An investigation of protocols for 2D and 3D models of human embryonic stem cell chondrogenic differentiation and tissue engineering

---

Nicola Carrinne FOSTER

Submitted for the Degree of Doctor of Philosophy

March 2020

Keele University

Abstract

Articular cartilage is prone to degradation as a result of aging, disease and injury, which can lead to the onset of osteoarthritis (OA). The avascular nature of the tissue renders its endogenous repair capacity notoriously poor and its aneural nature means that disease progression is often quite advanced before symptoms present. OA places a huge burden on the NHS and UK economy and there is an urgent need for alternative therapies, which offer patients a one-off durable treatment and mitigate or significantly delay the need for joint replacement. Tissue engineering offers a possible solution, wherein replacement cartilage is developed *in vitro* from undifferentiated cells.

Human embryonic stem cells (hESC) are readily available, pluripotent and demonstrate huge expansion capacity *in vitro*; all of which makes them an appealing cell source for tissue engineered constructs. This work sought to enhance the maturity of hESC-derived chondroprogenitors with the application of a range of 2D and 3D culture techniques and regimes of mechanical stimulation.

hESC were subjected to a directed differentiation protocol (DDP), described previously (Oldershaw et al. 2010), with the addition of an immobilised Wnt base and an acellular fibrin hydrogel to enable migration into a 3D environment. Addition of the hydrogel to differentiating monolayer hESC, always resulted in improved chondrogenic gene expression and the application of a Wnt platform significantly increased the migration of cells into the gel.

Hydrostatic pressure was applied to fibrin-encapsulated progenitors and was found to increase chondrogenic matrix deposition and gene expression. In addition, the application

of low level compressive forces to monolayer progenitors resulted in increased chondrogenic gene expression at low cell seeding densities.

Taken together, results suggest that both a 3D environment and the application of mechanical stimuli can significantly enhance the chondrogenic potential of hESC-derived chondroprogenitors. We believe that the work described here holds great potential for the development of a cell-based therapy for cartilage damage and degeneration.

Contents

Figures

Tables

Supplementary figures

Abbreviations

3D	Three-dimensional
4PBB	Four-point bending bioreactor
ACAN	Aggrecan protein
ACAN	Aggrecan
ACI	Autologous chondrocyte implantation
ALP	Alkaline phosphatase
APC	Adenomatous polyposis coli
APTES	3-Aminopropyltriethoxysilane
ASCOT	Autologous Stem Cells, Chondrocytes or the Two?
BMP2	Bone morphogenic protein 2
BMP4	Bone morphogenic protein 4
BMP7	Bone morphogenic protein 7
BMSC	Bone marrow-derived stroma cells
BSA	Bovine serum albumin
$CaCl_2$	Calcium chloride
CAMs	Cell adhesion molecules
CDK	Cyclin-dependent kinase
CDK4	Cyclin-dependent kinase 4
CDKN1A	Cyclin-dependent kinase inhibitor 1A
CDKN1C	Cyclin-dependent kinase inhibitor 1C
CDKN2D	Cyclin-dependent kinase inhibitor 2D
CHAD	Chondroadherin
CHAPS	3-[(3-Cholamidopropyl)dimethylammonio]-1-propanesulfonate
chErg	Chicken Erg
CHIR	CHIR99021 WNT pathway activator
CILP	Cartilage intermediate protein
CK1	Casein kinase 1
CKI	Cyclin dependent kinase inhibitor

COLVI	Collagen type VI
COL1	Collagen type I
COL11A2	Collagen type XI alpha 2 gene transcript
COL1A1	Collagen type I alpha I gene transcript
COL2	Collagen type II
COL2A1	Collagen type II alpha I gene transcript
COMP	Cartilage oligomeric matrix protein
CRG	Carrageenans
CS	Chondroitin sulphate
CsCl	Caesium chloride
C_T	Cycle threshold
DAPI	4',6-Diamidino-2-phenylindole
DDBM	Directed differentiation basal media
DDP	Directed differentiation protocol
DMMB	Dimethyl methylene blue
DMSO	Dimethyl sulfoxide
DPBS	Dulbecco's phosphate buffered saline
DS	Degrees of sulphation
Dsh	Dishevelled
DTT	DL-Dithiothreitol
E8	Essential 8
ECM	Extracellular matrix
ERK	Extracellular signal-related kinase
ESC	Embryonic stem cell
FACE	Fluorophore-assisted carbohydrate electrophoresis
FBS	Foetal bovine serum
FDA	Food and Drug Administration
FGF	Fibroblast growth factor
FGF2	Fibroblast growth factor 2
FN	Fibronectin
FOS	Fos proto-oncogene, AP-1 transcription factor subunit

FZD	Frizzled receptor
GAG	Glycosaminoglycan
Gal	Galactose
GalNAc	N-acetylgalactosamine
GAPDH	Glyceraldehyde 3-phaosphate dehydrogenase
GF	Growth factor/s
GlcA	Glucuronic acid
GlcNAc	N-acetylglucosamine
GSK3	Glycogen synthase kinase 3
GuHCl	Guanidine hydrochloride
HA	Hyaluronic acid
hADSC	Human adipose-derived stromal cells
HCl	Hydrochloric acid
HCl	Hydrochloric acid
HEPES	4-(2-hydroxyethyl)-1-piperazineethanesulfonic acid
hESC	Human embryonic stem cells
hESC	Human embryonic stem cells
HH	Hedgehog family
HMG	High-mobility group
HP	Hydrostatic pressure
HSPG	Heparan sulphate proteoglycan
HUVEC	Human vascular endothelial cells
ICC	Immunocytochemistry
IGF	Insulin-like family
IMS	Industrial methylated spirits
iPSC	Induced pluripotent stem cell
ITS	Insulin-Transferrin-Selenium-Sodium Pyruvate
IWP2	Inhibitor of Wnt production 2
JNK	Jun N-terminal kinase
KS	Keratan sulphate
LN	Laminin

MAP2K	MAP kinase kinase
MAP3K	MAP kinase kinase kinase
MAP3K3	Mitogen-activated protein kinase kinase kinase 3
MAPK	Mitogen-activated protein kinase
MAPK1	Mitogen-activated kinase 1
MEF	Mouse embryonic fibroblast
mESC	Murine embryonic stem cell
MMP13	Matrix metalloproteinase 13
MMPs	Matrix metalloproteinases
MSC	Mesenchymal stem cells
NaCl	Sodium chloride
NBF	Neutral buffered formalin
N-CAM	N-cadherin
NEAA	Non-essential amino acids
NICE	National Institute for Health and Care Excellence
OA	Osteoarthritis
OATS	Osteochondral autograft transfer
OCT4	Octamer-binding transcription factor 4
p38	p38 kinase isozyme
PCL	Poly(caprolactone)
PCM	Pericellular membrane
PEG	Poly(ethylene glycol)
PEGDA	poly(ethylene glycol) diacrylate
PG	Proteoglycan
PGA	Poly(glycolic acid)
PLA	Poly(lactic acid)
PLGA	Poly(lactic-co-glycolic acid)
PRELP	Protein/arginine-rich end leucine-rich repeat protein
PRG4	proteoglycan 4
PVA	Poly(vinyl alcohol)
qRT-PCR	Quantitative polymerase chain reaction

RA	Rheumatoid arthritis
RAC1	Rac family small GTPase 1
RGD	Arginylglycylaspartic acid
ROCK	Rho kinase
RT	Room temperature
RUNX2	Runt-related transcription factor 2
sAlg	Sulphated alginate
sAlg	Sulphated alginate
sAlg 0.0	Sulphated alginate with 0 degrees of sulphation
sAlg 0.8	Sulphated alginate with 0.8 degrees of sulphation
sAlg 2.0	Sulphated alginate with 2.0 degrees of sulphation
sGAG	Sulphated glycosaminoglycan
SLRP	Small leucine-rich repeat proteins
SO_3	Sulphur trioxide
SOX5	Sex determining region Y-Box 5
SOX6	Sex determining region Y-Box 6
SOX9	Sex determining region Y-Box 9
TAE	Tris-acetate-EDTA
TCF	T-cell factor
TCF/LEF	T-cell factor/lymphoid enhancer factor
TCP	Tissue culture plastic
TE	Tris-EDTA
TGF-ß	Transforming growth factor ß
TGT	Tissue Growth Technologies
Tnc	Tenascin-C
TRPV4	Transient receptor potential vanilloid 4
VTN	Vitronectin
w/c	Working concentration
Wnt	Wingless-related integration site
XPS	X-ray photoelectron spectroscopy
α-MEM	α-modified Eagle's medium

Publications and presentations

Associated publication

Some of the work from chapter 1 has been published in:

Foster, Nicola C., James R. Henstock, Yvonne Reinwald, and Alicia J. El Haj. 2015. D*ynamic 3D Culture: Models of Chondrogenesis and Endochondral Ossification*. Birth Defects Res C. 105 (1): 19–33. https://doi.org/10.1002/bdrc.21088.

Oral presentations

TERMIS (Tissue Engineering and Regenerative Medicine International Society) EU 2019

NC Foster, SJ Kimber, AJ El Haj. *Chondrogenic differentiation of human embryonic stem cells is enhanced with the application of a Wnt platform*. TERMIS EU meeting abstracts, 2019, page 1224

Poster presentations

TCES (Tissue and Cell Engineering Society) 2018

NC Foster, SJ Kimber, AJ El Haj. *Chondrogenic differentiation of human embryonic stem cells is enhanced with the application of a Wnt platform.* eCM meeting abstracts 2018, collection 4, page 29.

MSCA (Mercia Stem Cell Alliance) 2016

NC Foster, SJ Kimber, AJ El Haj. *The effects of the 3D environment and mechanical stimulation on the maturation of hESC-derived chondroprogenitors*.

TERMIS EU 2016

Y Reinwald, A Cheng, NC Foster, SJ Kimber, AJ El Haj. *Can the application of hydrostatic pressure to 3D ESC-models enhance the maturation of engineered cartilage tissue?*

TCES 2016

NC Foster, H Markides, E Hassan, AJ El Haj. *Tagging mechanoreceptors for promoting chondrogenesis.* eCM meeting abstracts 2016, collection 5, page 115.

Acknowledgements

I would like to thank my supervisor Alicia El Haj for giving me the opportunity to embark upon this PhD and for encouraging me to be more confident and positive in all that I do. I would also like to thank my co-supervisor Sue Kimber for offering more time and support than I could have hoped for and for providing a seemingly endless font of knowledge and insight – and of course, the cells!

Thank you also to Hari Markides, Katie Bardsley, Mike Rotherham and Tina Dale for their invaluable support and patience in the lab and to Nicola Bates for showing me how to culture these cells and for sending new batches when things went awry.

The work described in this thesis was funded by partially via the EPSRC as part of the Loughborough, Keele and Nottingham Universities' Centre for Doctoral Training and partially via the Institute for Science and Technology in Medicine at Keele University.

Finally, I would like to thank my family for their unfailing faith and support; particularly in the final year when childcare suddenly became an issue.

Chapter 1

Introduction

1.1 Clinical demand for tissue engineered articular cartilage

Articular cartilage is a smooth, tough tissue which reduces friction and acts as a shock absorber at articulating joints such as the knee, shoulder and hip. Unfortunately, the integrity of the tissue diminishes with age, and accelerated degradation as a result of disease and injury can lead to the development of osteoarthritis (OA). The avascular nature of cartilage renders its endogenous repair capacity notoriously poor and its aneural nature means that disease progression is often quite advanced before symptoms present.

Due to the complex nature of OA and its manifold indirect effects, estimating the cost of the disease to the UK poses a challenge. The musculoskeletal health budget for 2012-13 was £5.34 billion (Arthritis Research UK 2014). However, by 2017 the combined treatment costs of OA and rheumatoid arthritis (RA) were estimated at £10.2 billion. In addition to the direct costs of OA to the UK (figure 1-1), indirect costs arising as a result of lost revenue from missed work days (over 25 million per year) were estimated at £2.58 billion in 2017 (Arthritis Research UK 2017). This is predicted to rise to £3.44 billion by 2030. Additional costs associated with disability living allowance are estimated to exceed £5 billion per annum (Arthritis Research UK 2014) (Chen et al. 2012). Thus, OA places a huge burden on the NHS and UK economy and there is an urgent need for alternative approaches to current therapies, which offer patients a one-off durable treatment and mitigate or significantly delay the need for joint replacement. Tissue engineering offers a possible solution, wherein replacement cartilage is developed *in vitro* from undifferentiated cells, which can be obtained with little or no discomfort to the patient.

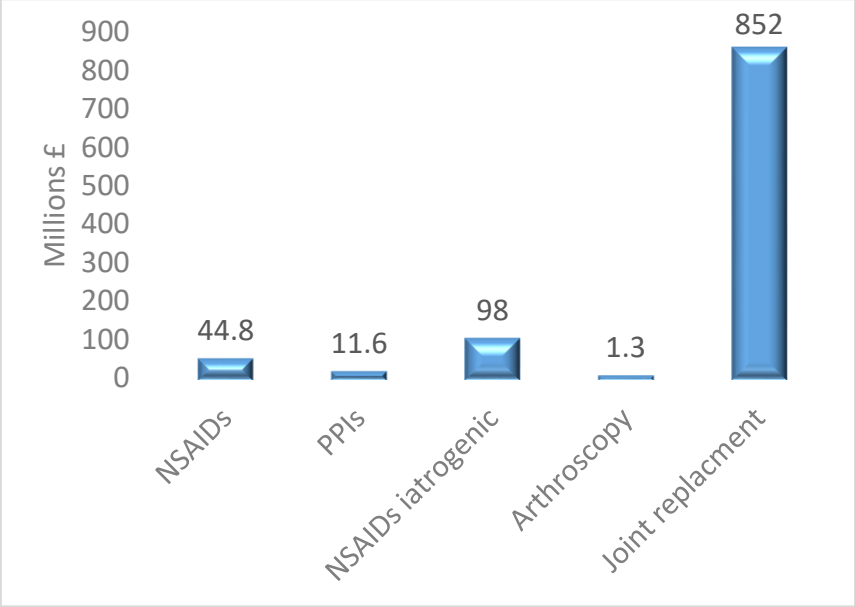

Figure 1-1. Estimated costs of OA treatments to the NHS in 2012. NSAIDs = non-steroidal anti-inflammatory drugs (e.g. ibuprofen, naproxen). PPIs = proton pump inhibitors often needed in conjunction with NSAIDs. NSAIDs iatrogenic = costs arising from gastrointestinal complications associated with use of NSAIDs. Arthroscopy = less invasive surgical procedure to remove damaged tissue/fluid. (A. Chen et al. 2012)

1.2 The musculoskeletal system

1.2.1 The skeleton

The skeletal system has roles in support, organ protection, movement, mineral homeostasis, blood cell production and triglyceride storage. It can be divided into the axial skeleton (skull, hyoid, auditory ossicles, vertebral column and thorax) and the appendicular skeleton (shoulders, limbs and hips). Where movement is required, articulating bones of the appendicular skeleton must interact with skeletal muscle in a carefully orchestrated manner. Many articulating bones are long bones (figure 1-2), such as the humerus and

ulna/radius of the arm. Long bones are composed of a diaphysis (shaft), proximal and distal epiphyses and metaphyses in between. The metaphyses have a layer of hyaline cartilage, termed the epiphyseal plate, which allows the bones to elongate. Once bones stop growing in length (during early adulthood), this layer mineralises to form bone and becomes the epiphyseal line. A thin layer of hyaline cartilage lines each epiphysis and the rest of the bone is covered in periosteum – a tough sheath of connective tissue which nourishes and protects the bone and contains osteoblasts to allow for appositional bone growth (increasing width). The medullary cavity in the centre of long bones contains fatty bone marrow and is lined by the endosteum, which contains a single layer of osteoblasts and a small amount of connective tissue. The diaphysis is primarily formed of dense cancellous bone, whereas the epiphyses consist mainly of trabecular tissue. Skeletal muscles attach to articulating bones at the point where they meet (joints). Attached via tendons, their contraction brings about movement of bones (Tortora and Grabowski 2003).

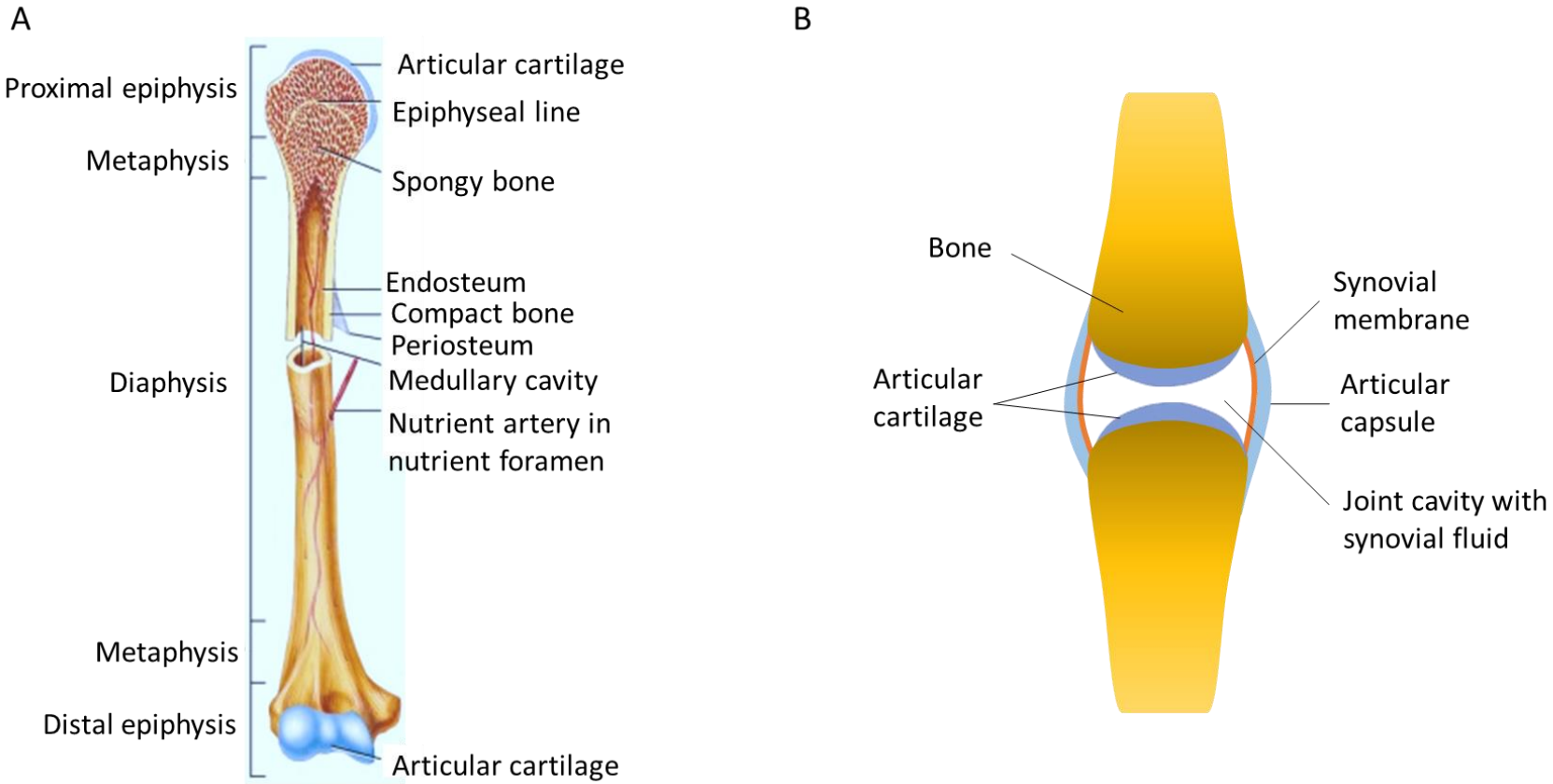

Figure 1-2. Structure of a long bone (A) and a synovial joint (B). Adapted from Tortora and Grabowski, Principles of Anatomy and Physiology, 10th edition, © John Wiley & Sons, Inc. (Tortora and Grabowski 2003).

1.2.2 Synovial joints

Joints can be fibrous, cartilaginous or synovial. Synovial joints, with their characteristic fluid-filled cavity, are the most common in the human body and there are six types. Examples include hinge joints such as at the knee or elbow which allow movement in one plane; condyloid joints at the knuckles or wrist which allow movement in two planes; and ball and socket joints at hip which enable movement around three axes (Tortora and Grabowski 2003). They are highly specialised to allow for load bearing and ultra-low friction movement between articulating bones. Synovial fluid, rich in hyaluronic acid (HA) and proteoglycan 4 (PRG4) (otherwise known as lubricin), serves to lubricate joints, but also has metabolic and regulatory functions in joint homeostasis by allowing the transfer of nutrients, waste products, growth factors, enzymes and range of other soluble molecules into and out of the non-vascularised synovial tissues. (Hui et al. 2012). Joint formation (figure 1-3) in humans first begins when the limb buds appear at around 4 weeks of gestation. Y-shaped mesenchymal condensations form, followed by an interzone at each future joint location. Cavitation occurs next and a liquid-filled synovial space appears. Proximal and distal ends of the developing limb acquire their characteristic interlocking shapes and finally, the formation of articular cartilage and other joint tissues, such as ligaments, complete the process by around week 14 (Pacifici, Koyama, and Iwamoto 2005; Mérida-Velasco et al. 1997).

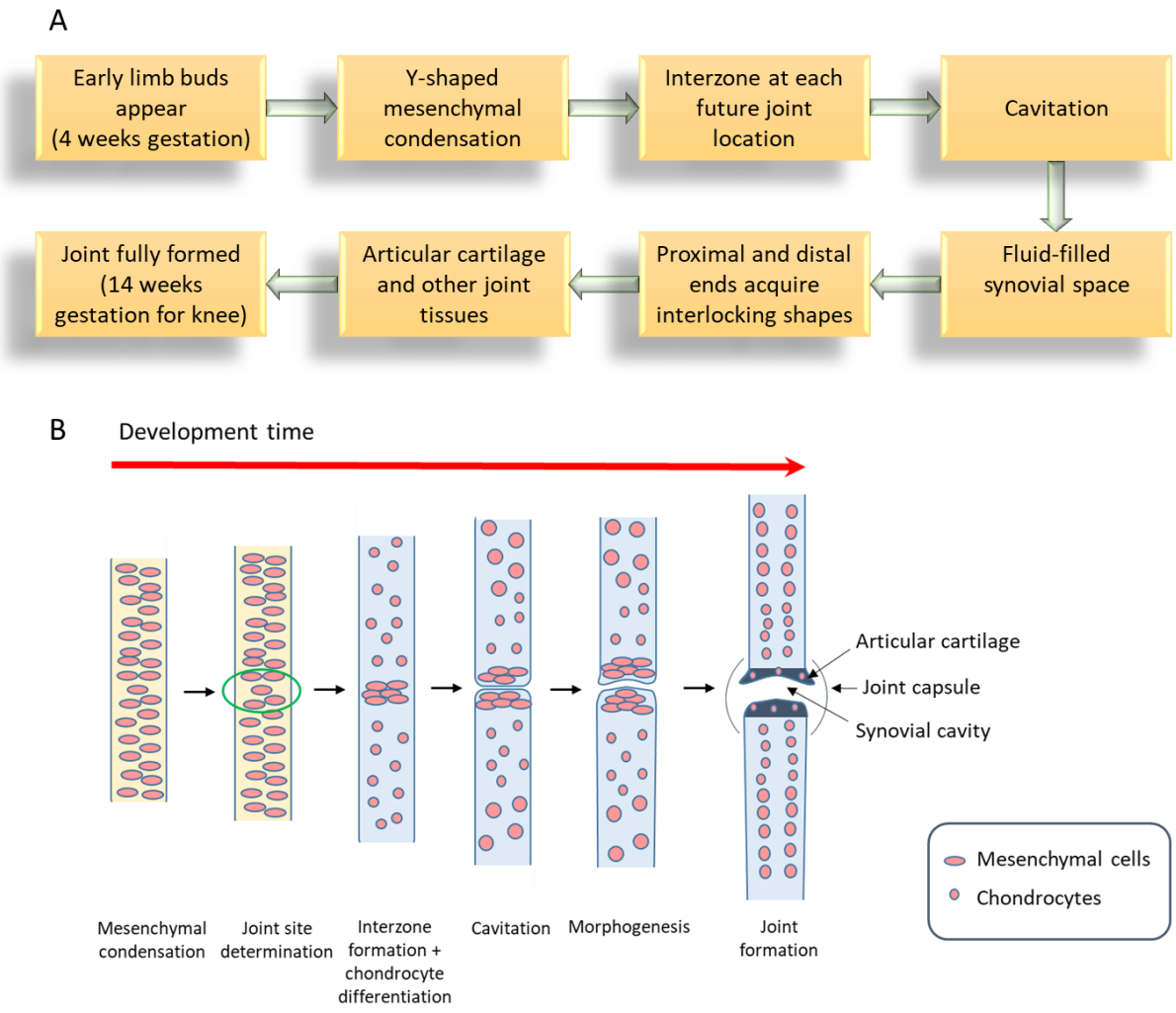

Figure 1-3. Synovial joint formation. A) Schematic of basic process of joint formation in humans B) Diagrammatical representation of joint formation. Adapted from Pacifici et al., 2005.

1.3 Articular cartilage

Found throughout the body – in structures such as the ear and nose, between vertebrae and also between articulating joints – cartilage is a key component of the musculoskeletal system. It is a tough, smooth, biphasic material – the solid phase composed of proteoglycans (PG), collagen and chondrocytes and the liquid phase mostly water and dissolved ions

(Guilak and Mow 2000; Mansour 2004; Foster et al. 2015). Hyaline cartilage (termed articular cartilage when located between articular joints) has a smooth "glassy" appearance and a highly specialised structure which differs from fibrocartilage and elastic cartilage (found in structures such as the intervertebral discs and epiglottis respectively).

1.3.1 The emerging model of hyaline cartilage ECM

The description of articular cartilage as a tissue with lubricating properties found on the ends of bones emerged as early as the 4th century and the first account of osteoarthritic cartilage was recorded in 1741. Up until the late 19th century, however, knowledge of the structure of articular cartilage remained very limited – fibrillar collagen and chondroitin sulphate were recognised as major components and zonal differences in chondrocyte distribution had been established (rounded cells in the deep tissue and flatter ones near the surface). Though it was also known to be an avascular tissue, its mode of mass transport was in dispute – one faction deemed the synovial fluid to be responsible, while the other favoured the subchondral blood vessels. With the development of the electron microscope and radio isotope technology in the mid-19th century, and improved chemical methods shortly thereafter, more detailed information about the structure of articular cartilage rapidly began to emerge (Benedek 2006). Around 1960 it was determined that chondroitin sulphate, along with smaller quantities of other polysaccharides such as keratan sulphate, were bound to a core protein and that these chondroitin sulphate-protein complexes probably formed aggregates (Partridge, Davis, and Adair 1961).

From this point a great deal of work, spanning the next five decades (figure 1-4) and pioneered by the likes of Helen Muir, Vincent Hascall, Stanley Sajdera, Dick Heinegård and Tim Hardingham, resulted in the model of articular cartilage that we have today (figure 1-

5). In 1969 Sajdera and Hascall published their “dissociative method” for extracting protein-polysaccharide complexes from bovine nasal cartilage (Sajdera and Hascall 1969). Unlike the earlier “disruptive” method which involved high speed homogenisation of the tissue and resulted in denaturisation and depolymerisation of its macromolecules, this new technique involved gentle agitation of samples in high ionic strength solutions to yield intact, disaggregated protein-polysaccharide complexes. This allowed for much closer interrogation of the tissue and from then on, a detailed picture of its structure began to emerge. In 1971 collagen type II (COL2) (described by Miller and Matukas in 1969) was identified as the tissue’s predominant collagen (Strawich and Nimni 1971). Bovine articular cartilage was incubated with papain at 4°C and washed with 0.15 M NaCl. Extraction with 0.45 M NaCl resulted in a 20% collagen in solution. After further purification to remove associated GAGs, a triple stranded molecule of COL2 was the only component observed.

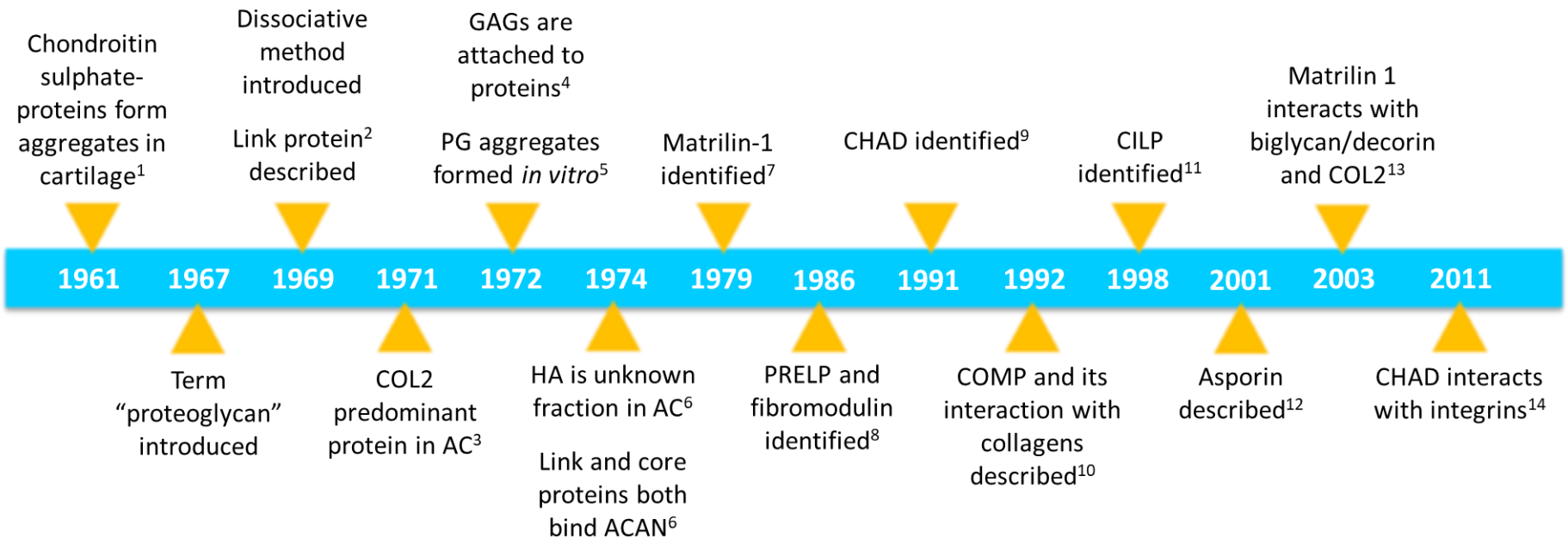

Figure 1-4. Timeline of developing model of articular cartilage. COL2 = collagen type II. GAG = glycosaminoglycan. PG = proteoglycan. HA = hyaluronic acid. PRELP = protein/arginine-rich end leucine-rich repeat protein. CHAD = chondroadherin. COMP = cartilage oligomeric matrix protein. CILP = cartilage intermediate protein. [1](Partridge, Davis, and Adair 1961) [2](Sajdera and Hascall 1969) [3](Strawich and Nimni 1971) [4](Rodén et al. 1972) [5](T. E. Hardingham and Muir 1972) [6](Timothy E. Hardingham and Muir 1974) [7](Paulsson and Heinegård 1979) [8](Heinegård et al. 1986) [9](Larsson et al. 1991) [10](Hedbom et al. 1992) [11](P. Lorenzo, Bayliss, and Heinegård 1998) [12](P. Lorenzo et al. 2001) [13](Wiberg et al. 2003) [14](Haglund et al. 2011).

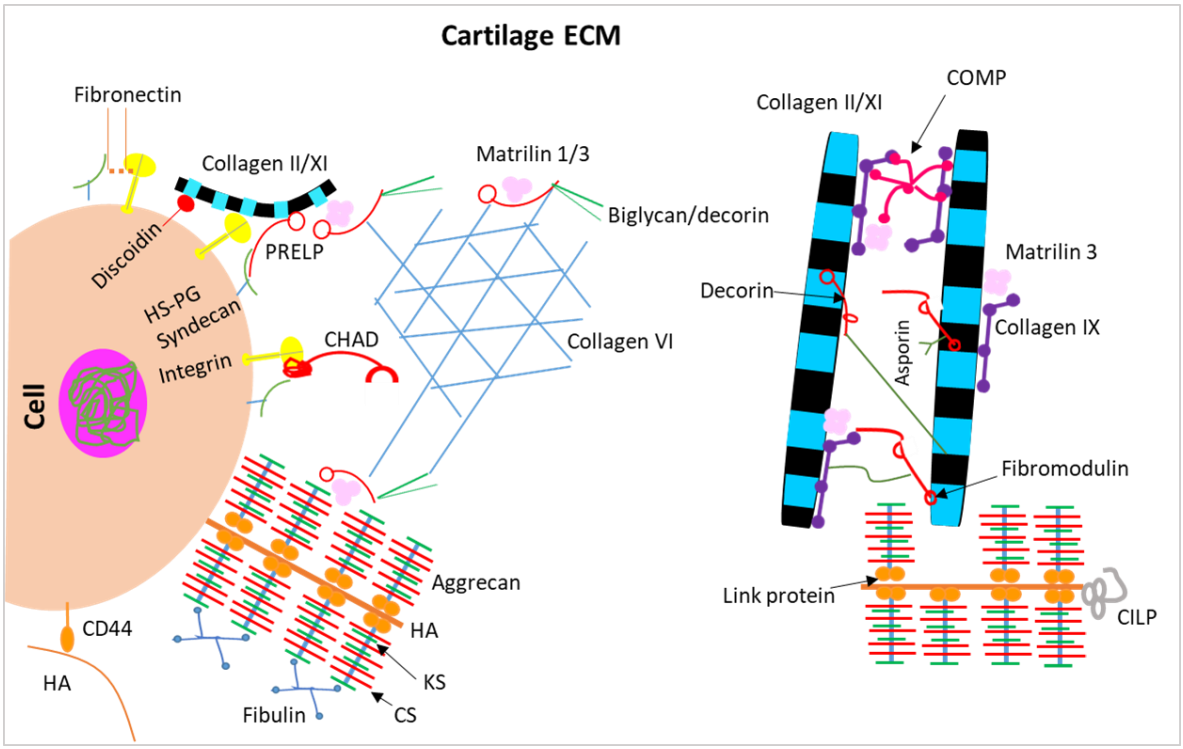

Figure 1-5. Dick Heinegård's final model of cartilage structure. CHAD = chondroadherin, COMP = cartilage oligomeric matrix protein, HA = hyaluronic acid, KS = keratan sulphate, CS = chondroitin sulphate, PRELP = protein/arginine-rich end leucine-rich repeat protein. Adapted from Hascall, 2014.

Isolation and characterisation of proteoglycans from cartilage tissue (usually bovine/porcine nasal or tracheal when much of the early work was conducted) via the dissociative method involves incubation with a dissociative solution of 3-4 M guanidine hydrochloride (GuHCl) to extract PGs, which are then re-aggregated with 0.5 M GuHCl. Aggregates are separated from unrelated proteins via caesium chloride (CsCl) density gradient centrifugation to produce an "A1 fraction" of PG aggregates. Further CsCl density centrifugation and incubation with dissociative 4M GuHCl results in a high density PG subunit and a lower density glycoprotein link (necessary for subsequent re-aggregation), which can be further separated into Link 1 and Link 2 with dissociative density gradients (V.

C. Hascall and Heinegård 1974). This method was utilised for much of the work that followed.

In 1971 Hardingham and Muir showed that small amounts of HA interacted with disaggregated PGs to give a stable increase in hydrodynamic size. Furthermore, this increase peaked at a HA concentration of 1%, suggesting that above this, HA molecules were competing for available PG. This interaction was specific for HA and it was estimated that 10-30 PG molecules were associated with each HA chain (T. E. Hardingham and Muir 1972). The following year the pair determined that each PG must have only one HA binding site, as they were unable to crosslink multiple HA chains. They also observed that each PG binds to a region around the size of a decasaccharide unit (4-5 nm) and, given that each PG occupies around 45 nm on a HA chain, deduced that they must be relatively spread out (Timothy E. Hardingham and Muir 1973). In 1974 they showed that the fraction isolated from cartilage, between the PG subunit and the glycoprotein link was in fact HA and that most PGs associated with it to form aggregates. Smaller, non-aggregating PGs with lower protein and keratan sulphate content were also identified (Timothy E. Hardingham and Muir 1974). Around the same time Hascall and Heinegård also observed large amounts of HA associated with PG aggregates (around 0.8%). These HA molecules were susceptible to degradation by chondroitinase, hyaluronidase and papain, but this was thwarted in the presence of chondroitin sulphate, which has a higher enzyme affinity; all of which suggests that HA is surrounded by PGs (V. C. Hascall and Heinegård 1974). Further work that year confirmed that most of the PGs in cartilage are aggregating, resistant to trypsin and papain digestion, and that link proteins are also present and necessary for their stabilisation (Vincent C. Hascall and Heinegård 1974; Heinegård and Hascall 1974). Further characterisation of

aggregating PGs followed in subsequent years, but the basic model is much the same as that shown in figure 1-8.

In 1979 Paulsson et al. reverted to the disruptive/associative method of proteoglycan extraction in order to preserve the secondary structure of polypeptides, which can be damaged by chaotropic salts such as GuHCl (Paulsson and Heinegård 1979). A series of chemical analyses revealed a novel molecule, termed “cartilage matrix protein” (later renamed matrilin 1), which formed stable complexes with link proteins and PG monomers and aggregates. This protein, thought to have a role in PG/collagen interactions, had a high molecular mass and was formed of two subunits joined by disulphide bridges. It was later found to interact with biglycan/decorin and COL2 (Wiberg et al. 2003). The discovery of two more novel matrix proteins (protein/arginine-rich end leucine-rich repeat protein (PRELP) and fibromodulin), each formed of a single polypeptide chain, followed a few years later (Heinegård et al. 1986; Vincent C. Hascall 2014). In 1991, Larsson et al. identified yet another matrix protein (later termed chondroadherin (CHAD)), which was subsequently found to interact with integrin α2ß1 (Haglund et al. 2011). Cartilage oligomeric matrix protein (COMP) and its interactions with collagens were described in 1992 (Hedbom et al. 1992) and the discovery of cartilage intermediate protein (CILP) followed in 1998 (P. Lorenzo, Bayliss, and Heinegård 1998). Finally in 2001, the identification of asporin, a protein unable to bind GAGs and thought to have a role in the stabilisation of collagen networks, completed Dick Heinegård’s final model (figure 1-5) (P. Lorenzo et al. 2001).

1.3.2 Development of articular cartilage *in vivo*

Chondrogenesis and the resulting production of articular cartilage is a complex process which varies depending on physiological location. During early embryonic development, human embryonic stem cells (hESC) in the limb buds give rise to a bi-potent mesendoderm population which develop into a mesenchymal core surrounded by an ectoderm (A. Cheng, Hardingham, and Kimber 2014). Condensed populations of mesenchymal stem cells form chondrification centres and subsequently differentiate into chondroprogenitors. Chondroblasts are then formed and they start to produce extracellular matrix (ECM) with an abundance of type II collagen and proteoglycans such as aggrecan (A. Cheng, Hardingham, and Kimber 2014). Eventually these cells lose contact with each other, become chondrocytes and organise into zones that form the growth plates of bones. Much of this initial cartilage model is replaced by bone via a process of endochondral ossification during foetal and postnatal development, but cartilaginous regions persist in the growth plates until early adulthood and remain at the ends of long bones as articular cartilage throughout life. (Oseni et al. 2011; A. Cheng, Hardingham, and Kimber 2014; Foster et al. 2015).

Sex determining region Y-Box 9 (SOX9) is a master transcription factor for all cartilage elements; its expression is switched on in both chondrogenic and osteogenic bone marrow-derived stromal cells (BMSC) prior to condensation and remains high in pre-chondrocytes and chondroblasts (Véronique Lefebvre and Smits 2005). Experiments with murine ESC have shown that there can be no expression of the key ECM proteins COL2 and ACAN when SOX9 expression is blocked (Bi et al. 1999). Furthermore, in its absence, mesenchymal cells are unable to differentiate into chondroblasts at all (Mori-Akiyama et al. 2003). The SOX9 protein has an Sry-related high-mobility group (HMG) box domain via which it binds to DNA

in order to initiate transcription of other genes such as *L-SOX5* (*SOX5*), *SOX6* and later, in cooperation with these two, *COL2A1* (Véronique Lefebvre and Smits 2005). No other transcription factors, upstream of SOX9, have been identified that may determine chondrocyte cell fate in all regions of cartilage. However, various homoebox transcription factors (Hox genes) coordinate the expression of genes involved in limb patterning during embryogenesis and may also be transducers of signalling pathways in chondrogenesis. For example, the *COL2A1* gene has multiple transcription factor recognition motifs in addition to those for SOX proteins. BMP2 signalling has been shown to activate the Hox gene *DLX-2*, which in turns leads to upregulation of *COL2A1* (Xu et al. 2001). The formation of a mesenchymal condensation in the developing limb bud requires successful cell contact, aggregation and fusion; all of which is reliant upon the expression of cell adhesion molecules (CAMs) such as N-cadherin (N-CAM), tenascin-C (Tnc), versican and thrombospondin-4 (Meech et al. 2005). *BARX2* is another Hox gene which helps to orchestrate chondrogenesis; it does so by regulating the expression of CAMs and its necessity for the formation of mesenchymal condensations and cartilage differentiation in the developing limbs of mice has been demonstrated (Meech et al. 2005). Furthermore, its expression is regulated by growth factors BMP4 and GDF5, and it was shown to act in conjunction with other targets of BMP signalling such as SOX9. BARX2 and COL2 proteins were shown to be co-expressed at the joint interzone and in the articular cartilage and, *in vitro*, BARX2 caused enhanced aggregation of bone marrow-derived cells (Meech et al. 2005). Additional proteins have been identified as transcriptional co-activators of SOX9 and their ablation shown to result in reduced expression of COL2. These include ZNF219 which brings about increased SOX9 activity on the *COL2A1* gene promoter (Takigawa et al. 2010); PGC-1 alpha which directly

interacts with SOX9 (Kawakami et al. 2005); and p300 which binds to the *COL2A1* promoter region (Tsuda et al. 2003).

SOX5 and SOX6 expression are activated in pre-chondrocytes and are very high in fully committed chondroblasts. Although they are not required for the determination of lineage commitment (normal precartilaginous condensations can form in their absence), low SOX5/SOX6 expression results in poor chondrogenic differentiation even when SOX9 expression is high (Smits et al. 2001). The three proteins bind to enhancer regions on the *COL2A1* gene and, together, can stimulate non-chondrogenic cells to express *COL2A1*, *ACAN* and other cartilage markers and are able to suppress hypertrophy; addition of transforming growth factor-ß (TGF-ß) and BMP4 can enhance this effect (Ikeda et al. 2004). Other cartilage matrix and regulatory genes have been shown to possess SOX binding regions, including collagen type XI alpha 2 (*COL11A2*) and *ACAN* (Véronique Lefebvre and Smits 2005). Thus, the SOX trio are master transcription factors for chondrogenesis and high expression of *SOX5*/*SOX6* is indicative of a more mature phenotype than expression of *SOX9* alone.

Prior to endochondral ossification, chondrocytes must first undergo a process of hypertrophy, which is characterised by an increase in cell volume, down-regulation of chondrogenic markers such as SOX9 and COL2, and upregulation of osteogenic markers such as collagen type X , RUNX2 and collagenases such as matrix metallopeptidase 13 (MMP13) (Mackie et al. 2008). Eventually, all chondrocytes in the growth plates of long bones become hypertrophic but, under normal (non-pathogenic) circumstances, articular chondrocytes do not. Quite how they escape growth plate maturation is unclear, but there are some well documented differences which make them distinct from those destined for

endochondral ossification. Pre-chondrocytes differentiate into chondroblasts which, unlike mature chondrocytes, are highly proliferative and responsible for laying down large amounts of ECM. Articular chondroblasts express high levels of lubricin (PRG4) and by the time they become mature chondrocytes (at the end of postnatal development) they also express high levels of ACAN, whereas both proliferation and COL2 expression are reduced (Rhee et al. 2005; Véronique Lefebvre and Smits 2005). Differential expression of the chicken Erg (chErg) transcription activator has also been observed between articular chondrocytes and growth plate chondrocytes (Iwamoto et al. 2000). Pre-hypertrophic chondrocytes express chErg, but a short-spliced variant was found to be expressed in cells taken from the articular cartilage of developing chicks. Furthermore, virally driven expression of the variant in the growth plate resulted in a failure of the tissue to undergo endochondral ossification, which indicates that chErg has a role in chondrocyte maturation. These differences suggest that the lineage commitment of chondrocytes in the growth plates and those in the epiphyses diverges early on in the process of joint formation.

1.3.3 Structure of articular cartilage

Articular cartilage is a highly specialised and organised form of hyaline cartilage which lines the surfaces of bones at diarthrodial joints. The liquid phase, consisting of water with dissolved ions such as sodium, accounts for around 80% of the tissue, whereas the remaining 20% is a solid phase consisting mainly of collagen fibrils cross-linked to proteoglycans. Chondrocytes are almost the only cell type in the tissue and constitute just 1-2% of the matrix volume, although this is higher in foetal and post-natal cartilage where growth rates are still high. In adult tissue these cells rarely divide and new cell production is a consequence of mitotic division rather than differentiation; they are, however,

metabolically active. Articular cartilage is avascular, aneural and, as a consequence of its isolation from the blood supply, relatively hypoxic (0.5-5% depending on depth of tissue) (Lafont 2010). Oxygen and nutrition are provided via diffusion from the subchondral bone and synovial fluid, therefore, cyclic movement and mechanical loading are key to maintaining normal structure and function by enabling water movement throughout the tissue. Chondrocytes are responsible for the production of ECM molecules as well as matrix metalloproteinases (MMPs), hyaluronidases and aggrecanases, which break down the matrix when necessary. The balance between anabolism and catabolism is carefully orchestrated by cellular responses to mechanical forces and soluble factors such as cytokines, growth factors and oxygen levels. Matrix synthesis, however, diminishes overall with increasing age. (Demoor et al. 2014; Poole et al. 2001; Sophia Fox, Bedi, and Rodeo 2009).

Unique zonal and regional organisation distinguish articular cartilage from that found in other regions (figure 1-6). The organisation and nature of ECM molecules varies with increasing depth, as does the morphology and arrangement of chondrocytes. The uppermost layer of tissue is termed the superficial zone and here cells are flattened and aligned parallel to the surface. Chondrocytes in this zone, along with synovial cells, produce lubricin which lubricates the surface and helps to achieve ultra-low friction movement of the joint. They also produce the lowest amounts of proteoglycan compared to other zones and the highest levels of COL2, the fibres of which are also aligned parallel to the surface. The greatest tensile strength and resistance to shear forces are found here at the articular surface and are achieved through a combination of densely packed COL2 fibrils (which provide strength) and parallel organisation of tissue, resulting in a tough, smooth outer

surface. This structure also acts as a filter for large macromolecules, thus protecting the cartilage from immune cells in the synovium. Below the superficial zone lies the transitional zone where cells, which are rounded and fewer in number, produce an extensive ECM rich in proteoglycans. Collagen fibres here have a larger diameter and a random arrangement. In the deep zone cell density and collagen content are lowest, whereas proteoglycan content and collagen fibril diameter are greatest; highest resistance to compressive forces is observed here. The calcified cartilage layer, visibly separated from the zone above by the tidemark, is mineralised and distinguished by the presence of hypertrophic chondrocytes which secrete collagen type X. This layer acts as a shock absorber for the subchondral bone beneath. (Bhosale and Richardson 2008; Poole et al. 2001).

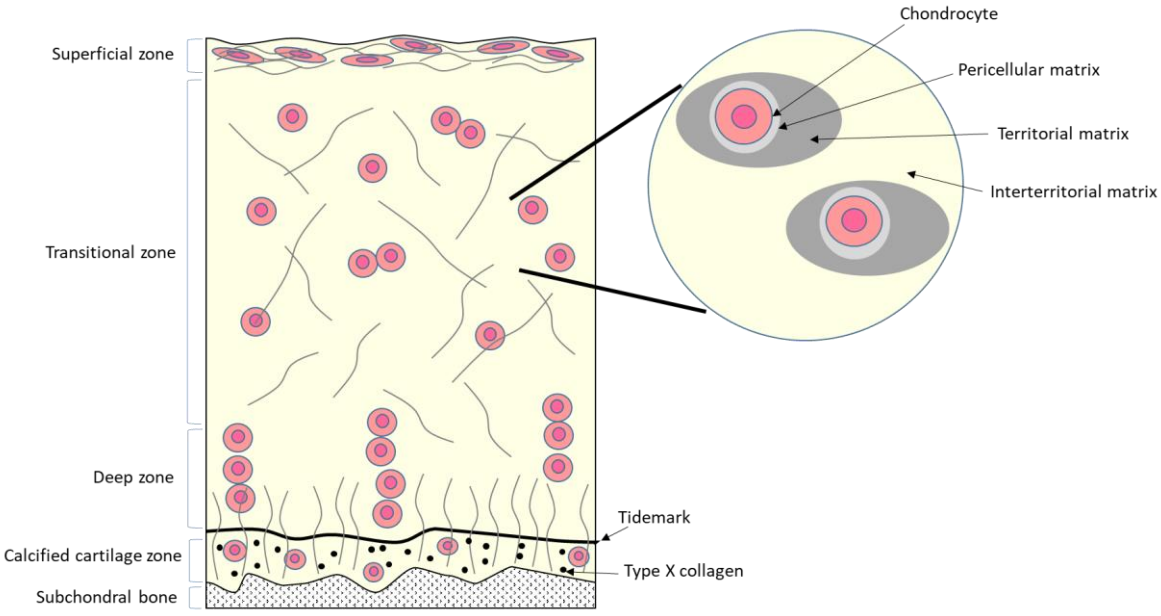

Figure 1-6. Structure of articular cartilage. Cells in the superficial zone are flattened and collagen fibres are aligned parallel to the articular surface. The transitional zone has fewer cells and collagen fibres are randomly arranged. In the deep zone cell density and collagen content are lowest, whereas proteoglycan content and collagen fibril diameter are greatest.

The calcified cartilage layer, visibly separated from the zone above by the tidemark, is mineralised and contains hypertrophic chondrocytes which secrete collagen type X.

In addition to zonal organisation, articular cartilage is organised into regions (figure 1-6), including the pericellular matrix (PCM), the territorial matrix and the interterritorial matrix. The PCM is similar to the rest of the ECM in many respects, but has fewer collagen fibrils and is rich in collagen type VI, which coats the cell surface (Keene, Engvall, and Glanville 1988) and co-localises with fibronectin (Hagiwara, Schröter-Kermani, and Merker 1993). The chondrocyte is anchored to the PCM via transmembrane proteins such as anchorin CII, which interact with COL2-expressing cells, and also via integrins, which interact with collagens and fibronectin in the pericellular space (Dürr et al. 1993). High levels of syndecan and glypicans also help to attach the chondrocyte to its immediate matrix and perlecan is an important cell surface molecule which helps to bind growth factors to the cell surfaces via its GAG chains (Gomes et al. 2002; Demoor et al. 2014). Levels of decorin, which has a role in limiting the diameter of collagen fibrils, are also high in this region (Poole et al. 2001). Together, the chondrocyte and PCM make up a structure called a chondron, rich in collagen types II, XI and IX, chondroitin-6 sulphate and keratan sulphate. Chondrocytes isolated separately from the PCM exhibit impaired phenotype and matrix production in subsequent culture, compared to intact chondrons. Fluorophore-assisted carbohydrate electrophoresis (FACE) analysis has also revealed significantly higher levels of chondroitin-6 sulphate and keratan sulphate in whole chondrons, all of which demonstrates the importance of the highly specialised PCM in maintaining articular cartilage phenotype (Q. G. Wang, El Haj, and Kuiper 2008).

Beyond the PCM lies the territorial matrix; collagen fibrils are more numerous here and they have a criss-cross arrangement, which forms a mesh around the chondrocytes in order to mediate mechanical impacts (Bhosale and Richardson 2008). These collagen fibrils extend out into the interterritorial matrix, which accounts for the majority of the ECM volume and is most remote from the chondrocytes. This region has the highest concentration of large aggregating proteoglycans (aggrecan) in addition to the collagens, proteoglycans and other non-collagenous proteins found throughout the tissue (table 1-1).

Table 1-1. Adult articular cartilage matrix components

Matrix component	Location	Function
Aggrecan	Throughout tissue. Main proteoglycan. Most concentrated in deep zone.	Provides compressive stiffness
Asporin	Surface of collagen fibrils	Possible role in stabilisation of collagen networks
Biglycan	Cell surface and pericellular matrix	Possible role in modulating growth factor and cytokine functions
Cartilage intermediate layer protein (CILP)	Transitional zone/interterritorial matrix	Unclear
Cartilage oligomeric matrix protein (COMP)	Between collagen fibrils	Helps to cross bridge collagen fibrils
CD44	Cell surface	Interacts with α2ß1 integrin, maintains cell morphology
Chondroadherin (CHAD)	Cell surface	Interacts with α2ß1 integrin, maintains cell morphology
Collagen type II	Main component of collagen fibrils (90%)	Provides tensile strength
Collagen type IX	Cross-linked to surface of macrofibrils	Enhances tensile properties and inter-fibrillar cross-linking
Collagen type VI	Pericellular matrix – cell surface	Aids chondrocyte attachment to matrix
Collagen type X	Hypertrophic cells in calcified layer	Aids cartilage mineralisation, provides functional strength and acts as shock absorber at bone interface
Collagen type XI	Within or on macrofibrils	Nucleates fibril formation
Decorin	On macrofibrils at articular surface	Regulates macrofibril formation
Fibromodulin	Surface of collagen fibrils	Stabilisation and organisation of the collagen network
Fibronectin	Enriched in PCM	Organisation of matrix
Hyaluronic acid	Throughout the ECM	Forms backbone of aggregating proteoglycans
Link protein	Aggregating proteoglycans	Assists binding of proteoglycans to hyaluronic acid
Lubricin	Articular surface and synovium	Lubricates joints
Lumican	Macrofibrils	Regulates macrofibril formation
Perlecan	Cell surface	Heparan sulphate binding proteoglycan. Cell-matrix adhesion
PRELP	Predominantly in the territorial matrix	Binds perlecan and collagens. Possible basement membrane anchor
Syndecan	Transmembrane	Heparan sulphate binding proteoglycan. Cell signalling.

1.3.4 Collagens in the extracellular matrix

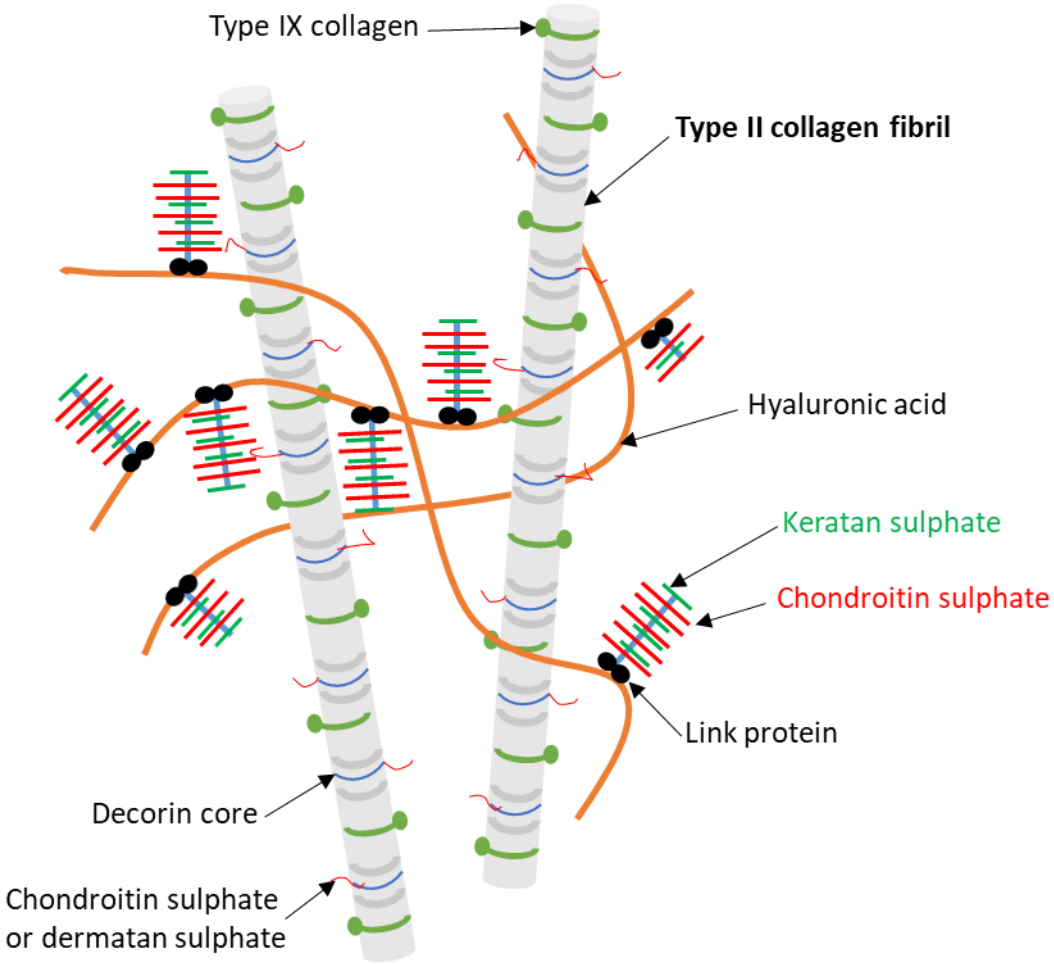

Figure 1-7. Interaction of the macrofibrillar collagen network with aggregating proteoglycans. Adapted from Poole et al. 2001.

Collagen is the most abundant protein found in animals and, of the 28 types identified in vertebrates, just five are found in articular cartilage where they comprise 60% of the tissue's dry weight. Collagens are all characterised as extracellular glycoproteins with a triple helical structure composed of three α polypeptide chains which intertwine to form a superhelix. (Exposito et al. 2010). Single procollagen chains are produced in the endoplasmic reticulum of collagen-producing cells. A number of post-translational modifications, orchestrated by enzymes, bring about the trimerisation of individual chains to form procollagen trimers,

followed by folding and disulphide bond formation. Procollagen trimers are processed further to produce collagen molecules with two short non-collagenous regions flanking the major triple helix. This robust structure is highly resistant to tensile forces and less susceptible to protease degradation than non-collagenous proteins, making it the ideal material for connective and load bearing tissues. (Canty and Kadler 2005; Exposito et al. 2010).

Fibrillar collagen molecules can associate via covalent crosslinks to form highly ordered structures called fibrils, which are usually composed of more than one type of collagen. In articular cartilage collagens type II, IX and XI associate to form large striated fibrils (figure 1-7), which crosslink and interact with proteoglycans to form a macrofibrillar collagen network through the territorial and interterritorial matrices. The diameter of these fibrils ranges from 20 nm in the superficial zone to as much as 120 nm in the deep zone (Poole et al. 2001). Collagen type II, which accounts for 80% of the collagenous component of articular cartilage, is a homotrimer formed from three α1(II) polypeptide chains. Small amounts of type XI collagen (a heterotrimer with an α1(XI), α2(XI) and α3(XI) chain) are present within and on the surface of fibrils and limit their lateral growth (Blaschke et al. 2000). Collagen type IX is a non-fibrillar heterotrimer (composed of an α1(IX), α2(IX) and α3(IX) chain), but the presence of a covalently bound GAG chain makes it technically a proteoglycan (Mendler et al. 1989). Bound to the surface of the fibrils, it interacts with COMP, heparin, matrilin 3, fibronectin and fibromodulin and is thought to have a role in stabilisation and organisation of the collagen network. Co-localisation of type IX collagen with fibronectin in the pericellular matrix suggests that it forms a molecular bridge between chondrocytes and collagen fibrils (Pihlajamaa et al. 2004; Parsons et al. 2011).

Collagen type VI is a non-fibrillar heterotrimer composed of α1, α2 and α3/α4/α5/α6 chains in a 1:1:1 ratio (Cescon et al. 2015). Found near to the cell surface in the PCM, it associates with decorin and HA to form a highly branched filamentous network which helps to anchor cells to the ECM (Keene, Engvall, and Glanville 1988; Poole et al. 2001). Collagen type X is a marker of hypertrophic cells and is generally found only in the calcified layer where it aids cartilage mineralisation and provides structural support. It is a short chain collagen molecule composed of three α1(X) polypeptides which are reinforced by a cluster of calcium ions (Ricard-Blum 2011).

1.3.5 Aggregating proteoglycans and GAGs

Proteoglycans are a structurally diverse group of molecules, which consist of a core protein covalently bound to one or more polysaccharide chains known as glycosaminoglycans (GAGs). The attached GAG chains can be chondroitin sulphate (CS), dermatan sulphate, keratan sulfate (KS), heparan sulfate or heparin. Many proteoglycans, including aggrecan and syndecan, carry two types of GAG chains, the size and ratio of which vary depending on age and health of the individual concerned. GAGs are large structures with numerous negatively charged sulphate and carboxylate groups, which attract cations into the ECM, thus generating an osmotic pressure which draws in water and keeps the space hydrated. Repulsive forces between the like charges of the GAG chains give proteoglycans their characteristic “bottlebrush” structure (figure 1-8). Aggrecan is by far the most abundant proteoglycan in articular cartilage and is able to form huge multi-molecular aggregates (figure 1-8). Each aggrecan monomer is around 90% carbohydrate – predominantly CS with smaller amounts of KS. Many of these monomers bind to the long chain GAG hyaluronan via a non-covalent interaction, which is stabilised by a link protein, resulting in the formation

of a large aggregating proteoglycan (figure 1-8). These complexes interact with other ECM components to give a hydrated gel capable of resisting strong compressive forces (T. E. Hardingham and Fosang 1992; Mansour 2004).

Versican is another aggregating proteoglycan composed of a core protein with CS chains, which also binds to HA with the aid of a link protein. Versican aggregates are thought to have anti-adhesive properties and create a loose, highly hydrated environment immediately around the cells of the interzone during joint morphogenesis, which promotes proliferation and migration. Expression of this proteoglycan diminishes in mature cartilage (Snow et al. 2005; Shepard et al. 2007).

HA, CS and KS are the three main types of GAG observed in articular cartilage and their distribution varies with depth in the tissue. HA accounts for 1-10% of the GAG content, KS 5-20% and CS around 80%. HA is unsulphated and composed of repeating disaccharide units of glucuronic acid (GlcA) and N-acetylglucosamine (GlcNAc) linked by a ß1,3-glycosidic bond. CS chains are composed of repeating disaccharide units of GlcA and N-acetylgalactosamine (GalNAc) and each unit can be sulphated at the GlcA C2 position, the GalNAc C4, GalNAc C6 or both GalNAc C4 and C6; sulphation at C4 or C6 is the most common. Increased sulphation at C6 sites relative to C4 sites as been reported as a function of age (Bayliss et al. 1999; A. Sharma et al. 2007). Again, the disaccharides are joined by a ß1,3-glycosidic bond. KS chains are composed of galactose (Gal) and GlcNAc repeating disaccharide units linked by a ß1,4 glycosidic bond. Sulphation can occur at position C6 of Gal and/or GlcNAc. Chain length and degree of sulphation have been shown to increase with age. (Kuiper and Sharma 2015; Bayliss et al. 1983; 1999).

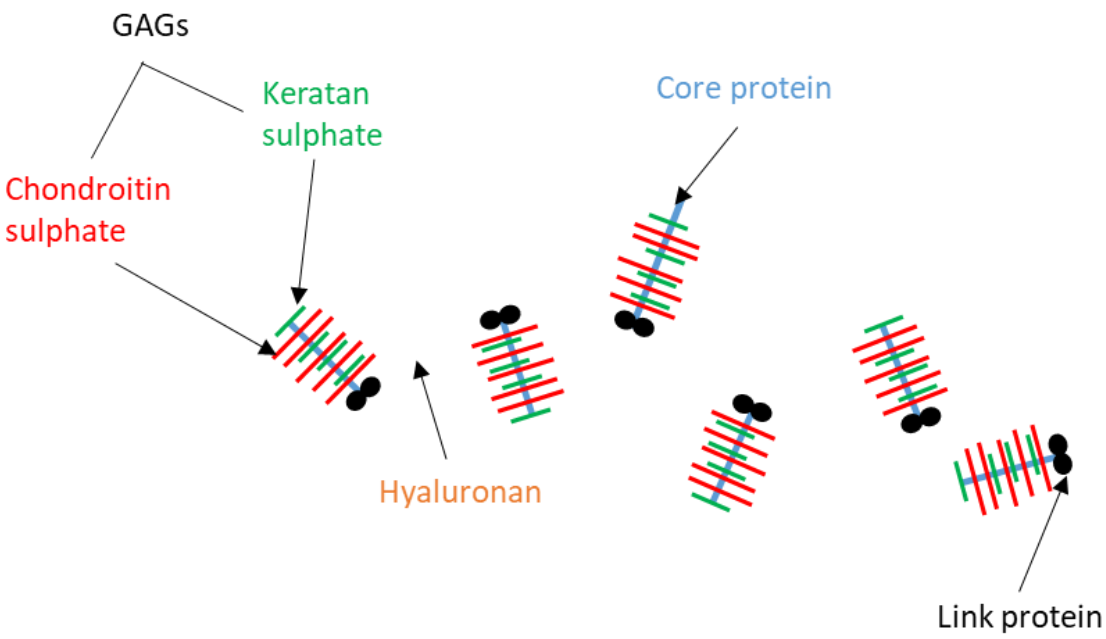

Figure 1-8. Basic structure of an aggregating proteoglycan complex. GAGs = glycosaminoglycans.

1.3.6 Other ECM molecules

Small leucine-rich repeat proteins (SLRPs) are a family of proteoglycans and proteins commonly found in articular cartilage and include decorin, biglycan, fibromodulin, lumican, PRELP, asporin and CHAD. By mass they account for a small proportion of total proteoglycans but are present in molar quantities similar to that of aggrecan. Decorin carries one chondroitin/dermatan sulphate chain and binds to collagen during fibril formation to reduce the final diameter; it is most concentrated in the superficial zone and PCM where fibril diameters are the smallest. Biglycan carries two chondroitin/dermatan sulphate chains and is otherwise highly homologous to decorin, but has a different pattern of expression and localisation. It does not bind to collagen and is found only near the cell surface and PCM, unlike decorin, which is also distributed in the wider ECM. The role of biglycan is not clear, but its ubiquitous expression and ability to bind molecules such as

transforming growth factor TGF-ß, BMP2 and BMP4, suggest that it may have a role in modulating growth factor and cytokine functions. Fibromodulin and lumican both carry KS chains and, like decorin, are thought to have a role in fibril synthesis. (T. E. Hardingham and Fosang 1992; Poole et al. 2001; Nastase, Young, and Schaefer 2012). PRELP has been shown to bind to perlecan and collagens. It binds to perlecan, a basement membrane heparan sulphate proteoglycan (HSPG), via a heparan-binding domain and, therefore, may have a role in anchoring the basement membrane of articular cartilage to the underlying connective tissue (Bengtsson et al. 2002). CHAD contains a binding motif for chondrocytes, a synthetic version of which maintains the rounded morphology of the cells *in vitro*. Binding of cells to both CHAD and the peptides also initiates signalling pathways such as ERK phosphorylation (Haglund et al. 2011; Paracuellos et al. 2017). This SLRP can also bind to collagen II and may, therefore, have a role in crosslinking in addition to maintenance of a mature phenotype and cartilage homeostasis (Paracuellos et al. 2017). Finally, there is evidence to suggest that asporin, which is thought to help stabilise collagen networks, contributes to OA pathogenesis, as it is abundantly expressed in OA cartilage and has also been shown to inhibit TGF-ß-induced chondrogenesis (Nakajima et al. 2007).

Additional ECM molecules such as COMP, CD44 and fibronectin have important roles in articular cartilage function and homeostasis. COMP is a matrix protein with a high affinity for collagen types II and IX and appears to have a role in fibril formation by helping to cross-bridge collagen fibrils (Holden et al. 2001; Geng et al. 2008). Cellular interactions with HA and other matrix molecules in the PCM are regulated by the cell surface receptor CD44. Adhesion of cells to HA via this glycoprotein has been shown to induce proliferation and expression of TGF-ß in a human chondrocyte-like cell line (Ishida et al. 1997). CD44 also

mediates the endocytosis of HA during tissue catabolism and is implicated in OA pathogenesis, where shedding of the cell surface receptor has been observed, along with a concurrent release of membrane-bound hyaluronidase into the surrounding matrix (Hida et al. 2015). Fibronectin is an ECM glycoprotein with multiple binding sites for both matrix components and cells. It interacts with collagen and proteoglycans and aids organisation of the collagen network, in addition to promoting cell adhesion via an arginylglycylaspartic acid (RGD) sequence. (Heinegård and Oldberg 1989; Chevalier 1993). The matrilins are a family of ECM proteins (matrilin-1, -3 and -4) which are abundant in embryonic/developing cartilage but are usually absent in healthy adult tissue. They have been shown to bind to aggrecan, collagen II fibrils and numerous other ECM components and may aid fibril formation (Nicolae et al. 2007; Heinegård and Oldberg 1989; Demoor et al. 2014).

1.3.7 Overall structure in relation to function

The unique structure of articular cartilage and distribution of the components described above serve to fulfil its role as a load-bearing connective tissue able to withstand high compressive and tensile forces and to provide smooth, frictionless movement at the joint. Repulsive forces between the negatively charged GAG chains create space in the ECM and this fixed charge also attracts cations such as sodium; the resulting osmotic pressure draws water into the space. One function of collagen fibrils is to provide tensile strength to resist the subsequent swelling. Application of a pressure gradient across the tissue or compression of the solid phase brings about water movement, which serves achieve mass transfer in an avascular environment. However, frictional resistance against this movement is very high which results in low permeability, slow water movement and generation of large shear forces. This viscoelastic behaviour means that sudden application of force, as a result

of exterior stimuli, results in slow deformation of the tissue, which acts as a shock absorber by distributing the pressure evenly across the articular surface. (Demoor et al. 2014; Blaschke et al. 2000; Sophia Fox, Bedi, and Rodeo 2009).

1.4 Cartilage ageing, damage and degradation

Reductions in chondrocyte population, matrix synthesis and hydration are observed in ageing cartilage; fewer cells result in lower levels of aggrecan and GAGs and, therefore, a reduced capacity to retain water. This inevitably compromises mass transfer, which leads to ineffective transport of nutrients and signalling molecules, and accumulation of cytotoxic waste products. Increased cartilage stiffness, resulting from excessive cross-linking of collagen, is also indicative of ageing tissue. As the integrity of the tissue is compromised, it is unable to resist the compressive and tensile forces exerted upon it and a gradual degeneration ensues. (Grogan and D'Lima 2010). Though ageing undoubtedly predisposes a joint to developing arthritis, there are multiple factors that contribute to the onset of the condition. Trauma to the joint surface as a result of sudden heavy impact or repetitive loading, for example, can cause chondrocyte death, reduced proteoglycan synthesis, disruption to the collagen matrix and swelling as a result of increased hydration. Production of inflammatory or catabolic molecules and reactive oxygen species have also been reported. (Grogan and D'Lima 2010)

Pathological changes observed in osteoarthritic joints (figure 1-9) include degradation of the articular cartilage, which progresses to a full thickness loss; thickening of the subchondral bone; accumulation of mineralised matrix; osteophyte (bone spur) formation at the joint surface; synovial inflammation; ligament degeneration with eventual rupture;

and hypertrophy of the joint capsule, which causes the characteristic enlargement of the area. Regions of the articular surface subject to the greatest mechanical forces are the first to display changes, and loss of the intact smooth, lubricated surfaces results in impaired movement of the joint. Innervated tissues, such as the subchondral bone, also undergo degeneration and are responsible for the pain associated with the later stages of OA. (Loeser 2010).

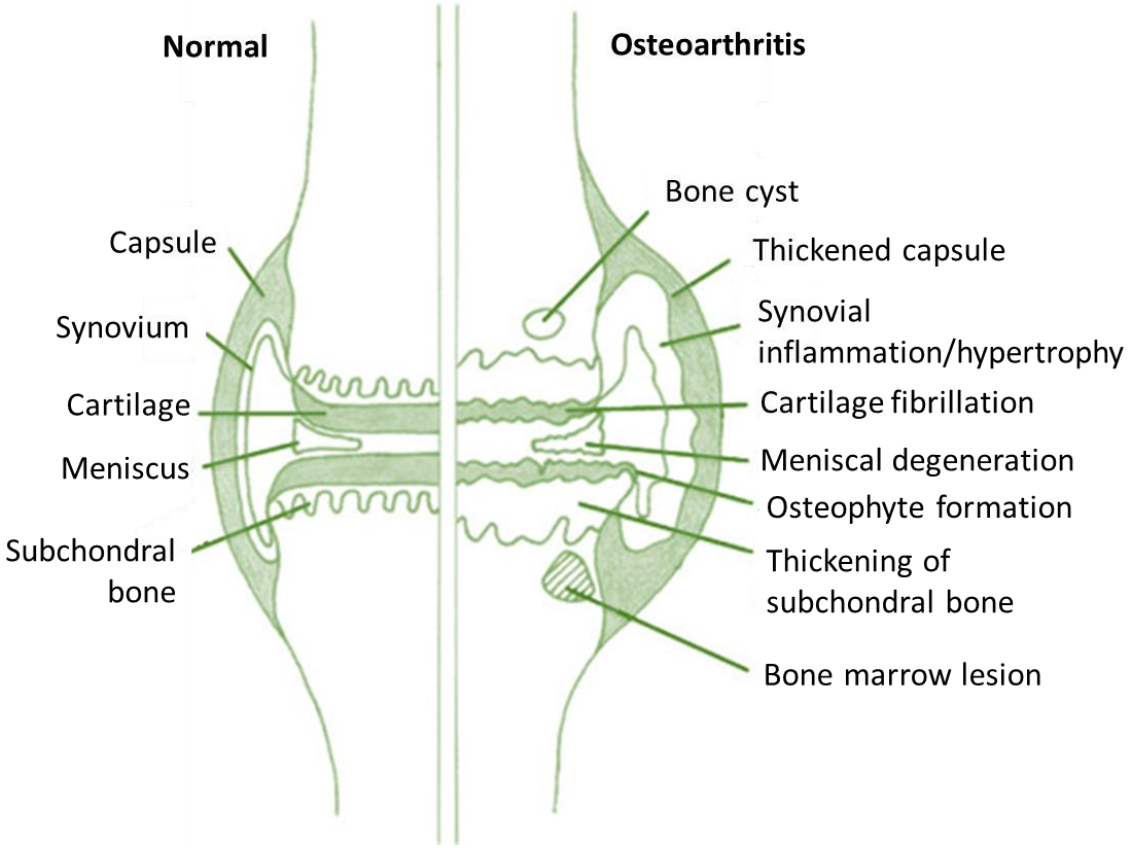

Figure 1-9. Pathology of OA in the human knee. The osteoarthritic joint displays degradation of articular cartilage, thickening of subchondral bone, osteophyte formation, synovial inflammation and hypertrophy of the joint capsule with characteristic enlargement of the area. Adapted from Loeser, 2010.

Owing to the work of Helen Muir in the 1970s, cartilage degeneration, previously thought a result of simple wear and tear, is now known to be a result of molecular and cellular processes. Her group showed that a canine model of OA expressed proteoglycans with higher levels of CS relative to KS, which mirrored the pattern of immature cartilage (McDevitt and Muir 1976). Due to the aneural nature of the tissue, OA remains asymptomatic until its late stages and insight into the changes that take place during the early stages is garnered primarily from animal models. Acute injuries to joints such as the knee are common, however, and can lead to the onset of OA, thus providing some opportunity for studying the earlier stages in humans. These early changes include increased water content and swelling, increased cell division and fibrillation of the articular surface. Prior to any visible changes to the tissue, an increase in proteoglycan synthesis is observed in animal models; however, in later stage human osteoarthritic cartilage, reports of proteoglycan synthesis vary widely. Collagen II has a low turnover in cartilage and its content in the tissue is not thought to change drastically, although modification of the network has been observed, as have higher levels of denatured collagen (thought to be a result of proteolytic enzyme activity) (Pilar Lorenzo, Bayliss, and Heinegård 2004; Bank et al. 2000; Hollander et al. 1994).

Although aggrecan and collagen type II are the main matrix components of articular cartilage, many of the other constituents described above, which have roles in matrix assembly and homeostasis have been implicated OA pathogenesis. Synthesis of COMP, fibronectin and CILP have been shown to increase in human early and late stage OA compared healthy tissue, whereas collagen synthesis is only upregulated in the late stages (Pilar Lorenzo, Bayliss, and Heinegård 2004). Cartilage from COMP-deficient mice appears

phenotypically normal, yet the animals develop severe early-onset arthritis, which may be due to instability of the tissue and exposure of more epitopes to invading immune cells (Geng et al. 2008). Insufficient COMP production, therefore, may be one factor which predisposes people to OA. Syndecan proteoglycans are also upregulated in osteoarthritic tissue. One member of the family, SYND4, hardly expressed at all in healthy adult tissue, is highly upregulated in both human OA and animal models. Its production is thought to be induced by proinflammatory cytokines associated with the condition and it actively contributes to pathogenesis by promoting aggrecanase activity and subsequent tissue degradation (Pap and Bertrand 2013). High levels of catabolic, proinflammatory cytokines such as interleukin (IL)-1 and tumour necrosis factor (TNF)-α, have been observed in osteoarthritic joints and contribute the destruction of articular cartilage (Goldring 2000). Pathways analysis of OA cartilage from human donors has also revealed dysregulated wingless-related integration site (Wnt) signalling in comparison with healthy tissue. Canonical and planar pathways were found to be downregulated, whereas the Ca^{2+}/Wnt pathway was activated (Thorfve et al. 2012). These are just a few examples of the large array of molecular changes that have been observed in degenerating articular cartilage. Whether these changes are the result of pathogenesis or a contribution to its onset remains to be seen in many cases, but such insights offer potential targets for the pharmaceutical management of the disease.

1.5 Current gold standard treatments

Current treatments for OA range from exercise, weight loss and the use of devices to reduce joint loading (e.g. walking frames) for milder cases, through to total joint replacement or fusion for the most severe cases (figure 1-10). Of these treatments, joint replacement is by

far the most expensive, costing the NHS an estimated total of £852 million in 2012 (A. Chen et al. 2012) (figure 1-1). Over 200 000 joint replacements were carried out by the NHS in 2015 (Arthritis Research UK 2017) and an increasing population means that this figure is set to rise.

Despite the relative success of the surgery, prosthetic joints are far from ideal. Implants remain functional for around 20 years (sometimes longer, but often less) before more traumatic revision surgery is required; after failure of the second implant, patients are often wheelchair-bound. Thus, arthroplasty is usually reserved for those aged over 50 and clinicians will opt for interventions such as arthroscopic lavage and debridement in order to delay its necessity for as long as possible. OA is also very common in smaller articulating joints, such as the interphalangeal joints of the fingers, and can be seriously debilitating and detrimental to quality of life. Here, however, arthroplasty is not an option.

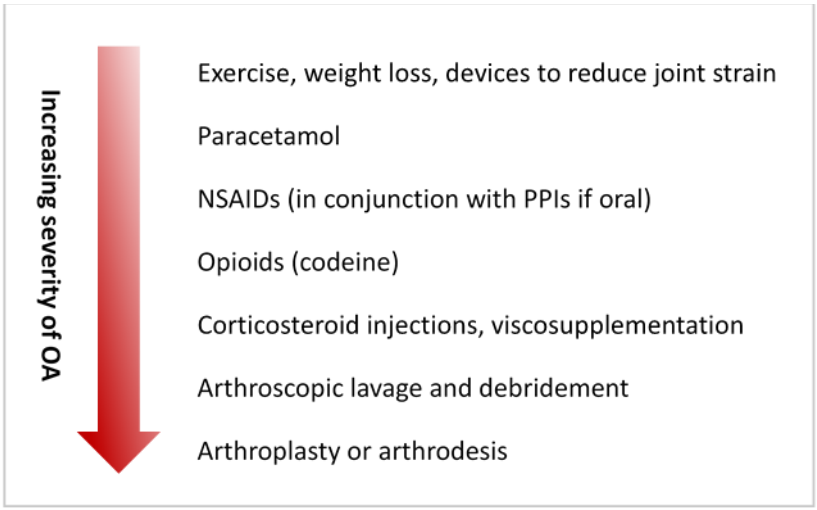

Figure 1-10. Current treatment available via the NHS for patients with OA.

1.6 Regenerative medicine approaches

1.6.1 Early procedures

Articular cartilage is a good candidate for regenerative medicine therapies, due to the limited treatment options, high incidence of disease/injury in all adult age groups and the relative accessibility of affected sites with minimally invasive techniques. Such techniques aim to either replace tissue with *in vitro* engineered alternatives, or to encourage endogenous repair with the application of a cellular therapy. A key measure of success is the regeneration of tissue functionally and structurally akin to that which has been damaged, as opposed to the formation of fibrous, scar tissue (a more common outcome). Debridement, subchondral bone drilling and micro-fracture (introduced in the 1940s, 1959 and 1997 respectively) are examples of attempts to promote endogenous repair mechanisms. Debridement is simply intended to remove damaged tissue, whereas micro-fracture and subchondral drilling induce bleeding, fibrous clot formation, subsequent recruitment of stem cells from the underlying bone marrow and the gradual formation fibrocartilage, which fills the defect (Insall 1967). Though still carried out today, these procedures have limited success and, in the case of debridement, it is unclear if there is any benefit at all (Thorlund et al. 2015). Significant improvements in pain and functionality have been reported following micro-fracture of the knee (Weber et al. 2018), but subchondral drilling has met with little success and, in some cases, resulted in worse post-operative function (Shah et al. 2007). Another technique is osteochondral autograft transfer (OATS), which involves transferring cartilage tissue from non-weight-bearing regions of the knee to the articular surface; although outcomes are encouraging, this option is limited by the

availability of donor tissue and is suitable only for lesions between 1 cm^2 and 4 cm^2 with a maximum depth of 10 mm (Shah et al. 2007).

1.6.2 Autologous chondrocyte implantation

Although the techniques described above give little hope of long-term repair, they are approved procedures which offer the opportunity for the application of cell/tissue engineered therapies. Autologous chondrocyte implantation (ACI), first performed on human patients in 1987, is one such therapy. Chondrocytes are isolated from a biopsy of healthy, autologous cartilage, expanded *in vitro* for 11-21 days, then injected into the defect and covered with a periosteal flap taken from the medial tibia (Brittberg et al. 1994). Second generation ACI involves the use of a collagen membrane instead of a periosteal patch, the hypertrophy of which can lead to complications in some patients. In 2017 first and second generation ACI were approved by the National Institute for Health and Care Excellence (NICE) for the treatment of cartilage defects of the knee. The extensive suturing and cell leakage associated with second generation ACI, however, has led to the development of matrix-assisted autologous chondrocyte transplantation, whereby chondrocytes are seeded onto a scaffold and then fixed in place with fibrin glue. Though this treatment is approved for use in the United States by the Food and Drug Administration (FDA), it has yet to be approved by NICE (Schuette, Kraeutler, and McCarty 2017). Other adaptations of ACI are in development and at various stages of the clinical trials process. The limited expansion capacity of chondrocytes may be overcome by substituting some or all of them with autologous BMSC. The ASCOT trial (Autologous Stem Cells, Chondrocytes or the Two?), which seeks to answer this question, is currently recruiting patients (Richardson et al. 2017).

Though there has been some success with cell therapies, tissue engineered cartilage grafts lack the mechanical strength to function as realistic alternatives to current gold standard treatments, particularly in areas subjected to high mechanical loading such as the hip, intervertebral disc or knee. Much work is now focused on selecting the optimum cells from which to derive chondrocytes; creating 3-dimensional (3D) scaffolds to provide adequate structural support and appropriate biochemical cues; and applying regimes of mechanical stimulation which stimulate the developing tissue in a fashion similar to that of the native environment.

1.6.3 Potential barriers to the success of regenerative therapies

Although tissue engineered constructs and cellular therapies often perform well *in vitro*, they are cultured in optimal growth conditions, which are not representative of the diseased state of the joint. Cytokines, which activate catabolic enzyme activity, are known to be elevated in OA joints. For example, IL-1α (a potent proinflammatory cytokine) was shown to be present in articular cartilage taken from patients with early stage OA and its co-localisation to chondrocytes throughput the tissue suggested that it was cell-derived rather than transported from the synovium (Towle et al. 1997). Other work has shown that chondrocytes taken from superficial zone cartilage of OA patients produce elevated levels of pro-inflammatory cytokines IL-1ß and TNF-α, in addition to numerous MMPs, which are known to be responsible for cartilage degradation (Tetlow, Adlam, and Woolley 2001). If native cartilage is unable to withstand these conditions, the chances of success for any transplanted material must be called into question. Challenging constructs/cells *in vitro* with addition of inflammatory mediators to the culture medium can give some indication of their likely response *in vivo*.

1.7 hESC as a potential cell source for therapies

In vitro production of cartilage for tissue engineering applications presents an array of challenges. Autologous chondrocytes are the most appealing cell source in terms of suitability for the patient, but their extraction and subsequent expansion is an invasive and lengthy process, which may ultimately yield cells with an endogenous predisposition towards pathogenesis. In addition, their expansion potential is limited to 2-3 passages; beyond this point they begin to de-differentiate towards a fibroblastic phenotype, which is of little use for the production of quality replacement tissue (Marlovits et al. 2004; Barlic et al. 2008). BMSC offer an alternative cell source and have been utilised with some success, but again their expansion capacity is limited and autologously-sourced cells may be predisposed towards a diseased phenotype (H. J. Kim and Park 2017). Human embryonic stem cells (hESC), however, are readily available, pluripotent and demonstrate huge expansion capacity *in vitro* – all of which makes them an appealing cell source for tissue engineered constructs (Metallo et al. 2008).

1.7.1 Chondrogenic differentiation of hESC

Protocols for differentiating hESC into a chondrogenic lineage have traditionally involved the initial formation of embryoid bodies, which are then dissociated and cultured in chondrogenic medium on a feeder layer of fibroblasts (usually murine) (A. Cheng, Hardingham, and Kimber 2014; Jukes et al. 2008; Hwang, Varghese, and Elisseeff 2008). However, these methods are far from ideal; the use of embryoid bodies results in a heterogeneous cell population, which may account for the high incidence of teratoma formation, and use of a xenogeneic feeder layer renders any resulting tissue unsuitable for clinical applications. More recent studies adopt protocols which avoid the need for

embryoid body formation by first differentiating hESC into BMSC and subsequently into chondrocytes (Boyd et al. 2009; G. Gong et al. 2010). Others report the use of a feeder-free layer in which cells are cultured on Matrigel or laminin in mouse embryonic fibroblast (MEF)-conditioned medium (Ludwig et al. 2006; Hwang et al. 2008). McKay et al. developed a human feeder cell line from placental stromal fibroblasts that were able to sustain hESC over long-term culture, resulting in a completely xeno-free product suitable for potential clinical applications (McKay et al. 2011). However, these feeder cells are obtained from first or early second trimester placentas, which limits their availability.

In vivo a broad range of genes and biomolecular signals regulate the differentiation of hESC into chondrocytes and the ultimate formation of cartilaginous tissue. For example, master transcription factor SOX9 (produced by chondro-progenitors) drives the early stages of chondrogenesis and is inhibited by runt-related transcription factor 2 (RUNX2) (the key transcription factor for osteogenesis) (A. Cheng, Hardingham, and Kimber 2014; Foster et al. 2015). Five families of growth factors also play major roles in this process: the TGF-ß super-family, the fibroblast growth factor family (FGF), the insulin-like family (IGF), the wingless family (Wnt) and the hedgehog family (HH) (Oseni et al. 2011). *In vitro* differentiation of embryonic stems cells (ESC) towards a chondrogenic lineage is usually achieved via culture in chondrogenic medium and the addition of one or a combination of growth factors such as TGFβ1, TGFβ3, bone morphogenic proteins 2/4/7 (BMP2, BMP4, BMP7) and IGF-1 (Koay, Hoben, and Athanasiou 2007; Toh et al. 2010; Nakagawa, Lee, and Reddi 2009).

In 2010 Oldershaw et al. developed a protocol to generate immature chondrocytes from hESC, based on the sequence of pathways that are active *in vivo* during early embryonic

development as the mesendoderm and mesoderm are forming. This three-stage, feeder-free process is carried out over 14 days and utilises a range of exogenous factors including WNT3A and activin-A to initiate a shift towards a mesendoderm population; FGF2 to enhance proliferation; BMP4 and GDF5, which are pro-chondrogenic cytokines; follistatin to block endoderm-specifying genes; and NT4 to promote cell survival. They demonstrated that, at the end of the process, up to 97% of cells from multiple embryonic cell lines expressed the *SOX9* gene. In addition, aggregates expressed high levels of chondrocyte-specific markers and very few markers that were indicative of a non-chondrocyte phenotype (Oldershaw et al. 2010). A modified version of the differentiation protocol was used to generate chondroprogenitors for the current study (figure 1-11).

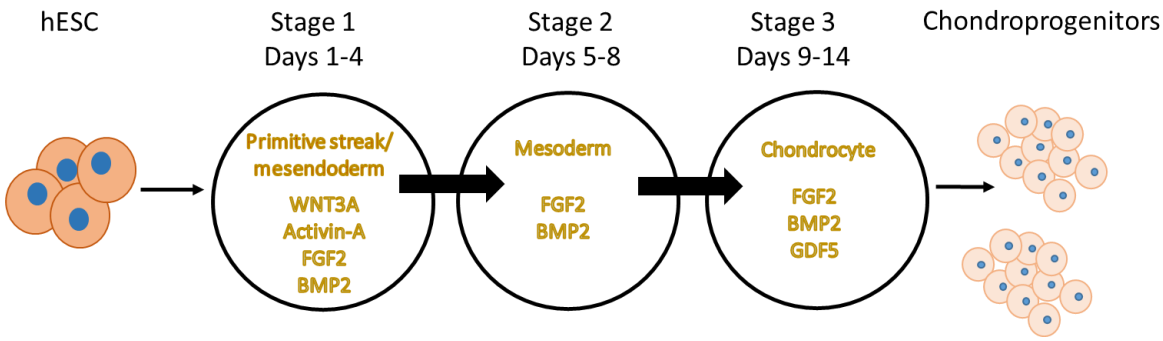

Figure 1-11. A 3-stage, 14-day differentiation protocol to generate hESC-derived chondroprogenitors. hESC are directed though a 14-day differentiation process in which exogenous growth factors are used to mimic the developmental environment experienced *in vivo*. Adapted from Oldershaw et al. 2010.

1.7.2 The role of Wnt in the stem cell niche

The stem cell niche is a microenvironment which provides the biochemical and biophysical cues necessary for the maintenance of properties such as self-renewal and pluripotency (S. J. Morrison and Spradling 2008). As cells migrate away from the niche and its signals, they

begin to differentiate in response to new environmental cues. Wnt proteins, highly conserved across species, are one such group of signalling molecules, with key roles in the self-renewal of numerous mammalian tissues. This family of proteins, with 19 members described to date, are around 350 amino acids long and all share the following key characteristics: multiple cysteine residues, a conserved serine residue for acetylation and lipidation, and a peptide sequence for secretion. Though able to stimulate cells via three different signalling pathways, Wnt influences pluripotency and stem cell renewal through activation of the non-canonical Wnt/ß-catenin pathway upon association with the membrane-bound receptors LRP6 and Frizzled (FZD) (figure 1-12). This triggers an intracellular signalling cascade which results in inhibition of the ß-catenin destruction complex, stabilisation of ß-catenin and its subsequent translocation to the nucleus where it binds to T-cell factor (TCF)/lymphoid enhancer factor (LEF) proteins, which in turn upregulate the transcription of target genes. (Jones and Wagers 2008; Clevers, Loh, and Nusse 2014; Mills, Szczerkowski, and Habib 2017; Zhan, Rindtorff, and Boutros 2017).

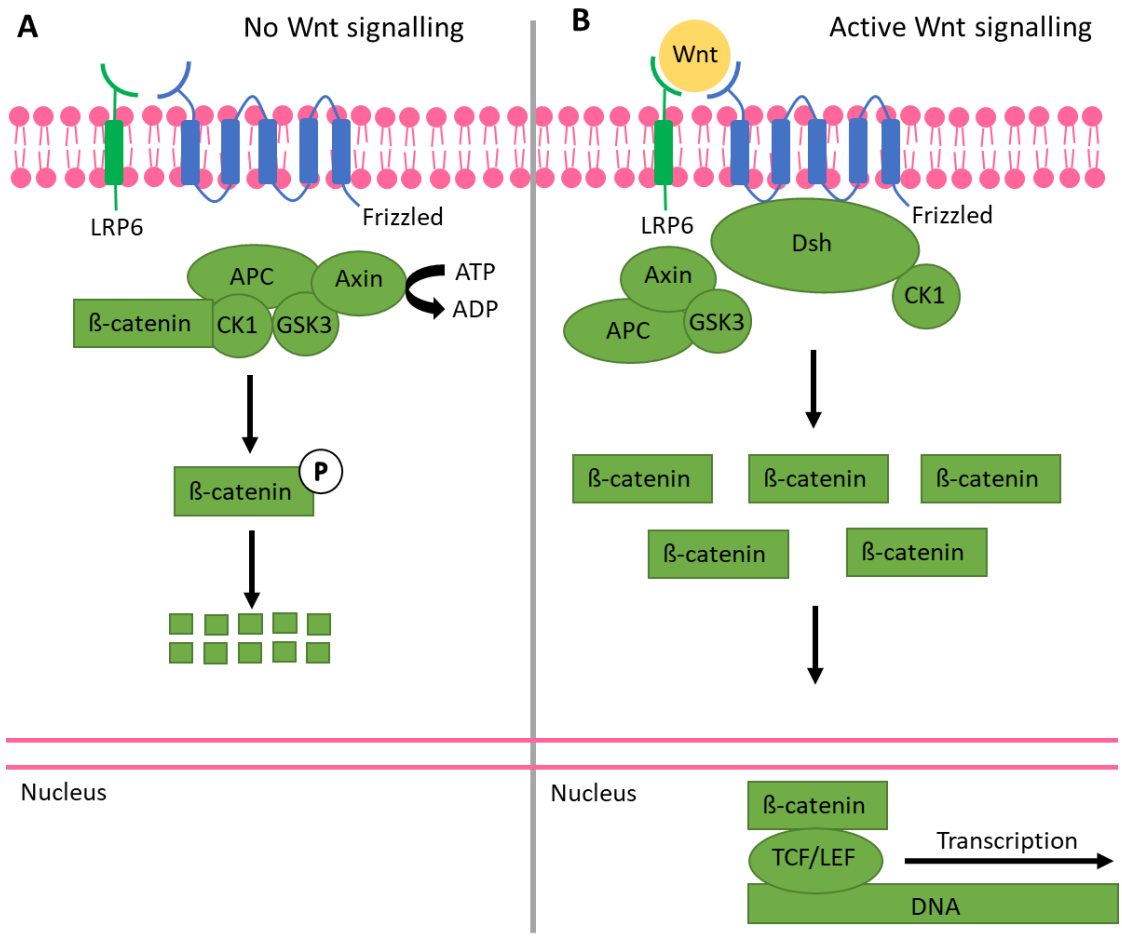

Figure 1-12. Overview of canonical Wnt signalling. A) In the absence of Wnt, ß-catenin is phosphorylated by the ß-catenin destruction complex, which includes adenomatosis polyposis coli (APC), Axin, casein kinase 1 (CK1) and glycogen synthase kinase 3 (GSK3). Phosphorylation targets ß-catenin for proteosomal degradation. B) In active signalling, Wnt ligands bind to Frizzled receptors and low-density lipoprotein receptor-related protein 6 (LRP6) co-receptors. Dsh proteins are recruited to the plasma membrane, where they inactivate the destruction complex. ß-catenin is stabilised and accumulates before translocating to the nucleus where it forms an active complex with TCF/LEF proteins and upregulates the transcription of target genes. (Zhan, Rindtorff, and Boutros 2017).

Wnt signalling has roles in a diverse range of cellular processes, including ESC differentiation, stem cell renewal and cancer progression. Canonical Wnt signalling has been shown to promote pluripotency in a range of stem cell types (Clevers, Loh, and Nusse 2014; Mills, Szczerkowski, and Habib 2017) including murine ESC (mESC) when WNT3A was added daily to the culture medium (ten Berge et al. 2011). However, there is much debate over the apparent dichotomous role of Wnt signalling in maintenance of plasticity/proliferation versus induction of differentiation, and the outcome seems very much dependent on both cell type and host species (Teo and Kahn 2010). In hESC, for example, Wnt activation of the ß-catenin pathway has been shown to lead to the disruption of self-renewal and the subsequent production of posterior primitive streak/mesoderm progenitors (Sumi et al. 2008; Gadue et al. 2006). Similarly, in the directed differentiation protocol (DDP) described by Oldershaw et al. in 2010, global Wnt signalling, via addition of WNT3A to the culture medium on days 1-3, was reported to initiate a shift towards a mesendoderm population and was critical for the subsequent successful production of chondroprogenitors. hESC differ from mESC in both their required culture conditions and their expression of pluripotency markers, with mESC expressing higher levels of *Klf4* and *Rex1* (Sokol 2011). Ethical restrictions mean that hESC are derived at a later developmental stage and it is often argued that they are more akin to mouse epiblast-derived stem cells than true ES cells and, therefore, have a narrower differentiation potential (Nichols and Smith 2011). These differences may account for the differential response of human and murine ESC to global Wnt signalling.

Post-translational fatty acid modification of secreted Wnt proteins by the Porcupine enzyme *in vivo* renders them hydrophobic and limits their movement through tissue fluid –

their effects are consequently short-ranged and can be as little as one- to two-cell diameters. This lipidation is essential in order to maintain the normal signalling activity of WNT3A and is thought to function by increasing local concentrations of the protein on plasma membranes (Willert et al. 2003). Unfortunately, for *in vitro* studies, where WNT3A is added globally to the culture medium (particularly in serum-free conditions), this hydrophobicity presents a barrier to its uniform delivery to cells and may result in the production of a heterogeneous population by the end of the culture period. CHIR99021 is a potent Wnt pathway activator which functions by inhibiting GSK3 in the ß-catenin destruction complex (figure 1-12), resulting in the accumulation of ß-catenin and its translocation to the nucleus in the same way as Wnt-initiated signalling. Soluble in low concentrations of dimethyl sulfoxide (DMSO), this small molecule has been successfully utilised to induce Wnt/ß-catenin signalling in a range of protocols for the differentiation and maintenance of ESC (Lian et al. 2013; W. Li et al. 2011; H. Kim et al. 2013). Replacement of WNT3A with CHIR99021 in Oldershaw et al.'s DDP is a recent modification which has reduced variability in the final cell population (personal communication).

In the stem cell niche Wnt molecules are presented to target cells via carrier proteins for long distance signalling, or on the surface of paracrine cells for close range effects. There is also evidence to suggest that the orientation of the protein is key to its function; association of mESC with immobilised WNT3A was shown to result in accumulation of LRP6 and ß-catenin destruction-complex-associated proteins at the point of contact (Habib et al. 2013). These Wnt-associated cells then underwent asymmetrical division with the axis of mitotic division in line with the bead upon which the Wnt was immobilised. Following cell division, proximal daughter cells retained pluripotency, whereas distal ones showed reduced

expression of pluripotent markers (Habib et al. 2013). In a later study Wnt was immobilised onto aldehyde-coated surfaces, such as glass and poly(caprolactone) (PCL), and cells (both ESC and BMSC) seeded onto these modified materials demonstrated higher levels of Wnt signalling and a concomitant increase in pluripotency/multipotency markers. In addition, BMSC migrating away from the Wnt-modified surface into collagen gels under osteogenic culture conditions, expressed higher levels of bone markers with increasing distance from the base, while those near to the polymer retained multipotency (Lowndes et al. 2016). A published protocol based on this work was utilised for chapter 3 of this study, where a "Wnt Platform" was used to drive the migration of differentiating hESC into fibrin hydrogels (Lowndes, Junyent, and Habib 2017).

1.8 3D models

3D models can support cell differentiation and proliferation to produce superior cartilaginous tissue with enhanced mechanical properties. A range of materials have been utilised as scaffolds for cartilage tissue engineering, including natural and synthetic polymers and polymer blends. These materials are generally used to produce hydrogels, sponges or fibrous meshes, which cells can either be seeded onto or encapsulated within. Scaffold structures which mimic that of the ECM and are robust enough to withstand the application of physical forces are optimal, although compromises are often necessary in order to support cell survival, especially in 3D models with encapsulated cells. Suitable biomaterials should promote cell viability; allow diffusion of nutrients and waste; integrate with the surrounding tissue; provide mechanical integrity; and have controllable degradation rates – rapid degradation can result in impaired mechanical strength, whereas the opposite can impede new cartilage production. (Chung and Burdick 2008). Though a

vast number of studies have produced scaffolds for cartilage tissue engineering from a wide range of materials, with varying structures and formulations (table 1-2 gives some examples from the last 15 years), few have managed to fulfil all of these criteria.

1.8.1 Hydrogels

Hydrogels, formed from natural and synthetic polymers such as alginate or poly(ethylene glycol) (PEG), are insoluble in water and can retain large volumes of liquid, creating a microenvironment for proliferating cells which mimics native tissue by allowing exchange of waste and nutrient molecules. They can also encapsulate cells more homogeneously than other scaffold materials and their viscoelastic mechanical properties more closely resemble those of the native cartilage (Hwang, Varghese, and Elisseeff 2007). In addition, this environment can be designed to release growth factors in a carefully controlled and time-dependent manner. Unfortunately, the hydrophilic nature of hydrogels renders them poor substrates for cell and protein adhesion, thus some groups have incorporated molecules such as RGD-containing peptides, which facilitate integrin binding (Hwang et al. 2006). Despite the well-documented advantages of hydrogel scaffolds, they lack the characteristic mechanical strength of native cartilage. Chemically crosslinking hydrogels via photo-polymerisation or redox polymerisation (as opposed to physically crosslinking them) can produce constructs with greater mechanical integrity. When mESC were cultured on dextran-poly(ethylene glycol) hydrogels, cells remained viable after three weeks and produced cartilaginous tissue. Degradation rates of the hydrogels could be extended from 3 to 7 weeks by changing the level of thiol substitution on the dextran biopolymer (Jukes et al. 2010). A three-layered hydrogel, seeded with murine BMSC, which allows cells to differentiate into “zone-specific chondrocytes”, has also been reported. Designed to mimic

the superficial, transitional and deep zones of articular cartilage, the PEG-based gel was supplemented with CS and metalloproteinase-sensitive peptides on the top layer, CS in the middle and HA on the bottom (Nguyen et al. 2011). An increased gradient of compressive modulus from the top layer to the bottom layer was observed and attributed to increasing levels of collagen X/proteoglycans and decreasing levels of collagen II. However, it is worth noting that the highest measurement recorded for compression modulus (1712 kPa in the "deep zone" of the construct) is still much lower than that of murine and human native articular cartilage (Cao et al. 2006; Shepherd and Seedhom 1999).

1.8.2 Meshes

Meshes are networks of fibres (woven or non-woven) often produced via electrospinning from blends of materials such as poly(lactic acid) (PLA), poly(glycolic acid) (PGA) and poly(lactic-co-glycolic acid) (PLGA). The void volumes (higher for non-woven meshes) and fibre diameter of the meshes can direct cell behaviour and they can be readily made with a range of porosities, degradation rates and mechanical properties. In addition, they offer the distinct advantage of superior mechanical strength compared to hydrogels and sponges. PCL scaffolds have lengthy resorption periods and high tensile/mechanical strengths, which make them good candidates for cartilage tissue engineering; however, their surface properties do not generally support cell attachment and proliferation. One study overcame this by electrospinning PCL concurrently with poly(vinyl alcohol) (PVA) in order to confer hydrophilicity and improved attachment onto the surface. When seeded with BMSC, improved cell proliferation and chondrogenic differentiation was observed *in vitro*, and improved healing of cartilage defects in a rabbit model was reported in addition (Shafiee et al. 2011). In a more recent study, electrospun PCL mats were loaded with TGF-ß1-laden

PLGA microspheres and the entire scaffold was then modified with cold atmospheric plasma in order to overcome the inherent hydrophobicity of the PCL. Improved vitronectin adsorption and subsequent cell attachment was observed, in addition to enhanced cell growth and chondrogenic differentiation of human BMSC (hBMSC) (Zhu et al. 2015). Despite their mechanical superiority and the ease with which their properties can be optimised, meshes are pre-fabricated into structures that are unlikely to be a perfect fit for the lesions they are covering *in vivo*, where reduced contact with the surrounding tissue may limit successful integration of the construct. In contrast, hydrogels can be injected into a defect and will occupy the space completely.

1.8.3 Sponges

Sponge structures can be achieved via salt-leaching, freeze-drying or gas foaming to give a wide range of properties which are determined by the combination of pore size, porosity, inter-connectivity and choice of biomaterial. Salt-leached sponge scaffolds made from a blend of PLGA and PLA and coated with fibronectin have been shown to enhance proliferation and chondrogenic differentiation of hESC compared to monolayer controls (Levenberg et al. 2003). Sponge scaffolds are often made from water-soluble polymers which are freeze-dried prior to the addition of a chemical cross-linker – this can lead to non-homogenous pore sizes and chemical distribution. “Cryogels”, however, are frozen after addition of a cross-linking agent and can yield structures with greater mechanical strength and more uniform pore sizes. A glucosamine-enriched gelatin/hyaluronic acid cryogel was recently developed and showed increased chondrogenic gene expression when seeded with primary chondrocytes and cultured for 21 days. Furthermore, when implanted into a rabbit cartilage defect model, the scaffolds generated neocartilage with increased collagen II and

GAG production compared to acellular controls. Incorporation of glucosamine, however, did lead to a reduction in mechanical strength and faster degradation of the constructs (C.-H. Chen et al. 2016). In another study, human osteoarthritic chondrocytes were seeded onto porous, cross-linked, freeze-dried hyaluronic acid scaffolds for 2 weeks. A significant reduction in cell number was observed, but chondrogenic markers and sulphated GAG (sGAG) increased (Bauer et al. 2016).

HA-based scaffolds are an attractive choice as they mimic the biochemistry of the native ECM more closely than other commonly-used biomaterials. They can be fabricated (often modified, cross-linked and in conjunction with other materials) as hydrogels, woven meshes, non-woven fibres and porous sponges. Rapid degradation rates and poor mechanical stability have limited the use of HA hydrogels so far, but when combined with other biomaterials (see C.-H.Chen et al. 2016 and Bauer et al. 2016 above), outcomes are more promising. hESC-derived chondrocytes were encapsulated in hydrogels composed of thiol-modified HA, thiol-modified gelatin and poly(ethylene glycol) diacrylate (PEGDA) in a 2:2:1 ratio and cultured for up to 4 weeks prior to implantation into a rat osteochondral defect model. Compared to controls, where only fibrous tissue was observed, cartilaginous repair tissue formed in the defect and was well integrated with native ECM, showing significantly higher levels of sGAG and collagen II (Toh et al. 2010). Silk fibroin is a natural polymer which has recently generated interest in the cartilage tissue engineering community. These scaffolds can be fabricated with a diverse range of structures (hydrogels, meshes and sponges), are biocompatible, have low immunogenicity and can be manipulated to give desired mechanical properties and proteolytic degradation. In addition, molecules such as HA, glucosamine and collagen can be incorporated into the structures

with relative ease (G. Cheng et al. 2018). When silk fibroin sponge scaffolds were embedded with mechano growth factor and TGF-ß3 and seeded with hBMSC, increased collagen II/aggrecan production and decreased collagen I production were observed *in vitro* and scaffolds had a compressive modulus similar to that of native cartilage (4.9 MPa compared to 5.5 MPa in rabbit tissue) (Luo et al. 2015). Furthermore, implantation into a rabbit osteochondral defect model resulted in repair tissue with better integration than non-functionalised controls and a more cartilaginous structure.

Table 1-2. Scaffolds used on cartilage tissue engineering.

Biomaterial	Cell type	Scaffold	Reference
Poly(lactic-co-glycolic acid) and poly(lactic acid) (50/50 blend)	Human ESC	Sponge	(Levenberg et al. 2003)
RGD-modified poly(ethylene glycol)	Murine ESC	Hydrogel	(Hwang et al. 2006)
Hyaluronic acid, thiol-modified gelatin and poly(ethylene glycol diacrylate)	Human ESC	Hydrogel	(Toh et al. 2010)
Dextran-poly(ethylene glycol)	Murine ESC	Hydrogel	(Jukes et al. 2010)
Poly(caprolactone) and poly(vinyl alcohol)	Lapine BMSC	Mesh	(Shafiee et al. 2011)
Poly(ethylene glycol) with chondroitin sulphate (CS) and matrix metalloproteinase-sensitive peptides incorporated into the top layer, CS incorporated into the middle layer and hyaluronic acid incorporated in the bottom layer	Murine bone marrow progenitors	Hydrogel	(Nguyen et al. 2011)
Poly(caprolactone) loaded with TGF-ß1-laden PLGA microspheres and then cold atmospheric plasma treated	Human BMSC	Mesh	(Zhu et al. 2015)
Thiol-modified, freeze dried, hyaluronic acid	Human articular chondrocytes	Sponge	(Bauer et al. 2016)
Gelatin/hyaluronic acid with glucosamine incorporated	Lapine articular chondrocytes	Sponge	(C.-H. Chen et al. 2016)
Silk fibroin functionalised with mechano growth factor and transforming growth factor ß3	Human BMSC	Sponge	(Luo et al. 2015)

1.9 Selection of biomaterials

hESC have been cultured in a range of hydrogels in a bid to produce cartilaginous tissue, including agarose (where viability was not always optimal) (Jukes et al. 2008; Diekman et al. 2012) and HA-based gels (S. Zhang et al. 2013; Toh et al. 2010). hESC-derived chondroprogenitors encapsulated in fibrin hydrogels have also been shown to produce repair tissue resembling native cartilage in a rat osteochondral defect model (A. Cheng et al. 2014). As a key component of the coagulation cascade, fibrin has unquestionable biocompatibility and has long been used as a "glue" in a number of surgical procedures. Given its physiological role in natural tissue repair processes, it is unsurprising that fibrin contains a host of cell/growth factor binding motifs and has an architecture which promotes cell infiltration and wound repair (Sproul, Nandi, and Brown 2018). Despite these advantages, fibrin in itself is not chondro-inductive and, in addition, it possesses weak mechanical properties and is prone to shrinkage and rapid degradation *in vitro* (Y. Li et al. 2015). Thus, as a vehicle for cell delivery to an osteochondral defect model, as described above (A. Cheng et al. 2014), the wound healing properties and pro-inflammatory nature of its cleavage products probably contributed to the success of fibrin as the choice of biomaterial. However, for the generation of replacement tissue to treat chronic, degenerative cartilage conditions, which require longer periods in culture, a biomaterial with chondro-inductive properties, superior mechanical strength and a slower rate of degradation would be preferable – though there are few options which meet all of these criteria.

Choice of biomaterial has also been reported to play a role in the cellular response to inflammatory conditions. Given that arthritic joints express high levels of pro-inflammatory

cytokines, such as IL-1ß and TNFα, this is an important consideration which may determine the success of any tissue engineered implant (Tetlow, Adlam, and Woolley 2001). Bovine articular chondrocytes cultured in the presence of IL-1ß and TNFα on either collagen, silk or PLA porous scaffolds demonstrated differential morphology and gene expression, depending on which material they were seeded onto (Kwon et al. 2013). Cells cultured on silk and collagen had a more rounded morphology and higher levels of GAG staining, while only silk scaffolds favoured higher expression of chondrogenic genes and lower expression of degradation-related genes. Thus, although PLA is commonly used in tissue engineering applications, it may not possess the biophysical properties necessary to perform well under inflammatory conditions *in vivo*.

HA-based scaffolds are an attractive choice as they mimic the biochemistry of the native ECM polysaccharides more closely than other commonly-used biomaterials. Unfortunately, they are also subject to rapid degradation rates and poor mechanical stability. For the production of a cartilage-like graft with requisite mechanical strength, it is necessary to combine HA with other biomaterials such as gelatin and PEGDA, as described in chapter 1.8 (Toh et al. 2010), or to form stiffer scaffolds such as freeze-dried sponges (Bauer et al. 2016). For potential injectable cell therapies, however, HA-based gels offer a promising strategy. Numerous studies have demonstrated that this material (generally modified or combined with a crosslinker to enhance its mechanical properties) promotes the viability and metabolic activity of chondrocytes and chondrocyte-like cell lines (H. Park et al. 2013; Yu et al. 2013; G. Wang et al. 2018). HyStem^{TM} is a commercially available hydrogel kit containing thiol-modified HA and a thiol-reactive crosslinker (PEGDA), the concentration of which can be adjusted to control the stiffness of the gel. An alternative version of this kit, containing

an additional component of thiol-modified denatured collagen fibrils (gelatin), was used by Toh et al. (2010) to encapsulate hESC-derived chondrogenic cells. These constructs were implanted into a rat osteochondral defect model and were reported to support long term cell viability and to result in regenerated tissue resembling native cartilage.

Gellan gum, an FDA approved food additive, has recently gained interest as a potential biomaterial for tissue engineering applications. Formed of tetrasaccharide repeating units (D-glucose, D-glucuronic acid, D-glucose and L-rhamnose), this polysaccharide is produced by the aerobic fermentation of *Sphingomonas paucimobilis* (Jansson, Lindberg, and Sandford 1983). It exhibits very low toxicity and only mild processing conditions are required to form a hydrogel, making it an attractive choice as a cell delivery material. The presence of glucuronic acid residues render this material structurally similar to native cartilage GAGs and its carboxylic groups confer a degree of functionality, which may be useful for the incorporation of other bioactive molecules (Oliveira et al. 2010). At elevated temperatures gellan gum forms a solution of disorganised coils, which associate into a strong double helix structure upon cooling to around 42°C. The addition of divalent cations (such as Ca^{2+}) during the gelling process crosslinks the helices by forming direct bridges, thus producing a construct with greater mechanical strength. Monovalent cations such as K^{+} can also crosslink the gel to a lesser extent by binding to the helices and balancing the repulsive negative forces of the carboxyl groups (Jansson, Lindberg, and Sandford 1983; Smith et al. 2007). Different temperature- and pH-dependent methods have been employed to produce a range of structures from gellan gum, including discs, membranes, fibres, particles and scaffolds (Oliveira et al. 2010). Numerous studies report good viability of cells encapsulated in hydrogels including human nasal chondrocytes (Oliveira et al. 2010), rat BMSC (Smith et

al. 2007) and porcine articular chondrocytes (Y. Gong et al. 2009). Compared to fibrin and agarose controls, gellan gum hydrogels seeded with porcine infrapatellar fad pad progenitors showed enhanced cell proliferation, elevated levels of sGAG and increased COL2 staining (although there was a concomitant increase in collagen type I protein (COL1), which may be indicative of a fibrocartilage phenotype) (Ahearne and Kelly 2013).

Incorporation of chondro-inductive biomaterials, either as a substrate for coating tissue culture plastic/cells or dissolved into the culture medium, is another potential means of enhancing the maturation of stem cell-derived chondroprogenitors. Biomimetic molecules, which mimic the structure of ECM components, have been used by a number of groups. Hydroxyl groups of alginates were replaced with sulphates by incubation with sulphur trioxide pyridine (SO_3/pyridine) in order to produce biomolecules which mimic the proteoglycans of native cartilage tissue (Mhanna et al. 2014). These sulphated alginates were cross-linked with calcium chloride to form a gel wherein bovine chondrocytes were encapsulated. Compared with non-sulphated controls, cell proliferation was significantly increased, although no change in expression of chondrogenic markers was observed. Another group reported that the same hydrogel enhanced proliferation of bovine chondrocytes by mediating fibroblast growth factor 2 (FGF2) signalling, much like heparan sulphate does *in vivo*; they also reported better retention of FGF2 in the constructs and increased cell spreading in response to increase levels of sulphation, which is indicative of improved adhesion to the biomaterial (Öztürk et al. 2016). These sulphated alginates have also been used in conjunction with collagen to create a layered substrate for the 2D culture of human adipose-derived stromal cells (hADSC), which was reported to result in improved binding of FGF2 and maintenance of multipotency (Mhanna et al. 2017).

Significant increases in *COL2A1* and *ACAN* gene expressions in human articular chondrocytes have been reported as a result of pre-coating tissue culture plastic (TCP) with ECM molecules such as decorin, HA, osteopontin and biglycan. Pre-culture on COL2-coated surfaces followed by high density pellet culture for 14 days results in tissue with superior matrix deposition as evidenced by safranin-O and COL2 staining (Grogan et al. 2014). A number of groups have reported the fabrication of biomimetic proteoglycans with increased resistance to proteolytic cleavage, which could be utilised in a similar way, although these have yet to be tested on cells (Prudnikova et al. 2017; S. Sharma et al. 2013). Finally, another option is to coat the cells themselves in a layer of ECM/biomimetic molecules in order to create a chondro-inductive microenvironment. Such methods have been adopted for other target tissues, the pancreas for example, where islet cells were micro-encapsulated in alginate in order to create a barrier which sequestered them from the immune system but still allowed for the transport of small molecules such as insulin, thus reducing the potential for an adverse immune response brought on by allogeneic material (Roshanbinfar and Salahshour Kordestani 2013). Micro-encapsulation in alginate has also been demonstrated for adipose- and bone marrow-derived stromal cells in a bid to create a protected micro-environment, which enhances viability for potential injectable cell therapies (Leslie et al. 2017). The substitution with or addition of chondro-inductive molecules to this micro-environment could yield higher quality chondroprogenitors compared to the basic directed differentiation protocol described by Oldershaw et al.

1.10 Mechanical stimulation

Articular cartilage is subject to cyclic compressive forces. Chondrocytes, like other cells types, possess integrins which enable the transduction of mechanical stimuli. In addition, it

has been shown that cartilage deformation leads to cell deformation, which may be another means of signal transduction. Matrix deformation, hydrostatic pressure gradients, fluid flow, streaming potentials and currents, and physicochemical changes all occur as a result of compression – given that cartilage is an avascular tissue, fluid flow is especially important for nutrient and waste transport (Guilak, Ratcliffe, and Mow 1995; Guilak et al. 1999; Grodzinsky et al. 2000).

1.10.1 Effects of biomechanical forces on natural cartilage development

It is widely accepted that biomechanical stresses and strains play a major role in the natural development, maintenance and degradation of cartilage. As early as the 1930s it was demonstrated that extrinsic mechanical forces affected the progression of skeletogenesis (Murray and Selby 1930; Nowlan, Sharpe, et al. 2010; Foster et al. 2015). Since then much work has been done to investigate the effects of immobilisation on joint development in chick embryos and other animal models such as mice and rats. The effects of mechanical stimuli on adult cartilage have been widely investigated and found to be important in maintenance of the tissue; however, given that tissue engineering approaches aim to develop functional constructs from stem or progenitor cell populations, it follows that elucidation of the effects of loading during embryogenesis may provide more useful insights.

Immobilisation has been shown to have detrimental effects on joint development, particularly in that it prevents formation of the cavity (figure 1-13) (Nowlan, Sharpe, et al. 2010). Further studies have demonstrated that lack of muscle contractions during chick embryogenesis prevent cavitation of articular joints such as the hip, knee and ankle and result in reduced cartilage volume (Ruano-Gil, Nardi-Vilardaga, and Tejedo-Mateu 1978;

Osborne et al. 2002). Supporting these findings, immobilisation after cavity formation was shown to resulted in a cavity that was not fully maintained (Mitrovic 1982) and increased movement was correlated to development of a wider cavity (Ruano-Gil, Nardi-Vilardaga, and Teixidor-Johé 1985). Mikic et al. immobilised chick embryos from 6 days so that limb development proceeded without mechanical loading. Compared to controls, samples taken from the upper and lower regions of the cartilage cones of immobilised chicks had a 50% reduced instantaneous modulus and significantly lower levels of proteoglycans and collagen (Mikic, Isenstein, and Chhabra 2004). Nowlan et al. measured the levels of stress, strain, hydrostatic pressure and fluid velocity at the mid-diaphyses of the long bones of developing chick embryos and used optical projection tomography to obtain 3D images of the developing limbs. They found that the highest mechanical forces were experienced shortly before formation of the bone collar, suggesting that high cycles of stimulus in the cartilage promote ossification (Nowlan, Murphy, and Prendergast 2008).

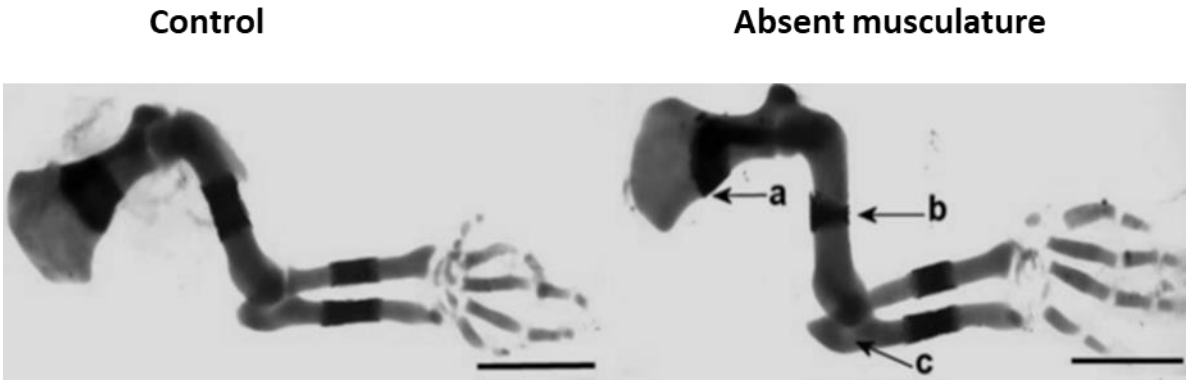

Figure 1-13. Effects of absent musculature on murine forelimb development. Mouse without muscle has reduced bone mass in the scapular blade (a), abnormal humeral

ossification centre (b) and non-cavitation of the elbow joint (c). Image adapted from Nowlan et al. 2010.

In mouse models immobilisation adversely affects the development of some joints but not others. For example, Nowlan et al. reported that mice with a reduced muscle phenotype demonstrated a substantial reduction in the joint line of the elbow, whereas no abnormalities were observed in the knee (Nowlan, Bourdon, et al. 2010). Kahn et al. looked at joint formation in muscleless and paralysed mouse embryos and noted the emergence of an interzone in the elbow joint with distinct cartilaginous regions, despite the lack of muscle contraction (Kahn et al. 2009). After this point, however, the joint failed to form and cells taken from the region did not express chondrogenic markers, suggesting that absence of mechanical stimuli results in the failure of progenitor cells to differentiate into chondrocytes. Thus, immobilisation appears to have a more pervasive effect on chick skeletogenesis than on that of mice. This may be accounted for by the contrasting mechanical environment that the two types of embryo are exposed to; the developing mouse (much like the human) experiences larger external forces which result from the natural movement of the mother and its littermates. Nowlan et al. later reported that these external stimuli induce larger forces in the hindlimb than the forelimb, which may explain why elbow joints are more adversely affected by lack of muscle contraction (Nowlan et al. 2012). The mouse model, therefore, is probably a more reliable one to adopt when attempting to gain insight into the effects of mechanical stimuli on human joint development.

1.10.2 Culturing cartilage constructs in a dynamic environment

Hydrostatic pressure (HP), direct compression and high- and low-shear fluid environments are the main types of force adopted in cartilage tissue engineering in an attempt to mimic the native environment of the tissue (Pörtner et al. 2005). A range of bioreactors have been designed to impart these forces including spinner flasks, rotating wall vessel bioreactors, perfusion bioreactors and concentric cylinder bioreactors. Turbulence during seeding and culture of bovine chondrocytes on PGA mesh discs was shown to result in cartilage-like constructs with significant increases in GAG, total collagen and equilibrium modulus, though these parameters were still much lower than those typical of the native tissue (Vunjak-Novakovic et al. 1996; Vunjak-Novakovic et al. 1999). Dynamic unconfined compression of chondrocytes on agarose discs resulted in a 6-fold increase in equilibrium modulus, which was approaching that of human articular cartilage, and a significant increase in GAG production (Mauck et al. 2000). Culture of hESC-derived mesenchymal stroma cells in perfusion bioreactors with a flow rate of 1 mL/minute has been shown to result in constructs with improved ECM production and enhanced mechanical properties (Tiğli et al. 2011). A range of studies have demonstrated that application of HP, the most-commonly adopted force, offers similar benefits (Takahashi et al. 1998; Carver and Heath 1999; Hu and Athanasiou 2006; Correia et al. 2012). Thus, it can be seen that a dynamic environment favours the *in vitro* production of *de novo* cartilage.

1.10.3 The role of hydrostatic pressure in cartilage development

As well as helping to maintain the adult tissue, mechanical stimuli contribute to embryogenesis and early cartilage formation. In pre-cartilaginous stages, the absence of gravity has been shown to reduce mesenchymal condensation in the limb buds of mouse

models (Duke and Montufar-Solis 1999). The exact mechanism of pre-cartilaginous condensation has yet to be elucidated, but the differential adhesion hypothesis predicts that cell-cell adhesion of mesenchymal progenitors is an important early step in the process (Responte et al. 2012). The strength of cell-cell adhesion has been shown to correlate to cell surface tensions in murine models (Foty and Steinberg 2005) and was inhibited by disruption of surface tension in zebra fish cells (Krieg et al. 2008). Thus, condensation may be initiated by cells possessing specific surface tensions; a parameter which can be influenced by mechanical forces such as HP.

Once cartilage has developed, these mechanical forces are converted into HP in the interstitial fluid, followed by shear stress as a result of fluid flow. It is difficult to accurately measure the effects of HP on cartilage development *in vivo*, but a number of studies have looked at the effects of mechanical loading on cartilage explants and found it to be important in balancing ECM turnover by stimulating cells and transporting large soluble molecules into and out of the tissue (Chan, Ferguson, and Gantenbein-Ritter 2011). Studies on human and animal intervertebral disc tissue have shown that physiological levels of HP (0.3 - 3 MPa) increase PG synthesis and metabolism and generally have an anabolic effect, whereas higher levels (3-10 MPa) inhibit PG production and have a catabolic effect (Handa et al. 1997; Ishihara et al. 1996). Continuous pressure, however, has been shown to produce no stimulatory effects at physiological levels; at low levels, comparable to atmospheric pressure, it may actually have a catabolic effect similar to that produced by excessive loading (Handa et al. 1997).

1.10.4 Hydrostatic pressure in cartilage tissue engineering

In vivo cartilage is subject to rapid cyclic loading of 3-10 MPa (up to 18 MPa in the hip) and human walking cadence is around 1 Hz (B. D. Elder and Athanasiou 2009). Thus, tissue engineering approaches tend to apply forces in this range – above this, detrimental effects (similar to the onset of osteoarthritis) have been observed (Kunitomo et al. 2009; Natoli and Athanasiou 2008). Cartilage tissue has been shown to respond to HP, but the nature of this response varies depending on the culture conditions and whether or not a scaffold is employed. For example, in 1993 Parkkinen et al. demonstrated that cyclic HP stimulated sulphate incorporation into bovine cartilage explants, but an identical regime inhibited it in primary chondrocytes cultured in monolayer (Parkkinen et al. 1993). Since then a number of other studies have reported similar variation. Elder et al. found that porcine chondrocytes cultured as pellets responded positively to 4 MPa of cyclic HP, whereas those cultured in alginate hydrogels did not (S. H. Elder et al. 2006). Although culture in hydrogels has been shown to promote chondrocyte differentiation, it does not favour direct cell-cell signalling, which may account for these results. Hydrogels, however, do offer the advantages of better hydration and nutrient exchange compared to pellets, and their softer structure allows their shape to be manipulated in order to fill cartilage defects. For these reasons, pellet culture was not considered for use in the current study.

There is a wealth of evidence to suggest that HP in the physiological range improves chondrogenesis in 3D cartilage constructs (table 1-3). Generally, cyclic HP with a force of 4-10 MPa, applied intermittently to 3D models at a frequency of around 1 Hz, has been shown to increase levels of total collagen (Hu and Athanasiou 2006; Meyer et al. 2011; Carroll, Buckley, and Kelly 2014), COL2 (Reza and Nicoll 2008; Correia et al. 2012) and GAG (Hu and

Athanasiou 2006; Sakao et al. 2008; Meyer et al. 2011; Correia et al. 2012; Carroll, Buckley, and Kelly 2014) deposition in the new tissue. Expressions of *SOX9*, *COL2A1* and *ACAN* mRNAs and GAG were also enhanced, providing further evidence that cells cultured in these conditions were differentiating towards a chondrogenic lineage (Sakao et al. 2008; Ogawa et al. 2009; Correia et al. 2012). A number of recent studies have found HP to have a positive effect on progenitors and chondrocytes cultured as pellets (Miyanishi et al. 2006; Safshekan et al. 2012; Vinardell et al. 2012). Miyanishi et al. found that 10 MPa of cyclic HP applied intermittently for 14 days enhanced expression chondrogenic markers even without the addition of growth factors such as TGF-β3; the combination of mechanical and chemical stimulation had an even greater impact. Safshekan et al. reported that human adipose-derived stem cells cultured as pellets with 5 MPa of cyclic HP expressed levels of *SOX9*, *COL2A1* and *ACAN* comparable to those expressed by native human cartilage tissue (though they did not attempt to quantify protein production). Though the results of these studies are promising, pellet culture does not offer the flexibility to create constructs with the desired morphologies and mechanical properties permitted by scaffolds such as hydrogels or meshes.

Table 1-3. Effects of hydrostatic pressure (HP) on 3D chondrogenic models

Cells and scaffold	HP parameters	Results	Reference
Self-assembled cartilage constructs	10 MPa IHP, 1 Hz, 4 hrs/day, 5 days/week for up to 8 weeks	Increased collagen and maintained GAG levels.	(Hu and Athanasiou 2006)
Porcine BMSC-derived chondrocytes suspended in agarose gel (2 donors)	10 MPa cyclic HP, 1 Hz, 1hr/day, 5 days/week for 42 or 21 days	Increased collagen and GAG content and dynamic modulus for one donor only.	(Meyer et al. 2011)
Porcine BMSC and infrapatellar fat pad derived multipotent stromal cells in agarose hydrogels	10 MPa cyclic HP at 1 Hz. 4 hr/day, 5 days/week for 5 weeks	Decreased metabolic activity, indicating decreased viability in both loaded and control samples.	(Carroll, Buckley, and Kelly 2014)
hASC on 2% agarose hydrogels	7.5 MPa cyclic HP, 4 h/day, 1 Hz for up to 21 days (no GFs)	hASC-chondrocytes: 5 MPa gave more GAG and COL2, lowest COL1 and highest *ACAN* gene expression. 0.4 MPa gave no significant changes.	(Puetzer et al. 2013)
Bovine IVD cells on PGA-PLLA fibrous scaffolds	5 MPa, 0.5 Hz, 4hrs/day from days 3-14.	Increased COL2 levels with more uniform distribution at day 14.	(Reza and Nicoll 2008)
Porcine chondrocytes in alginate beads or pellets	4 MPa cyclic HP, 1 Hz, 5400 cycles/ day for 7 days	Pellets exhibited classical anabolic response to dynamic HP, but alginate did not. Pellets had greater GAG content, higher rate of proline incorporation and more fibrous ECM.	(S. H. Elder et al. 2006)
Rabbit synovium-derived progenitor cells in alginate beads	1.0 to 5.0 MPa IHP, 0.5 Hz	5.0 MPa of IHP gave increased mRNA expression of PG, collagen II and *SOX9* and increased production of SOX9 protein and GAG.	(Sakao et al. 2008)
Human nasal chondrocytes in gellan gum hydrogels	0.4 MPa pulsatile HP 0.1 Hz, 3 hrs/day, 5 days/week for up to three weeks	Greater GAG and COL2 deposition and greater expression of *COL2* and *SOX9* genes.	(Correia et al. 2012)
hASC on porous collagen sponges	0-0.5 MPa cyclic HP, 0.5 Hz for one week	Increased expression of *COL2A1*, *ACAN* and *SOX9*. Higher rate of ECM accumulation and maintained cell number.	(Ogawa et al. 2009)

A major obstacle for cartilage tissue engineering is creating constructs with mechanical properties sufficient to withstand both the transplantation procedure and the relentlessly high forces experienced *in vivo*. Surprisingly few studies report on the mechanical properties of their constructs, but for those that do it is clear that culture without mechanical stimulation is unlikely to produce a construct that has the structure and strength to function as a suitable replacement for damaged cartilage. Bovine articular chondrocytes cultured for 6 weeks on PGA mesh discs in mixed conditions produced tissue with an equilibrium modulus, hydraulic permeability and dynamic stiffness significantly lower than native tissue (Vunjak-Novakovic et al. 1999). Snyder et al. recently cultured bone marrow-derived hBMSC on reinforced fibrin hydrogels in static conditions and, though the compressive modulus of the constructs was significantly higher than controls at 6.76 kPa, this is still around an order of magnitude below that of native human articular cartilage (Snyder et al. 2014). Other studies have achieved enhanced dynamic stiffness (up to 85 kPa) (Kopesky et al. 2010) and compressive modulus (up to 72 kPa) (Tiğli et al. 2011) on 3D scaffolds without mechanical stimulation, but the addition of HP has been shown to produce tissue with properties closer to those of native adult tissue. Carrol et al. reported that infrapatellar fat pat-derived stromal progenitors cultured on agarose hydrogels with 10 MPa cyclic HP for 5 weeks had a dynamic modulus of around 525 kPa (Carroll, Buckley, and Kelly 2014), which is again much higher than that reported by some of the earlier studies mentioned above. DuRaine et al. reported that leporine chondrocytes cultured to form scaffold-free self-assembled neocartilage with 10 MPa static HP for 1 hour per day produced tissue with a suture pull-out strength 33% that of native tissue (1.45 MPa) and an aggregate modulus of 90.4 kPa, which is around 35% that of human articular cartilage (DuRaine et al. 2015). These constructs were successfully transplanted into osteochondral

patellar defects of rabbits and left for three weeks. The animals were able to walk normally and when observed after sacrifice, though there were no signs of engraftment, the implants retained their cartilaginous properties. For just 42 days of culture this is impressive, though it would be interesting to see if the implants remained functional for a longer period and whether cyclic HP, which more closely mimics the natural environment, would have improved the mechanical properties even further.

1.10.5 Four-point bending bioreactor

As mentioned above, cartilage is subject to cyclic compressive forces which generate fluid flow and bring about matrix deformation, both of which impart mechanical signals to chondrocytes. For this reason, dynamic compressive forces are frequently applied as a means of enhancing the quality of tissue engineered cartilage constructs. These loads are detected by cell-surface mechano-sensitive ion channels, integrins and primary cilia, which initiate intracellular signalling cascades and orchestrate the cell's response to external cues (Musumeci 2016). Transient receptor potential vanilloid 4 (TRPV4) is a Ca^{2+}-permeable ion channel which was identified as a regulator of chondrogenic differentiation over 10 years ago, with similar expression patterns to other common markers such as *COL2A1* and *ACAN* (Muramatsu et al. 2007). Its activation in response to cyclic mechanical loading has been shown to result in enhanced matrix deposition (O'Conor et al. 2014). More recently, Piezo1 and Piezo2 were identified as fast-acting mechanosensitive ion channels, which are abundant in chondrocytes and allow rapid influx of Ca^{2+} in response to high levels of strain (Lee et al. 2014). Stimulation of trans-membrane integrins directly affects cytoskeletal actin organisation, again initiating signalling cascades. α1ß1, α10ß1, αvß5 and α5ß1 integrins have all been implicated in the response of chondrocytes to mechanical stimuli (Gilbert and

Blain 2018). Matrilin 1, abundant in developing tissue, has a key role in mediating mechanical stimuli and its presence was shown to be necessary in order for chondrocytes to elicit an anabolic response to loading regimes *in vitro* (Chen et al. 2016). Growth factors such as FGF2 are also released by chondrocytes in response to cyclic compression; perlecan-bound FGF2 is released as a result of turbulence and goes on to initiate mitogen-activated protein kinase (MAPK) signalling (Vincent et al. 2007).

Peake et al. used a four-point bending model to investigate the response of human osteoblast-like cells and the MG63 bone cell line to mechanical load in monolayer culture (M. A. Peake et al. 2000). They reported an up-regulation of Fos proto-oncogene, AP-1 transcription factor subunit (*FOS*), which could be blocked by the addition of ß1-integrin antibodies or inhibitors of stretch-activated ion channels, suggesting that the response was both mediated by surface integrins and a direct result of mechanical loading. The four-point bending bioreactor used in this work (chapter 2, figure 2-1) was designed to transmit tensile forces to cells cultured on glass slides, in a bid to recapitulate the microenvironment of osteoblasts *in vivo*. When this 4PBB system was developed, the maximum theoretical strain that could be applied to the glass coverslip was calculated using the standard beam deflection equation for four-point bending (below), where E = strain, t = coverslip thickness, L = distance between two outer loading parts, d = deflection and a = distance between two inner loading parts (M. Peake 2001).

$$E = td/a(L - 1.33a)$$

From this, it was determined that the uniaxial strain imparted to cells seeded onto the central 30 mm region of coverslips with a thickness of 0.22 mm was around 1000 microstrains (µE). This exceeded the minimum strain previously reported to induce new

bone formation *in vitro* (Thomas and el Haj 1996) and was comparable to the strains experienced by bone *in vivo* (Burr et al. 1996). In the current study, however, the model was adapted to impart compressive forces to chondroprogenitors by simply inverting the glass slide when cells were loaded into the chamber. When tension is applied to a surface, an equal compressive force is imparted to the opposite side; thus a compressive strain of around 1000 µE will be experienced by cells seeded onto this surface. Strains experienced *in vivo* by cartilage are reported to be around 2000 µE, even in low load-bearing regions such as the temporomandibular joints of rabbits (Kruse-Lösler et al. 2001). Therefore, it is likely that articular cartilage, in areas such as the knee, is exposed to much higher strains. Nevertheless, the loads applied by the 4PBB are at least approaching the physiological range and it was hoped that this model would provide insight into the short-term responses of hESC-derived chondroprogenitors to low levels of mechanical loading.

A number of studies have investigated the effects of mechanical stimulation on chondrocytes cultured in monolayer. Das et al. reported that application of cyclic strain lead to a modest increase in *ACAN* and lubricin expression in primary human chondrocytes, but a drastic reduction of chondrogenic markers in expanded chondrocytes (Das et al. 2008). A more recent study demonstrated that primary human chondrocytes responded to a similar (though more prolonged) regime of cyclic tensile strain with altered morphology, reduced elastic modulus and impaired chondrogenic matrix deposition (Liu et al. 2016). These findings indicate that monolayer chondrocytes do not respond well to mechanical stimulation. However, both of these studies utilised the commercially-available Flexcell® system which, although comparable to the 4PBB when used in tension, does not allow for

the application of compressive forces. Indeed, all other systems designed to impart compressive forces, require cells to be encapsulated in biomaterials.

1.11 Summary and hypotheses

The high incidence of OA, combined with the poor healing capacity of the tissue and the limited efficacy of current gold standard treatments render articular cartilage an obvious target for tissue engineered strategies and cell-based therapies. Human embryonic stem cells offer a potentially limitless source of cells and their successful differentiation into chondroprogenitors *in vitro* has been demonstrated; all of which makes them a much more appealing choice in comparison to the other cell types commonly utilised for this application. However, in order for them to be deemed safe for clinical use, the presence of pluripotent cells must be completely ablated and a more mature chondrogenic phenotype is desirable. In addition, it is preferable for cells to be housed in suitable biomaterials for their safe and effective application to defect sites, either as a tissue engineered scaffold or an injectable cell therapy.

The aim of this study is to develop several strategies which improve the maturation of hESC-derived chondroprogenitors in 2D and 3D culture environments. Three key hypotheses were tested:

- Application of an immobilised Wnt platform encourages the proliferation of differentiating cells and their subsequent migration into hydrogels in order to create a 3D construct with a more homogeneous population of chondroprogenitors
- Incubation of chondroprogenitors with biochemically relevant ECM molecules produces a more mature phenotype

- Application of mechanical forces, which mimic those experienced by chondrocytes *in vivo*, results in a more mature phenotype and enhance matrix deposition *in vitro*

Chapter 2

Materials and Methods

2.1 Materials

Unless stated otherwise, materials were obtained from their manufacturers or from a distributor within the United Kingdom.

Table 2-1. List of reagents, catalogue numbers and suppliers.

	Catalogue number	**Supplier**
1-Bromo-3-chloropropane (BCP)	B9673-200ML	Sigma-Aldrich, Inc.
2-Mercaptoethanol	M3148	Sigma-Aldrich, Inc.
2-Mercaptoethanol (50 mM) (Gibco™)	31350010	Fisher Scientific UK Ltd
2-Propanol	I9516	Sigma-Aldrich, Inc.
Acetone, for HPLC	10131560	Fisher Scientific UK Ltd
Activin A (human)	Qk001_ActA	Qkine Ltd.
Activin A (human)	120-14	PeproTech, Inc.
Agarose	BP1356-500	Fisher Scientific UK Ltd
AlamarBlue™ (Molecular Probes™)	10161053	Fisher Scientific UK Ltd
Ammonium acetate	A2706	Sigma-Aldrich, Inc.
Anti-Fibronectin antibody [F1]	ab32419	Abcam plc.
Anti-laminin antibody	ab11575	Abcam plc.
Anti-Nanog antibody	4903	New England Biolabs Ltd
Anti-SOX5 antibody - ChIP Grade	ab94396	Abcam plc.
Anti-SOX9 antibody [3C10]	ab76997	Abcam plc.
Anti-Vitronectin antibody [EP873Y]	ab45139	Abcam plc.
Aprotinin from bovine lung	A3428-10MG	Sigma-Aldrich, Inc.
B-27® Supplement	17504044	Fisher Scientific UK Ltd
BMP-2 (human)	120-02	PeproTech, Inc.
Bovine serum albumin (BSA)	BP9703-100	Fisher Scientific UK Ltd
Calcium chloride	793639	Sigma-Aldrich, Inc.

CHAPS hydrate	C3023-1G	Sigma-Aldrich, Inc.
CHIR99021 WNT pathway activator	72052	STEMCELL Technologies Inc.
Chloroform	C2432	Sigma-Aldrich, Inc.
Chondroitin sulphate	C9819	Sigma-Aldrich, Inc.
Collagen Type II monoclonal antibody	CIIC1	Developmental Studies Hybridoma Bank
Collagen type VI	Ab7538	Abcam plc.
Dekalb White eggs	N/A	Henry Stewart and Co. Limited
Dimethyl methylene blue (DMMB)	341088	Sigma-Aldrich, Inc.
Dimethyl sulfoxide (DMSO)	D5879	Sigma-Aldrich, Inc.
DL-Dithiothreitol (DTT)	D0632	Sigma-Aldrich, Inc.
DMEM/F-12, HEPES (Gibco™)	31330038	Fisher Scientific UK Ltd
DNA AWAY™	10223471	Fisher Scientific UK Ltd
DPX mounting medium	44581	Sigma-Aldrich, Inc.
Dulbecco's phosphate buffered saline without calcium and magnesium (Gibco™) (DPBS)	14190144	Fisher Scientific UK Ltd
EDTA (0.5 M), pH 8.0 (Invitrogen™)	AM9260G	Fisher Scientific UK Ltd
Eosin Y solution, alcoholic	HT110116	Sigma-Aldrich, Inc.
Essential 8 Medium (Gibco™) (E8)	15190617	Fisher Scientific UK Ltd
Ethanol (absolute)	E0650/17	Fisher Scientific UK Ltd
Ethidium bromide	E1510	Sigma-Aldrich, Inc.
FGF2 (Gibco™)	10202733	Fisher Scientific UK Ltd
FGF2 (Qkine)	Qk025_hFGF2	Qkine Ltd.
Fibrinogen	F3879-250MG	Sigma-Aldrich, Inc.
Fibronectin (human plasma)	FC010	EMD Millipore Corporation
Foetal Bovine Serum (FBS)	FB-1001	Biosera Europe
GDF-5 (human)	120-01	PeproTech, Inc.
Gel loading buffer	G2526	Sigma-Aldrich, Inc.

GeneRuler 50 bp DNA Ladder	SM0373	Fisher Scientific UK Ltd
Gluteraldehyde solution	G7776	Sigma-Aldrich, Inc.
Glycine	50046	Sigma-Aldrich, Inc.
Goat Anti-Mouse IgG H&L (Alexa Fluor® 488)	ab150113	Abcam plc.
Goat Anti-Rabbit IgG FITC	10006588	Bertin Bioreagent
Haematoxylin (Gill's Number 2)	GHS216	Sigma-Aldrich, Inc.
HEPES buffer solution	83264	Sigma-Aldrich, Inc.
Hexamethylenediamine	H11696	Sigma-Aldrich, Inc.
High Capacity cDNA Reverse Transcription Kit	4368814	Fisher Scientific UK Ltd
Histo-Clear (National Diagnostics)	NAT1330	Scientific Laboratory Supplies Limited
Histo-Clear HS200	H005	Scientific Laboratory Supplies Limited
Hydrochloric Acid (5M)	10605882	Fisher Scientific UK Ltd
HyStem™ Cell Culture Scaffold Kit	HYS010-1KT	Sigma-Aldrich, Inc.
IMS	I99050	Genta Environmental Ltd.
Insulin-Transferrin-Selenium-Sodium Pyruvate (ITS) (100X)	51300044	Fisher Scientific UK Ltd
Laminin	L2020-1MG	Sigma-Aldrich, Inc.
L-Glutamine (200 mM) (Gibco™)	25030024	Fisher Scientific UK Ltd
Live/Dead viability kit (Quant-iT™)	L3224	Fisher Scientific UK Ltd
Magnesium sulphate	M5921	Sigma-Aldrich, Inc.
Neutral buffered formalin	F5304	Sigma-Aldrich, Inc.
Non-Essential Amino Acids (100X) (Gibco™) (NEAA)	11140035	Fisher Scientific UK Ltd
Paraffin	GWAX010	Genta Environmental Ltd.
Penicillin-Streptomycin	15140122	Fisher Scientific UK Ltd
Phytagel™	P8169-100G	Sigma-Aldrich, Inc.

PicoGreen™ dsDNA Assay Kit (Quant-iT™)	P11496	Fisher Scientific UK Ltd
Poly(ethylene glycol) diacrylate (Alfa Aesar)	46497.MD	Fisher Scientific UK Ltd
Polycaprolactone	440744	Sigma-Aldrich, Inc.
Primocin	ant-pm-1	InvivoGen
ProFreeze (Lonza)	LZ12-769E	Scientific Laboratory Supplies Limited
Proteinase K (Invitrogen™)	25530015	Fisher Scientific UK Ltd
PureLink RNA Micro Scale Kit	12183016	Fisher Scientific UK Ltd
Purified Mouse Anti-Oct-3/4	611202	BD Biosciences
QuantiTect Primer Assays: ACAN COL2A1 COL1A1 COL10A1 GAPDH1 OCT4 NANOG RUNX2 SOX9 TRPV4	QT00001365 QT00049518 QT00037793 QT00096348 QT00079247 QT00210840 QT01025850 QT00020517 QT00001498 QT00077217	Qiagen
RNase-Free DNase Set	79254	Qiagen
RNeasy Mini Kit	74106	Qiagen
ROCK Inhibitor (ATCC® ACS-3030™)	Y27632	LGC Standards
Safranin-O	S2255-25G	Sigma-Aldrich, Inc.
Sodium bicarbonate	S5761	Sigma-Aldrich, Inc.
Sodium chloride	S7653	Sigma-Aldrich, Inc.
SYBR® Green PCR Master Mix	4309155	Fisher Scientific UK Ltd
TeSR™-E8™ Kit (E8)	5940	STEMCELL Technologies Inc.
Thrombin from human plasma	T4393-100UN	Sigma-Aldrich, Inc.
TRI Reagent	93289-100ML	Sigma-Aldrich, Inc.

Triton™ X-100	T8787	Sigma-Aldrich, Inc.
Tween® 20	P1379	Sigma-Aldrich, Inc.
Vitronectin (human)	A14700	Fisher Scientific UK Ltd
WNT3A protein (murine) (WNT3A)	1324-WN-10	R&D Systems, Inc.
α-modified Eagle's medium (α-MEM) (Lonza)	LZBE12-169F	Scientific Laboratory Supplies Limited

Table 2-2. List of equipment and suppliers/manufacturers.

AriaMx Tube Strips 8	401493	Agilent Technologies, Inc.
Mx3000P Optical Strip Caps 8	401425	Agilent Technologies, Inc.
Polypropylene pestle	Z359947-100EA	Sigma-Aldrich, Inc.
Biopsy punch (8 mm) (Kai)	BP-80F	Amazon.co.uk
Pestle	13236679	Fisher Scientific UK Ltd
Circular coverslips (10 mm diameter)	MIC3300	Scientific Laboratory Supplies Limited
Hanging cell culture insert (0.4 µm) (Millipore)	PIHT30R48	Fisher Scientific UK Ltd
Thin-walled 0.5 mL PCR tube (Ambion)	AM12275	Fisher Scientific UK Ltd
Superfrost glass microscope slides	10150061	Fisher Scientific UK Ltd

Table 2-3. List of media and solutions used in hESC culture and differentiation

Media/solution	Components
EDTA (0.5 mM)	500 µL 0.5 M EDTA, 500 mL DPBS, 0.9 g NaCl
Freezing media (hESC)	50% E8, 35% ProFreeze, 15% DMSO
Directed differentiation basal media (DDBM)	500 mL DMEM/F12, 5 mL NEAA, 10 mL B27 supplement, 5 mL ITS, 5 mL L-glutamine, 917 µL β-Mercaptoethanol

2.2 General cell culture techniques

In the interests of sterility, all cell culture procedures were conducted in a class II microbiological safety cabinet and disposable sterile plastic consumables were used. Cells and constructs were cultured in humidified, tri-gas controlled incubators with 21% oxygen, 5% carbon dioxide and 93% nitrogen. Unless stated otherwise, cells were cultured in 6-well plates.

2.2.1 Coating tissue culture plastic with vitronectin

It was necessary to coat TCP in vitronectin prior to cell seeding. To avoid freeze-thaw cycles, vitronectin (500 µg/mL) was thawed and divided into 60 µL aliquots, which were stored at -80°C for up to 6 months. Aliquots were thawed and diluted in Dulbecco's phosphate buffered saline (DPBS) to a concentration of 5 µg/mL (one 60 µL aliquot diluted in 6 mL DPBS is sufficient to coat six wells of a 6-well plate). The TCP was incubated with the diluted vitronectin at 37°C for 30 minutes or at room temperature (RT) for 60 minutes. The solution was removed and discarded prior to cell seeding.

2.2.2 Resuscitation of frozen cells

Frozen cryovials of hESC (MAN7 and MAN13) were provided by the Kimber Lab at the University of Manchester. Upon removal from liquid nitrogen storage dewars, cryovials were placed into an empty incubator at 37°C until around 90% of the contents had defrosted. The cryovial was then sprayed liberally with 70% industrial methylated spirits (IMS) and transferred to the class II microbiological safety cabinet. The cell suspension (approximately 1 cm^3) was then slowly transferred to a 50 cm^3 centrifuge tube containing 9 mL of medium at RT. The cells were centrifuged at 700 g for 3 minutes. The supernatant

was discarded, the cell pellet was loosened by gentle trituration and cells were resuspended in an appropriate volume of medium. If large clumps were still visible, cells were passed twice through a P1000 pipette tip until a homogeneous suspension was obtained.

2.2.3 Seeding cells

Each thawed vial of hESC was resuspended in 2 mL RT Essential 8 (E8) medium. Rho kinase (ROCK) inhibitor was added at a concentration of 10 µM in order to aid attachment and survival. The cell suspension was transferred to one vitronectin-coated well of a 6-well plate and incubated for 24 hours, at which point the ROCK inhibitor was removed. Medium was changed daily until cells reached 80% confluency.

2.2.4 Passaging cells

Cells were split at confluence using 0.5 mM EDTA, diluted in DPBS with 30 mM sodium chloride (NaCl) (table 2-3). Media was aspirated, cells were washed once with 1 mL EDTA per well and then incubated with a further 1 mL EDTA at 37°C for 3-5 minutes (depending on size of colonies desired for seeding). Incubation beyond 5 minutes may result in a single-cell suspension and, ultimately, loss of viability. EDTA was aspirated and 1 mL fresh RT E8 medium was added directly to the well using a 5 mL serological pipette. The medium was washed up and down and the tip of the pipette was used to physically dislodge the cells. The cells were then resuspended in the desired volume of E8 medium with 10 µM ROCK inhibitor and transferred to fresh wells of a 6-well plate. For culture cells were generally split at a ratio of 1:6. Cells were then incubated for 24 hours, at which point the ROCK inhibitor was removed.

2.2.5 Cryopreservation of cells

For long term storage, cells were detached from TCP as described in 2.2.3., resuspended in 10 mL appropriate medium (supplemented with 50% Profreeze with 15% DMSO) and transferred to a 50 mL centrifuge tube. They were then centrifuged at 700 g for 3 minutes and resuspended in cold freezing media (1 mL per well of cells). 1 mL cell suspension (approximately $2x10^6$ cells) was transferred to a cryovial and placed in a 2-propanol-filled Mr Frosty freezing container for controlled cooling to -80°C before being transferred to liquid nitrogen storage dewars.

2.2.6 Performing a cell count

To perform a cell count, cells were detached from one well as described in 2.2.3., but were incubated with EDTA for 6 minutes in order to obtain a single cell suspension. A Neubauer haemocytometer was prepared by exhaling onto the haemocytometer and adhering the coverslip to the resulting condensate. 10 µL of suspension was introduced by capillary action underneath the coverslip. Cells were then counted under a microscope. A mean was calculated from the four 1 mm^2 corner regions in order to give the number of cells per 0.1 µL. The mean was then multiplied by $1x10^4$ and again by the total number of mL of cell suspension in order to determine the number of cells. In order to avoid prolonged incubation with EDTA and compromised viability, this cell count was used as an estimate for the number of cells in the other wells.

2.3 Directed Differentiation Protocol (DDP)

A modified version of the protocol described by Oldershaw et al in 2010 was used to generate chondroprogenitors from hESC (Oldershaw et al. 2010). Since its publication the Kimber lab have worked to enhance this protocol, resulting in changes which yield chondroprogenitors with a more mature phenotype. The omission of follistatin and the substitution of BMP4 for BMP2 were changes that were adopted at the beginning of this work. The substitution of WNT3A for the small molecule CHIR99021 (CHIR) occurred during the course of the work, as recommended by the Kimber lab. In addition, Activin A (Peprotech) and FGF2 (Gibco^{TM}) were substituted with alternatives produced by Qkine towards the end of this study. The effect of each alteration was assessed via gene expression analysis (see supplementary figures 1-2). Finally, in this study, vitronectin was used as the cell substrate during the DDP, rather than commercially-available fibronectin or the fibronectin peptide donated by the University of Manchester. This decision was influenced by a number of factors: poor performance of commercially-available fibronectin in maintaining cell attachment; limited availability of the peptide produced by the University of Manchester; vitronectin performed equally as well as the peptide according to gene expression analysis (supplementary figure 3).

2.3.1 Preparation of directed differentiation basal medium (DDBM)

In order to prepare a bottle of DDBM (table 2-3), 20 mL DMEM/F12 was transferred from a fresh bottle into a 50 mL centrifuge tube. 10 mL B27 supplement, 5 mL non-essential amino acids (NEAA), 5 mL Insulin-Transferrin-Selenium-Sodium Pyruvate (ITS), 5 mL L-glutamine and 917 µL 2-mercaptoethanol were added. The mixture was then filter sterilised and transferred back into remaining DMEM/F12. For long-term storage, 40 mL aliquots were

transferred to 50 mL centrifuge tubes and stored at -20°C for up to six months. As required, aliquots were defrosted overnight at 4°C and stored at 4°C for up to one month. DDBM was allowed to reach RT before use in cell culture.

2.3.2 Preparation of growth factors (GF)

Lyophilised GF were stored as per manufacturers' instructions until required. Stock solutions were prepared as detailed in table 2-4 by reconstituting in 0.1% bovine serum albumin (BSA). Aliquots of stock solutions were stored at -80°C for up to six months. Working concentrations were prepared with 0.1% BSA as outlined in table 2-4 and stored for up to two weeks at 4°C. In later DDP runs, WNT3A was replaced with CHIR (a potent WNT pathway activator). A 10 mM stock solution was prepared by dissolving 1 mg in 215 µL sterile DMSO. 20 µL aliquots were stored at -80° and diluted, when needed, with DMSO to obtain a working concentration of 2 mM (table 2-4). The final concentration used in the medium was 2 µM. Aliquots of CHIR were protected from prolonged exposure to light as per manufacturer's instructions.

Table 2-4. Concentrations of growth factors used during DDP

Growth factor	Stock concentration (µg/mL)	Working concentration (µg/mL)	Final concentration (ng/mL)
WNT3A	10	10	25
Activin A	100	20	50/25/10*
FGF2	100	20	20
BMP-2	200	40	40/20*
GDF-5	100	20	20/40*

*final concentrations vary depending on day of DDP (table 2-5)

2.3.3 Initiating a DDP with hESC

On day 0 (D0) cells were seeded into two wells of a 6-well plate at a density of approximately $7x10^5$ cells per well (1:3 split of a confluent well), as described in 2.2.3. Two wells of a separate 6-well plate were also seeded with cells at the same density. The following day (D1), medium was aspirated from the both wells of the separate plate. Cells from one well were lysed with 350 µL buffer RLT (supplied in the RNeasy Mini Kit). The lysate was then transferred to a 1.5 mL centrifuge tube and stored at -80°C. Cells from the remaining well were fixed for 30 minutes with 10% neutral buffered formalin (NBF) and immunocytochemistry (ICC) was performed (chapter 2.22) in order to confirm pluripotency via octamer-binding transcription factor 4 (OCT4) expression (supplementary figure 4). Medium from the two remaining wells was aspirated, cells were washed once with DPBS and 2 mL per well of DDBM was added, supplemented with growth factors as outlined in table 2-5 and 2-6. Medium was changed daily and supplemented with growth factors detailed in table 2-5 and 2-6. Cells were split at a ratio of 1:4 on days 4 (D4) and 8 (D8) and at these points samples were also lysed with buffer RLT and stored at -80°C.

Table 2-5. GF supplementation for DDP using WNT3A

	GF (µL) per 2 mL DDBM for 1 well of a 6 well plate												
Day	**1**	**2**	**3**	**4**	**5**	**6**	**7**	**8**	**9**	**10**	**11**	**12**	**13**
WNT3A (10 µg/mL)	5	5	5										
Activin A (20 µg/mL)	5	2.5	1										
FGF2 20 (µg/mL)		2	2	2	2	2	2	2	2	2	2	2	2
BMP2 40 (µg/mL)			2	2	2	2	2	2	1	1			
GDF5 (20 µg/mL)									2	2	4	4	4

Table 2-6. GF supplementation for DDP using CHIR99021

	GF (µL) per 2 mL DDBM for 1 well of a 6 well plate												
Day	**1**	**2**	**3**	**4**	**5**	**6**	**7**	**8**	**9**	**10**	**11**	**12**	**13**
CHIR99021 (2mM)	2	2	2										
Activin A (20 µg/mL)	5	2.5	1										
FGF2 20 (µg/mL)		2	2	2	2	2	2	2	2	2	2	2	2
BMP2 40 (µg/mL)			2	2	2	2	2	2	1	1			
GDF5 (20 µg/mL)									2	2	4	4	4

2.3.4 Termination of DDP

At day 14 the DDP was terminated and cells were either cryopreserved or kept in culture for use in further experiments. The DDP was extended up to day 17 as necessary, dependent upon when chondroprogenitors were required for experimental purposes. This was preferable to using thawed cells, as recovery from cryopreserved cells was generally around 35%. At the point of termination one final sample was lysed with buffer RLT and stored at -80°C for subsequent gene expression analysis, along with samples from days 1, 4 and 8. Periodically, one well was fixed for 30 minutes with 10% NBF and ICC was performed (chapter 2.22) in order to assess chondrogenic potential via expression of either COL2, SOX5 or SOX9 (supplementary figure 6).

2.4 Preparation of fibrin hydrogels

2.4.1 Preparation of stock solutions

Sterile conditions were maintained for all of the following procedures. Fibrinogen was reconstituted in 30 mM NaCl to give a stock concentration of 50 mg/mL. 500 µL aliquots were transferred to 1.5 mL centrifuge tubes and stored at -20°C for up to six months. Thrombin was reconstituted in 30 mM NaCl to give a stock concentration of 100 UN/mL.

Aliquots of 100 µL were transferred to 0.5 mL centrifuge tubes and stored at -20°C for up to six months. Aprotinin was reconstituted in 30 mM NaCl to give a stock concentration of 1 mg/mL. Aliquots of 1 mL were transferred to 1.5 mL centrifuge tubes and stored at -20°C for up to six months. To obtain working concentrations these reagents were thawed at RT and diluted further with 30 mM NaCl.

2.4.2 Preparation of gels

To prepare a 200 µL gel, 60 µL cell suspension (cell density dependent on desired seeding density) was mixed with 80 µL fibrinogen (working concentration dependent on desired final concentration) in one 0.5 mL centrifuge tube. In a separate 0.5 mL centrifuge tube, 8 µL aprotinin (1 mg/mL) was combined with 20 µL thrombin (20 UN/mL) and 40 µL calcium chloride ($CaCl_2$) (100 mM). These volumes could be scaled up to make "master mixes" of each of the mixtures in larger containers. 60 µL aprotinin/thrombin/$CaCl_2$ mixture was transferred to a fresh 0.5 mL centrifuge tube. Next, 140 µL cell suspension/fibrinogen mixture was taken up into a P200 pipette tip, the pipette volume was increased to 200 µL, the mixture was added to the aprotinin/thrombin/$CaCl_2$. The entire mixture was then pipetted up and down twice, taken back into the same P200 pipette tip and transferred immediately to one well of a 48-well plate. The fibrin gel began to set immediately and became too viscous to pipette after around 20 seconds, therefore, it was important that this procedure was completed promptly. The gels were then incubated at 37°C for 30 minutes, at which point 500 µL of appropriate medium was added, with the addition of aprotinin at a concentration of 20 µg/mL. For acellular gels, the cell suspension was substituted with 60 µL of appropriate medium. To make 50 µL gels, the same process was used but with the following volumes: 15 µL cell suspension, 20 µL fibrinogen, 2 µL aprotinin,

5 µL thrombin and 10 µL $CaCl_2$. 50 µL gels were pipetted into a 96-well plate and 200 µL DDBM was added after 30 minutes of incubation.

2.5 Preparation of HyStem™ hydrogels

HyStem™ gels were made according to the manufacturer's instructions, with the exception that the Extralink component was replaced with PEGDA from a different source in order to increase the concentration of crosslinker in the gels. All procedures were carried out under aseptic conditions.

2.5.1 Preparation of reagents

A stock solution of PEGDA was made by dissolving 250 mg in 1 mL degassed water (supplied in HyStem™ kit) to give a concentration of 250 mg/mL. Aliquots were stored at -20°C for up to one month. The components of the HyStem™ kit were allowed to come to RT and then 1 mL degassed water was added to each bottle of lyophilised HyStem™ using a syringe and needle. The bottles were then placed horizontally on a rocker and left for 30 minutes at RT until the contents were completely dissolved.

2.5.2 Preparation of gels

In order to make ten 200 µL gels, 400 µL PEGDA was added to 1600 µL HyStem™ to give a final concentration of 50 mg/mL PEGDA. D14 chondroprogenitors were detached and a cell count was performed (as described in 2.2.4 and 2.2.6). $2x10^6$ cells were then resuspended in 2 mL of the HyStem™/PEGDA mixture. The resulting cell suspension was transferred to a 48-well plate, with 200 µL in each well. The gels were then incubated at 37°C for 30 minutes, at which point 500 µL medium was added with aprotinin at a concentration of 20 µg/mL.

2.6 Preparation of Phytagel™ (gellan gum) hydrogels

2.6.1 Preparation of reagents

A 1% solution was made by adding 100 µg of Phytagel™ to 10 mL dH_2O in a transparent, 20 mL glass container with a screw cap. The cap was loosened and the mixture was placed upright in a microwave (800 W) and heated for 5 seconds. A paper towel was wrapped around the neck of the container and the contents were swirled by hand for 2-3 seconds. The container was then heated for a further 5 seconds and this process was repeated until all of the Phytagel™ had dissolved. Complete dissolution via this method generally took around 3 minutes. Once dissolved, the lid was closed and the container was placed horizontally into a Bio-Rad GS Gene Linker UV Chamber oven and sterilised for 90 seconds at 257.3 nm. The container was then incubated at 37°C for at least 30 minutes, in order to allow the contents to cool. Allowing the mixture to cool to RT would have caused the gels to set; therefore, the container was maintained at 37°C until needed.

2.6.2 Preparation of gels

D14 chondroprogenitors were detached and a cell count was performed (as described in 2.2.4 and 2.2.6). $2x10^6$ cells were resuspended in 20 mL DDBM and divided equally between ten 50 mL centrifuge tubes. The tubes were centrifuged at 700 g for 3 minutes and the medium was carefully aspirated in order to leave as little liquid remaining as possible. In order to avoid premature gelation, the Phytagel™ solution was transferred from the incubator to the class II microbiological safety cabinet and kept in a beaker of warm water. 200 µL of Phytagel™ solution was then rapidly added to one cell pellet using a P1000 pipette tip. The mixture was drawn back into the pipette tip and transferred immediately to one cell of a 48-well plate. This process was repeated with the remaining cell pellets. The gels

were incubated for 10 minutes at 37°C, at which point 500 µL medium was added with aprotinin at a concentration of 20 µg/mL.

2.7 Creation of a PCL Wnt platform

2.7.1 Preparation of reagents

In a fume hood, a 2% solution of PCL was made by adding 300 mg PCL pellets to 15 mL 100% chloroform in a 20 mL glass tube with a screw cap. The solution was mixed with a magnetic stirrer and stir bar for one hour until completely dissolved. A solution of 1% 3-[(3-cholamidopropyl)dimethylammonio]-1-propanesulfonate (CHAPS) detergent (wt/vol) and 0.1% (wt/vol) BSA was prepared in DPBS and then filter sterilised. Aliquots were stored at 4°C for up to one month or at -20°C for up to six months. A 20 mM solution of 1,4-dithiothreitol (DTT) was prepared by adding 154.24 mg DTT to 50 mL DPBS. The solution was then filter sterilised and stored at 4°C for up to six months. A stock solution of WNT3A at 10 µg/mL was prepared in 1% CHAPS detergent and aliquots were stored at -80°C for up to six months. A working concentration (w/c) of 400 ng/mL in 1% CHAPS detergent was made immediately prior to use.

2.7.2 Preparation of polymers

15 mL 2% chloroform was transferred to three glass petri dishes (55 mm diameter), with 5 mL of solution per dish, and left for approximately 24 hours until a solid film had formed. Forceps were then used to transfer each film to a separate 50 mL centrifuge tube.

2.7.3 Modifying polymers with aldehydes

The following procedures were conducted in a fume hood. The lid was loosened on a bottle of hexamethylenediamine and it was heated gently on a hot plate for around 30 minutes

until a liquid was formed. 1250 µL of the liquid was added to 50 mL 90% 2-propanol. 15 mL of the mixture was added to each of the polymer sheets and the centrifuge tubes were placed on a roller for 90 minutes. The polymer sheets were removed from the centrifuge tubes, washed once in 100% 2-propanol and left to dry. 50 µL of 70% glutaraldehyde solution was added to 50 mL 70% ethanol. Each of the polymer sheets was incubated with 15 mL of the mixture for 5 minutes. The glutaraldehyde solution was then aspirated and the polymers were washed twice with 100% ethanol and left to dry.

2.7.4 Modifying polymers with WNT3A

An 8 mm biopsy punch was used to punch out discs of PCL from the polymer sheet. The discs were transferred to a 50 mL centrifuge tube containing 100% ethanol. Each disc was then transferred to a separate well of a 48-well plate, 500 µL ethanol was added to each well and they were left for 30 minutes. The discs were then transferred to a non-adherent 48-well plate and left to dry, then washed once in DPBS. 50 µL WNT3A solution (w/c) was pipetted carefully onto the top of each disc and they were incubated at RT for 1 hour, then washed once with DPBS. For inactivated WNT3A control polymers, the solution was removed after 1 hour, the discs were washed once in DPBS and then incubated with 200 µL of 20 mM DTT for 30 minutes at 37°C. They were then washed once in DPBS. For BSA control polymers, the WNT3A solution was substituted with 50 µL of 5% (wt/vol) BSA. Once the polymers were modified they seeded with cells immediately or stored at 4°C for up to 24 hours.

2.8 Stimulating cells with the four-point bending bioreactor (4PBB)

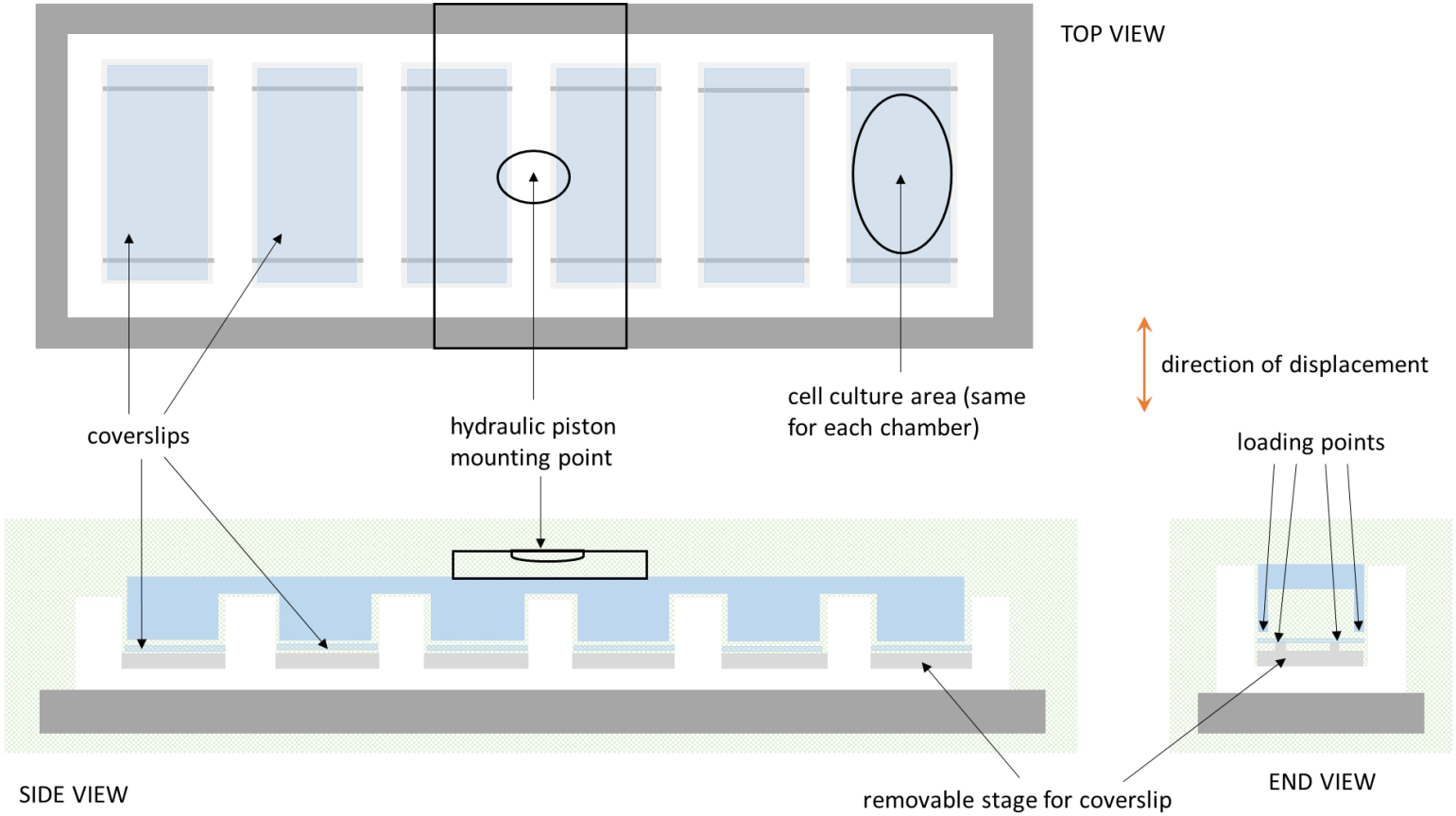

Figure 2-1. Schematic diagram of 4PBB. Diagrammatical representation of four-point bending loading apparatus for the application of uniaxial compression to hESC-derived chondroprogenitor coverslip cultures. Adapted from the thesis of Matthew Peake (M. Peake 2001).

2.8.1 Preparation of the bioreactor

In order to maintain sterility, the lids were removed from the two 4PBB chambers prior to use and submerged in 100% IMS for 2 hours, along with the pneumatic pistons. The IMS was removed and the lids and pistons were allowed to dry in the class II microbiological safety cabinet. The chambers were autoclaved and removed from their autoclave bags in the class II microbiological safety cabinet immediately prior to use. All components were handled with sterile forceps. The lid of the container was modified to allow for gas exchange by creating 5 holes which were plugged with the caps of T-175 culture flasks and sealed around the edges with Loctite All Plastics Superglue (figure 2-2 D-E).

2.8.2 Coating coverslips with vitronectin

No. 2 coverslips (table 2-2) were autoclaved, then transferred to 139 mm petri dishes (2 coverslips per dish). With the lids on, the petri dishes were transferred to a Bio-Rad GS Gene Linker UV Chamber oven and sterilised for 90 seconds at 257.3 nm. 1 mL vitronectin (5 µg/mL in DPBS) was carefully pipetted onto the surface of each coverslip (figure 2-2 A) and incubated at 37°C for 30 minutes or at RT for 60 minutes. Immediately prior to cell seeding, the vitronectin was carefully aspirated, ensuring that no liquid ran off the side of the coverslip. This was important in order to maintain surface tension when the cell suspension was added, so that cells remained only within the vitronectin-coated area.

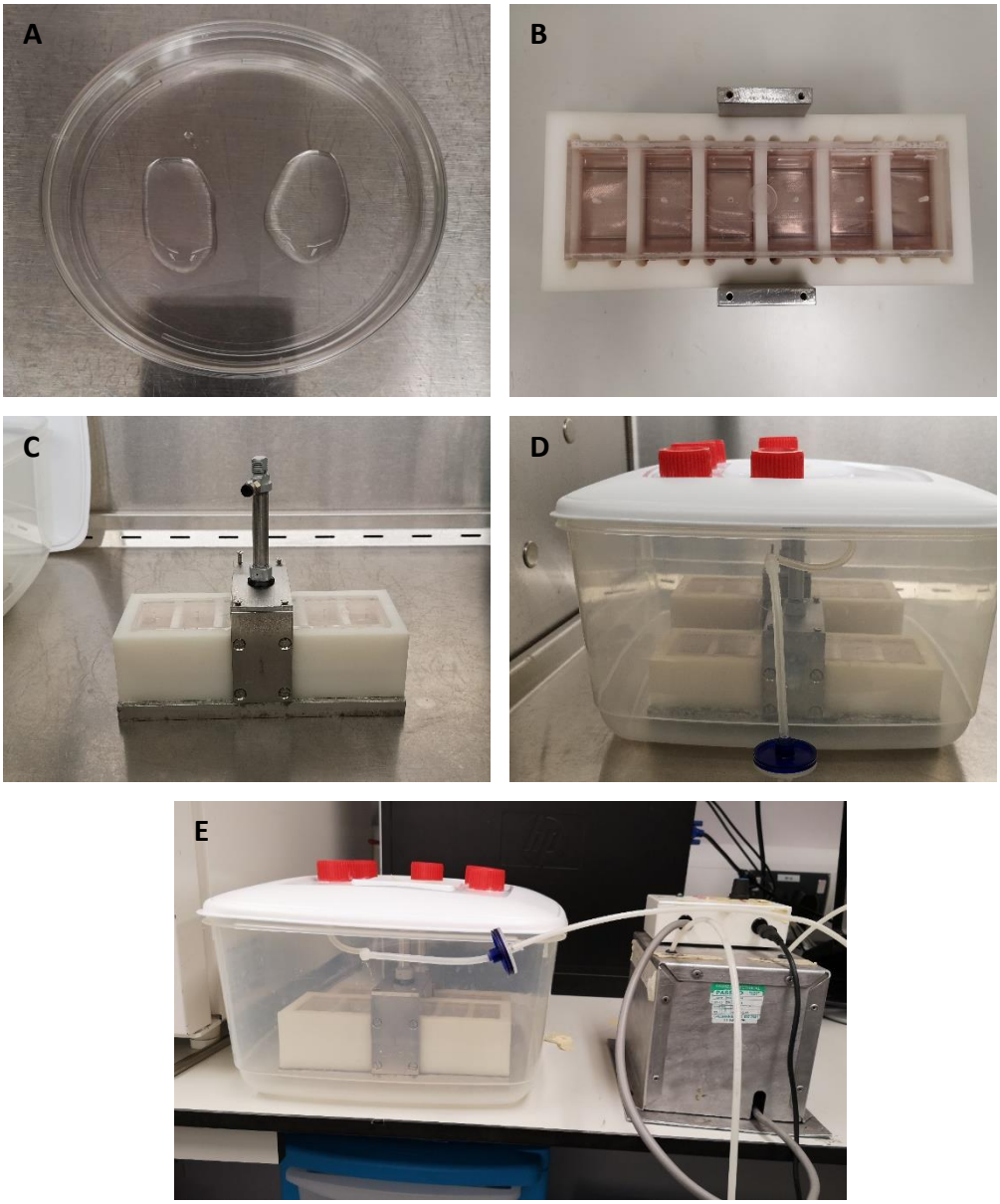

Figure 2-2. Loading of the 4PBB. Middle region of upper surface of coverslips are coated in vitronectin and cells are subsequently seeded onto this area (A). Cell-seeded coverslips are placed cell-side down into each well, medium is added and lid is placed on top (B). Pneumatic piston is secured into place (C). Inlet tube is attached to pneumatic piston (D). Inlet tube is attached to solenoid-mediated pneumatic switching system via a 0.2 µm syringe filter (E).

2.8.3 Seeding coverslips with cells

D14-16 chondroprogenitors were thawed as described in 2.2.2 and resuspended in an appropriate volume of D13 media (table 2-5) supplemented with ROCK inhibitor (10 µM). 1 mL cell suspension was carefully pipetted onto the surface of each vitronectin-coated coverslip and incubated for 24 hours at 37°C.

2.8.4 Application of compressive force

Using sterile forceps, each cell-seeded coverslip was transferred to one well of the 4PBB chamber and placed cell-side down. 5 mL of D13 media was added to each well and the lid was placed onto each chamber. The pneumatic piston was placed on top and screwed securely into place (figure 2-2 C). The two chambers were then transferred to a 10 L plastic container, which had previously been sprayed with 70% IMS and allowed to dry. The experimental chamber was placed on the side nearest to the inlet tube and the tube was attached to the pneumatic piston (figure 2-2 D). The lid was placed over the two chambers and closed securely. A solenoid-mediated pneumatic switching system was then attached to a syringe filter, which was in turn attached to the inlet tube, ensuring that air coming into the system was not contaminated (figure 2-2 E). The switching system was set to a frequency of 0.8 Hz and the alternating compressive force was applied for a period of 30 minutes. The control chamber was set up in exactly the same way, except that the piston was not connected to the pneumatic switching system, meaning that no compressive force was applied. After the stimulation period, the switching system was detached from the syringe filter and the plastic container and its contents were incubated at 37°C until the experiment was terminated, at which point the coverslips were carefully removed from the chambers and excess media was aspirated. The cells were then lysed by applying 570 µL

buffer RLT supplemented with 1% ß-mercaptoethanol directly to the coverslip. The lysate was transferred to a 1.5 mL centrifuge tube and stored at -80°C.

2.9 Stimulation with the Hydrostatic Bioreactor

This study utilised a custom-made hydrostatic bioreactor which was designed and built by Professor El Haj (ISTM, Keele University) and Tissue Growth Technologies (TGT) (Minnetonka, MN, USA). Figure 2-3 A details the components of the bioreactor. The sealed chamber (figure 2-3 B) is comprised of anodised aluminium and can house a standard cell culture plate with the lid removed. Ancillary equipment (figure 2-3 C) transfers pressure changes to the gas phase above the culture medium in the well plate. The chamber fits into a standard incubator, the air of which is compressed, recycled and fed through a continuously running scroll compressor via a heater, in order to maintain a temperature of 37°C. This air enters the chamber via a system of valves through a sterile filter, which can be autoclaved along with the chamber as required. A vacuum mechanism then removes the air from the chamber and directs it back into the incubator to be recycled. Operation of the system is controlled by TGT's GrowthWorks software. This allows for fine control of the sinusoidal waveform, with cyclical pressures between 0 kPa and 270 kPa, at frequencies ranging from 0.0001 Hz to 2 Hz. (Henstock et al. 2013). Owing to a catastrophic failure of this system, it was later re-fashioned and a commercially available microfluidic control system (OB1 MK3) was used to regulate the pressure in the chamber.

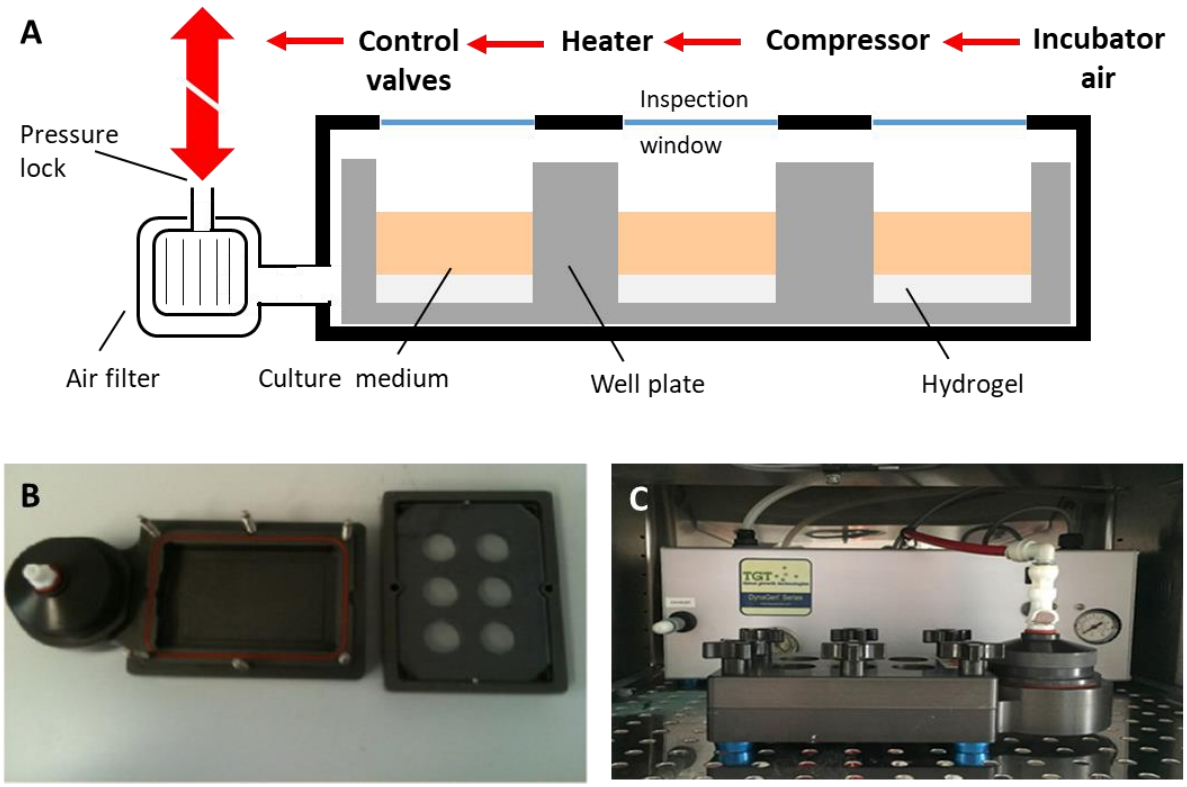

Figure 2-3. Hydrostatic bioreactor. Schematic cross-section of bioreactor chamber (A) shows how compressed incubator air is used to apply pressure to samples on a well plate. The bioreactor chamber with the lid removed (B) and the chamber connected to ancillary equipment (C) are also shown.

2.9.1 Preparation of samples for the bioreactor

50 µL fibrin hydrogels were prepared as described in 2.4.2. using chondroprogenitors which were derived as outlined in 2.3. The samples were left for 24 hours and then a live/dead assay (see chapter 2.19) was performed on one gel from each condition. Only gels with at least 50% viability were used. Acellular control hydrogels were also prepared for each condition.

2.9.2 Application of hydrostatic pressure

For all experiments the hydrostatic bioreactor chamber was opened only inside the class II microbiological safety cabinet and, during stimulation, the lid of the 96-well plate was removed and kept in aseptic conditions. On day 2, the 96-well plate containing the fibrin hydrogels was transferred to the bioreactor chamber. Cyclical hydrostatic pressure was applied to the samples for 1 hour at either 270 kPa or 170 kPa with a frequency of 1 Hz. A group of control gels were cultured in the same way, but did not receive any stimulation (static). After stimulation the gels were returned to the incubator. This process was repeated on days 3, 4 and 5. On day 7 the experiment was terminated and the samples were either snap-frozen and stored at -80°C for subsequent gene expression analysis, or fixed for 2 hours with 10% NBF for histological analysis.

2.10 Incorporation of sulphated alginates into the DDP

Sulphated alginates (sAlg) were a kind gift from Dr Rami Mhanna at the American University of Beirut, Lebanon. Details of the preparation of the alginates has been described previously (Mhanna et al. 2014). Alginates with two varying degrees of sulphation (DS) were used including 0.8 (sAlg 0.8), 2.0 (sAlg 2.0) and non-sulphated (sAlg 0.0). They were dissolved in DPBS at a concentration of 1 mg/mL.

2.10.1 Addition of sAlg to the culture medium

A DDP was initiated on either MAN7 or MAN13 hESC as described in 2.3.3. On D8 the cells were split as usual, but were seeded into a 24-well plate with 500 µL medium per well. For a 1:4 split 1 well of a 6-well plate (9 cm^2) was seeded into 18 wells (2 cm^2/well) of a 24-well plate. The cells were incubated for 24 hours, at which point the medium was changed to D9 medium supplemented with sAlg at varying concentrations (table 2-7). The DDP was

continued as usual, but on D12 the medium was again supplemented with sAlg. For control wells, the cells were cultured in appropriate medium (D9 or D12) without sAlg supplementation. The experiment was terminated on day 14 and cells were either lysed with 350 µL buffer RLT and stored at -80°C for gene expression analysis or fixed for 30 minutes with 10% NBF for analysis via immunocytochemistry.

Table 2-7. Volumes of sAlg solutions required on days 9 and 12 of DDP

	Volume of 1mg/mL sAlg solution (µL)	Volume of medium (µL)	Final volume (µL)
sAlg 0.0 (10 µg/mL)	5	495	500
sAlg 0.8 (10 µg/mL)	5	495	500
sAlg 2.0 (10 µg/mL)	5	495	500
sAlg 0.0 (10 µg/mL)	50	450	500
sAlg 0.8 (100 µg/mL)	50	450	500
sAlg 2.0 (100 µg/mL)	50	450	500

2.11 Pre-incubation of cells with ECM molecules

Either hESC or hESC-derived chondroprogenitors were detached as described in 2.2.4. $1x10^6$ cells were transferred to a 50 µL centrifuge tube along with 10 mL of appropriate medium and centrifuged for 3 minutes at 700 g. The cells were then resuspended in 1 mL appropriate culture medium supplemented with ECM molecules at the desired concentration and incubated for 10 minutes. ECM molecules used were vitronectin (VTN), fibronectin (FN), laminin (LN), HyStem™ or collagen type VI (COL VI). VTN is a ubiquitous cell adhesion molecule, which is commonly used to coat TCP for ESC culture and was, therefore, deemed a good starting point as proof of concept. FN is also a cell adhesion molecule, but with a more defined role in cartilage tissue (chapter 1.3.6) and thus more physiologically relevant in this model. Similarly, HA (Hystem™ and COL VI) are key structural molecules found in

articular cartilage (chapter 1.3.3 and 1.3.4). The cell suspension was then centrifuged and resuspended in appropriate medium at a density of $2.5x10^5$ cells/mL. 2 mL cell suspension was seeded into either vitronectin-coated 6-well plates or onto sterile, vitronectin coated circular coverslips (10 mm diameter), each housed within one well of a 6-well plate. The cells were then cultured for 4 days with daily medium changes, after which time they were either lysed with buffer RLT and stored at -80°C or fixed for 30 minutes with 10% NBF.

2.12 RNA isolation

Prior to RNA isolation all pipettes and surfaces were treated with DNA AWAY™. If frozen, samples were allowed to thaw and then placed on ice. Samples that were processed immediately after lysis were also kept on ice during processing. In order to isolate sufficient RNA from 3D constructs, it was necessary to homogenise the sample first. 2.12.2 – 2.12.4 (below) outline three different methods which were employed for this purpose.

2.12.1 Isolating RNA from cells in monolayer culture

Total RNA extraction was carried out using the RNeasy Mini Kit as per manufacturer's instructions. One volume of 70% ethanol was added to the lysate and mixed well by pipetting. Up to 700 µL of the solution was transferred to an RNeasy mini spin column and centrifuged at 10,000 g for 15 seconds. The flow-through was discarded and any remaining solution was passed through the spin column in the same way. The membrane was then washed with the following steps: 1) 700 µL buffer RW1 added, centrifuged at 10,000 g for 15 seconds, flow-through discarded 2) 500 µL buffer RPE added, centrifuged at 10,000 g for 15 seconds, flow-through discarded 3) 500 µL buffer RPE added, centrifuged at 10,000 g for 2 minutes, flow-through discarded. The spin column was then inserted into a fresh collection tube and centrifuged at 18,000 g in order to dry the membrane. The collection

tube was then replaced with a 1.5 mL centrifuge tube and 30 µL RNase-free water was pipetted directly onto the membrane and allowed to soak for 1 minute. The column was then centrifuged for 1 minute at 10,000 g, the elute was re-pipetted back onto the membrane and the column was centrifuged at 10,000 g for a further minute. Extracted RNA was quantified with a NanoDrop 2000 spectrophotometer and either kept on ice for immediate reverse transcription or stored at -80°C.

2.12.2 Isolating RNA from hydrogels using RNeasy Mini Kits

Samples were snap frozen either on dry ice or with a brief immersion into liquid nitrogen. 10 µL buffer RLT was then pipetted directly onto the sample and a disposable polypropylene pestle was used to crush it by hand. A further 350 µL buffer RLT was added, the sample was vortexed and centrifuged at 18,000 g for 3 minutes. The supernatant was carefully pipetted and mixed with an equal volume of 70% ethanol in a fresh 1.5 mL centrifuge tube. RNA was then extracted as described above in 2.12.1.

2.12.3 Isolating RNA from hydrogels with a low RNA yield

Smaller fibrin hydrogels yielded a particularly low concentration of RNA, therefore, it was necessary to use a combination of TRI Reagent and PureLink RNA Micro Scale Kits. Samples were snap frozen either on dry ice or with a brief immersion into liquid nitrogen and crushed by hand with a disposable polypropylene pestle. 1 mL TRI Reagent was added to the sample, along with 5 µL RNA carrier (provided in Micro Scale Kit). It was then shaken vigorously by hand and centrifuged at 18,000 g for 10 minutes. The supernatant was transferred to clean 1.5 mL centrifuge tube and incubated for 5 minutes at RT to allow complete dissociation of nucleoprotein complexes. 200 µL of chloroform was added and the sample was shaken vigorously by hand for 15 seconds, incubated at RT for 10 minutes and centrifuged at 12,000

g for 15 minutes at 4°C. Approximately 80% of the colourless upper aqueous phase was carefully pipetted and transferred to a fresh 1.5 mL centrifuge tube. An equal volume of 70% ethanol was added and mixed by pipetting up and down. The tube was then incubated at 4°C for 30 minutes. The resulting ethanol precipitation was transferred to a PureLink spin column, centrifuged at 12,000 g for 1 minute and the flow-through discarded. 350 µL of wash buffer I was added to the spin column, which was then centrifuged at 12,000 g for 1 minute and the flow-through discarded. 20 µL of DNase solution (10 µL DNase + 10 µL 2x DNase buffer) was pipetted directly onto the membrane and the sample was incubated at RT for 15 minutes. The membrane was then washed by the following steps: 1) 350 µL wash buffer I added, centrifuged for 15 seconds, flow-through discarded 2) 500 µL wash buffer II added, centrifuged for 15 seconds, flow-through discarded (this step was repeated once). In order to dry the membrane, the collection tube was replaced with a fresh one and the spin column was centrifuged at 12,000 g for 2 minutes. The collection tube was then replaced with a 1.5 mL centrifuge tube and 20 µL RNase-free water was pipetted directly onto the membrane and allowed to soak for 1 minute. The column was then centrifuged for 2 minutes at 12,000 g. Extracted RNA was quantified with a NanoDrop 2000 spectrophotometer and either kept on ice for immediate reverse transcription or stored at -80°C.

2.13 Reverse transcription

RNA was converted into cDNA using High Capacity cDNA Reverse Transcription Kits (Applied Biosystems) as per the manufacturer's instructions. A reverse transcription master mix was prepared using the following volumes of kit components (per sample of RNA): 2 µL 10x RT Buffer, 0.8 µL 25x dNTP Mix, 2 µL 10x RT random primers, 1 µL MultiScribe™ Reverse

Transcriptase, 0.2 µL RNase free water. The master mix was then briefly centrifuged and 6 µL was transferred to a thin-walled 0.5 mL PCR tube along with 14 µL of RNA. Samples were then centrifuged briefly and loaded into a thermal cycler which was programmed with the following steps: 1) 25°C for 10 minutes 2) 37°C for 120 minutes 3) 85°C for 5 minutes 4) held at 4°C until removed. cDNA was stored at -20°C.

2.14 Quantitative real-time polymerase chain reaction

Gene expression analysis was performed using SYBR® Green-based quantitative real-time polymerase chain reaction (qRT-PCR) with pre-optimised QuantiTect primer assays (Qiagen). SYBR® Green is a cyanine dye which preferentially binds to double-stranded DNA and, in doing so, exhibits a >1000-fold increase in fluorescence (Zipper et al. 2004; Dragan et al. 2012). The abundance of product, specified by the primer pair, can be determined during the course of amplification via the intensity of the fluorescent signal generated, which is measured at the end of each PCR cycle. The cycle number at which each sample has accumulated sufficient fluorescence to cross an arbitrary threshold (set by the thermal cycler to be above background levels and within the exponential phase of amplification) is recorded by the software as a cycle threshold (C_T) value. For each sample the C_T value for the housekeeping gene glyceraldehyde 3-phaosphate dehydrogenase (*GAPDH*) was used to normalise the C_T values for all other genes. Relative expression was calculated by using $2^{-\Delta CT}$ or $2^{-\Delta\Delta CT}$ as appropriate.

2.14.1 Preparation of samples

cDNA samples were diluted to 3 ng/µL in RNase free water. A "master mix" was prepared for each gene with the following volumes per sample: 7.5 µL SYBR™ Green PCR Master Mix, 2 µL QuantiTect 10x primer mix, 0.5 µL RNase free water. 10 µL of master mix was

transferred to each PCR tube (AriaMx Tube Strips 8) and 5 µL of cDNA from each sample was added either in triplicate or duplicate depending on the quantity of cDNA. The tubes were capped and centrifuged for 2 minutes in a microcentrifuge then transferred to an AriaMx Real-Time PCR System (Agilent Technologies).

2.14.2 Amplification of product

The thermal cycler was programmed as follows and as shown in figure 2-4:

- One cycle of 95°C for 10 minutes (hot start to denature activate DNA polymerase)
- 40 cycles of:
    - 95°C for 15 seconds (DNA melting)
    - 60°C for 1 minute (DNA extension)
        - Fluorescence measured
- 1 cycle of pre-programmed melt curve:
    - 95°C for 1 minute
    - 55°C for 30 seconds
    - 95°C for 30 seconds
        - Fluorescence measured as temperature is gradually increased from 55°C to 95°C

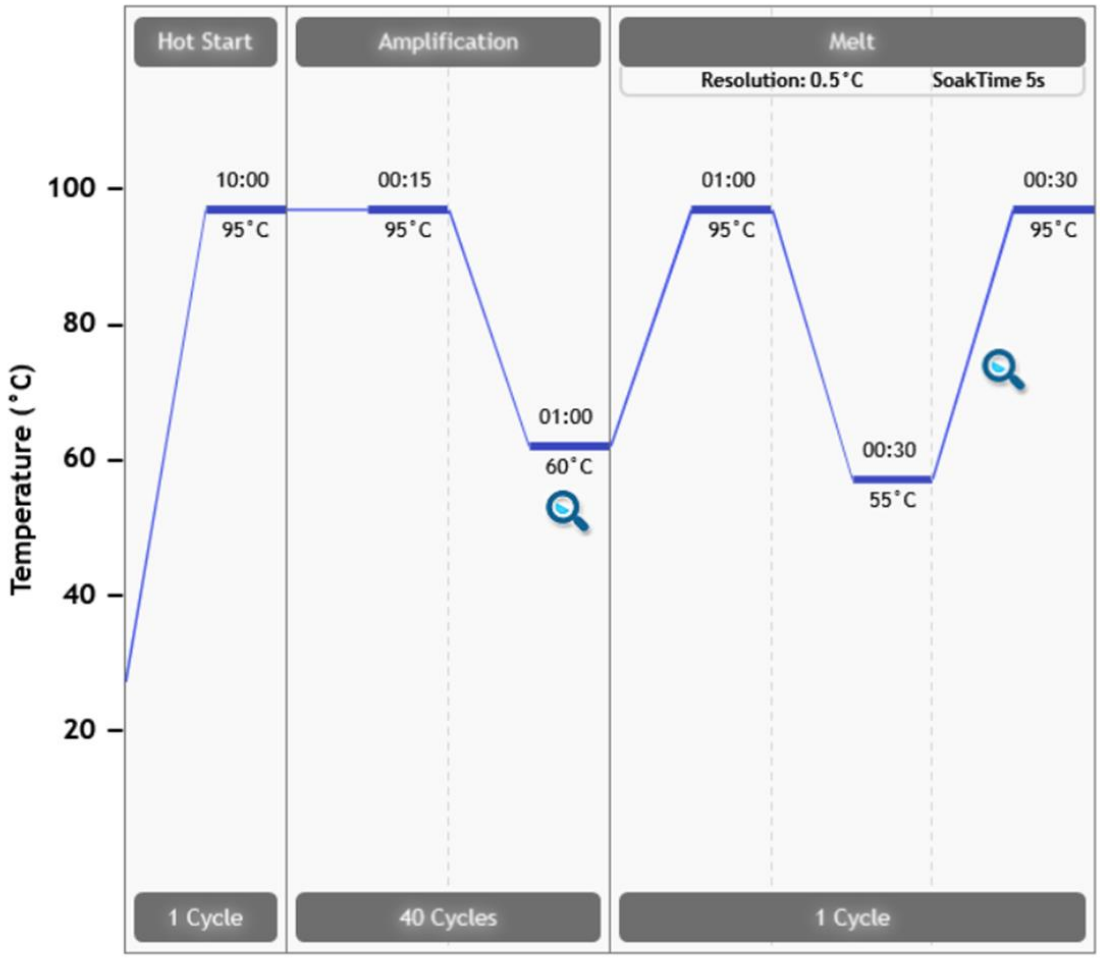

Figure 2-4. qRT-PCR thermal cycle programme. 1 hot start cycle to activate DNA polymerase, 40 cycles of product amplification and 1 cycle of melt curve formation.

2.14.3 qRT-PCR data analysis

Relative gene expressions in the form $2^{-\Delta CT}$ were calculated using Microsoft Excel.

2.15 Agarose gel electrophoresis

Although pre-optimised, commercially-available primers were used, some samples were fractionated by agarose gel electrophoresis following qRT-PCR amplification in order to confirm the presence of just one product per primer. A 2% (w/v) agarose solution was made

by adding 2 g agarose to 100 mL 1x tris-acetate-EDTA (TAE) buffer in a 250 mL glass bottle with a screw cap. The cap was loosened and the mixture was placed upright in a microwave (800 W) and heated for 10 seconds. A paper towel was wrapped around the neck of the container and the contents were swirled by hand for 2-3 seconds. The container was then heated for a further 10 seconds and this process was repeated until all of the agarose had dissolved. Complete dissolution via this method generally took around 1 minute. 5 µL ethidium bromide (10 mg/mL) was added to the solution, which was then swirled and poured into a gel setting chamber with well comb inserts and allowed to set for 1 hour. Ethidium bromide is a dye that undergoes enhanced fluorescence following UV excitation when bound to double-stranded DNA. This allows for visualisation of DNA bands within the gel. Once set, the gel was transferred to a BIO rad electrophoresis clear chamber which was pre-filled with 1x TAE buffer (pH 8). 2.5 µL gel loading buffer was added to each amplified PCR sample and 8 µL of the mixture was transferred to one well of the gel. 5 µL DNA ladder was added to the two wells at each side to allow comparison with samples. Gels were run for 1 hour at 100 V and visualised by fluorescence at 254 nm in a UV Transilluminator (Syngene). Images of the gels were captured with Syngene Genesnap software (supplementary figure 5).

2.16 Proteinase K digestion of cells and hydrogels

Monolayer cells were washed with DPBS, detached, transferred to 1.5 mL centrifuge tubes and centrifuged at 4000 g for 2 minutes in order to create a cell pellet. Hydrogels were washed with DPBS and transferred to 1.5 mL centrifuge tubes. 250 µL of Proteinase K (1 mg/mL dissolved in 100 mM ammonium acetate, pH 7.0) was added per 100 mg wet weight of tissue. Samples were vortexed, then incubated at 60°C with an additional vortex every

30 minutes until complete dissociation had occurred. This generally took around 2 hours. Proteinase K was inactivated by heating the samples to 100°C for 5 minutes in a heat block. They were then used immediately or stored at -20°C.

2.17 PicoGreen double stranded DNA assay

The Quant-IT^{TM} double stranded DNA assay was performed as per the manufacturer's instructions. 50 µL of Proteinase K digests (see 2.16 above) were used for this assay. DNA standards were prepared at concentrations of 20, 10, 5, 2.5, 1.25, 0.625 and 0.3125 µg/mL in 100 mM ammonium acetate. All samples and standards were then diluted 1:10 in 1x tris-EDTA (TE) buffer, ensuring there was sufficient volume for at least three aliquots of each sample at 50 µL per aliquot and four aliquots of each standard at the same volume. Each aliquot was transferred to 1 well of a 96-well plate. PicoGreen stock solution was diluted 1:200 in 1x TE buffer immediately prior to use. 50 µL of working solution was added to each sample/standard and incubated for 2 minutes then read using a Synergy 2 plate reader (excitation 480 nm, emission 520 nm). DNA concentrations were determined using a calibration curve of standards with linear regression. 10 mM ammonium acetate in 1x TE buffer was used as the 0 µg/mL standard.

2.18 DMMB sulphated GAG assay

Dimethyl methylene blue (DMMB) undergoes a rapid colour change in the presence of sGAG, which can be detected with a spectrophotometer. The remaining 200 µL of the Proteinase K digest (see 2.16 above) was used in this assay.

2.18.1 Preparation of DMMB solution

0.008 g DMMB was dissolved in 2 mL 100% ethanol in a glass beaker. 1.52 g glycine, 1.185 g NaCl and 500 mL dH_2O were added. The liquid was covered with foil and mixed for 2 hours with a magnetic stirrer. The pH was adjusted to 3.0 with hydrochloric acid (HCl) and stored in the dark at RT.

2.18.2 Preparation of samples

Chondroitin sulphate was used as the sGAG standard for this assay. Concentrations of 50, 25, 12.5. 6.25, 3.125, 1.5625 and 0.78125 µg/mL were prepared in 100 mM ammonium acetate. Aliquots of 50 µL were transferred to one well of a 96-well plate (4 aliquots per standard). 50 µL aliquots of digest were also transferred to one well of a 96-well plate (3 aliquots per sample). Plates were transferred to a Synergy 2 plate reader and an automated dispense unit was used to dispense 200 µL DMMB solution per well. Absorption at 530 nm was determined immediately after the solution was dispensed into each well in order to maximise reproducibility and to avoid formation of precipitation prior to reading. DNA concentrations were determined using a calibration curve of standards with linear regression. 100 mM ammonium acetate was used as the 0 µg/mL standard.

2.19 AlamarBlue™ metabolic activity assay

AlamarBlue™ contains a REDOX (reduction-oxidation reaction) indicator which changes from a blue, non-fluorescent form to a red, fluorescent form when taken up from the growth medium and chemically reduced by cells during metabolic activity. Damaged or non-viable cells have a lower metabolic activity and thus generate lower fluorescent signals. However, given that the same can be said of senescent cells or those not currently in the growth phase of the cell cycle, AlamarBlue™ may be considered a metabolic activity assay

rather than a true indicator of viability. (Rampersad 2012). Medium was aspirated from hydrogels or cells and replaced with medium containing 10% AlamarBlue™ solution. The samples were incubated in the dark at 37°C for an appropriate length of time until a visible colour change had occurred (generally 90 minutes for monolayer cells and around 4 hours for fibrin gels). In order to render any comparison valid, samples from the same experiment were incubated for an equal length of time. 4 x 50 µL of medium from each sample were then transferred to separate wells of a 96-well plate. Fluorescence was read on a Synergy 2 plate reader (excitation 530 nm, emission 590 nm). Excess solution was then removed from the samples, which were washed once with DPBS and fresh medium was added.

2.20 Cell viability assay

To assess the viability of cells within 3D constructs the LIVE/DEAD viability kit was used as per the manufacturer's instructions. Medium was aspirated from samples, which were then washed twice with DPBS and incubated with 2 µL/mL ethidium homodimer-1 and 0.5 µL/mL calcein-AM in DPBS in the dark for 20 minutes at 37°C. Samples were then washed once with PBS and imaged immediately with a Nikon Eclipse Ti-S Fluorescent microscope. Conversion of non-fluorescent calcein-AM to its fluorescent form by intracellular esterases is an indicator of live cells, whereas the compromised membrane integrity of dead cells leads to the uptake of red-fluorescent ethidium homodimer-1.

2.21 Histology

2.21.1 Preparation of samples

Porcine cartilage samples were obtained for use as positive controls for histological staining. A bone marrow biopsy Jamshidi needle was used to extract full depth articular cartilage

cores from porcine knee joints (donated by Hartshill Butchers, Stoke-on-Trent). The tissue was fixed overnight in 10% NBF at RT, then washed in DBPS and stored at 4°C. All hydrogels were washed in DPBS and incubated at RT for 2 hours (histology) or 1 hour (ICC) in 10% NBF. They were then washed in DPBS and stored at 4°C. Monolayer cells were washed in DPBS, incubated for 30 minutes at RT in 10% NBF, then washed again and stored at 4°C.

2.21.2 Paraffin embedding

Hydrogels and porcine cartilage tissue were dehydrated by immersion in the following alcohol series: 70% IMS for 2 hours, 80 % IMS for 1 hour, 90% IMS for 1 hour, 90% 2-propanol for 1 hour, 100% 2-propanol for 1 hour. Samples were then transferred to melted paraffin wax at 60°C in a wax embedder (Tissue-Tek Thermal Console) overnight. The following day, samples were transferred to fresh paraffin wax in an embedding mould with a labelled cassette and allowed to solidify on a cooling plate (Tissue-Tek Cryo Console).

2.21.3 3-Aminopropyltriethoxysilane coating of slides

In order to improve sample adhesion, standard Superfrost glass microscope slides were treated with APTES. Clean slides were soaked in acetone for 2 minutes to remove any trace residues and allowed to air dry. They were then immersed in 2% (v/v) APTES solution in acetone for a further 2 minutes. Coated slides were then washed in 2 baths of dH_2O for 2 minutes each, dried in an oven at 60°C and stored in their original boxes until needed.

2.21.4 Sectioning and de-paraffinisation of embedded samples

Sample blocks were trimmed to remove excess paraffin, positioned in the rotary microtome (Shandon AS325) and sectioned at 5 µm. Serial sections were taken, with 3-4 discontinuous sections per slide across ≥6 slides to allow for scrutiny of the same region with multiple

stains. Sections were transferred to a water bath with dH_2O at 40°C and collected onto APTES-coated slides. Slides were then placed in the oven overnight at 60°C and stored at RT. Prior to staining, it was necessary to deparaffinise samples. To this end, they were soaked in Histo-Clear for 10 minutes followed by a second soak with fresh Histo-Clear for a further 10 minutes. Slides were then rehydrated by immersion in 100%, 90%, 80%, 70% and 50% IMS for 2 minutes each and transferred to dH_2O.

2.21.5 Haematoxylin and eosin staining

Deparaffinised and rehydrated sections were immersed in Gill's number 2 haematoxylin for 4 minutes, then rinsed in running tap water, dipped twice in 0.3% acid alcohol (70% ethanol with 0.3% concentrated HCl), rinsed in running tap water, rinsed in Scott's tap water substitute (0.2% (w/v) sodium bicarbonate/2% magnesium sulphate (w/v) in dH_2O), rinsed in running tap water, dipped in eosin for 30 seconds, then rinsed for a final time in running tap water. They were then dehydrated by immersion in 50%, 70%, 80%, 90% and 100% IMS for 30 seconds each, cleared with two 5 minute soaks in Histo-Clear and mounted in DPX mounting medium. Stained samples were imaged with an EVOS Core XL microscope.

2.21.6 Safranin-O staining

Deparaffinised and rehydrated sections were immersed in 0.1% (w/v) Safranin O solution for 5 minutes then dehydrated by immersion in 50%, 70%, 80%, 90% and 100% IMS for 30 seconds each. They were then cleared with 2 x 5 minute soaks in Histo-Clear and mounted in DPX mounting medium. Stained samples were imaged with an EVOS Core XL microscope.

2.22 Immunocytochemistry

For intracellular epitopes (such as SOX9) samples were first permeabilised by incubation with 0.1% Triton-X at RT for 15 minutes. All samples were blocked for 2 hours with 2% BSA prior to staining. They were then incubated with primary antibody diluted in 0.1% BSA (at manufacturer recommended concentrations) overnight at 4°C with gentle rocking, followed by 3 x 5 minute washes in DPBS. Samples were then incubated with secondary antibody (diluted 1:500 in 0.1% BSA) for 2 hours (monolayer cells) or ≥4 hours (hydrogels) at RT with gentle rocking. 3 x 5 minute washes in DPBS were followed by incubation with 4',6-diamidino-2-phenylindole (DAPI) at a concentration of 0.5 µg/mL for 10 minutes (monolayer cells) or 30 minutes (hydrogels). Finally, 3 x 5 minute washes in DPBS were performed and samples were stored at 4°C in DPBS prior to imaging. Gels were imaged in situ with a laser confocal microscope (Olympus FLUOVIEW FV1200) and scans were taken at 9 µm intervals.

2.23 Statistical analysis

Analysis was performed using GraphPad Prism V6.01 and differences with a P-value of less than 0.05 ($p<0.05$) were considered significant. For individual experiments with >3 technical repeats values of gene expression, sGAG, DNA and sGAG/DNA were compared across groups using an ordinary one-way ANOVA with Tukey correction and comparison of column means. Where data from 3 independent experiments were available the mean of the technical repeats was used to calculate an overall mean for the 3 experiments; these values were then compared using an ordinary one-way ANOVA with Tukey correction and comparison of column means.

In some experiments, such as the Wnt platform in chapter 3, more than one variable was changed (in this case both substrate and incubation time). Where numbers of repeats were the same for each group, values of gene expression, sGAG, DNA, sGAG/DNA and metabolic activity were compared across groups using a regular two-way ANOVA with comparison of column means, with Tukey correction for multiple comparisons. In some cases, the number of repeats varied slightly for each group and in these cases an ordinary one-way ANOVA was performed instead, with Tukey correction and comparison of column means.

For comparison of paired samples from Alamar Blue assays (e.g. where an assay was performed on the same sample on days 9 and 12), a two-tailed paired T-test was performed.

Chapter 3

A 3D hESC chondrogenic model with an immobilised Wnt platform

3.1 Introduction

The stem cell niche is a local microenvironment, which provides the biochemical and biophysical cues necessary for the maintenance of properties such as self-renewal and pluripotency (S. J. Morrison and Spradling 2008). Signalling molecules, either secreted or membrane-bound on supporting cells, are presented in a highly controlled manner and influence factors such as proliferation, daughter cell fate, migration, morphology and cell death. As cells migrate away from the niche and its signals, they begin to differentiate in response to new environmental cues. Wnt ligands have been shown to play a key role in a number of stem cell niches – both embryonic and adult (Mills, Szczerkowski, and Habib 2017; Lowndes et al. 2016; Jones and Wagers 2008). In 2011, Berge et al. reported that mESC colonies showed enhanced pluripotent morphology and self-renewal capacity in response to increased Wnt signalling. Furthermore, this effect was blocked by Wnt antagonists Fx8CRD (which sequesters Wnt ligands) and inhibitor of Wnt production 2 (IWP2) (which blocks porcupine acetyltransferase and subsequent production of active endogenous Wnt), but could be rescued by addition of WNT3A to the culture medium (ten Berge et al. 2011). This blocking of Wnt activity led to differentiation towards an epiblastic stem cell fate and diminished expression of the pluripotency markers. Thus, in mESC Wnt signalling appears to play a major role in maintaining plasticity.

Highly conserved across species, Wnt has a key role in the self-renewal of numerous mammalian tissues (Clevers, Loh, and Nusse 2014). Wnt proteins are around 350 amino acids long and form a family with 19 members described to date, which all share the following key characteristics: multiple cysteine residues, a conserved serine residue for acetylation and lipidation, and a peptide sequence for secretion (Mills, Szczerkowski, and

Habib 2017). Although able to stimulate cells via three different signalling pathways, Wnt influences pluripotency and stem cell renewal through activation of the non-canonical Wnt/ß-catenin pathway upon association with the membrane-bound receptors LRP6 and FZD. This triggers an intracellular signalling cascade which results in inhibition of the ß-catenin destruction complex, stabilisation of ß-catenin and its subsequent translocation to the nucleus where it binds to TCF, which in turn upregulates transcription of target genes (figure 1-12) (Clevers, Loh, and Nusse 2014).

In vivo, the lipidation of Wnt proteins and their resulting hydrophobicity limits their mobility through tissue fluid and renders their effects short-ranged – within as little as one- to two-cell diameters (Clevers, Loh, and Nusse 2014). Therefore, in the stem cell niche Wnt molecules are presented to target cells via carrier proteins for long distance signalling, or on the surface of paracrine cells for more local effects. There is also evidence to suggest that the orientation of the ligand is key to its function. Association of mESC with immobilised WNT3A resulted in accumulation of LRP6 and ß-catenin destruction-complex-associated proteins at the point of contact. These Wnt-associated cells then underwent asymmetrical division with the cleavage plane in line with the bead upon which the Wnt was immobilised. Following cell division, proximal daughter cells retained pluripotency, whereas distal ones showed reduced expression of pluripotent markers (Habib et al. 2013). In a later study Wnt was immobilised onto aldehyde-coated surfaces, such as glass and PCL, and cells (both mESC and hBMSC) seeded onto these modified materials demonstrated higher levels of Wnt signalling and a concomitant increase in pluripotency markers. In addition, BMSC migrating away from the Wnt-modified surface into collagen gels under osteogenic culture conditions, expressed higher levels of bone markers with increasing distance from the Wnt

signal, while those near to the polymer retained multipotency, as evidenced by high *STRO-1* expression (Lowndes et al. 2016). This work resulted in a published a protocol which outlines how to construct what is termed a "Wnt platform" onto beads or glass surfaces in order to recreate a stem cell niche *in vitro*. It was demonstrated that this platform could maintain local stem cell populations, while generating more distant populations of differentiating cells (Lowndes, Junyent, and Habib 2017). Owing to the success of this system with an osteogenic model, the decision was taken apply to a chondrogenic model, using hESC and fibrin hydrogels. Fibrin was chosen as the biomaterial in this study, as it supports good viability of hESC, whereas collagen was previously found to result in high levels of cell death (data not shown).

One barrier to the clinical application of hESC-derived chondroprogenitors is the possible presence of residual pluripotent stem cells with the potential to form teratomas *in vivo*. It was hoped that the application of a modified version of the Wnt platform described above would have the dual effects of enhancing proliferation and inducing asymmetrical cell division in any remaining pluripotent hESC in order to mitigate the possibility of teratoma formation for potential future clinical applications.

3.2 Aims

The primary aims of this chapter were:

- To define a directed differentiation protocol for hESC using Wnt signalling and 3D culture
- To assess the effects of both the 3D model and the Wnt signalling on chondrogenic gene and protein expression
- To assess how Wnt signalling affects the migration of cells into hydrogels

3.3 Methods

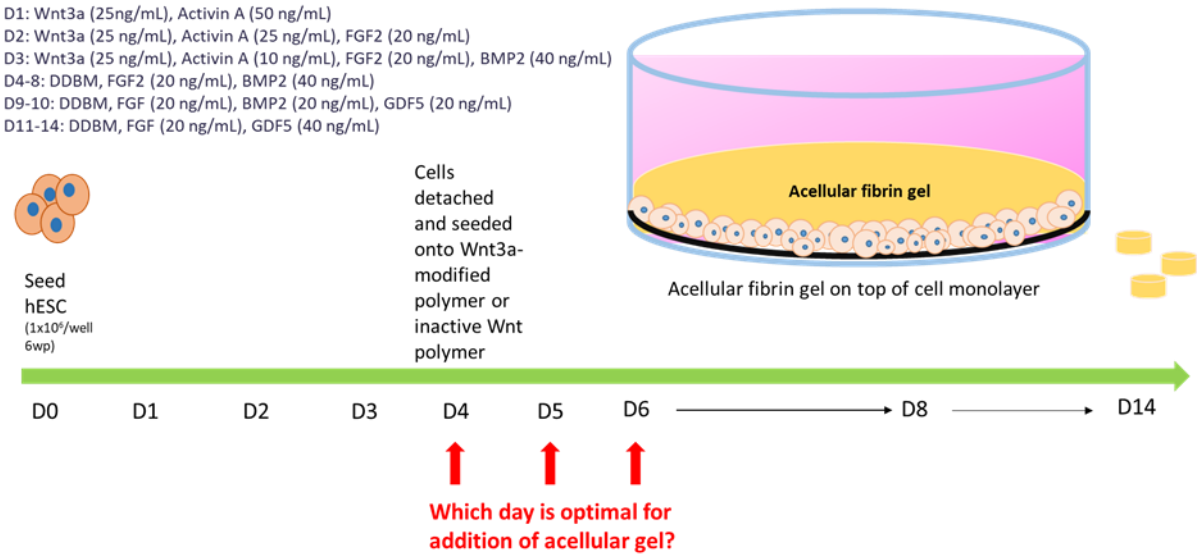

Figure 3-1. Schematic summary of the experimental procedure for chapter 3. A DPP was initiated on D1 using MAN7 hESC. The DDP proceeded to D14, with addition of a 200 µL acellular fibrin hydrogel on top of the differentiating monolayer of cells on either D4, D5 or D6. Medium was changed daily and supplemented appropriate growth factors. Aprotinin (20 µg/mL) was added to medium once gels were in place.

The experimental design for this chapter is summarised in figure 3-1. A directed DPP was initiated on MAN7 hESC as described in chapter 2.3. PCL discs were prepared and modified with WNT3A as described in chapter 2.7. On day 4 of the DPP, cells were detached and seeded onto Wnt-modified PCL discs in 48-well plates. For a 1:4 split, one confluent well of day 4 cells was seeded into 8 wells of a 48-well plate. For cell-only control samples (cell only), day 4 cells were split 1:4 into 6-well plates and then split 1:4 again on day 8 and cultured on TCP, as with a normal DDP. DTT-inactivated WNT3A polymers (DTT) and polymers incubated with 5% BSA instead of WNT3A (BSA) were also included as controls. The purpose of the pilot experiment was to determine the optimal day for the addition of

the acellular fibrin gel. Three initial experiments were conducted, in which gels were placed on top of the Wnt platform/cells on day 4, 5 or 6. For all subsequent experiments gels were added on day 5. The DPP was then continued until day 14 and, for all wells containing hydrogels, the medium was supplemented with aprotinin at a concentration of 20 µg/mL in order to limit protease degradation of the gels. In one experiment of the pilot study, a control group of cells was detached on day 11 and encapsulated in 200 µL cellular fibrin gels as described in chapter 2.4. These hydrogels were then cultured until day 14 in the same way as the other groups. This was done in order to rule out the possibility that the fibrin was responsible for the differences observed between experimental groups and cell only controls.

On days 7/9 and 12 of the pilot experiments, an Alamar Blue assay was performed (see 2.19). For all experiments, samples were taken on day 9 and again on day 14 when experiments were terminated. For Alamar Blue, PicoGreen and DMMB assays, there are no cell only controls as the monolayer DDP is performed in 6-well plates (as opposed to the 48-well plates in which the Wnt platform was cultured) and samples were, therefore, not comparable. Attempts to perform a monolayer DDP in 48-well plates were not successful, as cells quickly became over-confluent and lower seeding densities resulted in poor viability. For gene expression analysis, however, cell only controls were possible as RNA levels are normalised prior to cDNA synthesis. Samples were either snap frozen or fixed with 10% NBF. Gene expression analysis, PicoGreen assay, DMMB assay and ICC were performed on day 9 and day 14 samples. For gene expression analysis, RNA was isolated from the entire construct including the polymer base. This was followed by cDNA synthesis (2.13) and RT-qPCR (2.14). For PicoGreen and DMMB assays, however, the polymer was removed and the

hydrogel washed with DPBS prior to digestion with Proteinase K. For ICC polymers were removed after staining and gels were imaged with a laser confocal microscope (Olympus FLUOVIEW FV1200) from the bottom up. Scans were taken at 9 µm intervals for a distance of ≤300 µm. Images were then constructed using Imaris Image Analysis software. ICC and gene expression analysis was also performed on samples from three independent experiments. Cell migration was measured with Image J software using the images created with Imaris and the scale bars provided (figure 3-2).

Statistical analysis was performed as described in chapter 2.23.

3.4 Results

3.4.1 Determination of optimal day for addition of hydrogels

The purpose of the pilot study was to determine at which stage in the protocol to add the fibrin gels. The hydrogel was added either on day 4 (the same day that cells were seeded), day 5 or day 6.

3.4.1.1 Gene expression analysis

Gene expression analysis demonstrated elevated *ACAN* levels in D9 cultures compared to D14 in all three experiments. When gels were added on day 4, *ACAN* expression of the whole construct (including any cells remaining on the polymer base) peaked in the D9 Wnt and D9 DTT groups (figure 3-2 A). *ACAN* expression in D9 Wnt was significantly greater than in D14 Wnt ($p<0.05$), D9 BSA ($p<0.01$) and D14 cell only ($p<0.001$). In D9 DTT it was significantly greater than in D9 BSA ($p<0.05$) and D14 cell only ($p<0.01$). A similar pattern was observed for *ACAN* expression when gels were added on day 5 and 6, although expression was generally lower (figure 3-2 A-C). When gels were added on day 5, D9 BSA, D9 DTT and D14 BSA all had significantly greater expression than in D14 cell only ($p<0.05$, $p<0.001$ and $p<0.01$ respectively). D9 Wnt also demonstrated significantly higher expression than D14 Wnt ($p<0.05$). When gels were added on day 6 *ACAN* expression was significantly higher in D9 Wnt than in D9 DTT ($p<0.0001$), D9 BSA ($p<0.001$), D14 encapsulated cells ($p<0.0001$), D14 cell only ($p<0.0001$), D14 BSA ($p<0.001$), D14 DTT ($p<0.001$) and D14 Wnt ($p<0.001$).

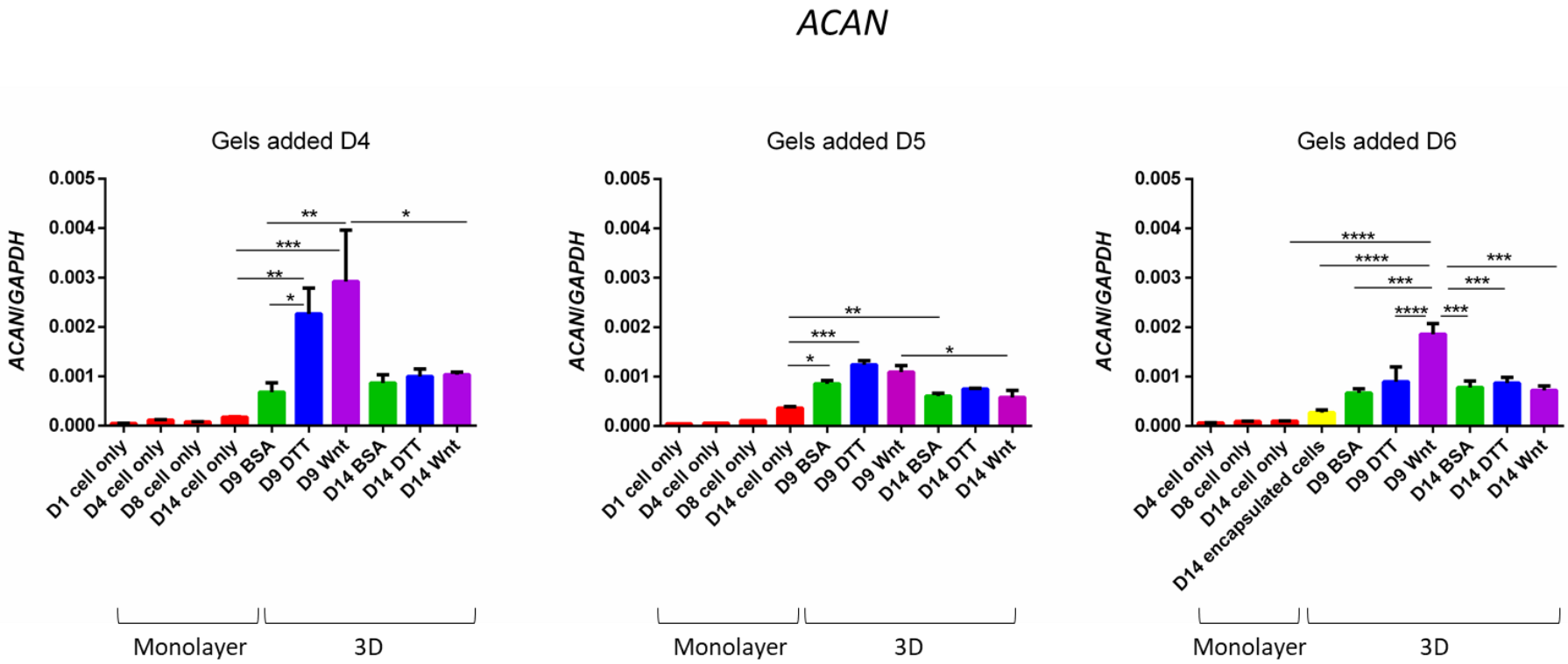

Figure 3-2. Aggrecan expression peaks on day 9 and is higher in all 3D constructs than in cell only controls. Gene expression is relative to *GAPDH* ($2^{-\Delta Ct}$). Data are expressed as the mean ± standard error, n=3-5 (technical repeats), *p<0.05, **p<0.01, ***p<0.001, ****p<0.0001.

In contrast, *COL1A1* gene expression was elevated at D14 in 2 out of 3 of the experiments (figure 3-3 A and B). Expression was not measured in one experiment due to insufficient cDNA resulting from low RNA yield. When gels were added on day 4, all day 14 constructs had significantly higher expression than D14 cell only (D14 BSA ($p<0.0001$), D14 DTT ($p<0.001$) and D14 Wnt ($p<0.0001$)) and significantly higher expression than their D9 counterparts ((D14 BSA ($p<0.0001$), D14 DTT ($p<0.001$) and D14 Wnt ($p<0.0001$). In addition, D14 DTT had significantly higher *COL1A1* expression than D14 cell only ($p<0.0001$), D9 DTT ($p<0.0001$), D14 BSA ($p<0.001$) and D14 Wnt ($p<.001$).

COL2A1 expression (figure 3-4) again peaked on day 14 in all experiments and was often significantly higher in day 14 3D samples than in day 14 cell only controls. When gels were added on day 4, all day 14 constructs had significantly higher expression than D14 cell only (D14 BSA ($p<0.0001$), D14 DTT ($p<0.0001$) and D14 Wnt ($p<0.0001$)) and significantly higher expression than their D9 counterparts ((D14 BSA ($p<0.0001$), D14 DTT ($p<0.0001$) and D14 Wnt ($p<0.0001$). In addition, D14 Wnt had significantly higher expression than D14 DTT ($p<0.05$). When gels were added on day 5 D14 DTT had significantly higher *COL2A1* expression than D14 cell only ($p<0.0001$), but although expression in D14 was generally higher, there were no other significant differences. When gels were added on day 6, D14 BSA showed significantly higher expression than D14 cell only ($p<0.05$), D14 encapsulated cells ($p<0.01$) and D9 BSA ($p<0.001$). D14 DTT also had significantly higher expression than D14 encapsulated cells ($p<0.05$). In the second two experiments, where gels were added on days 5 or 6, there were no significant differences between D14 polymer-based groups.

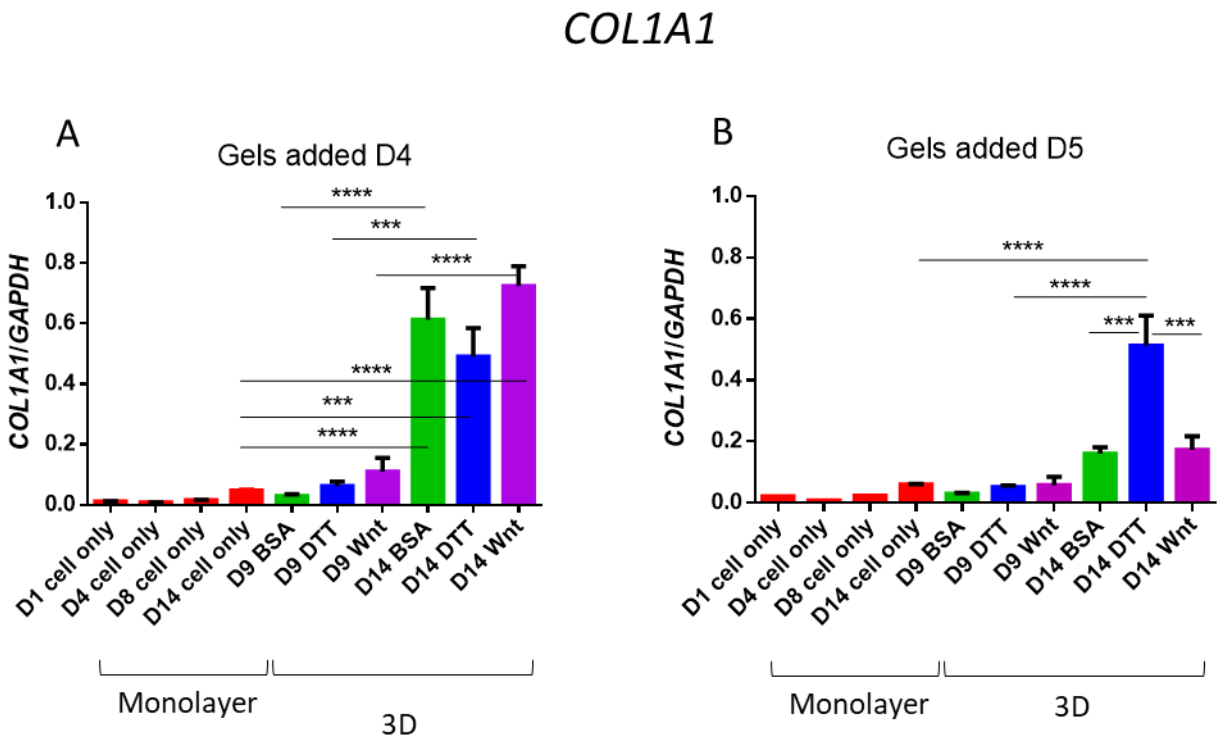

Figure 3-3. Collagen type I expression peaks on day 14 and is higher in all 3D constructs than in cell only controls. Gene expression is relative to *GAPDH* ($2^{-\Delta Ct}$). Data are expressed as the mean ± standard error, n=3-5 (technical repeats), *p<0.05, **p<0.01, ***p<0.001, ****p<0.0001

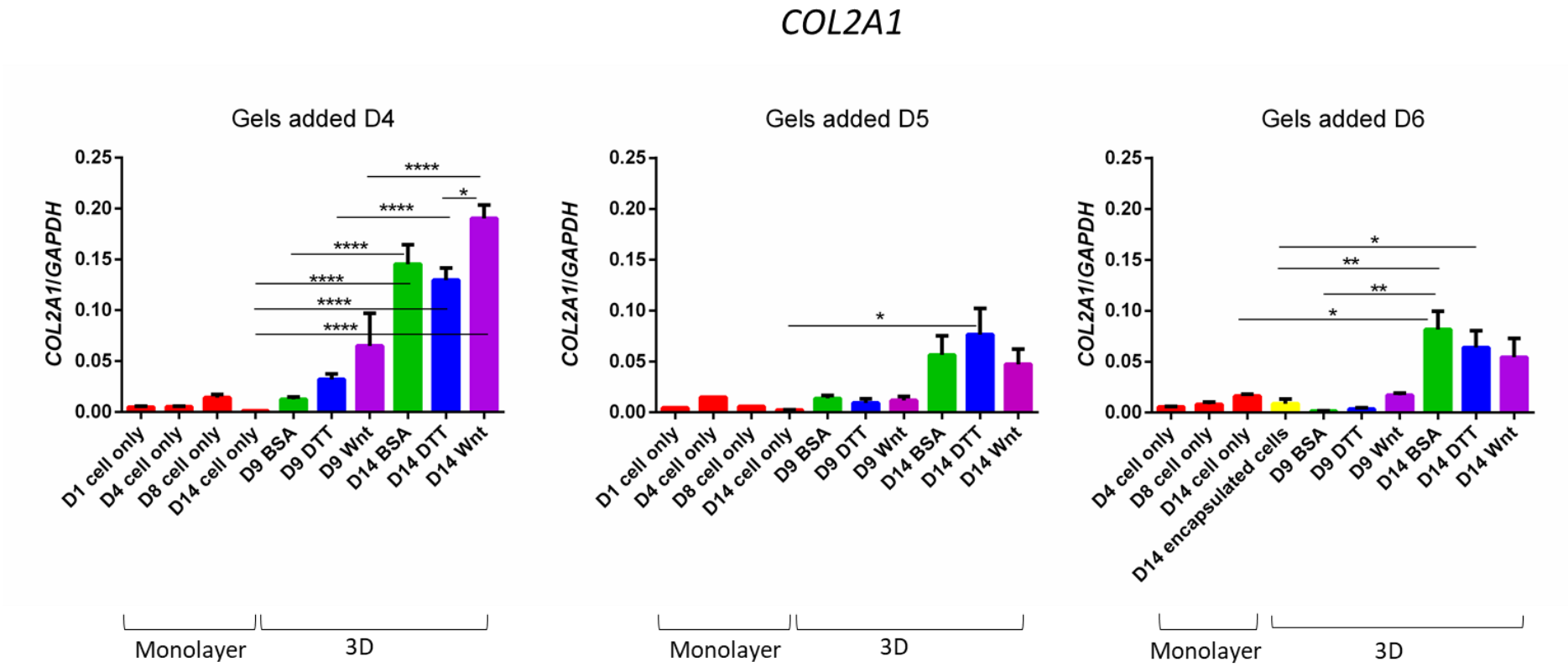

Figure 3-4. Collagen type II expression peaks on day 14 and is higher in all 3D constructs than in cell only controls. Gene expression is relative to *GAPDH* ($2^{-\Delta Ct}$). Data are expressed as the mean ± standard error, n=3-5 (technical repeats), *p<0.05, **p<0.01, ***p<0.001, ****p<0.0001.

SOX9 expression (figure 3-5) was always higher in polymer-based groups than in cell only controls and D14 encapsulated cells. When gels were added on day 4 expression in D9 Wnt was significantly higher than in D14 cell only ($p<0.05$) and D9 BSA ($p<0.05$). When gels were added on day 5, although expression was generally higher, there were no significant differences. When gels were added on day 6, *SOX9* expression was significantly higher in D9 BSA than in D14 cell only ($p<0.01$) and D14 encapsulated cells ($p<0.05$). It was also significantly higher in D9 DTT and D14 DTT than in D14 cell only ($p<0.05$ and 0.001 respectively).

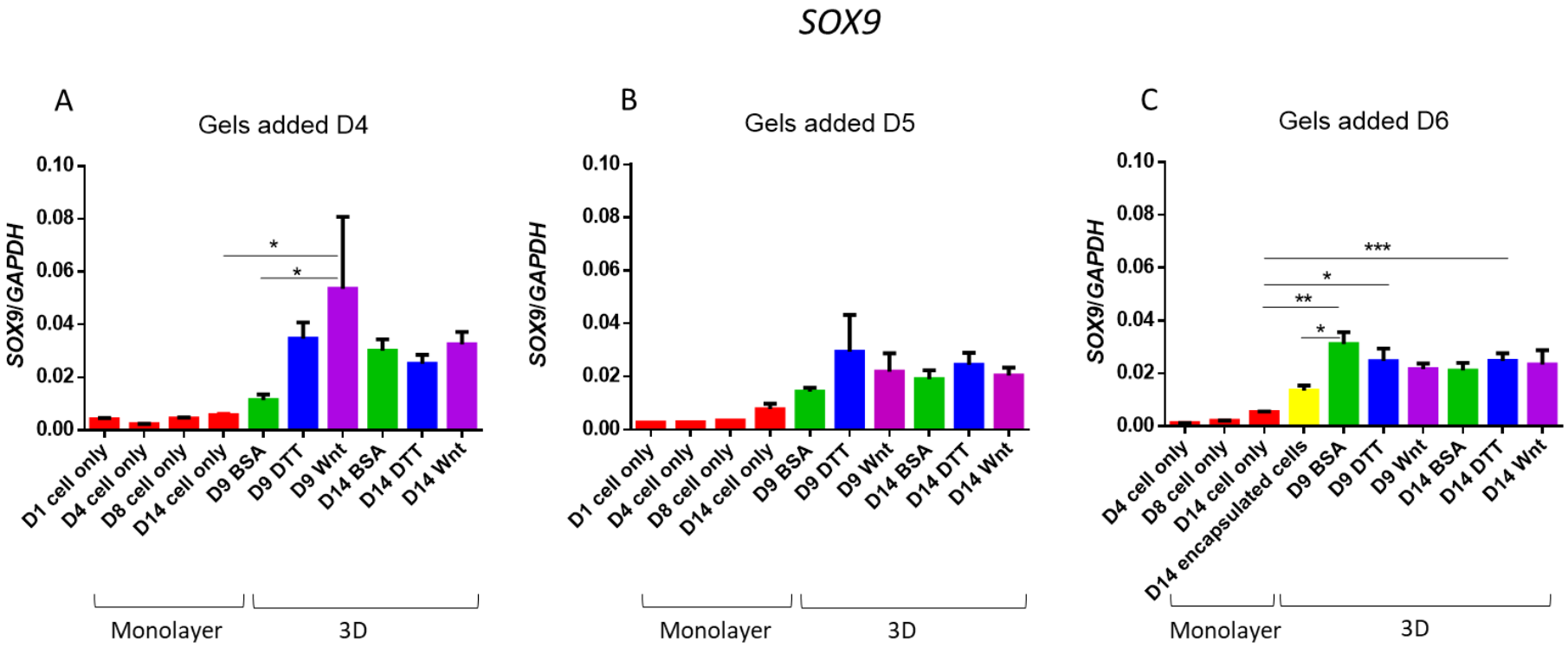

Figure 3-5. *SOX9* expression peaks on day 9 and is higher in all 3D constructs than in cell only controls. Gene expression is relative to *GAPDH* ($2^{-\Delta Ct}$). Data are expressed as the mean ± standard error, n=3-5 (technical repeats), *p<0.05, **p<0.01, ***p<0.001, ****p<0.0001.

3.4.1.2 Metabolic activity, DNA and sulphated GAG

Results show that metabolic activity increases with time in culture throughout the 14-day protocol. Overall, metabolic activity was lower in constructs where the hydrogel was added on D4 in comparison to when it was added on day 5 or 6, as evidenced by the lower levels of fluorescence on day 12 (figure 3-6). A lower overall metabolic activity may be an indication of reduced cell viability resulting from the addition of a gel so soon after cell seeding. Increased metabolic activity in each well by day 12 suggests that cell numbers increased with prolonged time in culture, as expected. When gels were added on day 4 (figure 3-6 A) D12 DTT had a significantly higher mean fluorescence than D7 DTT ($p<0.01$) and D12 Wnt was significantly higher than D7 Wnt ($p<0.01$). When gels were added on day 5, D12 BSA had significantly higher fluorescence than D9 BSA ($p<0.001$) and D12 DTT ($p<0.05$). In addition, D12 Wnt and D12 DTT had significantly higher fluorescence than their D9 counterparts ($p<0.05$ for both). When gels were added on day 6 the pattern was very similar, although the difference between day 12 and day 9 samples was more pronounced, with all day 12 groups having significantly higher metabolic activity than corresponding day 9 samples (D12 Wnt $p<0.01$, D12 DTT $p<0.01$ and D12 BSA $p<0.001$). In this experiment D12 Wnt also had significantly higher activity than D12 DTT ($p<0.05$), suggesting that the Wnt-modified polymer enhanced proliferation.

DNA assays support the conclusions drawn from the metabolic activity assays: D14 samples generally had higher levels of DNA (figure 3-7), indicating enhanced proliferation throughout the protocol. Unexpectedly, when gels were added on day 4 (figure 3-7 A), D9 DTT had significantly higher DNA content than D9 BSA ($p<0.001$) and D9 Wnt ($p<0.001$) and similar levels to day 14 samples. D14 DTT also had significantly more DNA than D14 BSA

($p<0.05$). As expected though, D14 Wnt had significantly more DNA than D9 Wnt ($p<0.01$). As with metabolic activity, DNA content was generally much higher in constructs when gels were added on day 5 (figure 3-7 B). Here day 14 samples had more DNA than their day 9 counterparts, but this difference was only significant in D12 DTT ($p<0.05$). When gels were added on day 6 (figure 3-7 C), all day 14 samples had significantly higher DNA content than corresponding day 9 samples (D14 BSA $p<0.01$, D 14 DTT $p<0.01$ and D14 Wnt $p<0.0001$), but the overall content was much lower than constructs in which gels were added on day 5, which suggests that addition of an acellular hydrogel at this point is more conducive to prolonged cell viability.

Patterns for sulphated GAG concentration in the pilot experiment (figure 3-8) very closely match the patterns observed for DNA content, suggesting that changes in levels of sulphated GAG were largely a result of variations in cell number. When gels were added on day 4 (figure 3-8 A), D9 DTT had significantly higher concentrations of sulphated GAG than D9 BSA and D9 Wnt (both $p<0.001$). D14 BSA and D14 Wnt both had significantly higher concentrations than their day 9 counterparts ($p<0.01$ and $p<0.0001$ respectively). When gels were added on day 5 (figure 3-8 B), day 14 concentrations were generally higher, but only D14 DTT was significantly higher than D9 DTT ($p<0.05$) and the same was true when gels were added on day 6 (figure 3-8 C), where D14 DTT was again significantly higher than D9 DTT ($p<0.01$). Once normalised to DNA content, there were no significant differences in sulphated GAG concentrations between groups (figure 3-8 D-E), except when gels were added on day 6 – here D9 Wnt had significantly higher concentrations than D9 BSA ($p<0.01$), D9 DTT ($p<0.001$) and D14 Wnt ($p<0.001$).

Based on these results, the decision was made to add hydrogels to cell/polymer constructs on day 5. Although chondrogenic gene expression was higher when gels were added on day 4, far greater cell numbers were observed when they were added on day 5.

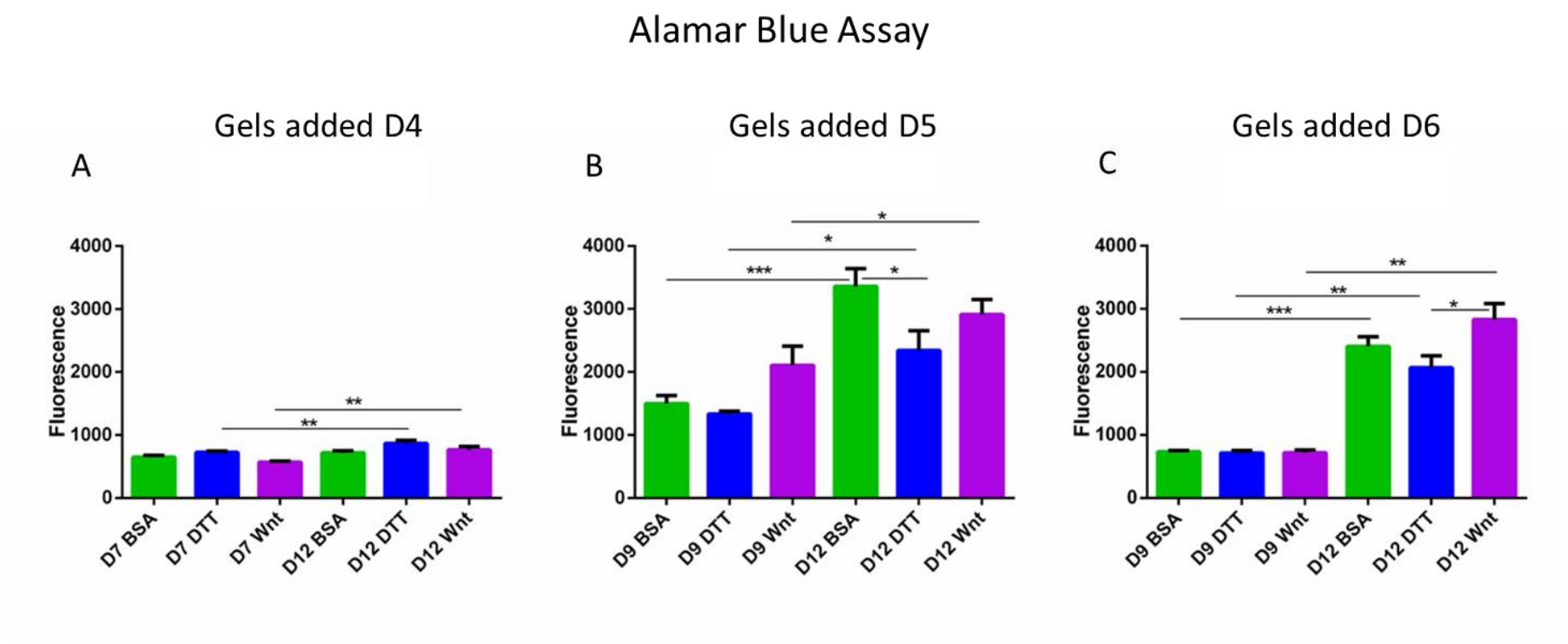

Figure 3-6. Day 12 groups generally have higher metabolic activity than day 9 groups. Metabolic activity was quantified using Alamar Blue assay. Overall, metabolic activity was higher when gels were added the day after cell seeding. Data are expressed as the mean ± standard error of fluorescence in arbitrary units, n=5-8 (technical repeats), *p<0.05, **p<0.01, ***p<0.001.

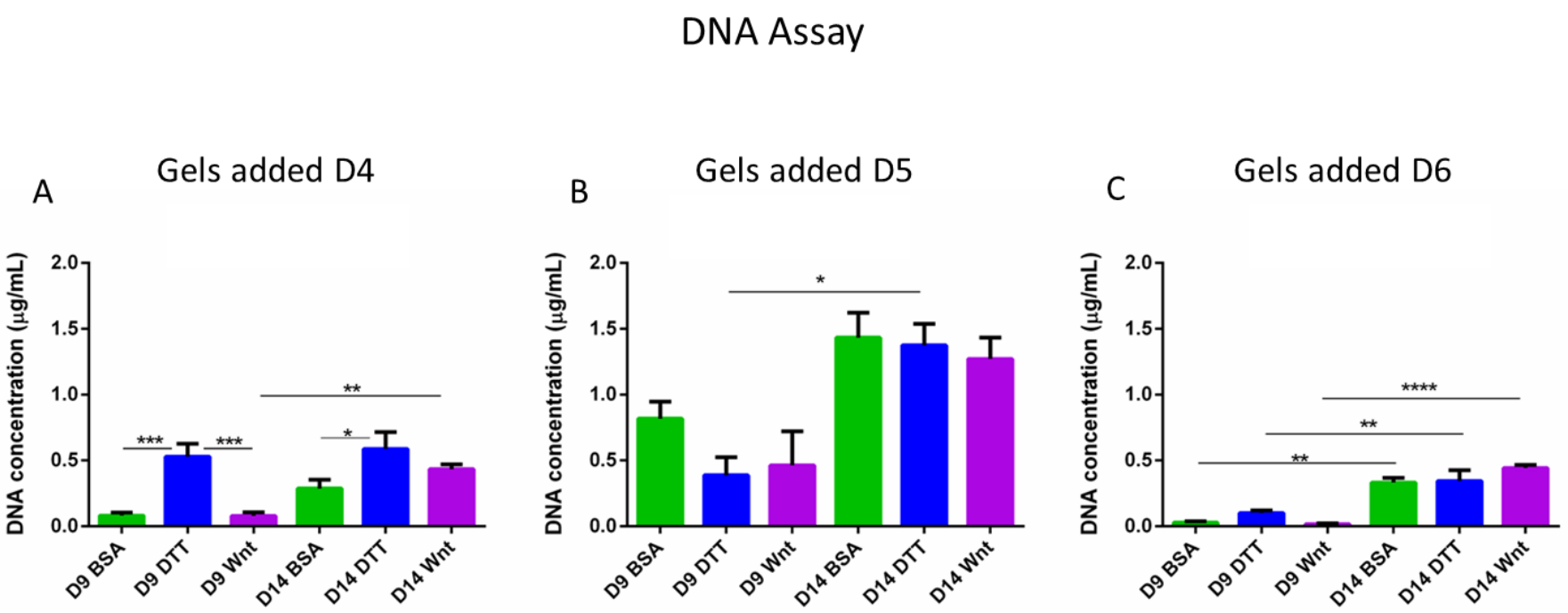

Figure 3-7. Day 14 groups generally have higher DNA content than day 9 groups. DNA was quantified using the PicoGreen assay. Overall, DNA content is higher in when gels were added on day 5. Data are expressed as the mean ± standard error of fluorescence in arbitrary units, n=4-5 (technical repeats), *p<0.05, **p<0.01, ***p<0.001, ****p<0.0001.

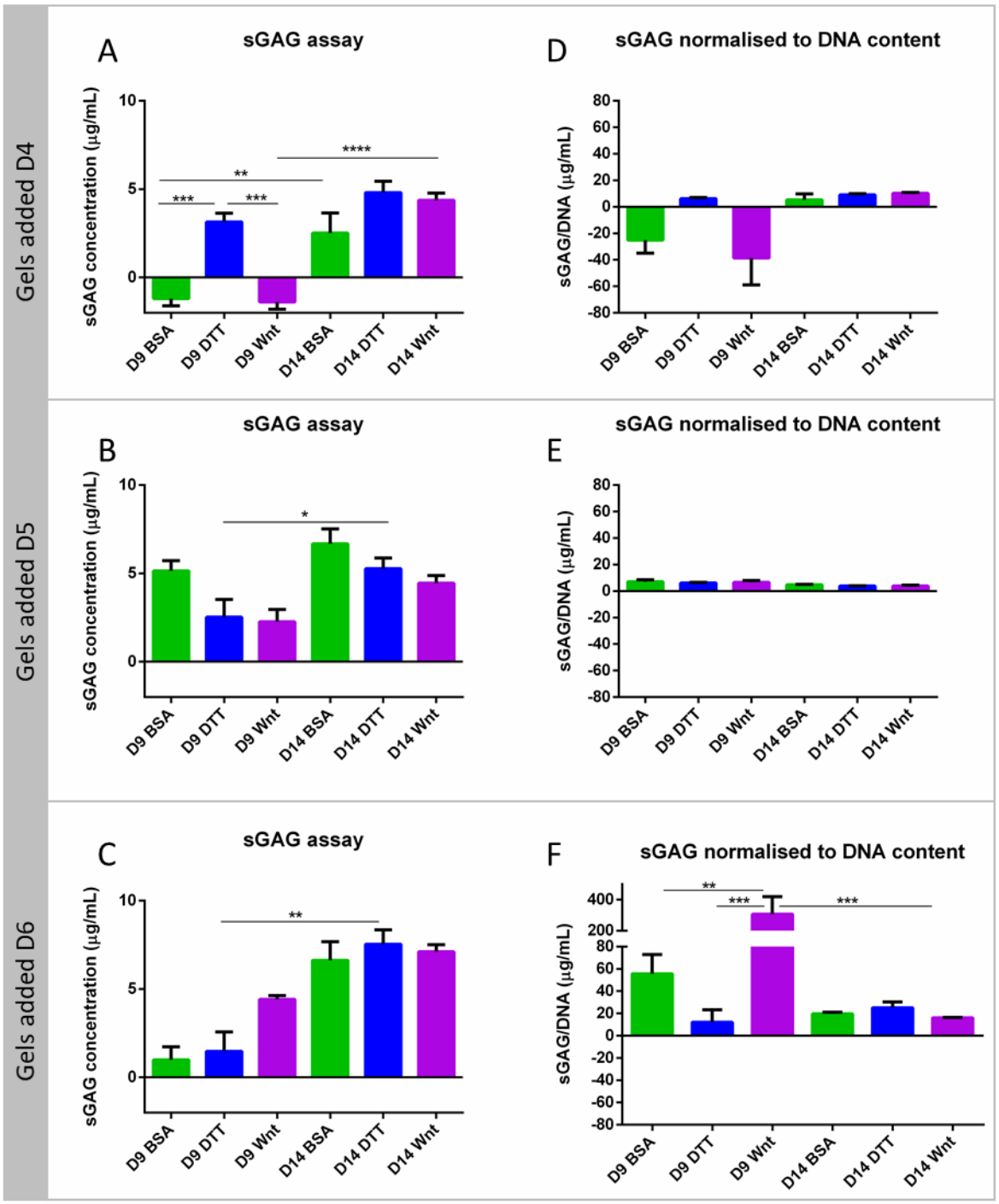

Figure 3-8. Levels of sulphated GAG were elevated in day 14 samples prior to DNA normalisation. sGAG was quantified using the DMMB assay. Normalised data (D-F) are expressed as a ratio of sGAG/DNA. Data are expressed as the mean ± standard error, n=4-5 (technical repeats), *p<0.05, **p<0.01, ***p<0.001.

3.4.2 Effects of Wnt3a when hydrogels are added on day 5

In pilot experiments chondrogenic gene expression was higher in constructs where the hydrogel was added on day 4. However, results of DNA and Alamar Blue assays indicate that adding the gel on day 5 was more conducive to cell survival. Therefore, in subsequent experiments the decision was taken to add the fibrin on day 5.

3.4.2.1 Gene expression analysis

For subsequent experiments, gels were added on day 5; this was repeated three more times and for two of these repeats, gene expression analysis was performed (figure 3-9). There were no significant differences in *ACAN* expression (figure 3-9 A) between any of the groups and mean relative expression was quite low (<0.002). For C*OL2* expression (figure 3-9 B) D14 BSA was significantly higher than D14 cell only ($p<0.05$), but there were no other significant differences between groups. *SOX9* expression (figure 3-9 C) was generally higher in D14 groups and was significantly higher in D14 BSA than in D9 BSA ($p<0.05$) and D14 cells ($p<0.01$). In addition, expression was significantly higher in D14 Wnt than in D9 Wnt ($p<0.05$) and in D14 cell only ($p<0.01$).

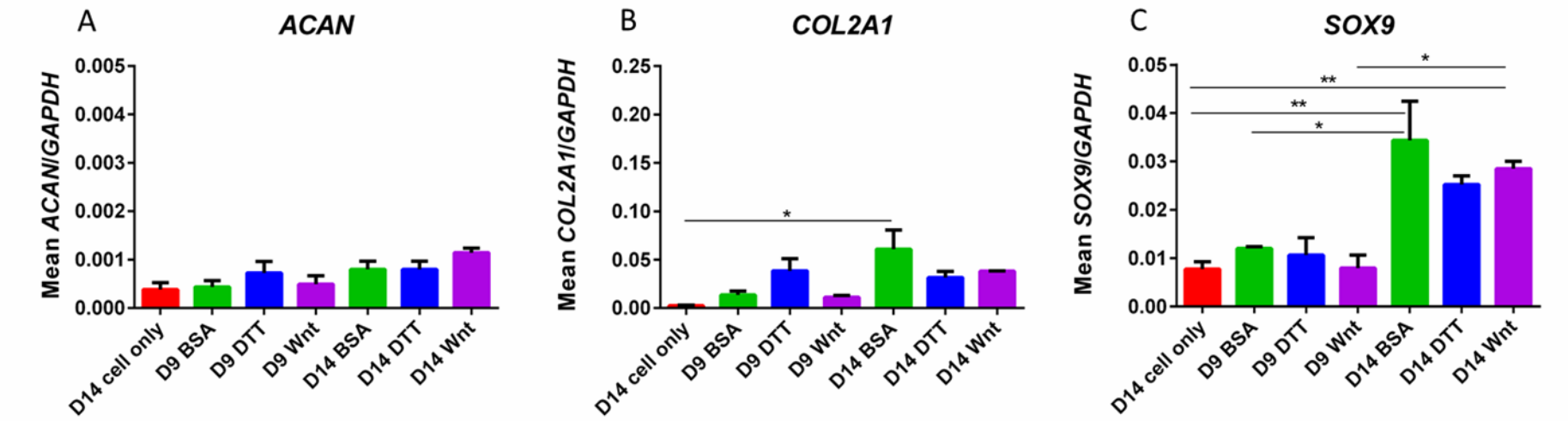

Figure 3-9. Immobilised WNT3A does not increase chondrogenic gene expression. Mean expression of *ACAN* (A), *COL2A1* (B) and *SOX9* (C) from three independent experiments, where hydrogels were added to cells on day 5. Data are expressed as the mean ± standard error, N=3, *p<0.05, **p<0.01.

3.4.2.2 Immunocytochemistry

SOX5 and SOX9 staining of constructs (figure 3-10 A) revealed that both proteins were more abundant in D9 Wnt groups compared to D9 BSA and D9 DTT. Image J software was used to quantify the fluorescent signal from these images (figure 3-10 B and C) and statistical analysis of the resulting values showed that the SOX5 signal in D9 Wnt was significantly higher than that of D9 DTT ($p<0.05$). In addition, the SOX9 signal of D9 Wnt was significantly greater than that of both D9 BSA ($p<0.05$) and D9 DTT ($p<0.05$). However, by day 14 there was little discernible difference between groups and no significant differences in mean fluorescence intensity values (figure 3-10). Although a strong SOX5 or SOX9 signal was often accompanied by a strong DAPI signal, there were numerous instances in the BSA and DTT groups where DAPI intensity was high, but SOX5 and SOX9 signals were very low (figure 3-10 A). This suggests that enhanced expression of the two chondrogenic proteins was not merely a result of an increase in cell numbers. DAPI staining (figure 3-10 D) was again significantly stronger overall in D9 Wnt groups compared to D9 DTT ($p<0.05$), indicating that these constructs had higher levels of DNA and, therefore, greater cells numbers. By day 14 these differences were again no longer discernible.

Merged images of SOX5 and SOX9 staining (figure 3-11) show that differentiated cells tended to migrate further than undifferentiated cells. This is evidenced by the band of SOX5- and SOX9-positive cells which can be seen in the top layer of the DAPI-stained cell population. This was particularly noticeable in D9 Wnt groups and was not observed in D9 BSA and D9 DTT, where SOX5 and SOX9 staining was quite weak. By day 14, this effect could be seen to some extent in all groups, but was again more evident in D14 Wnt where a thicker band of differentiated cells was clearly visible.

Supplementary figure 6 shows COL2, SOX5 and SOX9 staining of positive and negative (secondary antibody only) controls, which were monolayer D14 hESC-derived chondroprogenitors. This staining confirms that primary antibodies were effective at the concentrations used. Compared to positive controls (supplementary figure 6 A), COL2 staining of 3D constructs (figure 3-12) generally gave a very weak signal for all groups and was, therefore, not carried out beyond the first repeat. OCT4 staining was also carried out for D14 constructs in the first repeat (figure 3-12 B), in order to confirm that pluripotent cells were no longer present. A very small amount of OCT4 expression can be seen in all groups, although in D14 Wnt the level does not appear to be greater than that of the negative control (incubated with secondary antibody only).

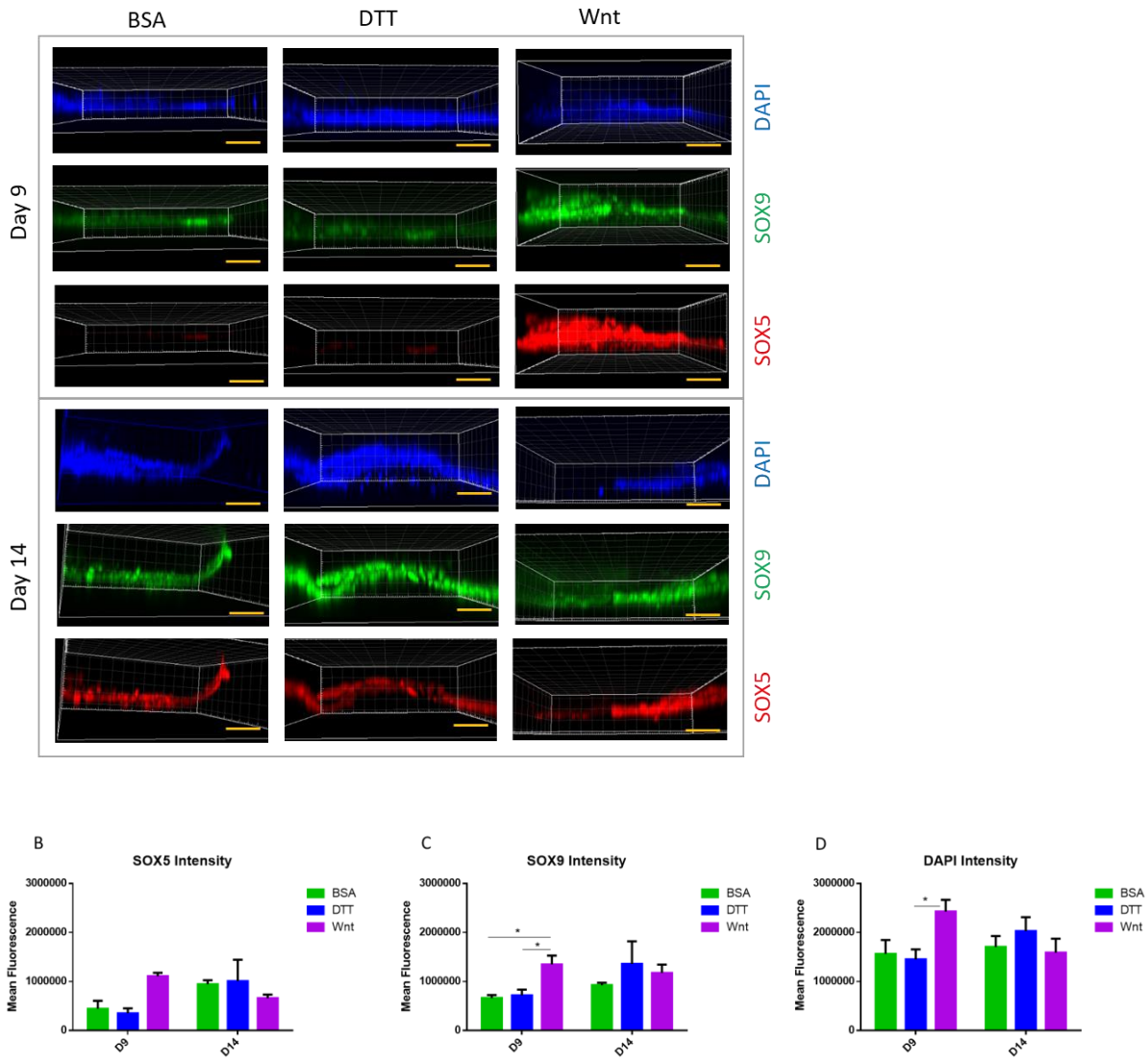

Figure 3-10. Day 9 samples express elevated chondrogenic proteins in response to WNT3A. A) Representative fluorescent images of hydrogels without the polymer base, where gels were added on day 5. Scans were taken from the bottom up every 9 µm with a laser confocal microscope, for a distance of ≤300 µm. Images were constructed using Imaris Image Analysis software. Scale bars = 100 µm. DAPI (blue), SOX5 (red), SOX9 (green). B) Mean SOX5 signal of all images from two independent experiments. N=2. C) Mean SOX9 signal of all images from three independent experiments. N=3. D) Mean DAPI signal of all images from three independent experiments. N=3. Data are expressed as the mean ± standard error (B-D).

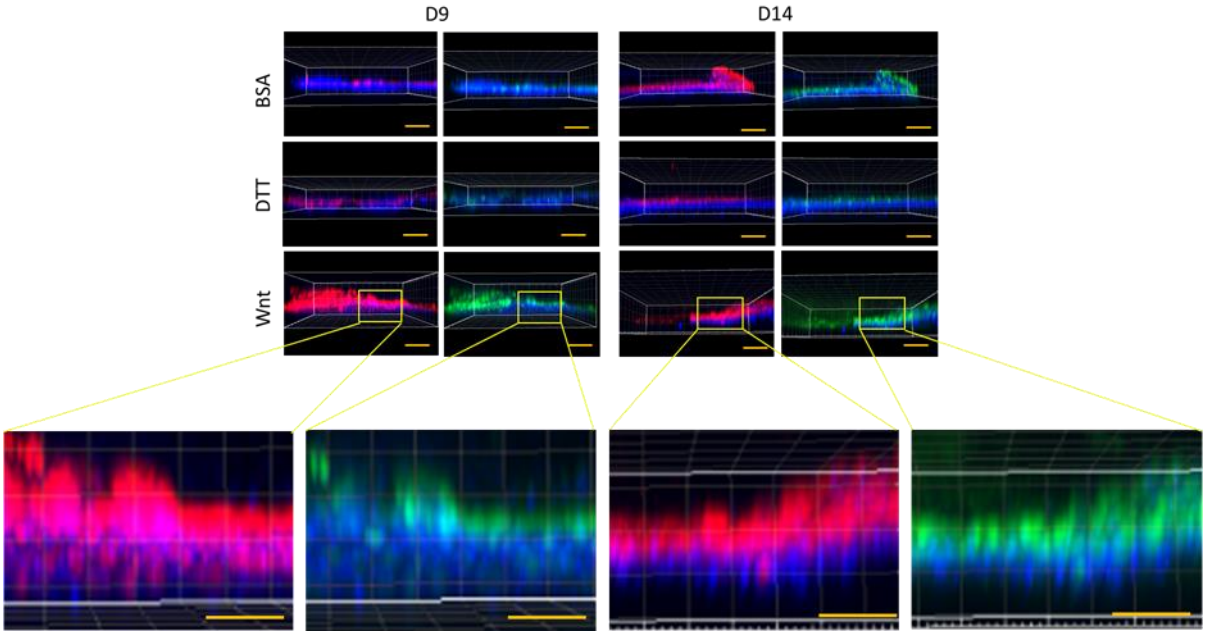

Figure 3-11. SOX5 and SOX9 staining of D9 and D14 samples merged with DAPI. Representative fluorescent images of hydrogels without the polymer base, where gels were added on day 5. Scans were taken from the bottom up every 9 µm with a laser confocal microscope, for a distance of ≤300 µm. Images were constructed using Imaris Image Analysis software. Scale bars = 100 µm. DAPI (blue), SOX5 (red), SOX9 (green).

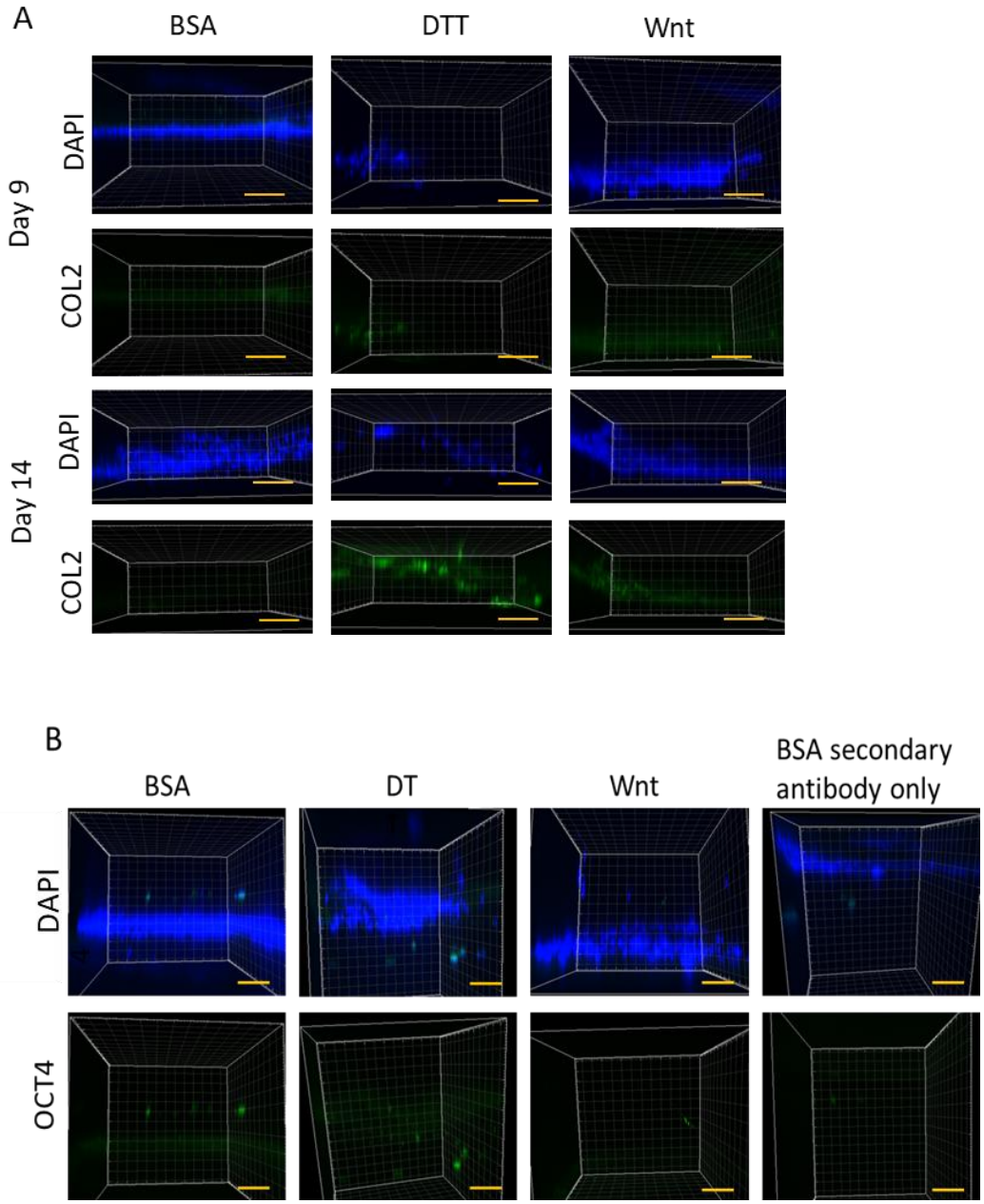

Figure 3-12. Constructs showed low expression of COL2 and OCT4. A) Representative fluorescent images of COL2 expression in D9 and D14 hydrogels from experiment 4. B) Fluorescent images of OCT4 expression in D14 hydrogels from experiment 2. Polymer bases were removed prior to imaging. Scans were taken from the bottom up every 9 µm with a laser confocal microscope, for a distance of ≤500 µm. Images were constructed using Imaris Image Analysis software. Scale bars = 100 µm. DAPI (blue), SOX9 (green).

3.4.2.3 Migration of cells into acellular fibrin hydrogels

Wnt modification resulted in greater migration in day 9 groups compared to both BSA and inactive Wnt controls. Migration of cells into acellular hydrogels was measured using all suitable images of DAPI staining, where a band of migrating cells was clearly visible in one optic plane (figure 3-13 A). The greatest migration was observed in D9 Wnt groups (figure 3-13 B), where cells moved significantly further than both D9 BSA ($p<0.01$) and D9 DTT ($p<0.01$). However, by day 14 this effect was lost and there were no significant differences between groups. In addition, cells from D14 groups migrated no further than their day 9 counterparts despite an additional 5 days in culture.

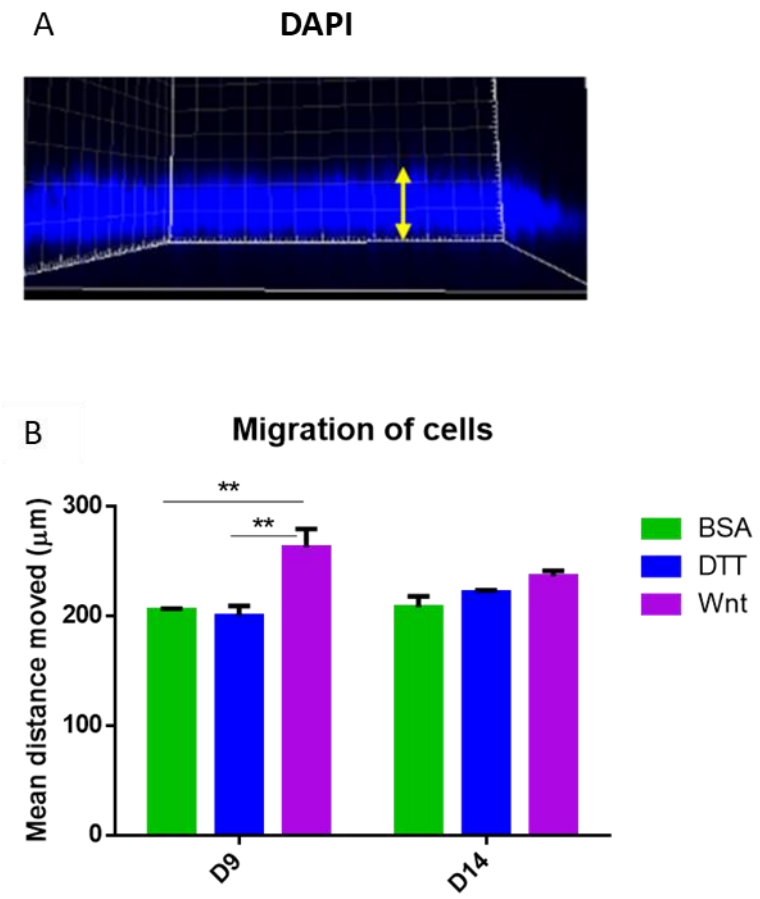

Figure 3-13. Quantification of cell migration. A) Representative image of a DAPI-stained hydrogel deemed appropriate for measuring migration of cells. Arrow indicates distance measured. In each image the maximum distance moved was measured and 2-3 gels were measured in each experiment. Distances were calculated using Image J software. B) Mean migration of cells from experiments 4, 5 and 6. N=3. Data are expressed as the mean ± standard error.

3.5 Discussion

Wnt signalling has key roles in a diverse range of cellular processes, including ESC differentiation, stem cell renewal and cancer progression. Canonical Wnt signalling has been shown to promote pluripotency in a range of stem cell types, including mESC when WNT3A was added daily to the culture medium (Anton, Kestler, and Kühl 2007; ten Berge et al. 2011; Clevers, Loh, and Nusse 2014). There is much debate over the apparent dichotomous role of Wnt signalling in maintenance of plasticity/proliferation versus induction of differentiation, and the outcome seems very much dependent on both cell type and host species (Teo and Kahn 2010). However, Wnt activation of the ß-catenin pathway has been shown to lead to the disruption of self-renewal and the subsequent production of posterior primitive streak/mesoderm progenitors in hESC (Sumi et al. 2008; Gadue et al. 2006). Therefore, in this study WNT3A (or a Wnt agonist) was added to the culture medium on days 1-3 in conjunction with Activin-A, in order initiate a shift towards a mesendoderm population. These cells were then seeded onto immobilised Wnt, which it was hoped would have the dual effects of enhancing proliferation and inducing asymmetrical cell division in any remaining pluripotent cells, as described previously in mESC (Habib et al. 2013).

First it was necessary to determine the optimal day for the addition of the acellular fibrin hydrogel to the cells. As with a normal DPP, the decision was made to split cells on day 4 and to seed them onto the Wnt-modified polymer at this point. Previous work with MAN7 hESC has revealed that seemingly minor environmental changes, which have a positive effect on other cells types, can be particularly detrimental to viability. Thus, addition of the gel on the same day as cell seeding, though providing the most prolonged Wnt signalling, was unlikely to prove optimal, as cells would not have had sufficient time to recover before

being subjected to further stress. Although addition of the gel on day 4 resulted in the highest expression of chondrogenic genes such as *ACAN* and *COL2A1*, lower metabolic activity and DNA content suggested that viability was indeed compromised. It should also be noted that this expression was based on RNA taken from the whole construct, including any cells remaining on the polymer base and may, therefore, represent a very heterogeneous cell population. Attempts were made to isolate RNA solely from the hydrogel after removal of the polymer base, but yield was too low to be of use. The DNA assays, however, were performed after polymers were removed and gels washed and are more representative of the cell population within the 3D constructs. Addition of the gels on day 6, again resulted in low DNA content, which may be due to loss of cells during media changes. hESC do not adhere to tissue culture plastic without prior addition of a substrate and, although some adherence was observed onto the Wnt-modified polymer, it is likely that the medium change on day 5 washed away some cells. In addition, it was considered preferable to offer cells a material to migrate into as soon as possible after seeding onto the immobilised Wnt, in order to maximise the DNA content of the constructs. Therefore, upon completion of the pilot experiments, the decision was taken to add the hydrogels on day 5 in subsequent experiments.

Expression of *COL1A1* was measured in two of the pilot experiments and, in a similar pattern to *COL2A1*, was found to peak at day 14 in all groups. When gels were added on day 5 *COL1A1* expression was significantly higher in D14 DTT than both D14 Wnt and D14 BSA. This is promising, as it suggests that immobilised Wnt favours lower *COL1A1* expression, which is more indicative of a hyaline cartilage phenotype. High levels of *COL1A1* may be indicative of an osteogenic phenotype. Preliminary experiments, however, revealed no

expression of collagen type X or *RUNX2*, a master regulator of osteogenesis (data not shown). Therefore, it seems unlikely that cells in this 3D model were differentiating towards an osteogenic lineage. However, high *RUNX2* expression has been reported in chondrocytes isolated from healthy, deep zone cartilage with lower levels of expression in those taken from the superficial zone (X. Wang et al. 2004). Thus the complete absence of expression in this study was unexpected, and future work should incorporate a positive control in order to confirm that the *RUNX2* primer used in the gene expression assay was amplifying the correct target gene.

Wnt signalling did not result in any significant changes in chondrogenic gene expression, except in the pilot experiment when gels were added on day 4. *ACAN* expression did not change significantly between day 9 and 14. In the pilot experiment, when gels were added on day 5, however, expression was significantly higher in D9 groups. Aggrecan is not an abundant protein and previous reports of increases in expression in response to the DDP, though significant, have been minor in comparison to other proteins (Oldershaw et al. 2010). In addition, there is generally a high level of variation in cell response during each DDP, with some runs proving more successful than others despite every attempt being made to keep conditions uniform. This variation, which may be due to batch to batch variation in the growth factors upon which the protocol relies so heavily, could account for the lack of consistent increases in *ACAN* expression in this study. *SOX9* expression again peaked on day 14. Although SOX9 protein expression was shown by Oldershaw et al. to peak on day 9, the variation in response described above may mean that cells matured more slowly in later experiments. This would also explain the relatively low expression of *COL2A1*,

which is a downstream gene target of *SOX9* and would, therefore, require a longer culture period to increase expression and accumulate in the ECM (V. Lefebvre et al. 1997).

Wnt signalling enhanced proliferation of cells and their subsequent migration into the hydrogels, but did not appear to enhance chondrogenic gene expression when gels were added on day 5. A significant increase in mean *COL2A1* expression between days 9 and 14 was only seen in the BSA control groups. It could be that the immobilised Wnt is inducing proliferation and migration rather than differentiation, whereas the lack of Wnt signalling in the BSA groups allows cells to differentiate in response to the growth factors in the culture medium, thus producing a more mature phenotype in these constructs. A similar effect was observed in human mesenchymal progenitors in response to immobilised fibronectin signalling – migration and proliferation were significantly upregulated at the expense of chondrogenic gene expression (Kalkreuth et al. 2014). In this example, however, cells were seeded onto hanging cell culture inserts and did not have the opportunity to migrate away from the proliferative signal and undergo subsequent differentiation. DAPI staining confirms that cells were indeed more abundant in D9 Wnt constructs and migration data indicates that these cells moved further from the polymer base (and its Wnt signal) compared to BSA and DTT groups. WNT3A has been shown to induce migration and proliferation in a wide range of cells types, including the human lens epithelial cell line HLE-B3 (Bao et al. 2012), murine BMSC (Shang et al. 2007), murine vascular smooth muscle cells (migration only) (Wu et al. 2014) and human BMSC (Lowndes et al. 2016); thus it is not surprising that hESC responded in the same way.

Migrating cells had enhanced chondrogenic markers, as evidenced by merged images of DAPI and SOX5/SOX9. In D9 Wnt hydrogels, a clear band of SOX5- and SOX9-positive cells

can be seen above the cell population at the base, whereas no such effect was observed for D9 BSA or D9 DTT. Canonical Wnt signalling may have enhanced proliferation in these cells, which resulted in greater migration into the hydrogel and, as cells moved further away from and lost contact with the immobilised Wnt, they were able to undergo differentiation. In order for differentiation to occur, however, cell proliferation must cease (Teo and Kahn 2010), which would explain why DNA content (as indicated by DAPI staining) and migration did not continue to increase after day 9 in the Wnt constructs. The same band of cells was still evident by day 14 and, by this point, the effect was also observed in the BSA-based constructs. It may be that cells in these groups were responding to weaker endogenous Wnt signals from undifferentiated cells at the base and migrating at a slower rate before finally catching up. Whatever the reason, migration and subsequent differentiation appear to occur at a faster rate in cells seeded onto immobilised Wnt. Immobilised growth factors, such as TGF-ß3 and BMP7, have been shown to promote chondrogenic differentiation in both adipose and bone marrow-derived mesenchymal cells when applied to porous polymer scaffolds (McCall, Luoma, and Anseth 2012; Lim et al. 2010). However, these are generally chondrogenic growth factors and do not have the added advantage of producing a population of migratory cells which can be separated from undifferentiated progenitors. Lowndes et al. (2016) are the only group to have utilised Wnt signalling in a similar fashion to that described here (albeit for osteogenic differentiation), but their use of human BMSC limits the scalability of the model for potential clinical applications, whereas hESC offer much greater expansion capacity.

Allowing differentiating cells to migrate into an acellular hydrogel resulted in a more mature phenotype than application of the DPP in monolayer. One limitation of the DPP is that it

produces chondroprogenitors rather than mature chondrocytes, as evidenced by low *CD44* expression, which is indicative of an under-developed ECM (Oldershaw et al. 2010). Although data for 3D constructs was from a heterogeneous cell population, expression of chondrogenic genes such as *ACAN*, *COL2A1* and *SOX9* was always higher than in D14 cell only controls and often significantly so. A barrier to the clinical application of hESC is the possible presence of residual pluripotent stem cells and their potential to form teratomas *in vivo*. Cheng et al (2014) sought to remove this obstacle with the application of the pluripotent cell-specific inhibitor PluriSIn1, which was earlier reported to be toxic to pluripotent cells at very low concentrations, while preserving progenitor and differentiated cells (Ben-David et al. 2013). However, when used at recommended concentrations, toxicity to hESC-derived chondroprogenitors was also observed. Although Oldershaw et al. reported no expression of pluripotent markers by day 14, this was rarely the case with DDPs conducted in this study (supplementary figures 1-3), where low levels of *OCT4* and *NANOG* were frequently detected by the end of the culture period. This may be due to the poor solubility of WNT3A in the culture medium in stage 1 of the protocol, which is deemed to be the most crucial stage for successful differentiation (Oldershaw et al. 2010). Substitution of WNT3A for CHIR99021, a potent and soluble Wnt agonist, certainly improved the outcome of DPPs (supplementary figure 1), but low levels of *OCT4* expression were still observed. It was hoped that the seeding of cells onto a Wnt-modified polymer with addition of an acellular hydrogel would result in a 3D model with a more homogeneous chondrogenic cell population; although further characterisation of cells is required to confirm this, results of ICC indicate that cells in the upper portion of the Wnt-based constructs are more chondrogenic. In addition, OCT4 staining of gels indicates that expression was almost entirely obliterated in all groups by D14 compared to positive controls (supplementary

figure 4), particularly in D14 Wnt gels. Due to limited numbers of constructs, OCT4 staining was only performed on one gel from each group in one experiment. In addition, low RNA yield meant that there was only sufficient cDNA to test for expression of the three chondrogenic genes. Future work should focus on testing for expression of pluripotency markers such as *OCT4* and *NANOG* in the D14 constructs, in order to rule out the potential presence of cells which render the constructs unsafe for clinical applications.

Although some migration into acellular hydrogels was observed, the maximum distance moved by the cells was under 300 µm, which represents less than one sixth of the whole 2 mm gel thickness. There was little change between days 9 and 14, which suggests that a longer culture period would not increase migration distance. The relative stiffness of fibrin in comparison to other materials may be a factor which limits migration – indeed preliminary experiments revealed that reducing the final fibrinogen concentration from 10 mg/mL to 8 mg/mL was necessary to see any meaningful migration at all. Therefore, substitution of fibrin for a material with a lower Young's modulus may be a means of enhancing migration in future experiments. Hyaluronan-based hydrogels would be one such option, which also offer the advantage of being chondro-inductive and may, therefore, have the added benefit of improving the expression of chondrogenic markers. It may be necessary to utilise only the top portion of the construct for clinical applications, in order to ensure that a more homogenous cell population is taken forward. Considering that a full thickness cartilage defect may be around 6 mm in depth at the knee (Cohen et al. 1999), it is unlikely that this model would ever yield a construct sufficient to treat such areas. However, in areas such as the wrist, where articular cartilage depth is less than 1 mm

(Pollock et al. 2013), this model could provide a promising tissue engineered alternative to current gold standard treatments.

3.6 Conclusion

hESC offer a promising cell source for tissue engineered alternatives for the treatment of cartilage defects. Their pluripotency and capacity for self-renewal are key factors in the success of the DDP, which can be used to produce large numbers of chondroprogenitors. However, it is these very factors which also render them a more hazardous option for clinical applications than other cell types. Any residual pluripotent cells have the potential to form teratomas *in vivo*, which is perhaps one reason why there are comparatively few clinical trials underway which utilise these cells.

One drawback of the DPP is that, by the end of the 14-day culture period, only immature chondrocytes are produced. In this study, addition of a 3D acellular hydrogel to differentiating monolayer hESC, always resulted in improved chondrogenic gene expression compared to D14 cell only controls; furthermore, this was true of both day 9 and day 14 constructs, suggesting that the differentiation process is accelerated in this model. In addition, the application of a Wnt platform significantly increased the migration of cells into the gel and ICC revealed that expression of chondrogenic proteins such as SOX5 and SOX9 was augmented by increased distance from the Wnt signal. The top portion of these constructs, with a more homogenous, chondrogenic population of cells, may offer a promising treatment solution for small cartilage defects. However, further optimisation is required to increase the migration of cells into the hydrogel in order to produce a thicker construct. In addition, cells need to be characterised further to ensure that they are not expressing pluripotent markers.

Chapter 4

Biomaterials to enhance the chondrogenic potential of hESC

4.1 Introduction

The directed differentiation protocol (DDP) described by Oldershaw et al. (2010) can produce large numbers chondroprogenitors, which offer great potential for use in cartilage cell therapies. However, for successful delivery to defect sites, as either tissue engineered grafts or injectable cell therapies, a carrier/scaffold material is usually necessary in order to protect cells from harmful shear forces and to aid manipulation. Hydrogels, formed from natural and synthetic polymers such as alginate or PEG, are insoluble in water and can retain large volumes of liquid, creating a microenvironment for proliferating cells which mimics native tissue by allowing exchange of waste and nutrient molecules. They can also encapsulate cells more homogeneously than other scaffold materials and their viscoelastic mechanical properties can be manipulated to more closely resemble those of the native cartilage (Hwang, Varghese, and Elisseeff 2007).

As a key component of the coagulation cascade, fibrin has unquestionable biocompatibility and has long been used as a "glue" in a number of surgical procedures. Given its physiological role in natural tissue repair processes, it is unsurprising that fibrin contains a host of cell/growth factor binding motifs and has an architecture which promotes cell infiltration and wound repair (Sproul, Nandi, and Brown 2018). Despite these advantages, fibrin in itself is not chondro-inductive and, in addition, it possesses weak mechanical properties and is prone to shrinkage and rapid degradation *in vitro* (Y. Li et al. 2015). Therefore, for the generation of replacement tissue to treat chronic, degenerative cartilage conditions, which require longer periods in culture, a biomaterial with chondro-inductive properties, superior mechanical strength and a slower rate of degradation would be preferable – though there are few options which meet all of these criteria.

Hyaluronic acid-based scaffolds and gellan gum (see chapter 1.9) are appealing alternatives for the production of hydrogels. Both have been used, with some success, to produce cartilaginous tissue from both stem cells (Toh et al. 2010; Ahearne and Kelly 2013) and primary chondrocytes (G. Wang et al. 2018; Oliveira et al. 2010). Due to poor mechanical stability, hyaluronic acid must be combined with other materials in order to form a hydrogel with the requisite stiffness; the HyStem^{TM} kit used in this study contains thiol-modified HA and a thiol reactive crosslinker (PEGDA). Gellan gum, on the other hand, requires only mild processing conditions and readily forms a stiff hydrogel when cooled.

Incorporation of chondro-inductive biomaterials, either as a substrate for coating tissue culture plastic/cells or dissolved into the culture medium, is another potential means of enhancing the maturation of stem cell-derived chondroprogenitors (see chapter 1.9). Biomimetic materials, such as sulphated alginates, have been shown to enhance the proliferation of bovine chondrocytes (Mhanna et al. 2014) and the pre-coating of TCP with ECM molecules such as decorin or HA has reportedly lead to increases in *COL2A1* and *ACAN* expression in human articular chondrocytes (Grogan et al. 2014). Another option is coat the cells in a layer of ECM/biomimetic molecules to create a chondro-inductive micro-environment. Micro-encapsulation in alginate has been shown to enhance the viability of injected BMSC (Leslie et al. 2017); the addition of chondro-inductive materials such as HA to this micro-environment could yield higher quality chondroprogenitors compared to the basic DDP used in this study.

4.2 Aims

The aims of this chapter were:

- To explore the use of alternative biomaterials for the 3D culture of hESC-derived chondroprogenitors
- To enhance the maturation of hESC-derived chondroprogenitors with the use of chondro-inductive ECM/biomimetic molecules

4.3 Methods

4.3.1 Comparison of 3D models

A DDP was applied to MAN7 hESC as described in chapter 2.3. Cells were harvested at day 14-16 and used to make 200 µL hydrogels with either fibrin (as described in chapter 2.4), HyStem^{TM} (chapter 2.5) or Phytagel^{TM} (gellan gum) (chapter 2.6). Cells were seeded at a final density of $0.5x10^6$/mL. Constructs were cultured for 7 days with daily medium changes supplemented with aprotinin at a concentration of 20 µg/mL in order to limit protease degradation of the gels. On day 7, a cell viability assay was performed on one of each type of gel as described in chapter 2.20. Samples were imaged using a Nikon Eclipse Ti-S Fluorescent microscope. The remaining constructs were either snap frozen and stored at -80°C or fixed with 10% NBF for 1 hour. ICC was conducted on fixed samples as described in chapter 2.22 and gels were stained with anti-SOX5 antibody (1 µg/mL) and anti-SOX9 antibody (1 µg/mL) and counterstained with DAPI. DNA and sulphated GAG assays were performed as described in chapters 2.17 and 2.18 respectively. RNA isolation, reverse transcription and gene expression analysis were performed as outlined in chapters 2.12.3,

2.13 and 2.14 respectively. This experiment was repeated three times, with chondroprogenitors derived from three separate DDP runs (see 4.4.1).

4.3.2 Addition of sulphated alginates to the DDP

A DDP was initiated on MAN7 or MAN13 hESC as described in chapter 2.3. On day 8 cells were split as usual (chapter 2.2), but seeded into 24-well plates. For a 1:4 split, 1 well of a 6-well plate was seeded into 20 wells of a 24-well plate. On day 9, the culture medium was changed as usual (table 2-6), but with addition of alginates or sulphated alginates diluted in DPBS as outlined in table 4-1. Alginates were added to the medium at a concentration of either 10 µg/mL or 100 µg/mL. Alginates with two different degrees of sulphation were used (0.8 and 2.0) in addition to non-sulphated alginate controls. Degree of sulphation (DS) is defined as the average number of sulfate groups per disaccharide repeating unit of alginate (Mhanna et al. 2014). 4 wells were cultured per condition and an additional 4 wells (VTN) were cultured in normal DDP medium without the addition of alginates. The medium was changed daily and alginates/sulphated alginates were added again on day 12. The experiment was performed three times with MAN7 cells and twice with MAN13 cells. Samples were imaged in situ on days 10 and 14 using a Nikon Eclipse Ti-S Fluorescent microscope (in bright field mode). On day 14, cells were either fixed with 10% NBF for 30 minutes and washed in PBS or lysed with 350 µL buffer RLT and stored at -80°C for subsequent gene expression analysis. Owing to limited sample numbers, ICC was performed on VTN, AlgS 0.8 10 and AlgS 2.0 10 groups only, and carried out as described in chapter 2.22 using collagen type II monoclonal antibody (3 µg/mL). RNA isolation, reverse transcription and gene expression analysis were performed as outlined in chapters 2.12.1, 2.13 and 2.14 respectively.

Table 4-1. Degrees of sulphation/concentrations of alginates added to medium on days 9 and 12.

Group	Degree of sulphation	Concentration (µg/mL)
VTN	N/A	N/A
Alg 10	0	10
AlgS 0.8 10	0.8	10
AlgS 2.0 10	2.0	10
Alg 100	0	100
AlgS 0.8 100	0.8	100
AlgS 2.0 100	2.0	100

4.3.3 Pre-incubating chondroprogenitors with ECM molecules

hESC-derived chondroprogenitors were pre-incubated with ECM molecules as described in chapter 2.11. As proof of concept, hESC were first pre-incubated with vitronectin at a concentration of 5 µg/mL in DDBM and seeded onto glass cover slides, which were coated with fibronectin (50 µg/mL) rather than vitronectin. Cover slides were transferred to 6-well plates and cells were cultured for two days, and then fixed with 10% NBF for 20 minutes. In order to determine if pre-incubation of cells had resulted in a coating with ECM molecules, ICC was carried out on fixed cells as described in chapter 2.22 using anti-Vitronectin antibody at a concentration of 1 µg/mL. In subsequent experiments, hESC-derived chondroprogenitors were pre-incubated with either fibronectin (50 µg/mL or as indicated in figures), HyStem^{TM} (500 µg/mL or as labelled) or collagen type VI (as indicated in figures). They were then seeded onto vitronectin-coated glass cover slides or 6-well plates and cultured for three days, at which point those on cover slides were fixed for 20 minutes with 10% NBF and those on TCP were lysed with buffer RLT for subsequent gene expression analysis. ICC was carried out on fibronectin-coated slides as described in chapter 2.22 using anti-fibronectin antibody at a concentration of 3 µg/mL. Owing to the structure of

HyStem^{TM}, which differs from naturally occurring hyaluronic acid, a suitable primary antibody could not be found; thus ICC was not performed. Instead, cells were stained for 5 minutes with 0.1% Safranin-O solution, as described in chapter 2.21.6, (without the necessity of deparaffinisation steps).

4.3.4 Statistical analysis

Statistical analysis was performed as described in chapter 2.23.

4.4 Results

4.4.1 Directed differentiation of MAN7 hESC

Chondrogenic gene expression increased between day 1 and day 15 in all three DDP runs performed on MAN7 hESC (figure 4-1). Mean *ACAN* and *SOX9* expressions were significantly greater by day 15 (both $p<0.05$). Expression of pluripotency marker *OCT4* decreased significantly ($p<0.01$), as expected, but was not completely ablated by day 15; indicating the likely presence of residual pluripotent stem cells in each population of chondroprogenitors.

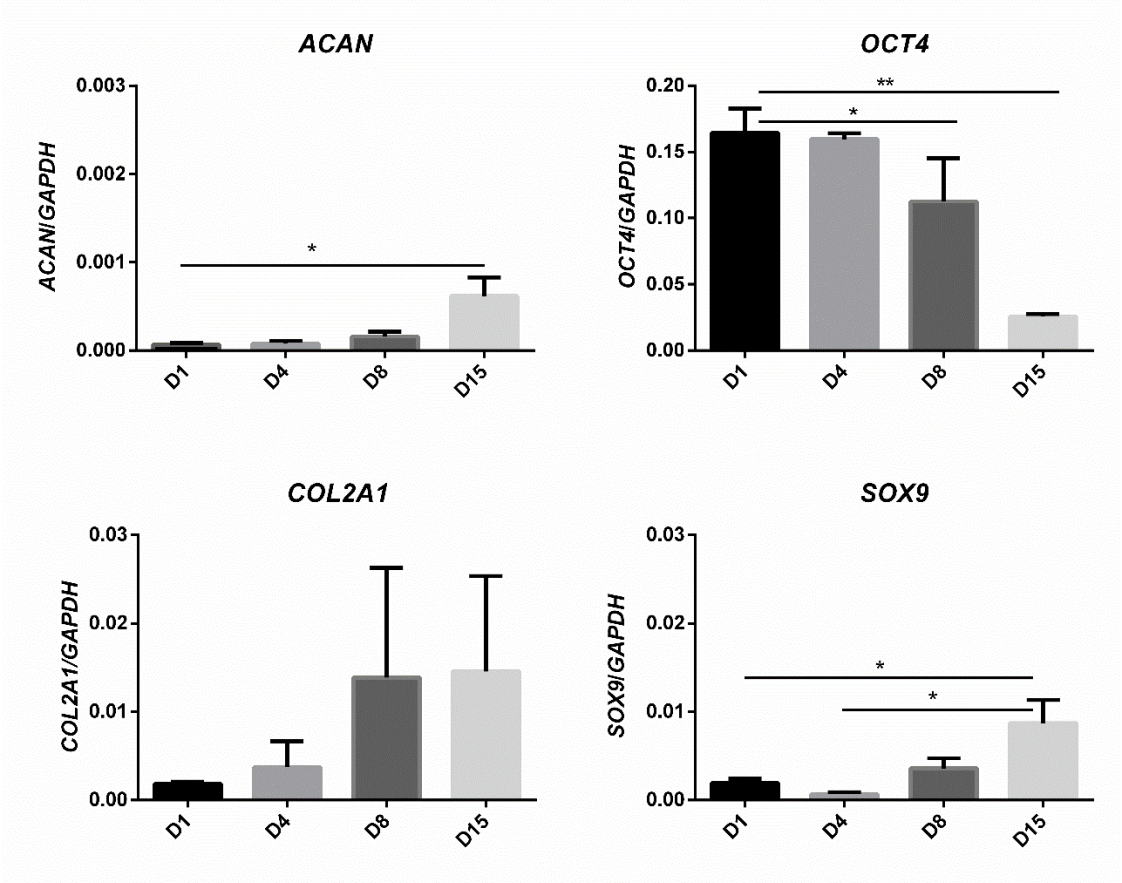

Figure 4-1. Chondrogenic gene expression increases and pluripotency gene expression decreases with progression of DDP. Mean expression ($2^{-\Delta Ct}$) of *ACAN*, *COL2A1*, *OCT4* and *SOX9* in MAN7 hESC subjected to directed differentiation for 15 days. Data are expressed as the mean ± the standard error, N=3 (biological repeats). *$p<0.05$, **$p<0.01$.

4.4.2 Comparison of 3D models indicates that fibrin and Phytagel™ are superior to HyStem™

Fibrin proved to be the best 3D model for supporting cell viability by day 7, whereas Phytagel™ constructs demonstrated around 40% viability and HyStem™ as low as around 10% (figure 4-2). Results demonstrate that fibrin constructs had significantly more DNA than both HyStem™ ($p<0.0001$) and Phytagel™ ($p<0.0001$) (figure 4-3 A). Fibrin constructs also had significantly higher levels of sGAG (figure 4-3 B) than HyStem™ ($p<0.0001$) and Phytagel™ ($p<0.01$) and Phytagel™ had significantly more than HyStem™ ($p<0.0001$). When normalised to DNA content, however, Phytagel™ constructs had a significantly higher sGAG/DNA ratio than both HyStem™ ($p<0.0001$) and fibrin ($p<0.0001$) (figure 4-3 C).

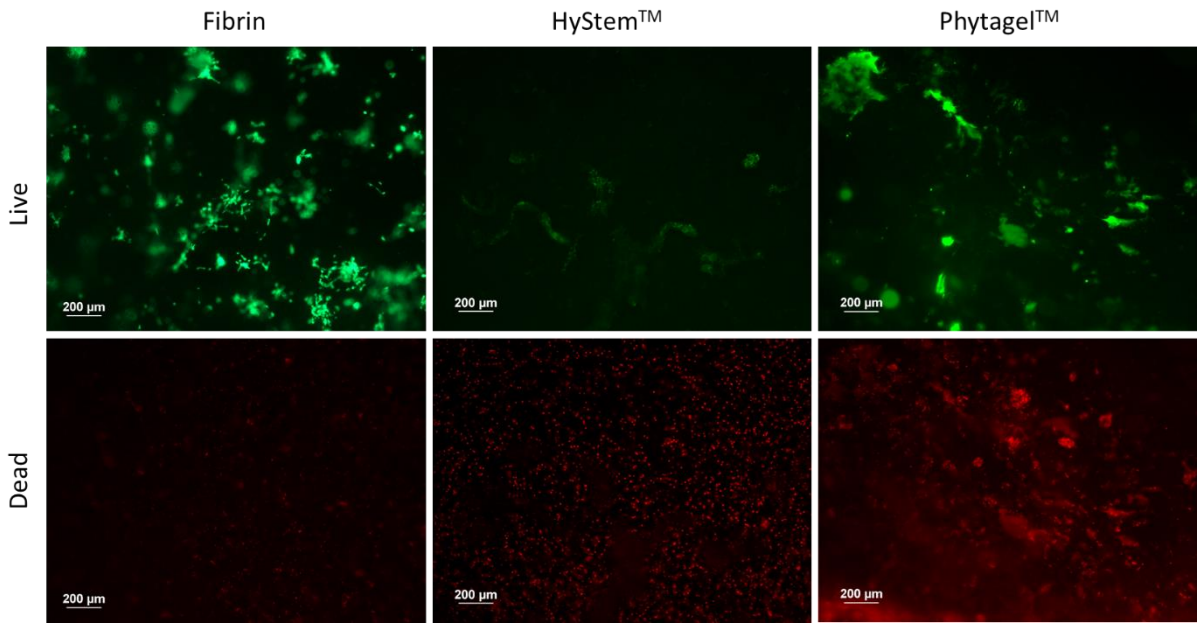

Figure 4-2. Fibrin-encapsulated chondroprogenitors demonstrate superior viability. Representative fluorescent images of hESC-derived chondroprogenitors encapsulated in either fibrin, HyStem™ or Phytagel™ and stained with LIVE/DEAD kit after 7 days of culture, n=2 (technical repeats). Green = calcein-AM (live). Red = ethidium homodimer-1 (dead). Scale bars = 200 µm.

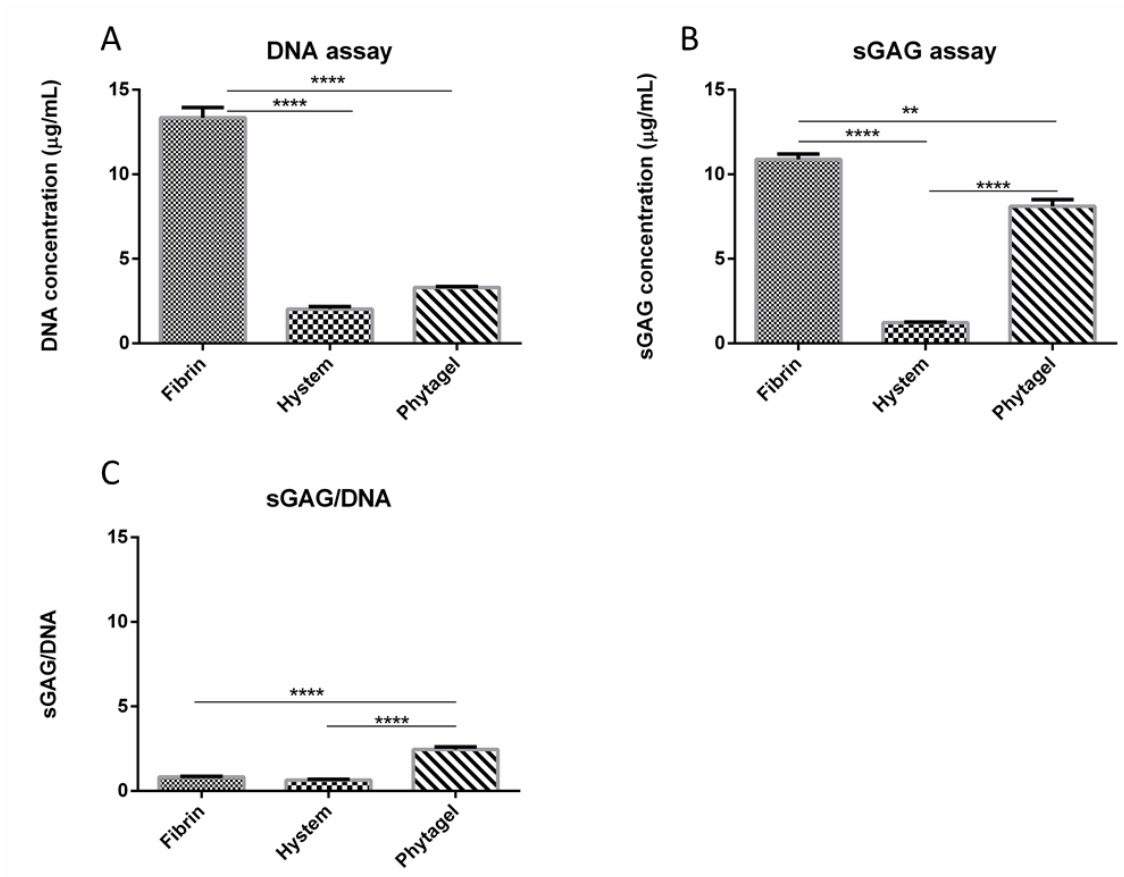

Figure 4-3. Fibrin-encapsulated chondroprogenitors contain more DNA and sGAG. PicoGreen double stranded DNA assay (A) and DMMB assay (B) performed on hESC-derived chondroprogenitors encapsulated in either fibrin, HyStem™ or Phytagel™ after 7 days of culture. sGAG was normalised to DNA content (C). Data are expressed as the mean ± the standard error, n=4 (technical repeats). **p<0.01, ****p<0.0001.

Similarly, gene expression analysis indicates that fibrin and Phytagel™ are more conducive to chondrogenic gene expression than HyStem™. *ACAN* expression of day 7 constructs was significantly higher in Phytagel™ than in fibrin ($p<0.05$) and higher than in HyStem™, though not significantly so (figure 4-4 A). *COL2A1* expression, however, was significantly higher in fibrin constructs than in both HyStem™ ($p<0.01$) and Phytagel™ ($p<0.001$) (figure

4-4 B). In the case of *COL2A1*, expression was actually lowest in Phytagel™ constructs. *SOX9* expression was similar in all constructs (figure 4-4 C).

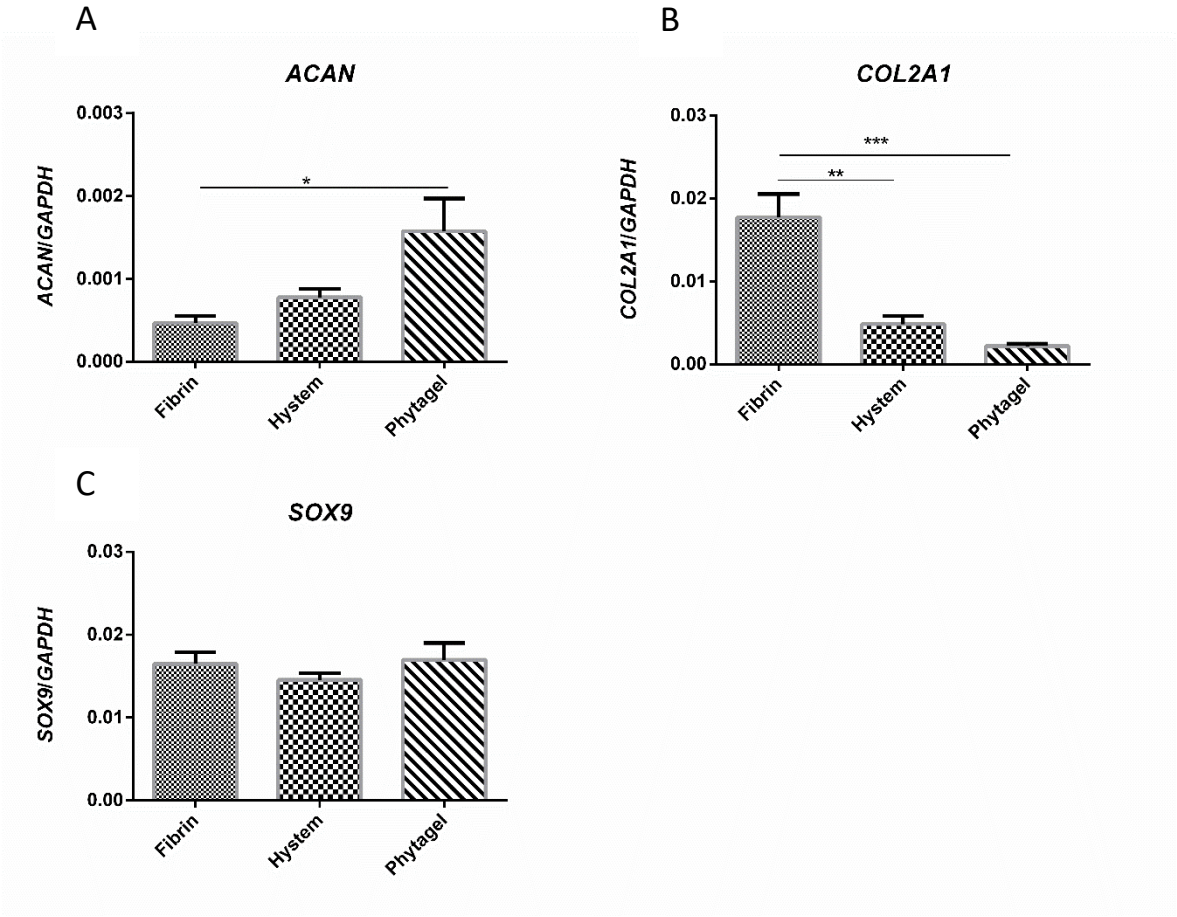

Figure 4-4. Fibrin and Phytagel™ constructs favour chondrogenic gene expression. qRT-PCR performed on hESC-derived chondroprogenitors encapsulated in either fibrin, HyStem™ or Phytagel™ after 7 days of culture. Gene expression is relative to *GAPDH* ($2^{-\Delta Ct}$). Data are expressed as the mean ± the standard error, n=4 (technical repeats). *p<0.05, **p<0.01, ***p<0.001.

ICC shows that expression of SOX5 and SOX9 proteins was higher in fibrin- and Phytagel™-encapsulated chondroprogenitors than in HyStem™ constructs, where there was no discernible expression of SOX5 and very little SOX9 visible (figure 4-5).

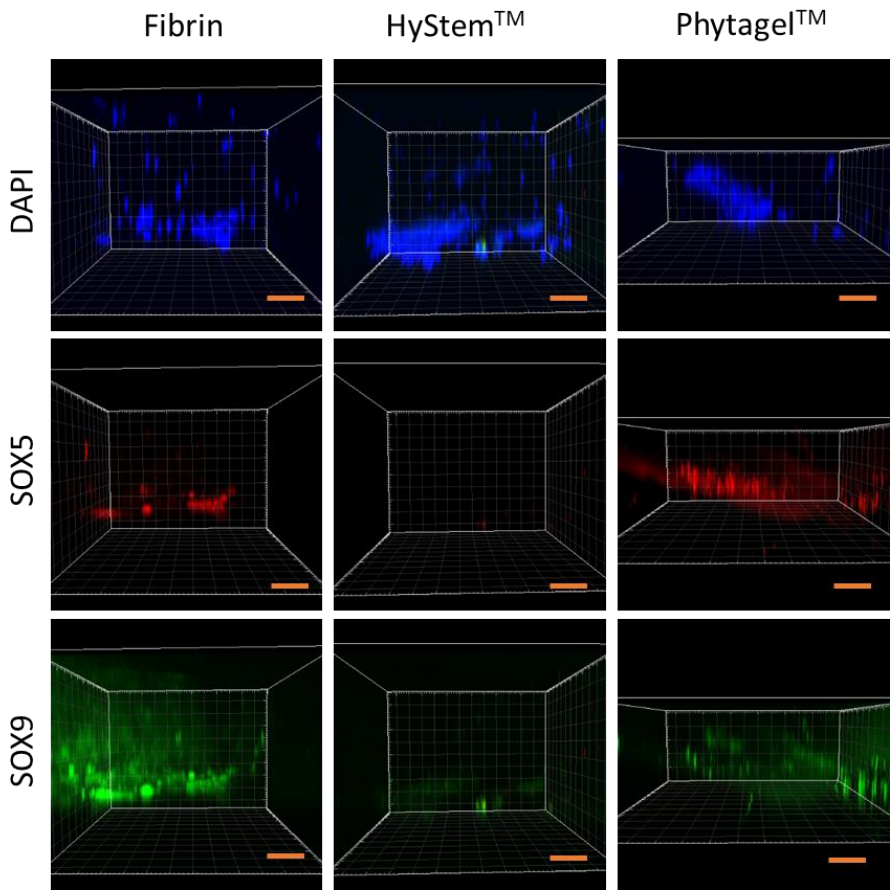

Figure 4-5. Fibrin and Phytagel™ constructs have greater expression of chondrogenic proteins. Representative fluorescent images of day 7 hydrogels. N=3 (biological repeats). Scans were taken from the bottom up every 9 µm with a laser confocal microscope, for a distance of ≤500 µm. Images were constructed using Imaris Image Analysis software. Scale bars = 100 µm. DAPI (blue), SOX5 (red), SOX9 (green).

4.4.3 Influence of sulphated alginates

In initial experiments AlgS 0.8 groups showed an improved response in terms of gene expression (figure 4-6) and, for this reason, these samples were selected for ICC in order to examine expression of COL2 protein (figure 4-9). In one experiment, where alginates were added to the medium of differentiating MAN13 hESC, AlgS 0.8 10 expressed significantly higher levels of *COL2A1* (figure 4-6 B) compared to VTN ($p<0.001$), Alg 10 ($p<0.05$) and AlgS 0.8 100 ($p<0.001$). The same group also expressed significantly higher levels of *SOX9* (figure 4-6 C) compared to VTN ($p<0.05$) and AlgS 0.8 100. *ACAN* expression (figure 4-6 A) was also higher in this group than in AlgS 0.8 100 ($p<0.01$), but for this gene, addition of the non-sulphated alginate at 10 μg/mL (Alg 10) resulted in the highest expression and was significantly greater than both VTN ($p<0.05$) and Alg 100 ($p<0.001$). A similar pattern was observed when alginates were added to differentiating MAN7 hESC; AlgS 0.8 10 again seemed to favour chondrogenic gene expression (data not shown). Overall, lower alginate concentrations (10 μg/mL) resulted in higher chondrogenic gene expression.

When this experiment was repeated, however, (twice for MAN7 and once for MAN13) the same patterns were not observed and statistical analysis of mean gene expressions from three independent experiments (figure 4-7) revealed no significant differences. Figure 4-8 demonstrates how the two cell lines compare in their responses to the sulphated alginates. Generally, they follow a very similar pattern; Alg 10, AlgS 0.8 10 and Alg 100 groups having a high level of variation, rather than consistent increases. Interestingly, addition of sulphated alginates with 2.0 DS at the higher concentration of 100 μg/mL always resulted in no expression of the chondrogenic genes examined, despite good RNA yield. For this reason, data for that group are absent. In both experiments performed with MAN13 the

same alginates, added at the lower concentration of 10 µg/mL, brought about the same ablation of expression, although this effect was not observed with MAN7 (figure 4-8).

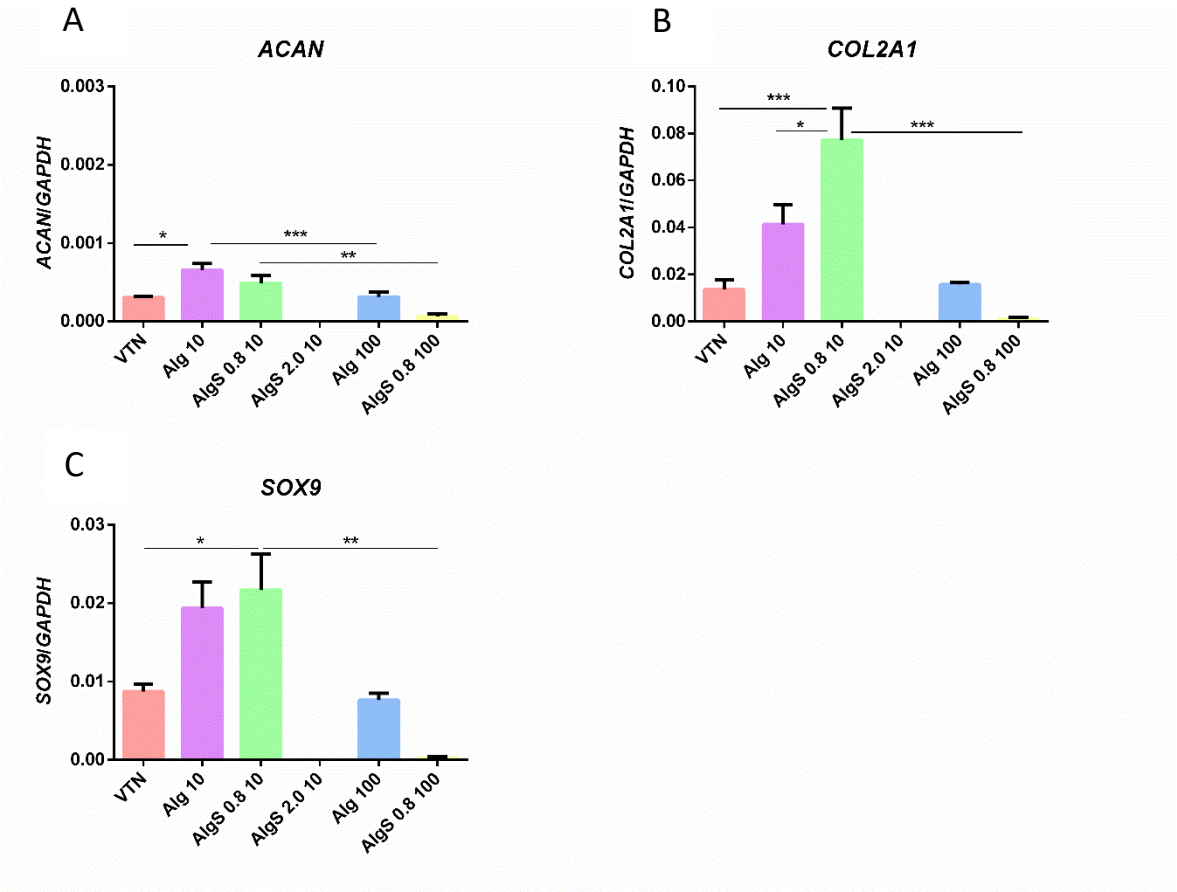

Figure 4-6. Initial results indicate that AlgS 0.8 10 enhances chondrogenic differentiation of MAN13 hESC. qRT-PCR performed on MAN13 D14 hESC-derived chondroprogenitors where alginates were added to the medium on days 9 and 12. VTN = vitronectin only control, Alg = alginates, AlgS = sulphated alginates, 10 = 10 µg/mL, 100 = 100 µg/mL, 0.8/2.0 = degrees of sulphation. Gene expression is relative to *GAPDH* ($2^{-\Delta Ct}$). Data are expressed as the mean ± the standard error, n=3 (technical repeats). *p<0.05, **p<0.01, ***p<0.001.

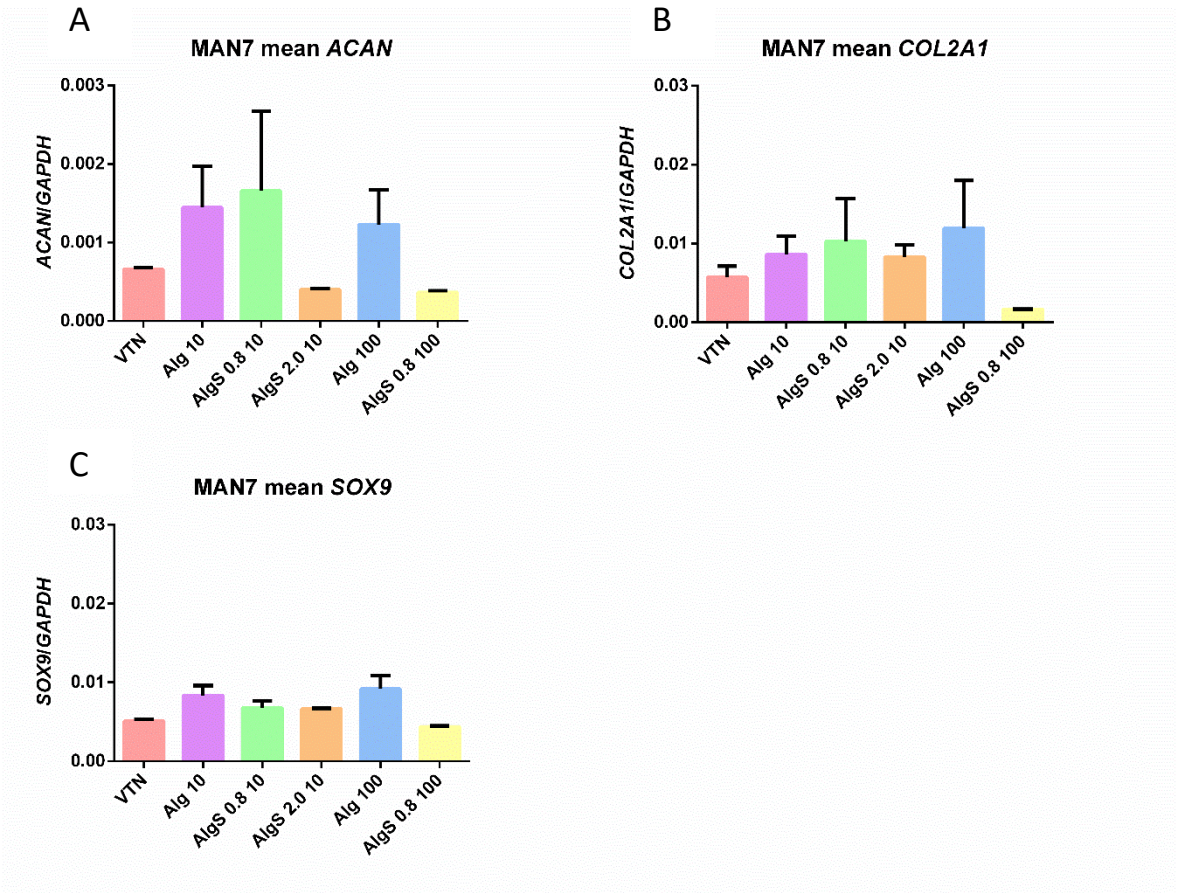

Figure 4-7. MAN7 mean gene expression reveals no significant differences between groups. qRT-PCR performed on D14 hESC-derived chondroprogenitors where alginates were added to the medium on days 9 and 12. VTN = vitronectin only control, Alg = alginates, AlgS = sulphated alginates, 10 = 10 µg/mL, 100 = 100 µg/mL, 0.8/2.0 = degrees of sulphation. Gene expression is relative to *GAPDH* ($2^{-\Delta Ct}$). Data are expressed as the mean ± the standard error and are from 3 independent experiments (N=3).

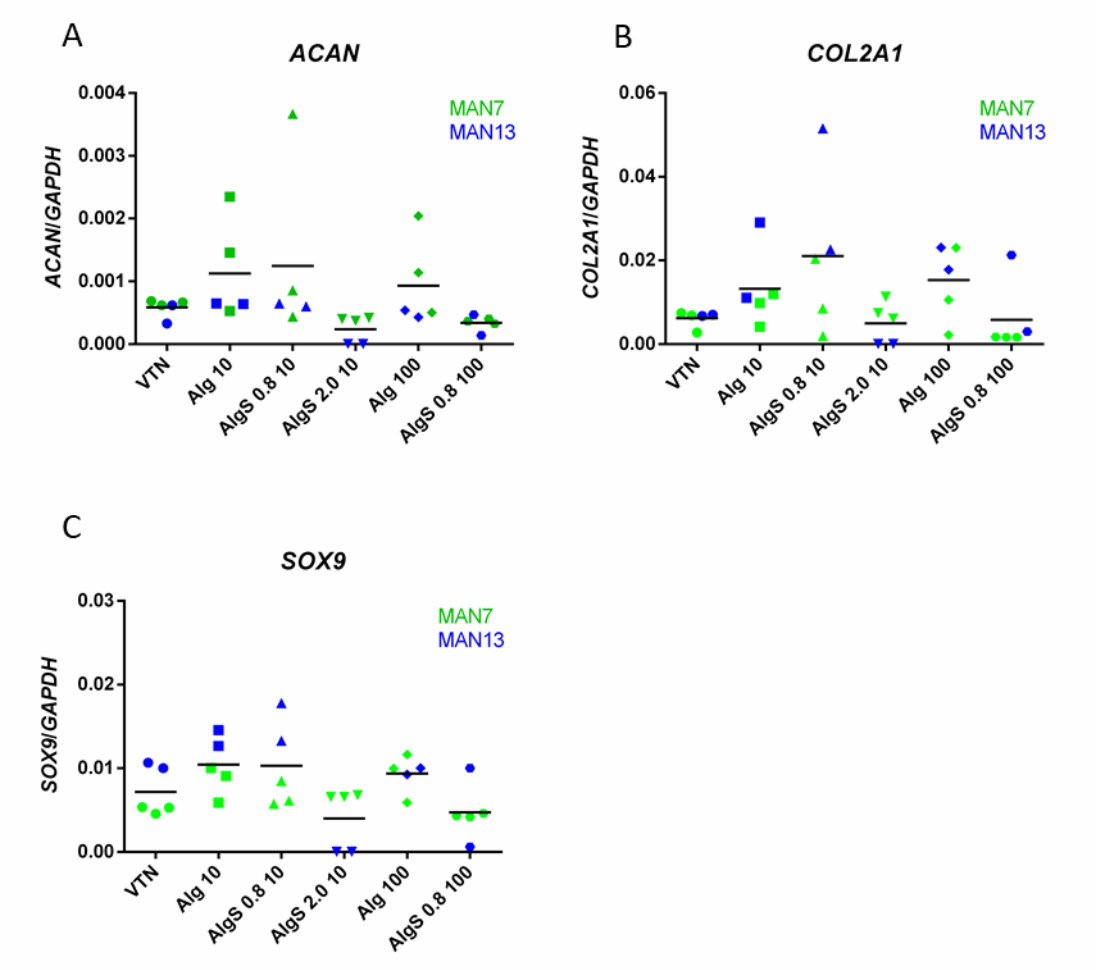

Figure 4-8. Responses of both hESC cell lines to sulphated alginates . qRT-PCR performed on D14 hESC-derived chondroprogenitors from two cell lines, where alginates were added to the medium on days 9 and 12. VTN = vitronectin only control, Alg = alginates, AlgS = sulphated alginates, 10 = 10 µg/mL, 100 = 100 µg/mL, 0.8/2.0 = degrees of sulphation. Gene expression is relative to *GAPDH* ($2^{-\Delta Ct}$). Results from each experiment are plotted as individual points. Black bars represent the mean of 5 independent experiments.

ICC (figure 4-9) indicates that COL2 protein expression is higher in cells supplemented with AlgS 0.8 10 compared to AlgS 2.0 10 and to VTN controls. However, COL2 staining was only performed for one experiment and further work is required to confirm this observation.

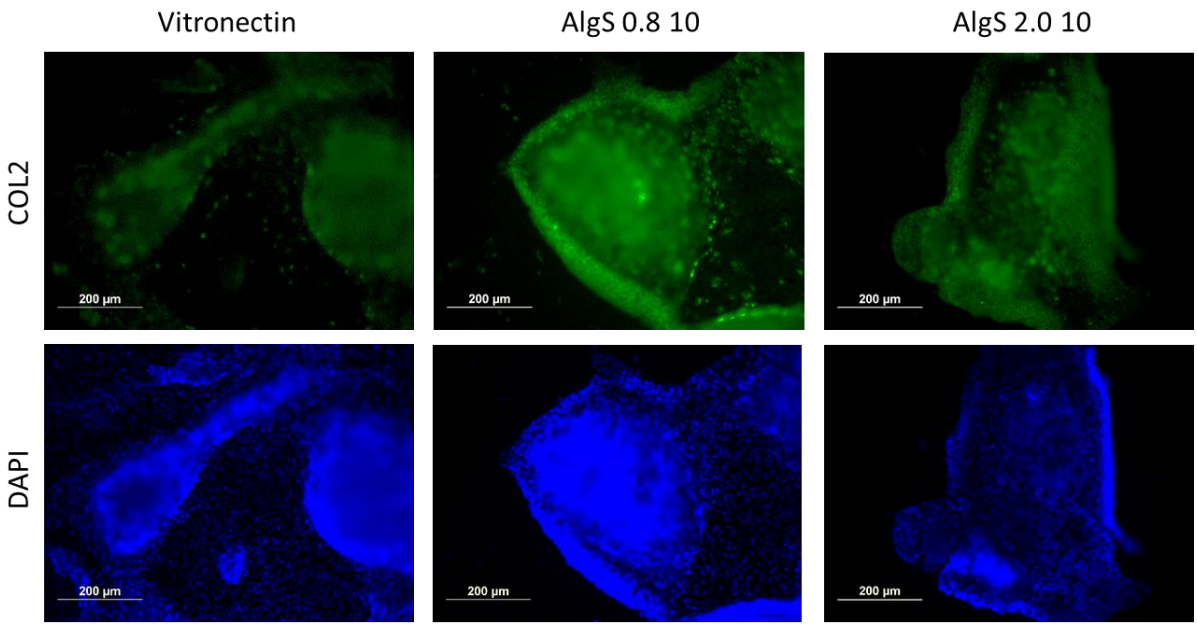

Figure 4-9. Expression of collagen type II protein may be higher in chondroprogenitors incubated with AlgS 0.8 10. Representative of fluorescent images of COL2 expression in D14 hESC-derived chondroprogenitors. Cells incubated with 10 µg/mL sulphated alginates with 0.8 degrees of sulphation for 7 days show higher COL2 staining intensity. Scale bars = 200 µm. DAPI (blue), COL2 (green).

4.4.4 Effects of pre-incubating cells with ECM molecules

hESC were initially pre-incubated with vitronectin in order to observe whether a coating of ECM molecules could be applied to cells with the method adopted. ICC reveals a clear layer of this protein around these cells (figure 4-10 middle and right), whereas there was no vitronectin present around control cells (figure 4-10 left). For subsequent experiments, molecules with important roles in cartilage ECM were selected to pre-incubate hESC-derived chondroprogenitors with. Fibronectin (figure 4-11) was detected in large amounts in both pre-incubated and control cells. However, the structure of protein network was different; fibres around the pre-incubated cells were shorter, more compact and appeared

to be extracellular, whereas fibres in the control samples were often observed closer to the nuclei. Gene expression analysis of cells pre-incubated with 50 µg/mL fibronectin (figure 4-12) revealed a trend of increase in expressions (not significant) of *ACAN*, *COL2A1* and *SOX9*. The subsequent dose response experiment (figure 4-13) entailed incubation of hESC-derived chondroprogenitors with fibronectin at a range of concentrations, from 5-500 µg/mL. In this experiment, no increases in *ACAN* and *COL2A1* expression were detected in comparison to controls (0 µg/mL), with the exception of 5 µg/mL, where a small increase in *COL2A1* expression was observed. However, this increase was not significant.

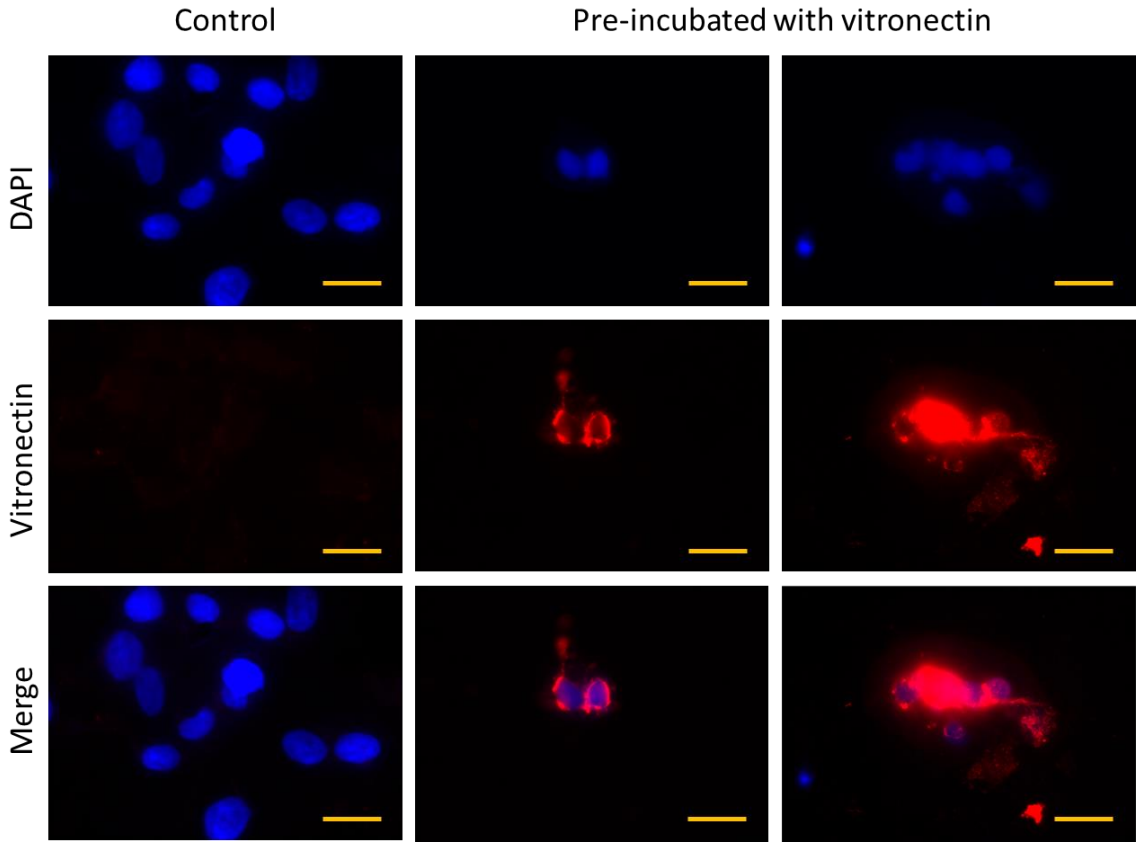

Figure 4-10. Chondroprogenitors appear to be coated in vitronectin. Representative of fluorescent images of hESC pre-incubated with vitronectin for one hour and cultured for three days (middle and right) or control (left). Scale bars = 20 µm. DAPI (blue), vitronectin (red).

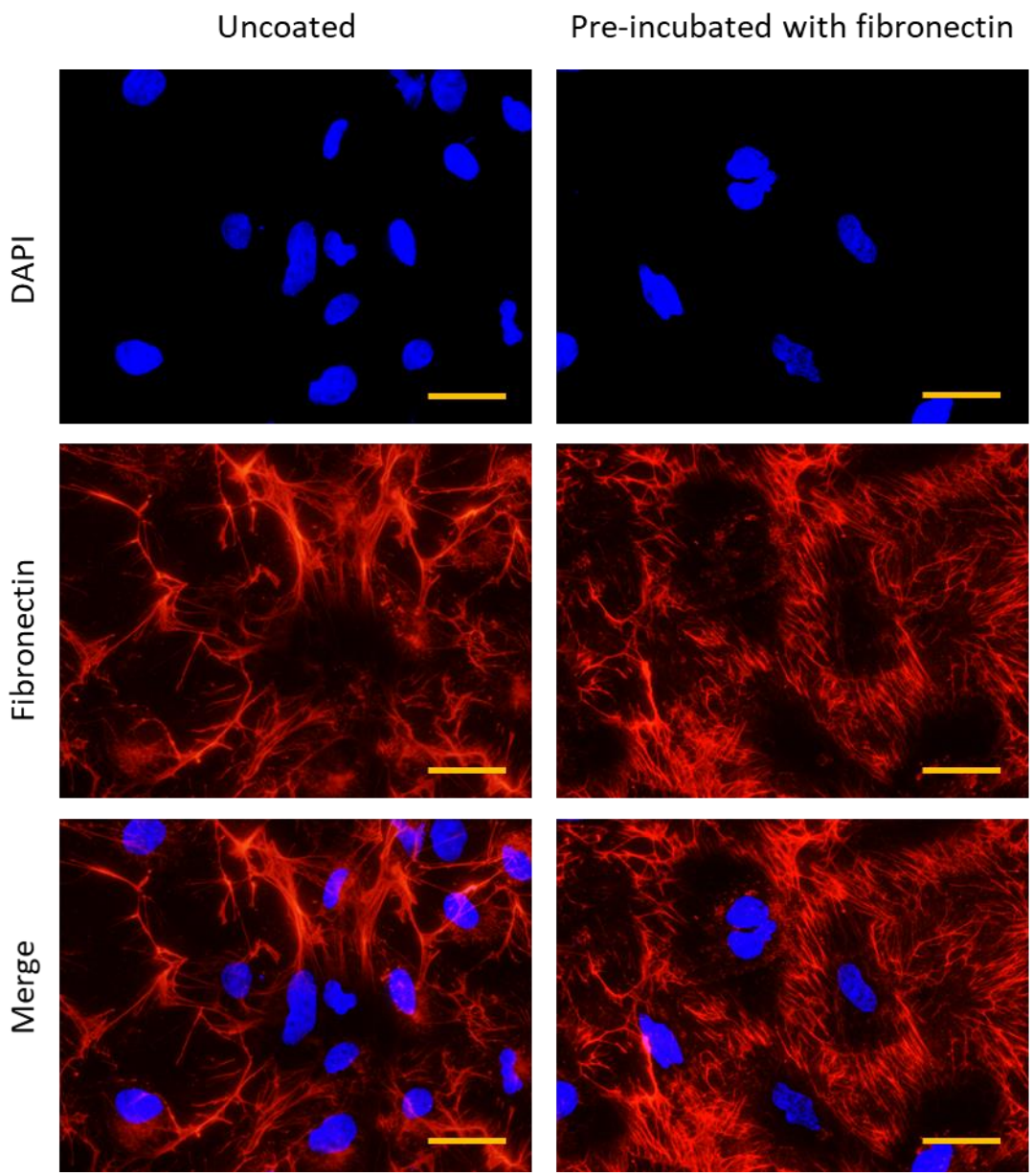

Figure 4-11. Fibronectin is present in both pre-incubated and control cells. Representative of fluorescent images of hESC-derived chondroprogenitors pre-incubated with fibronectin for one hour and cultured for three days (right) or control (left). Scale bars = 20 µm. DAPI (blue), fibronectin (red).

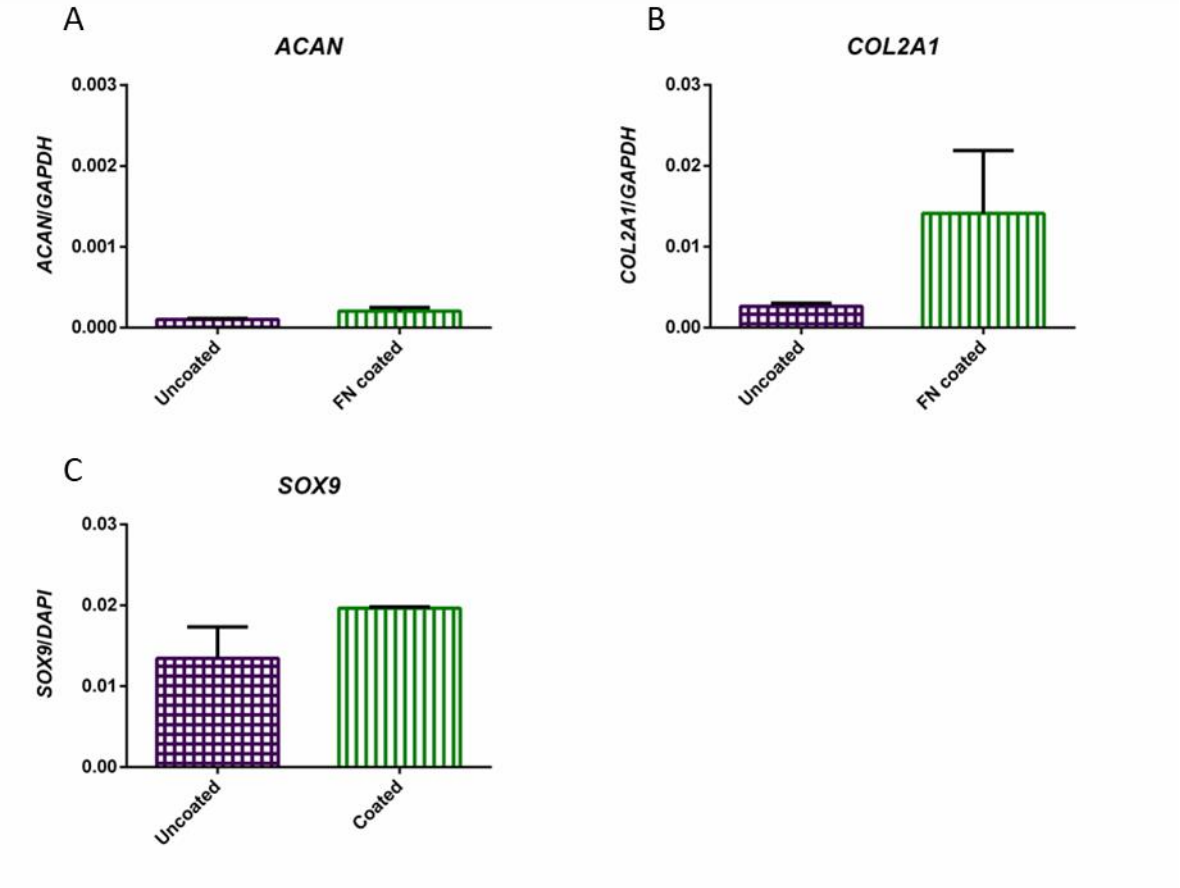

Figure 4-12. Initial experiments indicate that pre-incubation with fibronectin may increase chondrogenic gene expression. hESC-derived chondroprogenitors incubated with fibronectin at a concentration of 50 µg/mL for one hour and cultured for three days. Data are from one experiment with two technical repeats (n=2) and expressed as the mean ± standard error. Significance not determined due to lack of repeats. Expressions of all three chondrogenic genes are elevated compared to controls, though not significantly so. Gene expression is relative to *GAPDH* ($2^{-\Delta Ct}$).

In three independent experiments, chondroprogenitors incubated with 500 µg/mL HA (HyStem™) (the concentration recommended by the supplier for preparing hydrogels), demonstrated no increase in expression of *ACAN* or *COL2A1* (figure 4-14). Safranin-O staining, however, was unquestionably more intense in HA-treated cells compared to

controls (figure 4-15), which is indicative of enhanced sulphated GAG deposition. The subsequent dose response experiment (figure 4-16) entailed incubation of hESC-derived chondroprogenitors with HA at a range of concentrations, from 50-500 μg/mL. No significant differences in *ACAN* expression were observed between any of the groups. A pre-incubation concentration of 100 μg/mL resulted in significantly higher C*OL2A1* expression than in cells pre-incubated with 300 μg/mL ($p<0.01$) or 500 μg/mL ($p<0.05$), but although there was a trend of increased *COL2A1* expression compared to control cells, this increase was not significant.

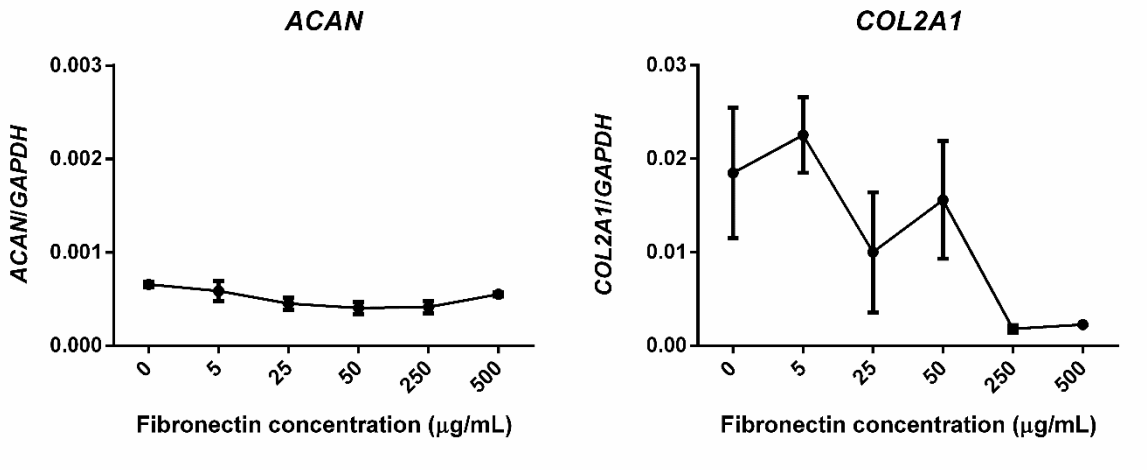

Figure 4-13. Effects of fibronectin dose response on chondrogenic gene expression. hESC-derived chondroprogenitors incubated with fibronectin at a range of concentrations for one hour and cultured for three days. Data are from one experiment with three technical repeats (n=3) and are expressed as the mean ± standard error. Gene expression is relative to *GAPDH* ($2^{-\Delta Ct}$).

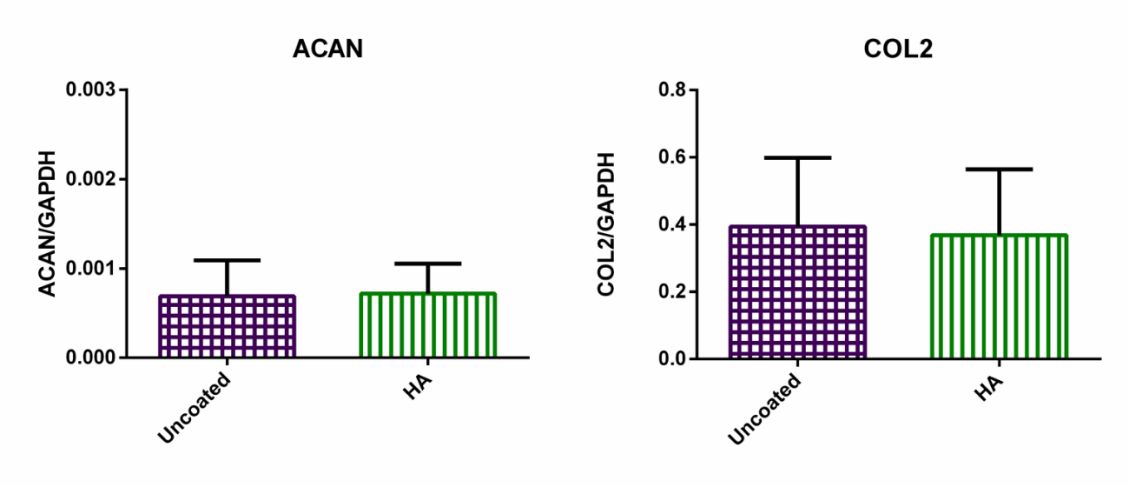

Figure 4-14. Pre-incubation of cells with hyaluronic acid does not affect chondrogenic gene expression. Cells incubated with HyStem^{TM} (HA) at a concentration of 500 µg/mL for one hour and cultured for three days. Data are from three independent experiments (N=3) and are expressed as the mean ± standard error. Gene expression is relative to *GAPDH* ($2^{-\Delta Ct}$).

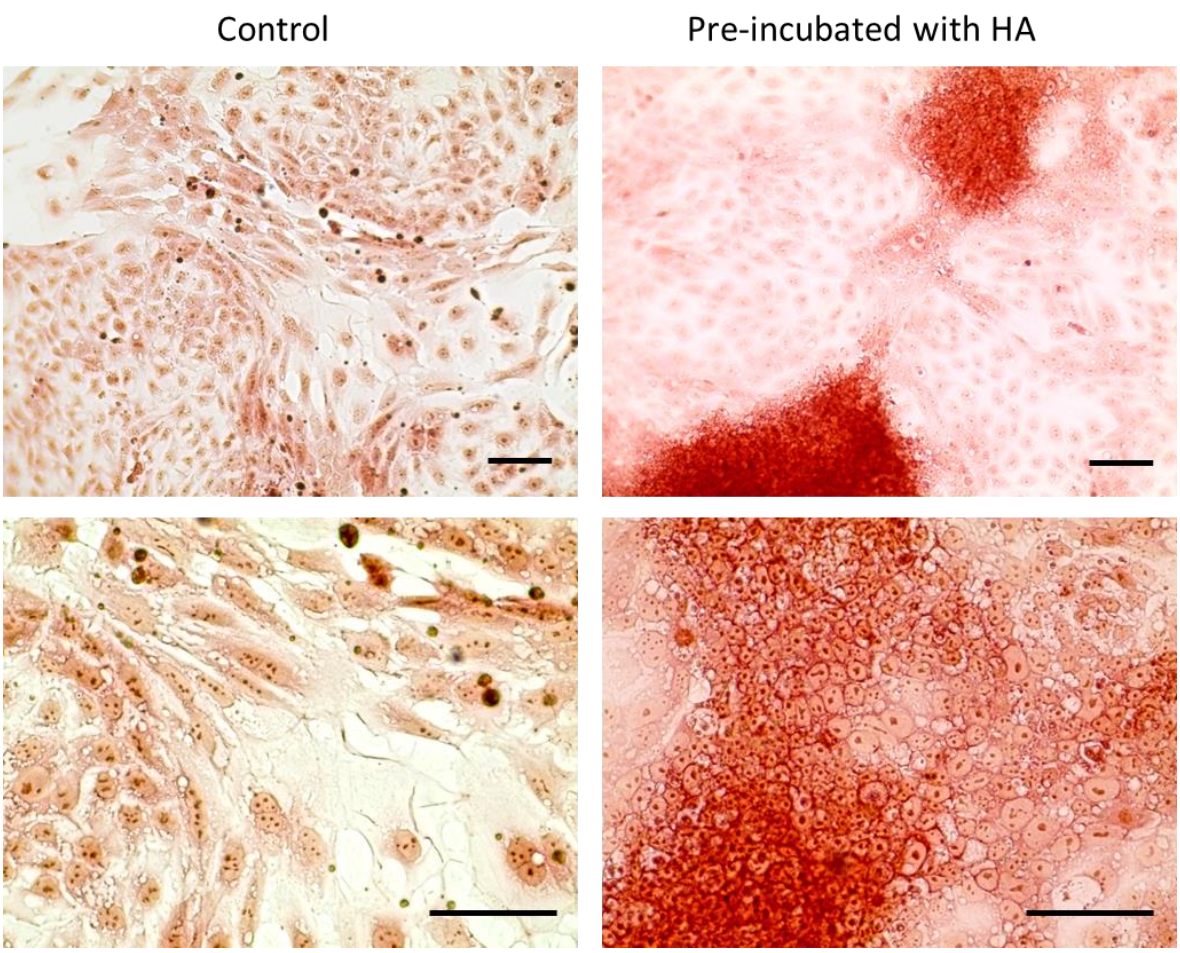

Figure 4-15. Cells pre-incubated with HA produce more chondrogenic ECM. Representative images of hESC-derived chondroprogenitors incubated with HyStem™ (HA) at a concentration of 500 µg/mL and cultured for three days, then stained with Safranin-O. Scale bars = 200 µm.

Finally, cells incubated with COLVI at a range of concentrations from 0.05 – 50 µg/mL showed no significant differences in expression of *ACAN* or *COL2A1* compared to controls (figure 4-17).

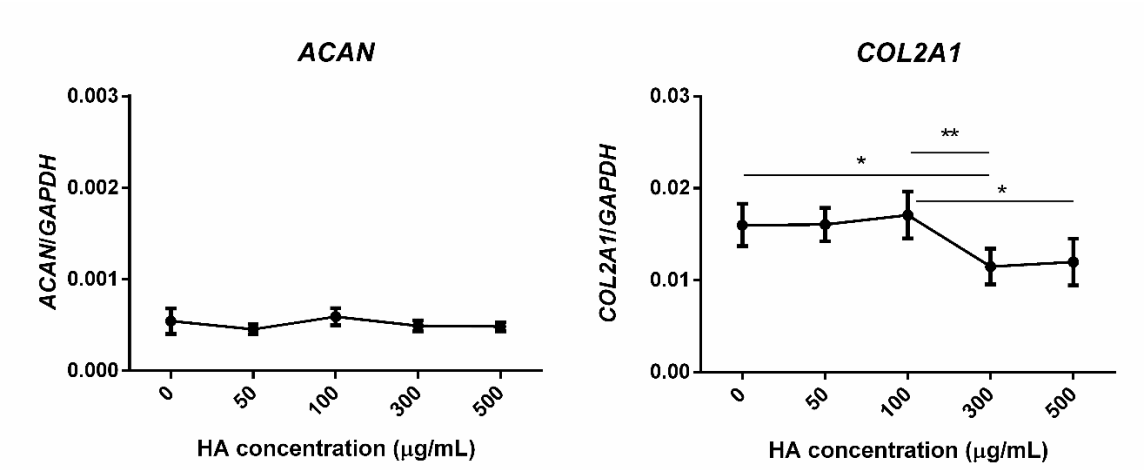

Figure 4-16. Effects of HA dose response on chondrogenic gene expression. Cells were incubated with HA at a range of concentrations and cultured for three days. Data are from one experiment with five technical repeats (n=5) and are expressed as the mean ± standard error. Gene expression is relative to *GAPDH* ($2^{-\Delta Ct}$).

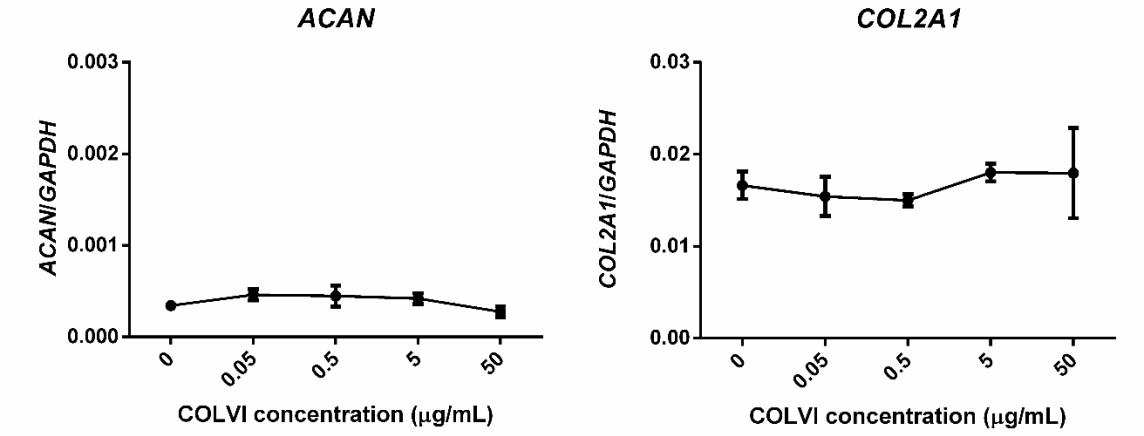

Figure 4-17. Effects of COLVI dose response on chondrogenic gene expression. Cells were incubated with collagen type VI at a range of concentrations and cultured for three days. Data are from one experiment with three technical repeats (n=3) and are expressed as the mean ± standard error. Gene expression is relative to *GAPDH* ($2^{-\Delta Ct}$).

4.5 Discussion

4.5.1 3D culture is optimum in fibrin hydrogels

Fibrin proved the most suitable 3D model for supporting the viability of hESC-derived chondroprogenitors. The inevitable generation of shear stresses and the resulting formation of single cells during the formulation of the gels probably contributed to the relatively high level of anoikis-induced cell death in all three models (Olson 2008). Addition of a ROCK inhibitor, routinely applied when passaging cells for monolayer culture (chapter 2.2.3), may be a means of enhancing cell survival in future work. Given its physiological role in the clotting cascade, its numerous cell/growth factor binding motifs and an architecture which promotes cell invasion, it is not surprising that fibrin proved the most biocompatible of the hydrogels (Sproul, Nandi, and Brown 2018).

Gellan gum demonstrated superior viability to HyStem^{TM} and often proved at least as effective as fibrin in promoting a chondrogenic phenotype. Numerous other studies have reported that gellan gum enhances viability, proliferation and expression of chondrogenic markers (Ahearne and Kelly 2013; Oliveira et al. 2010; Vilela et al. 2018). In this study, viability of cells encapsulated in gellan gum was lower than those encapsulated in fibrin, but this may well be due to the method by which the constructs were prepared. Prior to gelation, it was necessary to keep the gellan gum at 37°C and, in order to form a gel, cell pellets were rapidly resuspended in 200 µL of this liquid, generating unavoidably high levels of shear force. The rapid setting also resulted in a non-homogenous cell distribution within the gel. In addition, it was not possible to prepare the gels in culture medium (as with fibrin), because the cations present caused immediate gelation. This meant that cells were deprived of nutrition for around 20 minutes whilst the gels were allowed to fully set and for

a period of time afterwards until the medium had diffused inside; indeed, this was also the case with HyStem™ constructs. To overcome this, attempts were made to form a more concentrated solution into which cells already resuspended in culture medium could be added; unfortunately, however, the formation of a solution above 1% proved impossible due to the poor solubility of the Phytagel™. Despite this, the improved chondrogenic gene expression and sGAG deposition suggest that gellan gum remains a promising biomaterial for the 3D culture of hESC-derived chondroprogenitors, and that it may be worth exploring alternative methods of gel formation in order to promote cell viability. Modifications, such as methacrylation (Vilela et al. 2018) or reduction of molecular weight (by means of oxidative cleavage) (Gong et al. 2009), have been employed in order to render gellan gum suitable for injectable therapies. Vilela et al. showed that hADSC encapsulated in methacrylated gellan gum produced significantly more *de novo* cartilage than untreated controls when injected into a rat model with induced chondral lesions. Furthermore, the constructs performed at least as well as microfracture-treated controls and produced a higher *COL2A1*:*COL1A1* ratio *in vitro*. Gong et al. showed that chondrocyte-seeded gels with a reduced molecular weight and a subsequent slower rate of gelation, exhibited greater cell proliferation and viability, superior matrix formation and better phenotype maintenance than agarose controls.

Surprisingly, HyStem™ constructs (consisting primarily of HA) demonstrated very poor viability and did not prove to be chondro-inductive, even in regions with high numbers of viable cells, as evidenced by ICC. One previous study reported good long-term viability and production of cartilaginous tissue in hESC-seeded HA hydrogels (Toh et al. 2010). However, they did not state the concentration of PEGDA used to crosslink the HA; in the current study

it was necessary to increase the concentration to 50 mg/mL in order to obtain a hydrogel with any structural integrity. The manufacturer recommends using concentrations of PEGDA up to 40 mg/mL and previous work has reported the use of 50 mg/mL without loss of viability in fibroblasts (Y. D. Park, Tirelli, and Hubbell 2002). However, it may be that these higher concentrations are detrimental to less robust cells and that different effects will be induced in different cell types, such as chondrocytes and hESC-derived chondroprogenitors. HA-based 3D models have been shown to support chondrogenesis in multiple studies (Toh et al. 2010; Jooybar et al. 2019; G. Wang et al. 2018; Chung and Burdick 2009), so the presence of viable cells with no SOX5 protein expression and very low SOX9 expression compared to the other models was unexpected. Given the key role of HA in the ECM of articular cartilage, a tissue engineered environment which mimics this biochemistry should prove optimal. However, the viable cells observed in these constructs may have been more fibroblastic in nature; high levels of *COL1A1* (a marker of fibrocartilage) were frequently expressed in cells at the end of the directed differentiation protocol. Alternatively, it may be that the increased stiffness of the other two models proved more beneficial than the chondro-inductive biochemistry of the HA-based gels. Numerous studies have shown that softer hydrogels favour chondrogenic differentiation; one group found that a stiffness of 0.5 MPa resulted in the greatest proteoglycan production and expressions of *ACAN*, *COL2* and *SOX9* in murine chondrocytes cultured on polyacrylamide surfaces (Allen, Cooke, and Alliston 2012), whereas a host of other studies have shown that stiffnesses in the range of 30-90 kPa are optimal (Y. Zhang, Chen, and Pei 2016). Although the mechanical properties of the hydrogels were not measured in the current investigation, it was obvious from the difficulty experienced in manipulating the HyStem^{TM} constructs, which flowed under their own weight, that they were more akin to a liquid than a viscoelastic solid. The fibrin and

Phytagel™ constructs, however, were soft but had viscoelastic properties – slow deformation under the application of force and the ability to revert to their original shape upon its removal.

4.5.2 Biomaterials for potential cell delivery applications

Injectable cells therapies are an appealing option for the treatment of damaged/diseased joints, as they are minimally invasive, less costly and aim to promote endogenous repair of the tissue rather than replacing it. However, injection of cells generates larger shear forces which can compromise viability and reduce the efficacy of treatments. Microencapsulation of single cells or small aggregates can provide a protective microenvironment, which reduces the shear stress experienced by the cells upon injection and promotes survival. To this end, attempts were made to encapsulate hESC-derived chondroprogenitors in relevant ECM molecules via pre-incubation with solutions of fibronectin, HA and COLVI.

Initial results indicated that fibronectin-treated cells displayed enhanced chondrogenic gene expression. An adhesive glycoprotein which forms part of the ECM of articular cartilage, fibronectin facilitates the binding of other ECM proteins, GAGs and collagen via cell membrane-bound integrins such as α5ß1, α4ß1 and αvß3 (Singh and Schwarzbauer 2012). Therefore, it is reasonable to expect that it might augment chondrogenic matrix deposition. Fibronectin has been shown to be vital for embryogenesis and early differentiation events; mice lacking FN expression demonstrated deficient mesodermal migration, proliferation, differentiation and adhesion (George et al. 1993). In addition, it has been identified as a major bioactive molecule produced by MEFs (upon which hESC were traditionally cultured) (Braam et al. 2008) and it aids hESC attachment and self-renewal *in vitro* (Baxter et al. 2009; Soteriou et al. 2013). However, due to endogenous production of

the protein, it was not possible to confirm that the cells had indeed been coated with fibronectin during the incubation period prior to culture. One way of confirming this in future work would be to use commercially available, fluorescently-labelled fibronectin in this initial pre-incubation process and to perform confocal imaging of the cells, which are stained with a fluorescent membrane dye, over a time course in order to determine the precise location of the protein and its persistence.

Chondroprogenitors pre-incubated with HA showed greater sGAG deposition compared to controls, although enhanced expression of *ACAN* and *COL2* was not observed. A previous study has shown that BMSC suspended in pure HA demonstrated improved homing to and repair of articular cartilage in a guinea pig OA model, with increased COL2 deposition and enhanced safranin-O staining throughout the tissue (Sato et al. 2012), which suggests that addition of HA to the culture environment can be chondro-inductive. Again, it was not possible to confirm the successful coating of chondroprogenitors with HA, but given that it has been shown to associate strongly with the cell surface receptor CD44 in the presence of other matrix molecules (Lesley et al. 1992; Y. Kim and Kumar 2014), and that CD44 is expressed by these hESC-derived chondroprogenitors (Oldershaw et al. 2010), it is likely that the HA was bound to the cells. Commercially-available fluorescein HA could be utilised in future work in order to confirm attachment to the cells during pre-incubation. In order to confirm the increase in production of cartilaginous matrix, the presence of specific proteins such as COL2 would need to be determined with the application of techniques such as immunofluorescence or enzyme-linked immunosorbent assays (ELISA).

Individually, the ECM molecules explored in these experiments did not produce consistent significant increases in cartilage-specific makers when added to the culture medium of

hESC-derived chondroprogenitors. Collagen type VI which, in normal articular cartilage, binds to the cell surface and co-localises with fibronectin (Keene, Engvall, and Glanville 1988; Hagiwara, Schröter-Kermani, and Merker 1993) conferred no detectable benefit on gene expression and, for this reason, the decision was taken not to pursue this line of investigation. However, when combined with other materials and used to microencapsulate cells, these molecules have proved beneficial in other studies. A range of cells types, including ADSC and BMSC, demonstrated improved viability post-injection when encapsulated in cross-linked, shear-thinned alginate (Aguado et al. 2012). BMSC encapsulated in fibronectin-functionalised alginate showed improved viability and proliferation compared to alginate only controls (Sayyar et al. 2015) and the addition of HA to alginate microcapsules resulted in increased sGAG production and improved viability (Cañibano-Hernández et al. 2017). Therefore, it may be necessary to anchor these ECM molecules to other biomaterials which can be used to more effectively encapsulate cells, in order to observe significant responses. Another option would be to functionalise fibrin or gellan gum hydrogels (explored earlier in this chapter and shown to promote viability) with molecules such as fibronectin, HA or COLVI (or their cell binding fragments) in order to improve cell viability and response. Gellan gum is particularly appealing, as it can be used to form a sheared fluid gel, rendering it suitable for injectable therapies (García, Alfaro, and Muñoz 2016).

4.5.3 Effects of biomimetic sulphated molecules

Addition of sulphated alginates to the culture medium, particularly at lower concentrations with low degrees of sulphation, enhanced expression of chondrogenic genes and proteins in a number of experiments. Mhanna et al. (2017) claim that these molecules mimic the

action of sGAG which, in addition to providing structural support, have key roles in the binding of cytokines, chemokines and growth factors and in cell-ECM attachment (Sarrazin, Lamanna, and Esko 2011). CS typically has 1-2 sulphated groups per disaccharide repeating unit (chapter 1.3.5) and the alginates used in this study had either 0.8 or 2 per unit; thus, there is indeed a degree of structural similarity. Although Mhanna et al. reported increased levels of proliferation in chondrocytes encapsulated in sulphated alginate hydrogels, however, they did not observe any increase in chondrogenic markers (Mhanna et al. 2014). Similarly, in the current study, results from three independent experiments showed no significant difference in response to sulphated alginates in terms of chondrogenic gene expression. This may be due to the large variation in response of the hESC to the DDP, which resulted in large standard deviations between experiments. Though not significant, addition of Alg 0.8 10 to the culture medium tended to result in higher chondrogenic gene expression and ICC suggests that COL2 deposition was also enhanced.

Sulphated polysaccharides are an appealing biomaterial for cartilage tissue engineering. Carrageenans are naturally-occurring sulphated polysaccharides which have recently generated interest for tissue engineering applications. Like the sulphated alginates used in this study, they have structural similarity to the sGAG which are native to articular cartilage, but no processing is required to bring about their sulphation. Derived from seaweeds, there are 6 different carrageenans (CRG), of which Kappa (k), Iota (I) and Lambda (λ) have the best viscoelastic and gelling properties (Yegappan et al. 2018). hADSC encapsulated in hydrogels formed from k-carrageenan were reported to show good viability, proliferation and expression of chondrogenic markers over a 21-day period (Popa et al. 2015). Other studies have shown that functionalising carrageenans with molecules such as TGF-ß1 (Rocha et al.

2011) or combining them with materials such as fibrin/HA (Pereira et al. 2009) results in the production of cartilage-specific ECM in hADSC and human articular chondrocytes respectively. In other work, hASC encapsulated in k-Carrageenan hydrogels containing magnetic nanoparticles showed enhanced chondrogenic gene expression in response to magnetic stimulation (Popa et al. 2016). Therefore, sulphated polysaccharides offer promising opportunities for cartilage tissue engineering, though whether they are able to support the viability of hESC-derived chondroprogenitors remains to be seen.

4.6 Conclusion

A broad range of biomaterials have been utilised for cartilage tissue engineering. Compared to other cell types such as BMSC, hESC-derived chondroprogenitors provide a limitless source of cells for this application; yet their sensitivity to environmental changes means that a narrower range of suitable biomaterials are available in which to culture them. Fibrin and gellan gum proved optimal in the promotion of cell viability and, if functionalised with chondro-inductive/biomimetic molecules, may offer promising materials for the production of both cartilaginous constructs and injectable cell therapies.

Chapter 5

Effects of mechanical stimulation on hESC-derived chondroprogenitors

5.1 Introduction

Articular cartilage is subject to cyclic compressive forces and it is widely accepted that biomechanical stresses and strains play a major role in the natural development, maintenance and degradation of the tissue. Chondrocytes possess integrins and ion channels which enable the transduction of these mechanical stimuli. In addition, it has been shown that cartilage deformation leads to cell deformation, which may be another means of signal transduction via disruption of cell surface receptors and the associated cytoskeleton. Matrix deformation, hydrostatic pressure gradients, fluid flow, streaming potentials and currents, and physicochemical changes all occur as a result of compression. Given that cartilage is an avascular tissue, fluid flow is especially important for nutrient and waste transport (Guilak, Ratcliffe, and Mow 1995; Guilak et al. 1999; Grodzinsky et al. 2000). Once cartilage is fully developed, these mechanical forces are converted into HP in the interstitial fluid, followed by shear stress as a result of fluid flow. Studies on human and animal intervertebral disc tissue have shown that physiological levels of HP (0.3 - 3 MPa) increase proteoglycan synthesis and metabolism and generally have an anabolic effect, whereas higher levels (3-10 MPa) inhibit proteoglycan production and have a catabolic effect (Handa et al. 1997; Ishihara et al. 1996). *In vivo* cartilage is subject to rapid cyclic loading of 3-10 MPa (up to 18 MPa in the hip) and human walking cadence is around 1 Hz (B. D. Elder and Athanasiou 2009). Thus, tissue engineering approaches tend to apply forces in this range – above this, detrimental effects (similar to the onset of osteoarthritis) have been observed (Kunitomo et al. 2009; Natoli and Athanasiou 2008).

There is a wealth of evidence to suggest that HP in the physiological range improves chondrogenesis in 3D cartilage constructs. Generally, cyclic HP with a force of 4-10 MPa,

applied intermittently to 3D models at a frequency of around 1 Hz, has been shown to increase levels of total collagen (Hu and Athanasiou 2006; Meyer et al. 2011; Carroll, Buckley, and Kelly 2014), *COL2A1* (Reza and Nicoll 2008; Correia et al. 2012) and GAG (Hu and Athanasiou 2006; Sakao et al. 2008; Meyer et al. 2011; Correia et al. 2012; Carroll, Buckley, and Kelly 2014) deposition in the new tissue. Expressions of GAGs and *SOX9*, *COL2* and *ACAN* mRNAs were also enhanced, providing further evidence that cells cultured in these conditions were differentiating towards a chondrogenic lineage (Sakao et al. 2008; Ogawa et al. 2009; Correia et al. 2012). A number of recent studies have found HP to have a positive effect on progenitors and chondrocytes cultured as pellets (Miyanishi et al. 2006; Safshekan et al. 2012; Vinardell et al. 2012). Miyanishi et al. found that 10 MPa of cyclic HP applied intermittently for 14 days enhanced expression chondrogenic markers even without the addition of growth factors such as TGF-β3; the combination of mechanical and chemical stimulation had an even greater impact. Safshekan et al. reported that human adipose-derived stem cells cultured as pellets with 5 MPa of cyclic HP expressed levels of *SOX9*, *COL2A1* and *ACAN* transcripts comparable to those expressed by native human cartilage tissue (though they did not attempt to quantify protein production). Though the results of these studies are promising, pellet culture does not offer the flexibility to create constructs with the desired morphologies and mechanical properties that scaffolds such as hydrogels or meshes permit, as extensive processing is required to release the cells from the rigid ECM which forms around the pellet.

Dynamic compressive forces are frequently applied as a means of enhancing the quality of tissue engineered cartilage constructs. Adult cartilage tissue is exposed to cyclic compressive loads, which are important for both nutrient exchange and for the

transduction of external stimuli via cell-surface mechano-sensitive ion channels and integrins, which initiate intracellular signalling cascades and orchestrate the cell's response to external cues (Musumeci 2016). Compressive forces are also necessary for the normal development of cartilage tissue during embryogenesis (Ruano-Gil, Nardi-Vilardaga, and Tejedo-Mateu 1978; Mitrovic 1982; Nowlan, Sharpe, et al. 2010). Here, however, mechanical cues are imparted by the mother and buffered by the amnion and are, therefore, lower than those experienced by mature tissue. Furthermore, during the very early stages of development, there is no extensive ECM to transmit these mechanical cues, but there is a pericellular matrix rich in matrilins, ACAN, COMP and collagen types VI, II and IX, which interact with specific integrins in response compressive forces (Gilbert and Blain 2018). Matrilin 1, abundant in developing tissue, has a key role in mediating mechanical stimuli and its presence was shown to be necessary in order for chondrocytes to elicit an anabolic response to loading regimes *in vitro* (Y. Chen et al. 2016). Growth factors such as FGF2 are also released by chondrocytes in response to cyclic compression; perlecan-bound FGF2 is released as a result of turbulence and goes on to initiate mitogen-activated protein kinase (MAPK) signalling (Vincent et al. 2007).

Stimulation of mechanoreceptors such as membrane-bound ion channels, integrin receptors and primary cilia stimulate intracellular signalling pathways in response to forces such as compression, deformation, hydrostatic pressure and release of soluble factors. Transient receptor potential vanilloid 4 (TRPV4) is Ca^{2+}-permeable ion channel which was identified as a regulator of chondrogenic differentiation over 10 years ago, with similar expression patterns to other common markers such as *COL2* and *ACAN* (Muramatsu et al. 2007). Its activation in response to cyclic mechanical loading has been shown to result in

enhanced matrix deposition (O'Conor et al. 2014). More recently, Piezo1 and Piezo2 were identified as fast-acting mechanosensitive ion channels, which are abundant in chondrocytes and allow rapid influx of Ca^{2+} in response to high levels of strain (Lee et al. 2014). Stimulation of trans-membrane integrins directly affects cytoskeletal actin organisation, again initiating signalling cascades. α1ß1, α10ß1, αvß5 and α5ß1 integrins have all been implicated in the response of chondrocytes to mechanical stimuli (Gilbert and Blain 2018).

Peake et al. used a four-point bending model to investigate the response of human osteoblast-like cells and the MG63 bone cell line to mechanical load in monolayer culture (M. A. Peake et al. 2000). They reported an up-regulation of *C-FOS,* which could be blocked by the addition of ß1-integrin antibodies or inhibitors of stretch-activated ion channels, suggesting that the response was both mediated by surface integrins and a direct result of mechanical loading. The four-point bending bioreactor used in this work (chapter 2, figure 2-1) was designed to transmit tensile forces to cells cultured on glass slides, in a bid to recapitulate the microenvironment of osteoblasts *in vivo*. In the current study, however, the model was adapted to impart compressive forces to chondroprogenitors by simply inverting the glass slide when cells were loaded into the chamber. It was hoped that this model would provide insight into the short-term responses of hESC-derived chondroprogenitors to low levels of mechanical loading.

5.2 Aims

The primary aims of this chapter were to:

- Explore the effects of low level cyclic hydrostatic pressure on a 3D hESC chondrogenic model
- Explore the effects of low level compressive forces on hESC-derived chondroprogenitors in monolayer culture

5.3 Methods

5.3.1 Investigating the effects of hydrostatic pressure

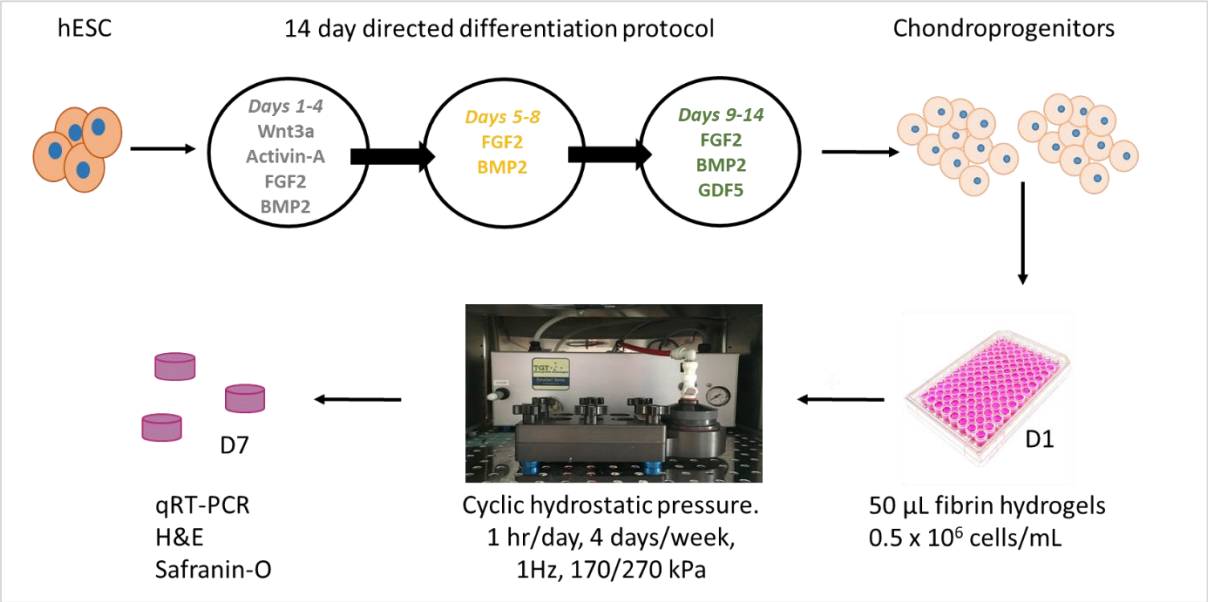

Figure 5-1. Schematic summary of the experimental procedure for investigating the effects of hydrostatic pressure on a 3D hESC-chondrogenic model.

Chondroprogenitors were derived from hESC using a 14-day DDP as described in chapter 2.3. The cells were then encapsulated in 50 µL fibrin hydrogels as described in chapter 2.4 at a final seeding density 0.5 x 10^6 cells/mL and a final fibrinogen concentration of 10 mg/mL. Acellular constructs were prepared for each condition. The following day constructs were transferred to the hydrostatic bioreactor chamber. In this first experiment the TGT system described in chapter 2.9 was used to apply either 170 kPa or 270 kPa cyclic hydrostatic pressure was applied for 1 hour at a frequency of 1 Hz and fresh day 15 chondroprogenitors were used. In the second experiment the pressure was regulated using the OB1 MK3 microfluidic control system and constructs were subjected to 270 kPa hydrostatic pressure for 1 hour at a frequency of 1 Hz. Day 15 chondroprogenitors were

thawed, seeded and cultured for a further two days prior to encapsulation in fibrin hydrogels. As the OB1 MK3 control system uses compressed air (rather than drawing air from the incubator, as with the TGT system) the culture medium was supplemented with 4-(2-hydroxyethyl)-1-piperazineethanesulfonic acid (HEPES) buffer (25mM) prior to stimulation and changed again to DDBM without HEPES buffer afterwards.

Following stimulation, the plate was removed from the chamber and constructs were returned to the incubator. This regime was repeated on the subsequent three days. Unstimulated controls were prepared and incubated alongside stimulated samples. On day 7 constructs were either fixed for 2 hours with 10% NBF and stored in PBS at 4°C for subsequent histological analysis/ICC, or snap frozen and stored at -80°C for subsequent gene expression analysis. Histology was carried out as described in chapter 2.21; 5 µm sections were prepared and stained haematoxylin and safranin-O. Samples were imaged with an EVOS Core XL microscope. Porcine articular cartilage was sectioned and stained in the same way and used a positive control to assess levels of safranin-O staining. In order measure staining intensity, Image J software was used; images were converted to 8-bit black and white, thresholds were adjusted to exclude white regions and a mean pixel intensity was calculated from three areas of equal size per image. Data was collected in this way from three images per group. ICC was performed on whole gels stimulated with the OB1 MK3 system (one from each condition) and scans were taken from the bottom up every 9 µm with a laser confocal microscope, for a distance of 500 µm. Images were constructed using Imaris Image Analysis software. RNA was isolated as described in chapter 2.12.3, reverse transcription was performed as described in chapter 2.13 and qRT-PCR was performed on the resulting cDNA as described in chapter 2.14.

5.3.2 Exploring the effects of compressive forces using the 4PBB

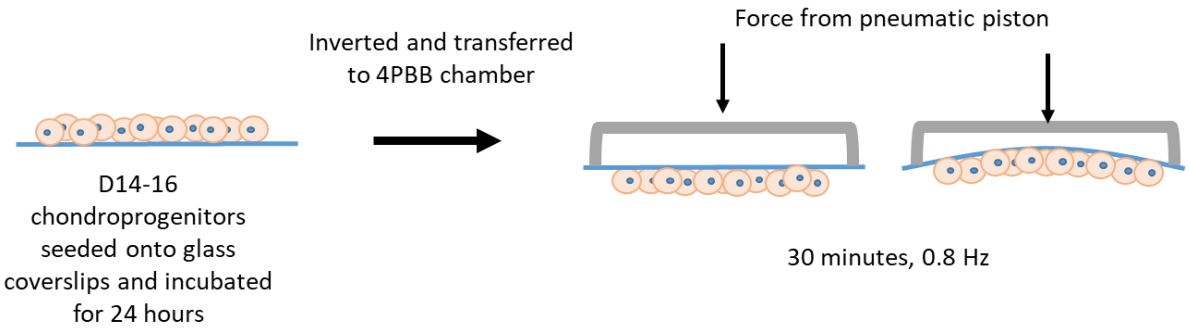

Figure 5-2. Schematic summary of the experimental design for application of the four-point bending model to hESC-derived chondroprogenitors. After one application of mechanical force for 30 minutes are 0.8 Hz, cells are incubated for a further 24 hours and lysed for subsequent gene expression analysis.

Chondroprogenitors were derived from hESC using a 14-day DDP, as described in chapter 2.3 and cryopreserved as described in chapter 2.2.5. Cells were thawed as required (chapter 2.2.2), seeded onto glass coverslips at a density of either 2.5 x 10^5 cells/mL (low) or 3.75 x 10^5 cells/mL (high) and stimulated with the 4PBB as described in chapter 2.8. After a further 24 hours of incubation cells were lysed with 570 µL buffer RLT supplemented with 1% ß-mercaptoethanol. The lysate was transferred to a 1.5 mL centrifuge tube and stored at -80°C. RNA isolation was performed as described in chapter 2.12.1, reverse transcription was carried out as described in chapter 2.13 and qRT-PCR was performed on the resulting cDNA as described in chapter 2.14.

5.3.3 Statistical analysis

Statistical analysis was performed as described in chapter 2.23.

5.4 Results

5.4.1 Directed differentiation of hESC

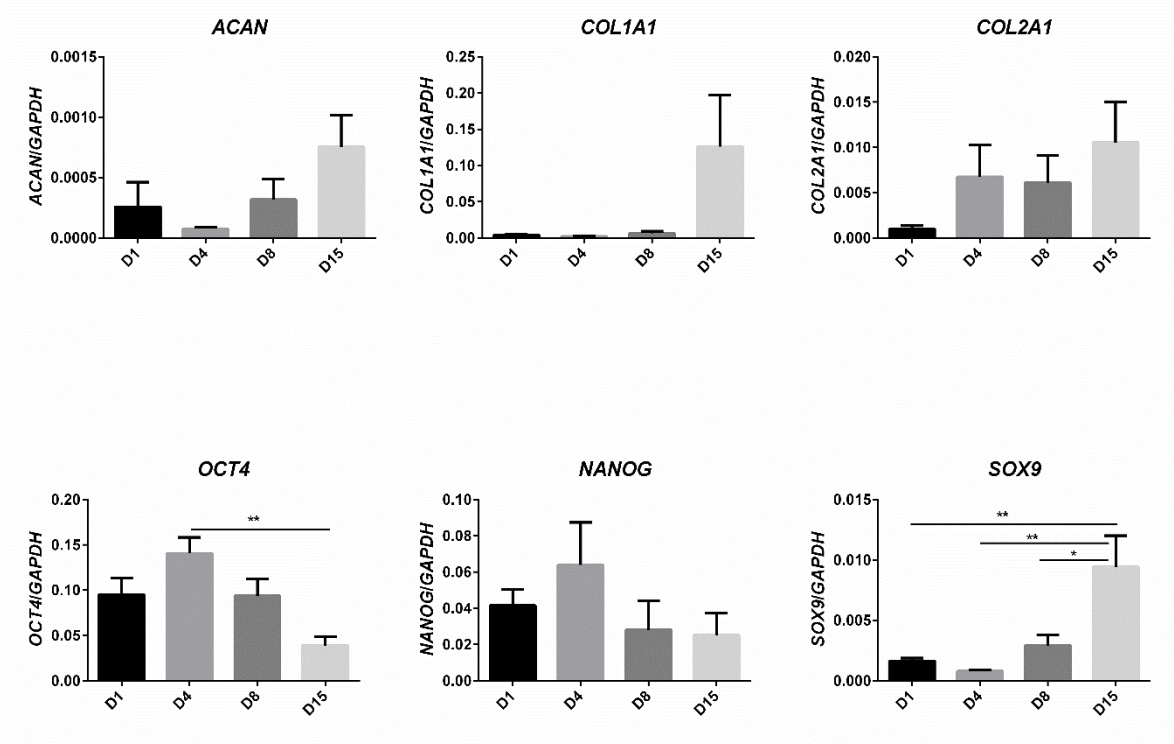

Figure 5-3. Chondrogenic gene expression increases and pluripotency gene expression decreases with progression of DDP. Representative expression pattern of *ACAN*, *COL1A1*, *COL2A1*, *OCT4*, *NANOG* and *SOX9* in MAN7 hESC subjected to directed differentiation for 15 days. Expression is relative to *GAPDH* ($2^{-\Delta Ct}$). Data are expressed as the mean ± standard error, N=5-7 (biological repeats), *p<0.05, **p<0.01.

Chondrogenic gene expression increased between day 1 and day 15 in all DDP runs performed on MAN7 hESC (figure 5-3). Mean *SOX9* expression was significantly greater in D15 cells than in D1 (p<0.01), D4 (p<0.01) and D8 cells (p<0.05). Expression of pluripotency markers *OCT4* and *NANOG* decreased overall, but there was a small initial expected increase on day 4 and expression was not completely ablated by day 15; this is indicative of the

presence of residual pluripotent stem cells in each population of chondroprogenitors. However, *OCT4* expression was significantly reduced between D4 and D15 ($p<0.01$). *COL1A1* expression showed a large increase by day 15, which may be indicative of a fibrocartilage phenotype. Large standard error bars are reflective of the variation typically observed between DDP runs.

5.4.2 Application of hydrostatic pressure enhances cartilaginous matrix deposition

Results from one experiment with 3 technical repeats (n=3) show that, compared to cell only controls, expression of *ACAN* (figure 5-4 A) was significantly higher when hydrogels were subjected to 270 kPa cyclic hydrostatic pressure using the TGT system ($p<0.05$). There were no other significant differences in *ACAN* expression. *COL1A1* expression (figure 5-4 B) demonstrated no significant differences between any of the groups, but it was generally higher in 3D constructs than in cell only controls. *COL2A1* expression (figure 5-4 C) was significantly higher in cells stimulated with both 170 kPa ($p<0.05$) and 270 kPa ($p<0.01$), compared to cell only controls, but not significantly higher than static controls. *SOX9* expression (figure 5-4 D) was significantly higher in gels stimulated with 270 kPa than in both static ($p<0.01$) and cell only ($p<0.001$) controls and significantly higher in those stimulated with 170 kPa than in cell only controls ($p<0.01$).

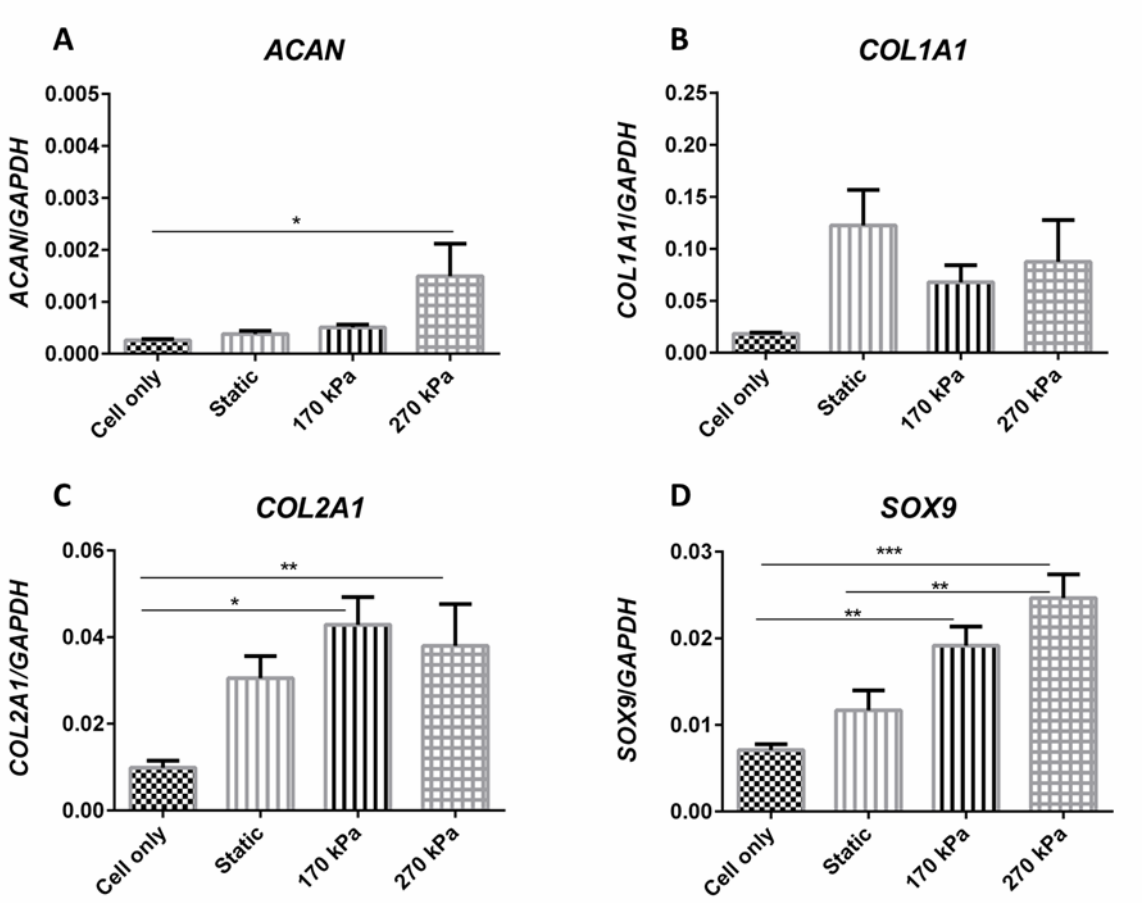

Figure 5-4. Chondrogenic gene expression is enhanced by the application of hydrostatic pressure. Gene expression is relative to *GAPDH* ($2^{-\Delta Ct}$). Data are expressed as the mean ± standard error, n=3 (technical repeats), *p<0.05, **p<0.01, ***p<0.001.

Safranin-O staining (figure 5-5) shows that application 170 kPa and 270 kPa cyclic hydrostatic pressure using the TGT system resulted in visibly enhanced matrix deposition compared to static and acellular controls. Two samples from each group were analysed and representative images are shown in figure 5-5. Image analysis shows that constructs stimulated at 170 kPa had significantly greater levels of safranin-O staining compared to static cellular controls and stimulated acellular controls ($p<0.05$ for both). In addition, constructs simulated at 270 kPa had significantly higher levels of staining than acellular

controls ($p<0.05$), but there was no significant difference between the two stimulated cellular groups. As expected, porcine articular cartilage had a significantly higher degree of staining than static cellular ($p<0.001$), 270 kPa acellular ($p<0.001$) and 270 kPa cellular ($p<0.05$) groups, but not significantly more so than 170 kPa cellular.

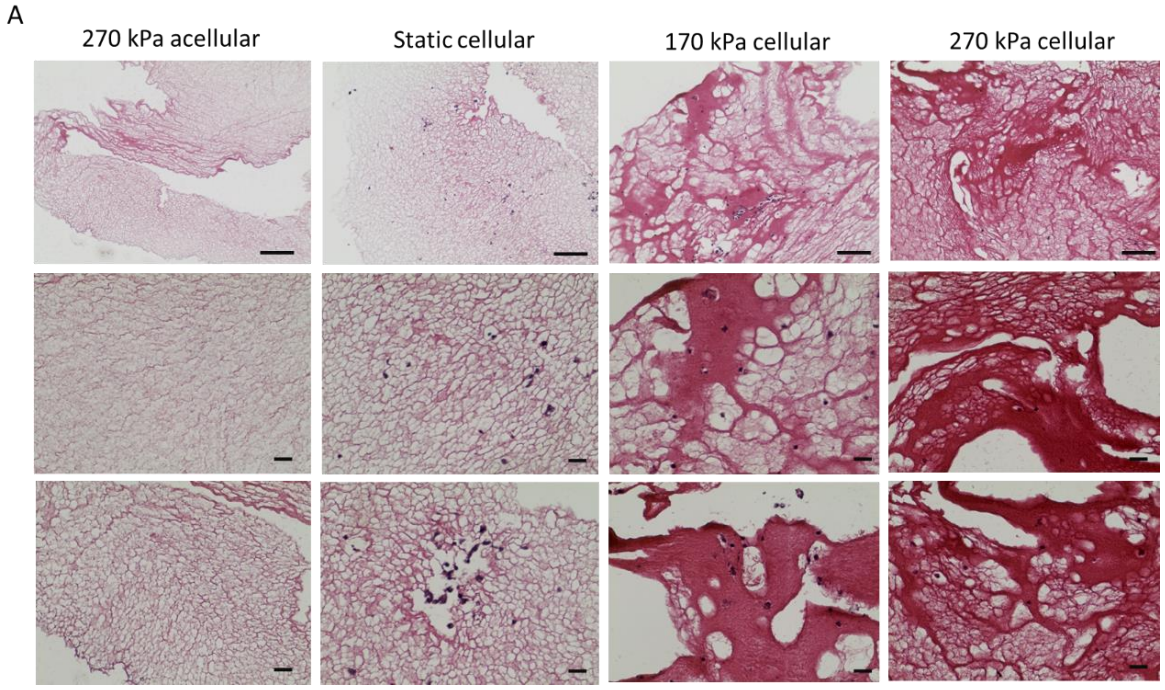

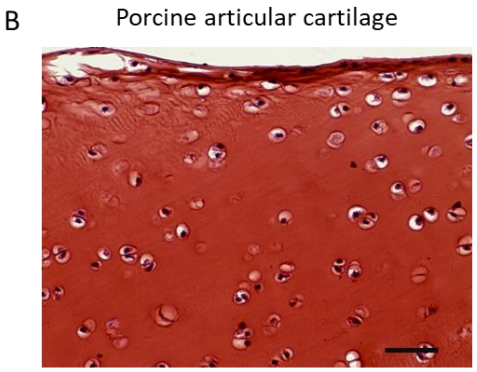

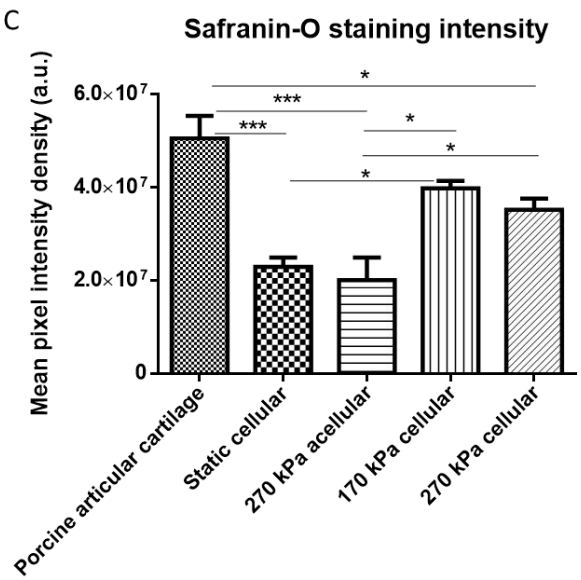

Figure 5-5. Chondrogenic matrix deposition is enhanced by the application of cyclic hydrostatic pressure. A) hESC-derived chondroprogenitors were encapsulated in fibrin gels at 0.5 x 10^6 cells/mL and cultured for 7 days. Gels stimulated in the hydrostatic bioreactor (TGT control system) for 1 hour/per day, 4 days at 1 Hz at either 270 kPa or 170 kPa. Static controls received no stimulation. B) Representative image of porcine articular cartilage. 5 µm paraffin sections stained with haematoxylin and Safranin-O (A and B). Scale = 500 µm. C) Safranin-O staining intensity assessed via pixel density of images. Data obtained from 3 images per group. Data are expressed as the mean ± standard error, n=3 (technical repeats), *p<0.05, ***p<0.001.

ICC was performed on whole constructs stimulated with the OB1 MK3 system. Analysis of one gel from each condition suggests that 270 kPa cyclic hydrostatic pressure results in more COL2 deposition than in static controls (figure 5-5). By immunofluorescence on whole gels, COL2 fluorescence intensity is visibly (figure 5-5 A) and measurably (figure 5-5 B) higher in the stimulated sample than in the static control. However, DAPI intensity (figure 5-5 A) is also higher in the stimulated sample which suggests that this construct contained more cells. When normalised to DAPI, COL2 expression is very similar in both gels (figure 5-5 C).

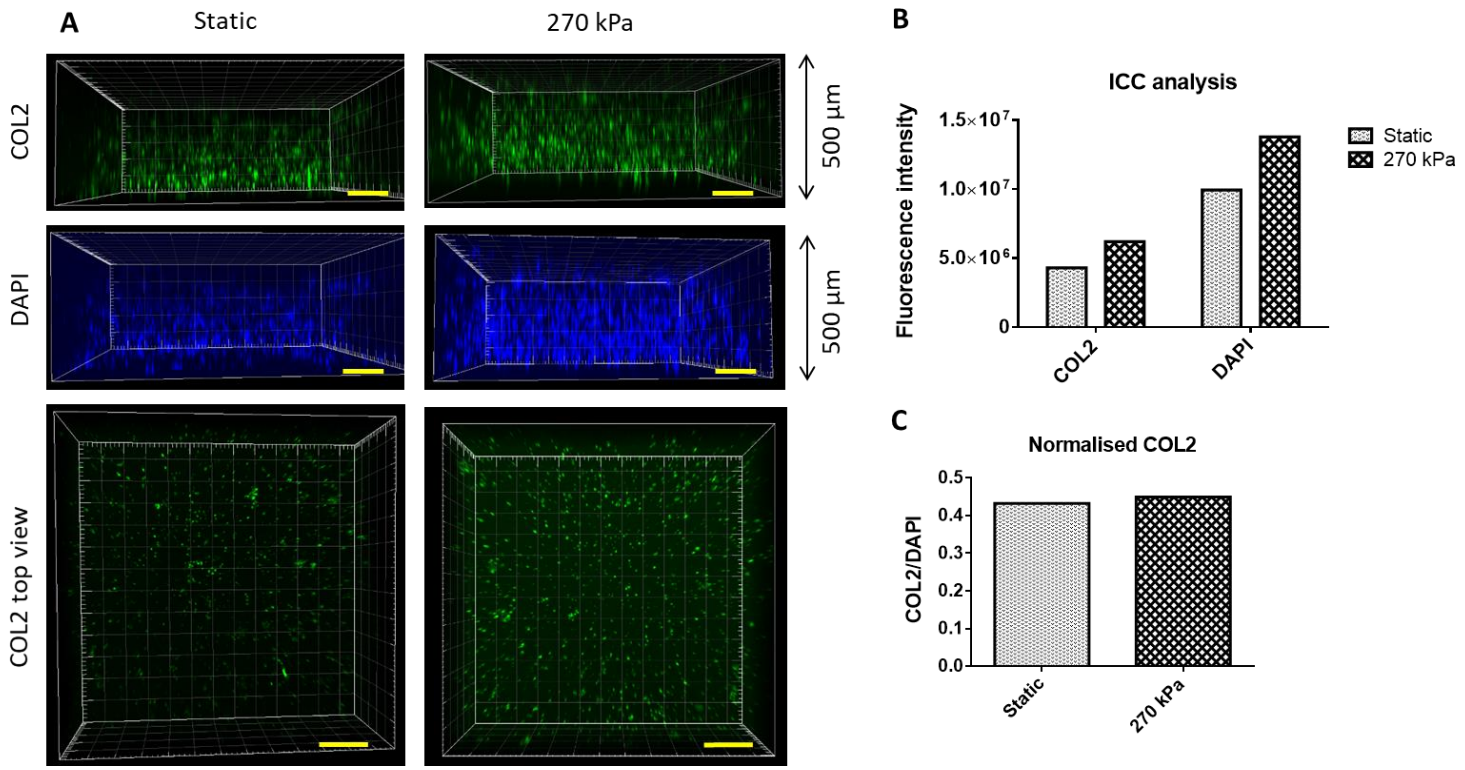

Figure 5-6. Hydrostatic pressure may increase the number of collagen type II-expressing cells. hESC-derived chondroprogenitors encapsulated in fibrin hydrogels at 0.5 x 10^6 cells/mL and cultured for 7 days. Gels stimulated in the hydrostatic bioreactor (OB1 MK3 control system) for 1 hour/per day, 4 days at a frequency of 1 Hz and a pressure of 270 kPa. Static controls received no stimulation. Scans were taken from the bottom up every 9 µm with a laser confocal microscope, for a distance of ≤500 µm. Images were constructed using Imaris Image Analysis software. Scale bars = 200 µm. N=1.

5.4.3 Effects of the 4PBB are dependent on cell seeding density

Chondrogenic gene expression of cells seeded at the lower density of 2.5 x 10^5/mL always showed a trend of upregulation in response to stimulation from the 4PBB. In three independent experiments, each with three technical repeats (figure 5-7), *ACAN* expression (figure 5-7 A) was significantly higher in stimulated samples in one repeat ($p<0.01$) (figure 5-7 A3). *COL2A1* (figure 5-7 B) and *SOX9* (figure 5-7 C) expressions were also significantly higher in one repeat (figure 5-7 B2 and C2) ($p<0.05$ in both cases). *TRPV4* expression (figure 5-7 D) was significantly enhanced in two repeats (figure 5-7 D2 and D3) (both $p<0.01$). Mean gene expression from three independent experiments showed a similar trend but differences were not significant (data not shown).

When cells were seeded at the higher density of 3.75 x 10^5/mL (figure 5-8), the reverse pattern was often observed; chondrogenic gene expression was down-regulated in response to stimulation with the 4PBB. Expressions of *ACAN* (figure 5-8 A) were significantly increased in unstimulated cells compared to stimulated samples in two out of three repeats (figure 5-8 A2 and A3) ($p<0.001$ and $p<0.05$ respectively). The same was true for *SOX9* expression (figure 5-8 C2 and C3) ($p<0.01$ and $p<0.05$ respectively) and *TRPV4* expression, which was significantly lower in stimulated samples in one repeat (figure 5-8 D2) ($p<0.05$). *COL2A1* showed a similar trend of reduced expression in one repeat (figure 5-8 B1), but differences were not significant. With the exception of *SOX9* (figure 5-9), where mean expression from was significantly reduced ($p<0.05$), mean gene expressions from three independent experiments were not significantly different between stimulated and unstimulated samples, though the same trend of down-regulation was observed.

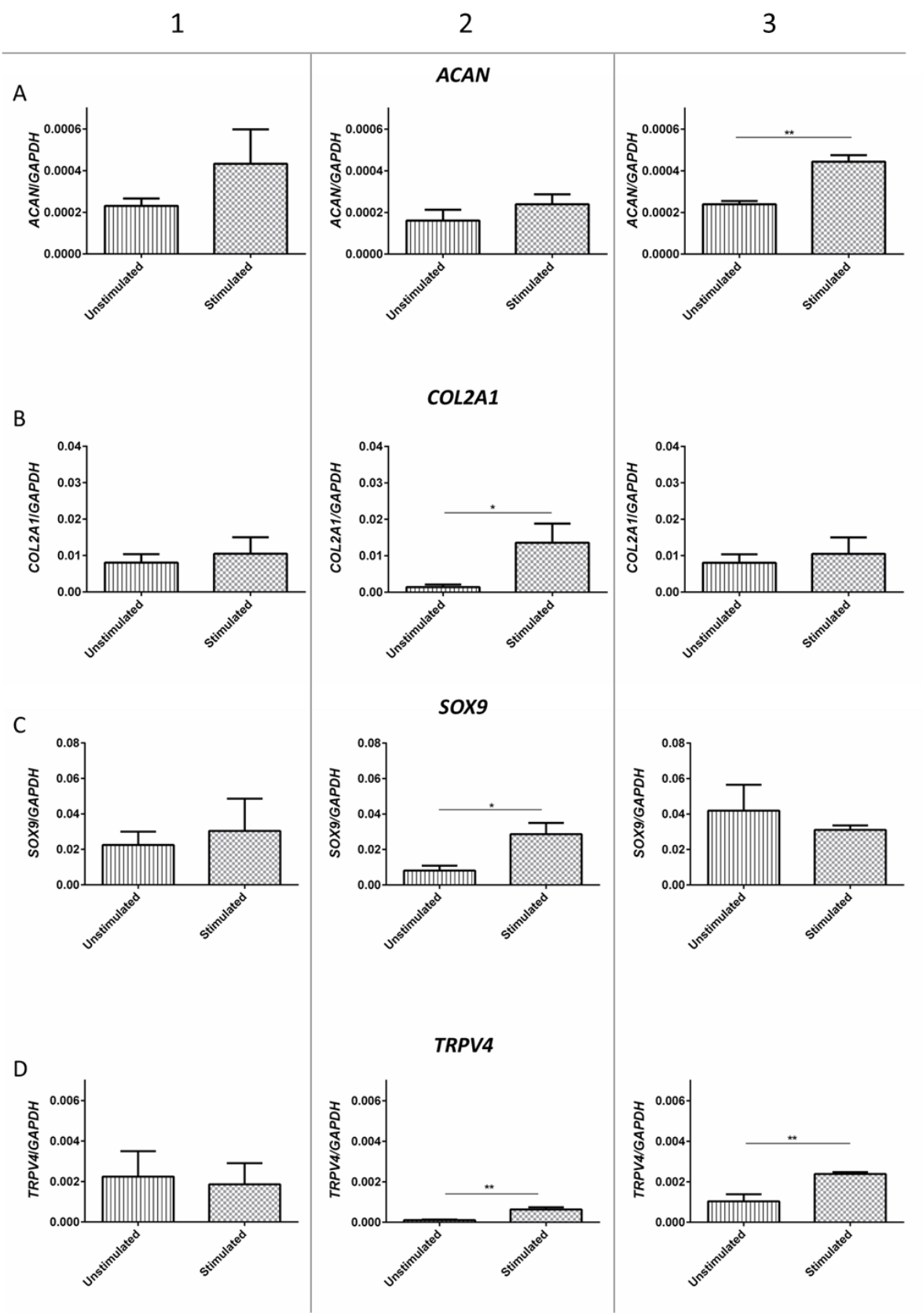
1
2
3
A
ACAN
ACAN/GAPDH
0.0000
0.0002
0.0004
0.0006
**
Unstimulated
Stimulated
B
COL2A1
COL2A1/GAPDH
0.00
0.01
0.02
0.03
0.04
*
C
SOX9
SOX9/GAPDH
0.00
0.02
0.04
0.06
0.08
*
D
TRPV4
TRPV4/GAPDH
0.000
0.002
0.004
0.006
**

Figure 5-7. Stimulation with the 4PBB enhances chondrogenic gene expression at lower cell seeding density. hESC-derived chondroprogenitors seeded at a density of 2.5 x 10^5 cells/mL in 3 independent experiments (1-3). qRT-PCR was performed 24 hours post stimulation. Gene expression is relative to *GAPDH* ($2^{-\Delta Ct}$). Data are expressed as the mean ± the standard error. 3 technical repeats performed per experiment (n=3). *p<0.05, **p<0.01

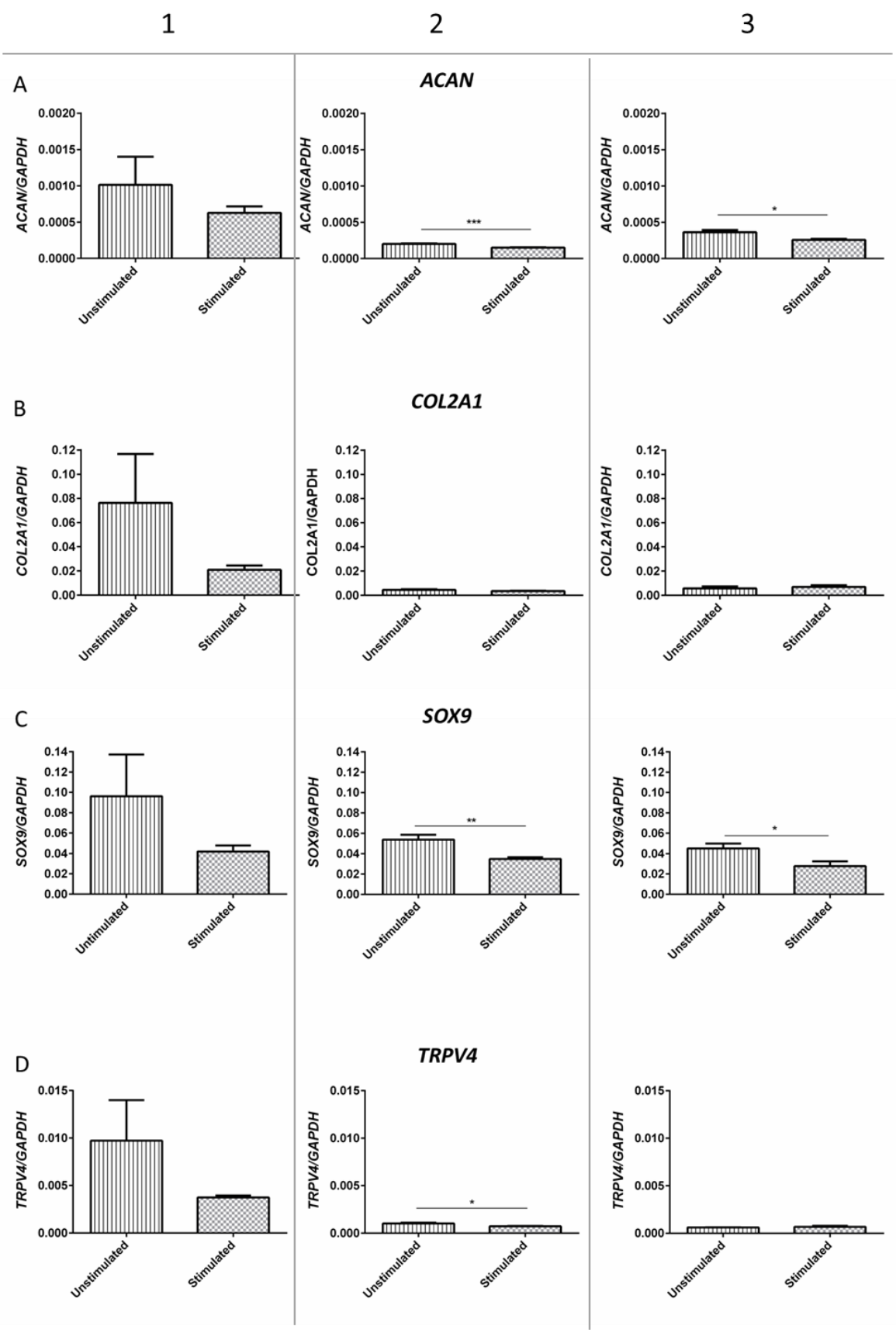
1
2
3
A
ACAN
ACAN/GAPDH
0.0020
0.0015
0.0010
0.0005
0.0000
***
*
Unstimulated
Stimulated
B
COL2A1
COL2A1/GAPDH
0.12
0.10
0.08
0.06
0.04
0.02
0.00
C
SOX9
SOX9/GAPDH
0.14
**
Untimulated
D
TRPV4
TRPV4/GAPDH
0.015
0.010
0.005
0.000

Figure 5-8. Stimulation with the 4PBB reduces chondrogenic gene expression at higher cell seeding density. hESC-derived chondroprogenitors seeded at a density of 3.75 x 10^5 cells/mL in 3 independent experiments (1-3). qRT-PCR was performed 24 hours post stimulation. Gene expression is relative to *GAPDH* ($2^{-\Delta Ct}$). Data are expressed as the mean ± the standard error. 3 technical repeats performed per experiment (n=3). *p<0.05, **p<0.01, ***p<0.001.

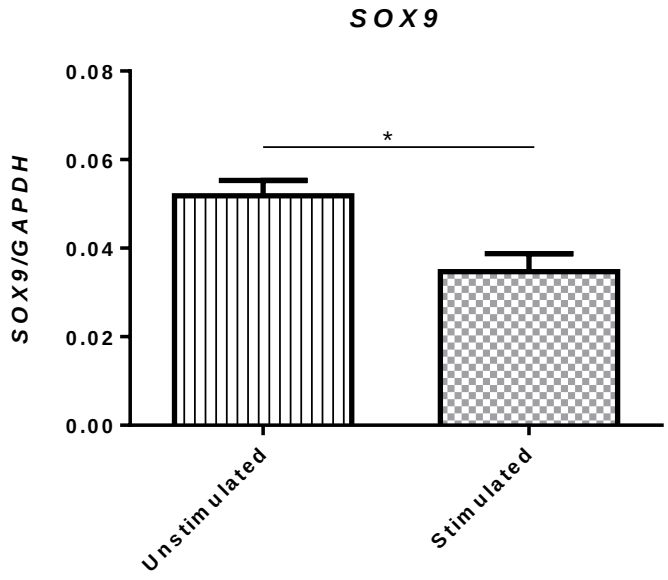

Figure 5-9. Mean gene expression confirms that stimulation with the 4PBB is detrimental to *SOX9* gene expression at higher cell seeding densities. hESC-derived chondroprogenitors seeded at a density of 3.75 x 10^5 cells/mL. qRT-PCR was performed 24 hours post stimulation. Gene expression is relative to *GAPDH* ($2^{-\Delta Ct}$). Data are from three independent experiments (N=3) and are expressed as the mean ± the standard error. *p<0.05.

5.5 Discussion

Our results show a clear relationship between the dynamic environment and the expression of chondrogenic genes. Both a 3D model and a dynamic environment are necessary to promote a more mature phenotype in hESC-derived chondroprogenitor/fibrin constructs. In most cases, chondrogenic gene expression was significantly higher in hydrogels subjected to cyclic hydrostatic pressure when compared cell only controls (monolayer), though not when compared to static controls (except in the case of *SOX9*). For pre-differentiated cells, the use of a 3D model alone was not sufficient to bring about a significant enhancement of *ACAN* and *COL2A1* expression – genes which code for the two major ECM molecules in articular cartilage.

Proteoglycan deposition and matrix density were undoubtedly improved by the application of hydrostatic pressure – here the presence of cells is the only factor which distinguishes static controls from acellular. The staining intensity of the two stimulated, cellular groups, however, is approaching the level of the porcine articular cartilage. Again, deposition of COL2 appears elevated in stimulated samples, though further work is required to confirm this. Higher COL2 staining intensity could be a result of increased cell numbers in constructs subjected to hydrostatic pressure, as indicated by a concomitant increase in DAPI intensity. Previous studies have reported an increase in proliferation in response to hydrostatic pressure. Murine BMSC exposed to 90 kPa sustained HP for a 1 hour period showed an increased S-phase fraction and proliferative index (M. Zhang et al. 2012; Zhao et al. 2015). In an earlier study, human vascular endothelial cells (HUVEC) exposed to sustained HP also demonstrated increased proliferative activity; although here, no attempts were made to quantify the level of pressure exerted by the system (Schwartz et al. 1999). Proliferation

markers and DNA assays should be incorporated into future experiments in order to determine if hydrostatic pressure improves the proliferative capacity of hESC-derived chondroprogenitors; if this were the case then it would be of great benefit, as expansion of these cells is very limited, especially after cryopreservation.

In the case of *SOX9*, expression was significantly greater in gels subjected to 270 kPa hydrostatic pressure than in static controls, but this was not true of those subjected to 170 kPa, which suggests that there may be some benefit in using higher pressure regimes. Adult articular cartilage is exposed to compressive forces as high as 18 MPa (B. D. Elder and Athanasiou 2009) and numerous studies have reported that pressures in the region of 4-10 MPa are beneficial for tissue engineered cartilaginous constructs (see table 1-3, chapter 1). However, the use of pressures similar to those observed in adult tissue *in vivo* may not be appropriate for immature tissue engineered cartilage, which is more akin to that observed during earlier developmental stages. Therefore, it is unsurprising that relatively low levels of hydrostatic pressure led to the striking changes in proteoglycan deposition which were observed in this study. Given that *SOX9* codes for the master regulator of chondrogenesis, of which *COL2* is a downstream target, it may be that these day 7 constructs represent an early stage in the process and that a longer time in culture would have brought about increases in matrix protein-coding genes that were also significantly higher than in static controls. Other studies have reported significant increases in *ACAN* and *COL2*, along with increased cartilaginous matrix production in response to hydrostatic pressure after 2 weeks (Reza and Nicoll 2008), 4 weeks (Zhao et al. 2015), 3 weeks (Correia et al. 2012) and even 8 weeks (Hu and Athanasiou 2006) of culture in hBMSC, hADSC and primary chondrocytes (both human and bovine). Few report significant differences after just 7 days, however.

Application of compressive strains with the 4PBB at low seeding densities appears to enhance chondrogenic gene expression. Though not significant, the trend across three independent experiments shows increasing expression in response to stimulation and individual experiments often showed significant increases. As with previous experiments (chapter 3 and 4), this lack of consistency across multiple experiments may be a result of the initial variation in response of hESC to the DDP. Another explanation may lie in issues experienced with cell seeding. When developing this system, the authors determined that cells should be confined to the middle 3 cm portion of the coverslip in order to receive the full 1000 μE strain. In practice this was difficult to achieve and a proportion of the population would adhere outside of this region.

Increases in *ACAN*, *COL2A1* and *SOX9* were generally accompanied by an increase in *TRPV4*, which suggests that the mechanical stimuli were transduced by this ion channel. Previous studies have shown a similar pattern of gene expression and an increase in SOX9-dependent reporter activity upon pharmacological activation of *TRPV4*, all of which were blocked by addition of the TRPV4 antagonist ruthenium red to the culture medium or by the use of a small interfering RNA for TRPV4 (Muramatsu et al. 2007). More recently, addition of the TRPV4 agonist 4alpha-phorbol-12,13-didecanoate (4α-PDD) resulted in improved collagen deposition and tensile strength in self-assembled articular cartilage constructs derived from bovine chondrocytes (Eleswarapu and Athanasiou 2013). In other work, both dynamic loading of porcine chondrocyte-laden agarose gels and addition of the TRPV4 agonist GSK101 were shown to increase expression of *COL2A1*, *TGFß3* and pro-anabolic/anti-catabolic genes (O'Conor et al. 2014). These effects were abrogated by the presence of the TRPV4 antagonist GSK205. Interestingly, unlike the work described by Muramatsu et al.

(above) and that of the current study, no increase in *SOX9* expression was observed in response to GSK101; the authors suggest that TRPV4 signal transduction may be via an alternative pathway in mature chondrocytes (O'Conor et al. 2014). TRPV4 activation has been reported previously in hESC-derived cells in response to mechanical stimulation, though there is little to be found relating to hESC and chondrogenesis. hESC-derived cardiomyocytes subjected to uniaxial stretch responded with directional realignment and this effect was blocked with the TRPV4 antagonists RN1734 and HC060747 (Y. Qi et al. 2015). Therefore, it seems plausible that TRPV4 channel activation and subsequent increased SOX9 activity are responsible for the response of hESC-derived chondroprogenitors to stimulation via the 4PBB. However, the use of TRPV4 agonists and antagonists along with SOX9 reporter systems would be required to confirm this. Limitations of the system rendered such work impossible in the time available; the susceptibility of the rudimentary apparatus to infection, loss of cells due to detachment during stimulation and poor RNA yield meant that a large number of experiments were unsuccessful.

At higher seeding densities, unstimulated controls often show higher chondrogenic gene expression and, in the case of *SOX9*, mean expression across three independent experiments was significantly higher in this group. In order for cells to experience the uniaxial strain imparted by the system, they must be in contact with the coverslip. hESC-derived chondroprogenitors tend to form aggregates rather than a homogenous monolayer, thus larger aggregates form when they are seeded in large numbers and confined to the same area as those seeded at a lower density. Consequently, a larger number of cells are not in direct contact with the coverslip and, therefore, are subject to a

much lower level of strain. This explains why there was frequently no significant change in chondrogenic gene expression of stimulated cells compared to unstimulated controls, but quite why this would result in significantly lower *SOX9* expression overall is unclear.

5.6 Conclusion

Articular cartilage is subject to cyclic compressive loads during normal development and function. These forces, converted into hydrostatic pressure and shear flow by the interstitial fluid, are detected and transduced by chondrocytes, initiating signalling cascades and bringing about transcriptional changes which are essential for both development and maintenance of the tissue. Therefore, it is only logical that tissue engineering strategies should seek to recapitulate this dynamic environment *in vitro*. Fibrin-encapsulated, hESC-derived chondroprogenitors can respond to cyclic hydrostatic pressure with increased chondrogenic gene expression and matrix deposition. At low seeding densities, cyclic compressive forces imparted by the 4PBB may also result in enhanced chondrogenic gene expression in hESC-derived chondroprogenitors. Results indicate that both types of dynamic environment favour higher levels of proliferation, although more work is needed to confirm this.

Chapter 6

Discussion, future work and concluding remarks

6.1 Summative discussion

Articular joint disease and degeneration pose a huge financial burden to the NHS and severely impair the quality of life for those affected. As yet, there is no effective and enduring alternative to the current gold standard treatment of joint replacement, which is both costly and invasive. Therefore, there is a great need for the development of treatments such as tissue engineered cartilage grafts and cell therapies, which can replace damaged tissue and promote endogenous repair mechanisms. Much research is underway in the fields of rheumatology, stem cell biology and regenerative medicine (to name but a few), in a bid to find alternative, effective treatments for conditions such as OA and RA. As with many other target tissues, the appropriate source of material for cell-based therapies remains in hot dispute. Autologous chondrocytes, which offer the distinct advantages of immune-compatibility and of producing unquestionably superior ECM, have already been utilised with some success (Schuette, Kraeutler, and McCarty 2017). However, the necessity of their isolation from the patient and subsequent expansion *in vitro* prior to application renders significant scalability impossible and may discourage major investment from pharmaceutical companies wishing to produce an "off the shelf" product. In addition, one has to question whether cells isolated from OA/RA patients will retain an endogenous predisposition towards pathogenesis and whether the diseased environment into which they are implanted would be detrimental to the successful function of these healthy cells. For these reasons, allogeneic multipotent/pluripotent stem cells are a more attractive prospect for many researchers. BMSC have successfully been used to generate chondrocytes for a number of years, but their expansion capacity is very limited and their isolation from healthy donors is a painful and invasive procedure. hESC and, more recently,

induced pluripotent stem cells (iPSC) can also be used to generate chondrocytes, but offer the added advantage of potentially limitless expansion capacity. In addition, the protocol described by Oldershaw et al. for producing chondroprogenitors from hESC forgoes the problematic step of embryoid body formation, resulting in a population of cells which require minimal processing and are more heterogeneous (Oldershaw et al. 2010). Barriers to the clinical translation of these cells are their immature phenotype and the potential for the residual pluripotent cells to form teratomas *in vivo*. Cheng et al (2014) sought to remove the latter obstacle with the application of the pluripotent cell-specific inhibitor PluriSIn1, which was earlier reported to be toxic to pluripotent cells at very low concentrations, whilst preserving progenitor/differentiated cells (Ben-David et al. 2013). However, when used at recommended concentrations, toxicity to hESC-derived chondroprogenitors was also observed.

The purpose of this study was to investigate a range of culture techniques, dynamic regimes and biomaterials with the intention of producing a protocol for enhancing the chondrogenic potential of hESC-derived chondroprogenitors and obtaining a more mature phenotype. This thesis is the first to report the use of hESC-derived chondroprogenitors differentiated in monolayer on an immobilised Wnt platform to create a 3D chondrogenic model. In addition, it is the first to report the effects of hydrostatic pressure on an hESC-derived 3D chondrogenic model and the first to report the application of a four-point bending model to monolayer hESC-derived chondroprogenitors. Chapter 3 demonstrates that providing differentiating cells with a 3D environment to migrate into enhances expression of chondrogenic markers compared to 2D culture and that inclusion of an immobilised Wnt platform accelerates this process. Given that all other methods of chondrogenic

differentiation utilise 3D culture and that natural cartilage development occurs in a complex 3D environment, this is unsurprising. However, unlike the pellet culture or embryoid body formation favoured by more traditional protocols, this model allows cells to migrate in response to environmental cues and results in a layered structure, which is more analogous to the native tissue. Although fibrin has proven to be a useful 3D model for the Kimber lab's hESC (explored in chapter 4), there are a range other biomaterials whose chondro-inductive properties ought to render them a more suitable choice for producing tissue engineered cartilage. It was hoped that the substitution of fibrin for one of these materials would build on the work described in chapter 3 and produce a superior 3D chondrogenic model. However, none of the biomaterials tested were able to support cell viability to the same degree as fibrin, despite reports of success in other hESC lines (Toh et al. 2010). The ultimate aim of this work was to subject the optimised 3D chondrogenic model to mechanical stimulation in a bid to recapitulate the dynamic native environment and to produce a more mature construct. Initial work with our custom-made hydrostatic bioreactor indicated that fibrin-encapsulated cells did indeed respond positively to regimes of mechanical stimulation, as evidenced by increased chondrogenic gene expression and matrix deposition. Unfortunately, the system failed in the first year of this study and repair/replacement proved impossible, despite a great deal of effort. The group did recently manage to acquire a comparable system, but there was insufficient time to remaining to repeat the work described in chapter 5 using freshly-differentiated cells.

Another means of imparting mechanical stimulation, the 4PBB, was also adopted in this study. This device is more limited than the hydrostatic bioreactor, in that it can only be used to stimulate cells in monolayer and is an open system, which leaves them prone to infection

and can, therefore, only be used for brief incubation periods. The intention with this system was to interrogate the cellular response to mechanical cues more closely by identifying receptors and pathways activated as a result of stimulation and by examining the effects of their inhibition. Unfortunately, the high incidence of infection and the tendency of the cells to detach during stimulation, meant that the many experiments yielded no results. Despite this, there is evidence that cells responded to the 4PBB with up-regulated chondrogenic gene expression when seeded at a low density and that their response is mediated via MAPK signalling.

Pluripotent stem cells are much more susceptible to seemingly minor environmental changes than multipotent and terminally differentiated cells, such as BMSC or articular chondrocytes. Although this broadens the scope for potential applications, it also presents an array of challenges for culturing the cells. A major obstacle in this study was the variation in response of MAN7 and MAN13 hESC to the DDP. Although an increase in chondrogenic gene expression and a decrease in pluripotency markers were generally observed with time, there was a great deal of variation in levels of expression between runs. This produced large standard errors when means were calculated from multiple experiments, which meant that observed differences were rarely significant. In addition, hESC are less robust than other cell types and do not adhere well to tissue culture plastic; again this presented obstacles when trying to culture and differentiate the cells and progress was, therefore, particularly slow. Despite the many advantages of using pluripotent stem cells for tissue engineering applications, the fact that these issues remained a huge hindrance to progress throughout the three years of this study suggests that more work is required to render hESC cell therapies translatable. It may be, however, that commercially available hESC lines are less

susceptible to these issues, in which case the application of cyclic hydrostatic pressure to the 3D hESC model of chondrogenesis described in chapter 3 could result in a superior tissue engineered cartilaginous construct.

6.2 Future work

Chapter 3 outlines the production of a 3D hESC chondrogenic model with an immobilised Wnt platform. In order to confirm that the WNT3A is accelerating the migration and subsequent differentiation of hESC in the fibrin hydrogel, a number of factors would need to be established. Firstly, it would be useful to confirm that MAN7 and MAN13 hESC are actually Wnt responsive with the use of a TCF/LEF reporter system as described previously (Fuerer and Nusse 2010). In addition, it was never confirmed in this study that the WNT3A was efficiently bound to the PCL surface. This method was adapted from a protocol which describes the adsorption of WNT3A to glass surfaces, which have different chemical properties to PCL (Lowndes, Junyent, and Habib 2017). In order to ascertain whether the protein is indeed bound, a number of techniques could be employed, including simple ICC using anti-WNT3A antibodies; techniques such as X-ray photoelectron spectroscopy (XPS) to characterise the surface of the polymer; or Wnt activity assays involving cells that express luciferase or green fluorescent protein upon induction of Wnt/ß-catenin signalling. In addition, it would be useful rule out the presence of residual pluripotent stem cells on this model (particularly the upper portion of the gel) by repeating the work and including gene expression analysis and ICC for the presence of makers such as OCT4.

Future work involving the Wnt platform model should be tested with additional ESC cell lines in order to show that the observed effects are reproducible. There was also no attempt

made in this study to determine the mode of action in this model. Even without Wnt in its active form, the addition of a hydrogel to a differentiating monolayer of cells resulted in increased expression of chondrogenic markers. It is possible that the change in cell-liquid interface brought about environmental changes, such as hypoxia, which drove the resulting physiological changes. Inclusion of primers for hypoxia markers such as hypoxia inducible factor 1 alpha (HIF-1α) or glucose transporter 1 (Glut-1) into gene expression analysis would be a simple way of testing this hypothesis (Le and Courter 2008). In addition, sensors could be used to measure oxygen levels in this model, even without the addition of cells, which would mitigate the necessity of repeating the entire experiment.

Acquisition of positive controls for use in gene expression analysis and ICC is also important for future work. Primary human chondrocytes would be the ideal control for gene expression analysis, in order to determine whether the increases in expressions of *COL2A1*, *ACAN*, and *SOX9* observed in this study are meaningful and approaching the levels observed in the native tissue. Given the limited availability of primary human joint tissue, another option is to obtain commercially available, pre-transcribed cDNA. It is also necessary to confirm that the protein expression shown with ICC is comparable to native tissue. In this case, however, the cross-reactivity of many antibodies means that articular cartilage from xenogeneic sources would suffice (as in chapter 5 where porcine tissue was used as a control for the presence of sulphated GAG).

Despite difficulties encountered when testing alternative biomaterials (chapter 4), gellan gum emerged as a potential alternative to fibrin. As mentioned earlier, alterations to the gel preparation and the inclusion of ROCK inhibitor may enhance the survival of hESC-derived chondroprogenitors encapsulated in gellan gum. If this is the case, it would be

interesting to see if this material proved more chondro-inductive when used in place of fibrin in both 3D models. Although gellan gum and fibrin appeared to possess enhanced mechanical properties, there is currently no data to show this. Therefore, it would be useful to determine the mechanical properties of these biomaterials with compression testing using a Bose machine. This may confirm the hypothesis that stiffer materials result in increased expression of chondrogenic markers.

Now that the OB1 MK3 bioreactor is available, the work involving hydrostatic pressure bears repeating. This would involve culture and chondrogenic differentiation of MAN7 and MAN13 hESC, as the recovery of pre-differentiated frozen stocks proved insufficient when attempts were made to repeat the work. It would also be interesting to incorporate cyclic hydrostatic pressure into the culture of the 3D model described in chapter 3. Finally, there were indications that both the hydrostatic bioreactor and the 4PBB brought about an increase in proliferation. To confirm this, PicoGreen assays could be carried out on samples after stimulation and BrdU or EdU proliferation assays could be incorporated into samples during culture.

6.3 Concluding remarks

The data presented in this thesis explores methods of enhancing the maturation of hESC-derived chondroprogenitors with a range of 2D and 3D culture techniques. Application of an immobilised Wnt platform and a 3D environment to hESC undergoing differentiation resulted in a more rapid increase chondrogenic markers and the production of a construct with potential for use in tissue engineering applications. Furthermore, application of cyclic hydrostatic pressure resulted in enhanced chondrogenic gene expression and matrix

deposition in an existing 3D hESC chondrogenic model. Although further work is required, we believe that the work described here holds great potential for the development of a cell-based therapy for cartilage damage and degeneration.

References

Aguado, Brian A., Widya Mulyasasmita, James Su, Kyle J. Lampe, and Sarah C. Heilshorn. 2012. 'Improving Viability of Stem Cells During Syringe Needle Flow Through the Design of Hydrogel Cell Carriers'. *Tissue Engineering. Part A* 18 (7–8): 806–15. https://doi.org/10.1089/ten.tea.2011.0391.

Ahearne, Mark, and Daniel J. Kelly. 2013. 'A Comparison of Fibrin, Agarose and Gellan Gum Hydrogels as Carriers of Stem Cells and Growth Factor Delivery Microspheres for Cartilage Regeneration'. *Biomedical Materials (Bristol, England)* 8 (3): 035004. https://doi.org/10.1088/1748-6041/8/3/035004.

Allen, Jessica L., Margaret E. Cooke, and Tamara Alliston. 2012. 'ECM Stiffness Primes the TGFβ Pathway to Promote Chondrocyte Differentiation'. *Molecular Biology of the Cell* 23 (18): 3731–42. https://doi.org/10.1091/mbc.E12-03-0172.

Anton, Roman, Hans A. Kestler, and Michael Kühl. 2007. 'Beta-Catenin Signaling Contributes to Stemness and Regulates Early Differentiation in Murine Embryonic Stem Cells'. *FEBS Letters* 581 (27): 5247–54. https://doi.org/10.1016/j.febslet.2007.10.012.

Arthritis Research UK. 2014. 'Arthritis in the UK – Facts and Statistics'. 2014. file:///C:/Users/rsf66/Downloads/Arthritis%20key%20facts.PDF.

Arthritis Research UK. 2017. 'Arthritis: The Nation's Joint Problem'. file:///C:/Users/rsf66/Downloads/State_of_the_nation_report_web_160817.pdf.

Bank, R. A., M. Soudry, A. Maroudas, J. Mizrahi, and J. M. TeKoppele. 2000. 'The Increased Swelling and Instantaneous Deformation of Osteoarthritic Cartilage Is Highly Correlated

with Collagen Degradation'. *Arthritis and Rheumatism* 43 (10): 2202–10. https://doi.org/10.1002/1529-0131(200010)43:10<2202::AID-ANR7>3.0.CO;2-E.

Bao, Xiu-li, Hui Song, Zhuo Chen, and Xin Tang. 2012. 'Wnt3a Promotes Epithelial-Mesenchymal Transition, Migration, and Proliferation of Lens Epithelial Cells'. *Molecular Vision* 18: 1983–90.

Barlic, Ariana, Matej Drobnic, Elvira Malicev, and Nevenka Kregar-Velikonja. 2008. 'Quantitative Analysis of Gene Expression in Human Articular Chondrocytes Assigned for Autologous Implantation'. *Journal of Orthopaedic Research: Official Publication of the Orthopaedic Research Society* 26 (6): 847–53. https://doi.org/10.1002/jor.20559.

Bauer, Christoph, Manuela Berger, Renate R. Baumgartner, Sonja Höller, Hannes Zwickl, Eugenia Niculescu-Morzsa, Florian Halbwirth, and Stefan Nehrer. 2016. 'A Novel Cross-Linked Hyaluronic Acid Porous Scaffold for Cartilage Repair'. *Cartilage* 7 (3): 265–73. https://doi.org/10.1177/1947603515611949.

Baxter, Melissa A., Maria V. Camarasa, Nicola Bates, Fiona Small, Patricia Murray, David Edgar, and Susan J. Kimber. 2009. 'Analysis of the Distinct Functions of Growth Factors and Tissue Culture Substrates Necessary for the Long-Term Self-Renewal of Human Embryonic Stem Cell Lines'. *Stem Cell Research* 3 (1): 28–38. https://doi.org/10.1016/j.scr.2009.03.002.

Bayliss, M. T., D. Osborne, S. Woodhouse, and C. Davidson. 1999. 'Sulfation of Chondroitin Sulfate in Human Articular Cartilage. The Effect of Age, Topographical Position, and Zone of Cartilage on Tissue Composition'. *The Journal of Biological Chemistry* 274 (22): 15892–900.

Bayliss, M T, M Venn, A Maroudas, and S Y Ali. 1983. 'Structure of Proteoglycans from Different Layers of Human Articular Cartilage.' *Biochemical Journal* 209 (2): 387–400.

Ben-David, Uri, Qing-Fen Gan, Tamar Golan-Lev, Payal Arora, Ofra Yanuka, Yifat S. Oren, Alicia Leikin-Frenkel, et al. 2013. 'Selective Elimination of Human Pluripotent Stem Cells by an Oleate Synthesis Inhibitor Discovered in a High-Throughput Screen'. *Cell Stem Cell* 12 (2): 167–79. https://doi.org/10.1016/j.stem.2012.11.015.

Benedek, T. G. 2006. 'A History of the Understanding of Cartilage'. *Osteoarthritis and Cartilage* 14 (3): 203–9. https://doi.org/10.1016/j.joca.2005.08.014.

Bengtsson, Eva, Matthias Mörgelin, Takako Sasaki, Rupert Timpl, Dick Heinegård, and Anders Aspberg. 2002. 'The Leucine-Rich Repeat Protein PRELP Binds Perlecan and Collagens and May Function as a Basement Membrane Anchor'. *Journal of Biological Chemistry* 277 (17): 15061–68. https://doi.org/10.1074/jbc.M108285200.

Berge, Derk ten, Dorota Kurek, Tim Blauwkamp, Wouter Koole, Alex Maas, Elif Eroglu, Ronald K. Siu, and Roel Nusse. 2011. 'Embryonic Stem Cells Require Wnt Proteins to Prevent Differentiation to Epiblast Stem Cells'. *Nature Cell Biology* 13 (9): 1070–75. https://doi.org/10.1038/ncb2314.

Bhosale, Abhijit M., and James B. Richardson. 2008. 'Articular Cartilage: Structure, Injuries and Review of Management'. *British Medical Bulletin* 87: 77–95. https://doi.org/10.1093/bmb/ldn025.

Bi, W., J. M. Deng, Z. Zhang, R. R. Behringer, and B. de Crombrugghe. 1999. 'Sox9 Is Required for Cartilage Formation'. *Nature Genetics* 22 (1): 85–89. https://doi.org/10.1038/8792.

Blaschke, Ulrich K., Eric F. Eikenberry, David J. S. Hulmes, Hans-Joachim Galla, and Peter Bruckner. 2000. 'Collagen XI Nucleates Self-Assembly and Limits Lateral Growth of Cartilage Fibrils'. *Journal of Biological Chemistry* 275 (14): 10370–78. https://doi.org/10.1074/jbc.275.14.10370.

Boyd, Nolan L., Kelly R. Robbins, Sujoy K. Dhara, Franklin D. West, and Steven L. Stice. 2009. 'Human Embryonic Stem Cell-Derived Mesoderm-like Epithelium Transitions to Mesenchymal Progenitor Cells'. *Tissue Engineering. Part A* 15 (8): 1897–1907. https://doi.org/10.1089/ten.tea.2008.0351.

Braam, Stefan R., Laura Zeinstra, Sandy Litjens, Dorien Ward-van Oostwaard, Stieneke van den Brink, Linda van Laake, Franck Lebrin, et al. 2008. 'Recombinant Vitronectin Is a Functionally Defined Substrate That Supports Human Embryonic Stem Cell Self-Renewal via AVβ5 Integrin'. *STEM CELLS* 26 (9): 2257–65. https://doi.org/10.1634/stemcells.2008-0291.

Brittberg, M., A. Lindahl, A. Nilsson, C. Ohlsson, O. Isaksson, and L. Peterson. 1994. 'Treatment of Deep Cartilage Defects in the Knee with Autologous Chondrocyte Transplantation'. *The New England Journal of Medicine* 331 (14): 889–95. https://doi.org/10.1056/NEJM199410063311401.

Burr, D. B., C. Milgrom, D. Fyhrie, M. Forwood, M. Nyska, A. Finestone, S. Hoshaw, E. Saiag, and A. Simkin. 1996. 'In Vivo Measurement of Human Tibial Strains during Vigorous Activity'. *Bone* 18 (5): 405–10.

Cañibano-Hernández, Alberto, Laura Saenz Del Burgo, Albert Espona-Noguera, Gorka Orive, Rosa M. Hernández, Jesús Ciriza, and Jose Luis Pedraz. 2017. 'Alginate Microcapsules Incorporating Hyaluronic Acid Recreate Closer in Vivo Environment for Mesenchymal Stem

Cells'. *Molecular Pharmaceutics* 14 (7): 2390–99. https://doi.org/10.1021/acs.molpharmaceut.7b00295.

Canty, Elizabeth G., and Karl E. Kadler. 2005. 'Procollagen Trafficking, Processing and Fibrillogenesis'. *Journal of Cell Science* 118 (7): 1341–53. https://doi.org/10.1242/jcs.01731.

Cao, Li, Inchan Youn, Farshid Guilak, and Lori A. Setton. 2006. 'Compressive Properties of Mouse Articular Cartilage Determined in a Novel Micro-Indentation Test Method and Biphasic Finite Element Model'. *Journal of Biomechanical Engineering* 128 (5): 766–71. https://doi.org/10.1115/1.2246237.

Carroll, S. F., C. T. Buckley, and D. J. Kelly. 2014. 'Cyclic Hydrostatic Pressure Promotes a Stable Cartilage Phenotype and Enhances the Functional Development of Cartilaginous Grafts Engineered Using Multipotent Stromal Cells Isolated from Bone Marrow and Infrapatellar Fat Pad'. *Journal of Biomechanics* 47 (9): 2115–21. https://doi.org/10.1016/j.jbiomech.2013.12.006.

Carver, S. E., and C. A. Heath. 1999. 'Influence of Intermittent Pressure, Fluid Flow, and Mixing on the Regenerative Properties of Articular Chondrocytes'. *Biotechnology and Bioengineering* 65 (3): 274–81.

Cescon, Matilde, Francesca Gattazzo, Peiwen Chen, and Paolo Bonaldo. 2015. 'Collagen VI at a Glance'. *J Cell Sci* 128 (19): 3525–31. https://doi.org/10.1242/jcs.169748.

Chan, Samantha C. W., Stephen J. Ferguson, and Benjamin Gantenbein-Ritter. 2011. 'The Effects of Dynamic Loading on the Intervertebral Disc'. *European Spine Journal: Official Publication of the European Spine Society, the European Spinal Deformity Society, and the*

European Section of the Cervical Spine Research Society 20 (11): 1796–1812. https://doi.org/10.1007/s00586-011-1827-1.

Chen, A., C. Gupte, K. Akhtar, P. Smith, and J. Cobb. 2012. 'The Global Economic Cost of Osteoarthritis: How the UK Compares'. Research article. Arthritis. 2012. https://doi.org/10.1155/2012/698709.

Chen, Chih-Hao, Chang-Yi Kuo, Yan-Jie Wang, and Jyh-Ping Chen. 2016. 'Dual Function of Glucosamine in Gelatin/Hyaluronic Acid Cryogel to Modulate Scaffold Mechanical Properties and to Maintain Chondrogenic Phenotype for Cartilage Tissue Engineering'. *International Journal of Molecular Sciences* 17 (11). https://doi.org/10.3390/ijms17111957.

Chen, Yupeng, Jack Cossman, Chathuraka T. Jayasuriya, Xin Li, Yingjie Guan, Vera Fonseca, Kun Yang, et al. 2016. 'Deficient Mechanical Activation of Anabolic Transcripts and Post-Traumatic Cartilage Degeneration in Matrilin-1 Knockout Mice'. *PLOS ONE* 11 (6): e0156676. https://doi.org/10.1371/journal.pone.0156676.

Cheng, Aixin, Timothy E. Hardingham, and Susan J. Kimber. 2014. 'Generating Cartilage Repair from Pluripotent Stem Cells'. *Tissue Engineering. Part B, Reviews* 20 (4): 257–66. https://doi.org/10.1089/ten.teb.2012.0757.

Cheng, Aixin, Zoher Kapacee, Jiang Peng, Shibi Lu, Robert J. Lucas, Timothy E. Hardingham, and Susan J. Kimber. 2014. 'Cartilage Repair Using Human Embryonic Stem Cell-Derived Chondroprogenitors'. *Stem Cells Translational Medicine* 3 (11): 1287–94. https://doi.org/10.5966/sctm.2014-0101.

Cheng, Gu, Zahra Davoudi, Xin Xing, Xin Yu, Xin Cheng, Zubing Li, Hongbing Deng, and Qun Wang. 2018. 'Advanced Silk Fibroin Biomaterials for Cartilage Regeneration'. *ACS Biomaterials Science & Engineering* 4 (8): 2704–15. https://doi.org/10.1021/acsbiomaterials.8b00150.

Chevalier, Xavier. 1993. 'Fibronectin, Cartilage, and Osteoarthritis'. *Seminars in Arthritis and Rheumatism* 22 (5): 307–18. https://doi.org/10.1016/S0049-0172(05)80010-1.

Chung, Cindy, and Jason A. Burdick. 2008. 'Engineering Cartilage Tissue'. *Advanced Drug Delivery Reviews* 60 (2): 243–62. https://doi.org/10.1016/j.addr.2007.08.027.

Chung, Cindy, and Jason A. Burdick. 2009. 'Influence of Three-Dimensional Hyaluronic Acid Microenvironments on Mesenchymal Stem Cell Chondrogenesis'. *Tissue Engineering. Part A* 15 (2): 243–54. https://doi.org/10.1089/ten.tea.2008.0067.

Clevers, Hans, Kyle M. Loh, and Roel Nusse. 2014. 'An Integral Program for Tissue Renewal and Regeneration: Wnt Signaling and Stem Cell Control'. *Science* 346 (6205): 1248012. https://doi.org/10.1126/science.1248012.

Cohen, Z. A., D. M. McCarthy, S. D. Kwak, P. Legrand, F. Fogarasi, E. J. Ciaccio, and G. A. Ateshian. 1999. 'Knee Cartilage Topography, Thickness, and Contact Areas from MRI: In-Vitro Calibration and in-Vivo Measurements'. *Osteoarthritis and Cartilage* 7 (1): 95–109. https://doi.org/10.1053/joca.1998.0165.

Correia, Cristina, Ana L. Pereira, Ana R. C. Duarte, Ana M. Frias, Adriano J. Pedro, João T. Oliveira, Rui A. Sousa, and Rui L. Reis. 2012. 'Dynamic Culturing of Cartilage Tissue: The

Significance of Hydrostatic Pressure'. *Tissue Engineering. Part A* 18 (19–20): 1979–91. https://doi.org/10.1089/ten.TEA.2012.0083.

Das, R. H. J., H. Jahr, J. A. N. Verhaar, J. C. van der Linden, G. J. V. M. van Osch, and H. Weinans. 2008. 'In Vitro Expansion Affects the Response of Chondrocytes to Mechanical Stimulation'. *Osteoarthritis and Cartilage* 16 (3): 385–91. https://doi.org/10.1016/j.joca.2007.07.014.

Demoor, Magali, David Ollitrault, Tangni Gomez-Leduc, Mouloud Bouyoucef, Magalie Hervieu, Hugo Fabre, Jérôme Lafont, et al. 2014. 'Cartilage Tissue Engineering: Molecular Control of Chondrocyte Differentiation for Proper Cartilage Matrix Reconstruction'. *Biochimica et Biophysica Acta (BBA) - General Subjects*, Matrix-mediated cell behaviour and properties, 1840 (8): 2414–40. https://doi.org/10.1016/j.bbagen.2014.02.030.

Diekman, Brian O., Nicolas Christoforou, Vincent P. Willard, Haosi Sun, Johannah Sanchez-Adams, Kam W. Leong, and Farshid Guilak. 2012. 'Cartilage Tissue Engineering Using Differentiated and Purified Induced Pluripotent Stem Cells'. *Proceedings of the National Academy of Sciences of the United States of America* 109 (47): 19172–77. https://doi.org/10.1073/pnas.1210422109.

Dragan, A. I., R. Pavlovic, J. B. McGivney, J. R. Casas-Finet, E. S. Bishop, R. J. Strouse, M. A. Schenerman, and C. D. Geddes. 2012. 'SYBR Green I: Fluorescence Properties and Interaction with DNA'. *Journal of Fluorescence* 22 (4): 1189–99. https://doi.org/10.1007/s10895-012-1059-8.

Duke, P. J., and D. Montufar-Solis. 1999. 'Exposure to Altered Gravity Affects All Stages of Endochondral Cartilage Differentiation'. *Advances in Space Research: The Official Journal of the Committee on Space Research (COSPAR)* 24 (6): 821–27.

DuRaine, G. D., B. Arzi, J. K. Lee, C. A. Lee, D. J. Responte, J. C. Hu, and K. A. Athanasiou. 2015. 'Biomechanical Evaluation of Suture-Holding Properties of Native and Tissue-Engineered Articular Cartilage'. *Biomechanics and Modeling in Mechanobiology* 14 (1): 73–81. https://doi.org/10.1007/s10237-014-0589-1.

Dürr, J., S. Goodman, A. Potocnik, H. von der Mark, and K. von der Mark. 1993. 'Localization of Beta 1-Integrins in Human Cartilage and Their Role in Chondrocyte Adhesion to Collagen and Fibronectin'. *Experimental Cell Research* 207 (2): 235–44. https://doi.org/10.1006/excr.1993.1189.

Elder, Benjamin D., and Kyriacos A. Athanasiou. 2009. 'Hydrostatic Pressure in Articular Cartilage Tissue Engineering: From Chondrocytes to Tissue Regeneration'. *Tissue Engineering. Part B, Reviews* 15 (1): 43–53. https://doi.org/10.1089/ten.teb.2008.0435.

Elder, Steven H., Shawn W. Sanders, William R. McCulley, Misti L. Marr, Joon W. Shim, and Karen A. Hasty. 2006. 'Chondrocyte Response to Cyclic Hydrostatic Pressure in Alginate versus Pellet Culture'. *Journal of Orthopaedic Research: Official Publication of the Orthopaedic Research Society* 24 (4): 740–47. https://doi.org/10.1002/jor.20086.

Eleswarapu, Sriram V., and Kyriacos A. Athanasiou. 2013. 'TRPV4 Channel Activation Improves the Tensile Properties of Self-Assembled Articular Cartilage Constructs'. *Acta Biomaterialia* 9 (3): 5554–61. https://doi.org/10.1016/j.actbio.2012.10.031.

Exposito, Jean-Yves, Ulrich Valcourt, Caroline Cluzel, and Claire Lethias. 2010. 'The Fibrillar Collagen Family'. *International Journal of Molecular Sciences* 11 (2): 407–26. https://doi.org/10.3390/ijms11020407.

Foster, Nicola C., James R. Henstock, Yvonne Reinwald, and Alicia J. El Haj. 2015. 'Dynamic 3D Culture: Models of Chondrogenesis and Endochondral Ossification'. *Birth Defects Research. Part C, Embryo Today: Reviews* 105 (1): 19–33. https://doi.org/10.1002/bdrc.21088.

Foty, Ramsey A., and Malcolm S. Steinberg. 2005. 'The Differential Adhesion Hypothesis: A Direct Evaluation'. *Developmental Biology* 278 (1): 255–63. https://doi.org/10.1016/j.ydbio.2004.11.012.

Fuerer, Christophe, and Roel Nusse. 2010. 'Lentiviral Vectors to Probe and Manipulate the Wnt Signaling Pathway'. *PloS One* 5 (2): e9370. https://doi.org/10.1371/journal.pone.0009370.

Gadue, Paul, Tara L. Huber, Patrick J. Paddison, and Gordon M. Keller. 2006. 'Wnt and TGF-β Signaling Are Required for the Induction of an in Vitro Model of Primitive Streak Formation Using Embryonic Stem Cells'. *Proceedings of the National Academy of Sciences of the United States of America* 103 (45): 16806–11. https://doi.org/10.1073/pnas.0603916103.

García, M. Carmen, M. Carmen Alfaro, and José Muñoz. 2016. 'Rheology of Sheared Gels Based on Low Acyl-Gellan Gum'. *Food Science and Technology International = Ciencia Y Tecnologia De Los Alimentos Internacional* 22 (4): 325–32. https://doi.org/10.1177/1082013215599296.

Geng, Hui, Stefan Carlsen, Kutty Selva Nandakumar, Rikard Holmdahl, Anders Aspberg, Åke Oldberg, and Ragnar Mattsson. 2008. 'Cartilage Oligomeric Matrix Protein Deficiency Promotes Early Onset and the Chronic Development of Collagen-Induced Arthritis'. *Arthritis Research & Therapy* 10 (6): R134. https://doi.org/10.1186/ar2551.

George, E. L., E. N. Georges-Labouesse, R. S. Patel-King, H. Rayburn, and R. O. Hynes. 1993. 'Defects in Mesoderm, Neural Tube and Vascular Development in Mouse Embryos Lacking Fibronectin'. *Development (Cambridge, England)* 119 (4): 1079–91.

Gilbert, Sophie J., and Emma J. Blain. 2018. 'Chapter 4 - Cartilage Mechanobiology: How Chondrocytes Respond to Mechanical Load'. In *Mechanobiology in Health and Disease*, edited by Stefaan W. Verbruggen, 99–126. Academic Press. https://doi.org/10.1016/B978-0-12-812952-4.00004-0.

Goldring, M. B. 2000. 'Osteoarthritis and Cartilage: The Role of Cytokines'. *Current Rheumatology Reports* 2 (6): 459–65.

Gomes, R., C. Kirn-Safran, M. C. Farach-Carson, and D. D. Carson. 2002. 'Perlecan: An Important Component of the Cartilage Pericellular Matrix'. *Journal of Musculoskeletal & Neuronal Interactions* 2 (6): 511–16.

Gong, Guochun, Deborah Ferrari, Caroline N. Dealy, and Robert A. Kosher. 2010. 'Direct and Progressive Differentiation of Human Embryonic Stem Cells into the Chondrogenic Lineage'. *Journal of Cellular Physiology* 224 (3): 664–71. https://doi.org/10.1002/jcp.22166.

Gong, Yihong, Chunming Wang, Ruenn Chai Lai, Kai Su, Feng Zhang, and Dong-an Wang. 2009. 'An Improved Injectable Polysaccharide Hydrogel: Modified Gellan Gum for Long-

Term Cartilage Regenerationin Vitro'. *Journal of Materials Chemistry* 19 (14): 1968–77. https://doi.org/10.1039/B818090C.

Grodzinsky, A. J., M. E. Levenston, M. Jin, and E. H. Frank. 2000. 'Cartilage Tissue Remodeling in Response to Mechanical Forces'. *Annual Review of Biomedical Engineering* 2: 691–713. https://doi.org/10.1146/annurev.bioeng.2.1.691.

Grogan, Shawn P., Xian Chen, Sujata Sovani, Noboru Taniguchi, Clifford W. Colwell, Martin K. Lotz, and Darryl D. D'Lima. 2014. 'Influence of Cartilage Extracellular Matrix Molecules on Cell Phenotype and Neocartilage Formation'. *Tissue Engineering. Part A* 20 (1–2): 264–74. https://doi.org/10.1089/ten.tea.2012.0618.

Grogan, Shawn P, and Darryl D D'Lima. 2010. 'Joint Aging and Chondrocyte Cell Death'. *International Journal of Clinical Rheumatology* 5 (2): 199–214. https://doi.org/10.2217/ijr.10.3.

Guilak, F., W. R. Jones, H. P. Ting-Beall, and G. M. Lee. 1999. 'The Deformation Behavior and Mechanical Properties of Chondrocytes in Articular Cartilage'. *Osteoarthritis and Cartilage* 7 (1): 59–70. https://doi.org/10.1053/joca.1998.0162.

Guilak, F., and V. C. Mow. 2000. 'The Mechanical Environment of the Chondrocyte: A Biphasic Finite Element Model of Cell-Matrix Interactions in Articular Cartilage'. *Journal of Biomechanics* 33 (12): 1663–73.

Guilak, F., A. Ratcliffe, and V. C. Mow. 1995. 'Chondrocyte Deformation and Local Tissue Strain in Articular Cartilage: A Confocal Microscopy Study'. *Journal of Orthopaedic Research:*

Official Publication of the Orthopaedic Research Society 13 (3): 410–21. https://doi.org/10.1002/jor.1100130315.

Habib, Shukry J., Bi-Chang Chen, Feng-Chiao Tsai, Konstantinos Anastassiadis, Tobias Meyer, Eric Betzig, and Roel Nusse. 2013. 'A Localized Wnt Signal Orients Asymmetric Stem Cell Division in Vitro'. *Science (New York, N.Y.)* 339 (6126): 1445–48. https://doi.org/10.1126/science.1231077.

Hagiwara, H., C. Schröter-Kermani, and H. J. Merker. 1993. 'Localization of Collagen Type VI in Articular Cartilage of Young and Adult Mice'. *Cell and Tissue Research* 272 (1): 155–60.

Haglund, Lisbet, Viveka Tillgren, Laura Addis, Christina Wenglén, Anneliese Recklies, and Dick Heinegård. 2011. 'Identification and Characterization of the Integrin A2β1 Binding Motif in Chondroadherin Mediating Cell Attachment'. *Journal of Biological Chemistry* 286 (5): 3925–34. https://doi.org/10.1074/jbc.M110.161141.

Handa, T., H. Ishihara, H. Ohshima, R. Osada, H. Tsuji, and K. Obata. 1997. 'Effects of Hydrostatic Pressure on Matrix Synthesis and Matrix Metalloproteinase Production in the Human Lumbar Intervertebral Disc'. *Spine* 22 (10): 1085–91.

Hardingham, T. E., and A. J. Fosang. 1992. 'Proteoglycans: Many Forms and Many Functions'. *FASEB Journal: Official Publication of the Federation of American Societies for Experimental Biology* 6 (3): 861–70.

Hardingham, T. E., and Helen Muir. 1972. 'The Specific Interaction of Hyaluronic Acid with Cartilage Proteoglycans'. *Biochimica et Biophysica Acta (BBA) - General Subjects* 279 (2): 401–5. https://doi.org/10.1016/0304-4165(72)90160-2.

Hardingham, Timothy E., and Helen Muir. 1973. 'Binding of Oligosaccharides of Hyaluronic Acid to Proteoglycans (Short Communication)'. *Biochemical Journal* 135 (4): 905–8.

Hardingham, Timothy E., and Helen Muir. 1974. 'Hyaluronic Acid in Cartilage and Proteoglycan Aggregation'. *Biochemical Journal* 139 (3): 565–81.

Hascall, V. C., and D. Heinegård. 1974. 'Aggregation of Cartilage Proteoglycans. I. The Role of Hyaluronic Acid'. *The Journal of Biological Chemistry* 249 (13): 4232–41.

Hascall, Vincent C. 2014. 'A Tribute to Dick Heinegård'. *Matrix Biology* 39 (October): 2–4. https://doi.org/10.1016/j.matbio.2014.08.005.

Hascall, Vincent C., and Dick Heinegård. 1974. 'Aggregation of Cartilage Proteoglycans II. OLIGOSACCHARIDE COMPETITORS OF THE PROTEOGLYCAN-HYALURONIC ACID INTERACTION'. *Journal of Biological Chemistry* 249 (13): 4242–49.

Hedbom, E., P. Antonsson, A. Hjerpe, D. Aeschlimann, M. Paulsson, E. Rosa-Pimentel, Y. Sommarin, M. Wendel, A. Oldberg, and D. Heinegård. 1992. 'Cartilage Matrix Proteins. An Acidic Oligomeric Protein (COMP) Detected Only in Cartilage'. *The Journal of Biological Chemistry* 267 (9): 6132–36.

Heinegård, D., and V. C. Hascall. 1974. 'Aggregation of Cartilage Proteoglycans. 3. Characteristics of the Proteins Isolated from Trypsin Digests of Aggregates'. *The Journal of Biological Chemistry* 249 (13): 4250–56.

Heinegård, D., T. Larsson, Y. Sommarin, A. Franzén, M. Paulsson, and E. Hedbom. 1986. 'Two Novel Matrix Proteins Isolated from Articular Cartilage Show Wide Distributions among Connective Tissues'. *The Journal of Biological Chemistry* 261 (29): 13866–72.

Heinegård, D., and A. Oldberg. 1989. 'Structure and Biology of Cartilage and Bone Matrix Noncollagenous Macromolecules'. *FASEB Journal: Official Publication of the Federation of American Societies for Experimental Biology* 3 (9): 2042–51.

Henstock, J. R., M. Rotherham, J. B. Rose, and A. J. El Haj. 2013. 'Cyclic Hydrostatic Pressure Stimulates Enhanced Bone Development in the Foetal Chick Femur in Vitro'. *Bone* 53 (2): 468–77. https://doi.org/10.1016/j.bone.2013.01.010.

Hida, Daisuke, Ben T. Danielson, Cheryl B. Knudson, and Warren Knudson. 2015. 'CD44 Knock-down in Bovine and Human Chondrocytes Results in Release of Bound HYAL2'. *Matrix Biology : Journal of the International Society for Matrix Biology* 48 (October): 42–54. https://doi.org/10.1016/j.matbio.2015.04.002.

Holden, Paul, Roger S. Meadows, Kathryn L. Chapman, Michael E. Grant, Karl E. Kadler, and Michael D. Briggs. 2001. 'Cartilage Oligomeric Matrix Protein Interacts with Type IX Collagen, and Disruptions to These Interactions Identify a Pathogenetic Mechanism in a Bone Dysplasia Family'. *Journal of Biological Chemistry* 276 (8): 6046–55. https://doi.org/10.1074/jbc.M009507200.

Hollander, A. P., T. F. Heathfield, C. Webber, Y. Iwata, R. Bourne, C. Rorabeck, and A. R. Poole. 1994. 'Increased Damage to Type II Collagen in Osteoarthritic Articular Cartilage Detected by a New Immunoassay'. *The Journal of Clinical Investigation* 93 (4): 1722–32. https://doi.org/10.1172/JCI117156.

Hu, Jerry C., and Kyriacos A. Athanasiou. 2006. 'The Effects of Intermittent Hydrostatic Pressure on Self-Assembled Articular Cartilage Constructs'. *Tissue Engineering* 12 (5): 1337–44. https://doi.org/10.1089/ten.2006.12.1337.

Hui, Alexander Y., William J. McCarty, Koichi Masuda, Gary S. Firestein, and Robert L. Sah. 2012. 'A Systems Biology Approach to Synovial Joint Lubrication in Health, Injury, and Disease'. *Wiley Interdisciplinary Reviews. Systems Biology and Medicine* 4 (1): 15–37. https://doi.org/10.1002/wsbm.157.

Hwang, Nathaniel S., Shyni Varghese, and Jennifer Elisseeff. 2007. 'Cartilage Tissue Engineering: Directed Differentiation of Embryonic Stem Cells in Three-Dimensional Hydrogel Culture'. *Methods in Molecular Biology (Clifton, N.J.)* 407: 351–73. https://doi.org/10.1007/978-1-59745-536-7_24.

Hwang, Nathaniel S., Shyni Varghese, and Jennifer Elisseeff. 2008. 'Derivation of Chondrogenically-Committed Cells from Human Embryonic Cells for Cartilage Tissue Regeneration'. *PloS One* 3 (6): e2498. https://doi.org/10.1371/journal.pone.0002498.

Hwang, Nathaniel S., Shyni Varghese, H. Janice Lee, Zijun Zhang, Zhaohui Ye, Jongwoo Bae, Linzhao Cheng, and Jennifer Elisseeff. 2008. 'In Vivo Commitment and Functional Tissue Regeneration Using Human Embryonic Stem Cell-Derived Mesenchymal Cells'. *Proceedings of the National Academy of Sciences* 105 (52): 20641–46. https://doi.org/10.1073/pnas.0809680106.

Hwang, Nathaniel S., Shyni Varghese, Zijun Zhang, and Jennifer Elisseeff. 2006. 'Chondrogenic Differentiation of Human Embryonic Stem Cell-Derived Cells in Arginine-Glycine-Aspartate-Modified Hydrogels'. *Tissue Engineering* 12 (9): 2695–2706. https://doi.org/10.1089/ten.2006.12.2695.

Ikeda, Toshiyuki, Satoru Kamekura, Akihiko Mabuchi, Ikuyo Kou, Shoji Seki, Tsuyoshi Takato, Kozo Nakamura, Hiroshi Kawaguchi, Shiro Ikegawa, and Ung-il Chung. 2004. 'The

Combination of SOX5, SOX6, and SOX9 (the SOX Trio) Provides Signals Sufficient for Induction of Permanent Cartilage'. *Arthritis and Rheumatism* 50 (11): 3561–73. https://doi.org/10.1002/art.20611.

Insall, J. N. 1967. 'Intra-Articular Surgery for Degenerative Arthritis of the Knee. A Report of the Work of the Late K. H. Pridie'. *The Journal of Bone and Joint Surgery. British Volume* 49 (2): 211–28.

Ishida, Osamu, Yoshiya Tanaka, Isao Morimoto, Masaharu Takigawa, and Sumiya Eto. 1997. 'Chondrocytes Are Regulated by Cellular Adhesion Through CD44 and Hyaluronic Acid Pathway'. *Journal of Bone and Mineral Research* 12 (10): 1657–63. https://doi.org/10.1359/jbmr.1997.12.10.1657.

Ishihara, H., D. S. McNally, J. P. Urban, and A. C. Hall. 1996. 'Effects of Hydrostatic Pressure on Matrix Synthesis in Different Regions of the Intervertebral Disk'. *Journal of Applied Physiology (Bethesda, Md.: 1985)* 80 (3): 839–46. https://doi.org/10.1152/jappl.1996.80.3.839.

Iwamoto, Masahiro, Yoshinobu Higuchi, Eiki Koyama, Motomi Enomoto-Iwamoto, Kojiro Kurisu, Helena Yeh, William R. Abrams, Joel Rosenbloom, and Maurizio Pacifici. 2000. 'Transcription Factor Erg Variants and Functional Diversification of Chondrocytes during Limb Long Bone Development'. *The Journal of Cell Biology* 150 (1): 27–40.

Jansson, Per-Erik, Bengt Lindberg, and Paul A. Sandford. 1983. 'Structural Studies of Gellan Gum, an Extracellular Polysaccharide Elaborated by Pseudomonas Elodea'. *Carbohydrate Research* 124 (1): 135–39. https://doi.org/10.1016/0008-6215(83)88361-X.

Jones, D. Leanne, and Amy J. Wagers. 2008. 'No Place like Home: Anatomy and Function of the Stem Cell Niche'. *Nature Reviews. Molecular Cell Biology* 9 (1): 11–21. https://doi.org/10.1038/nrm2319.

Jooybar, Elaheh, Mohammad J. Abdekhodaie, Mansour Alvi, Abbas Mousavi, Marcel Karperien, and Pieter J. Dijkstra. 2019. 'An Injectable Platelet Lysate-Hyaluronic Acid Hydrogel Supports Cellular Activities and Induces Chondrogenesis of Encapsulated Mesenchymal Stem Cells'. *Acta Biomaterialia* 83 (January): 233–44. https://doi.org/10.1016/j.actbio.2018.10.031.

Jukes, Jojanneke M., Leonardus J. van der Aa, Christine Hiemstra, Theun van Veen, Pieter J. Dijkstra, Zhiyuan Zhong, Jan Feijen, Clemens A. van Blitterswijk, and Jan de Boer. 2010. 'A Newly Developed Chemically Crosslinked Dextran-Poly(Ethylene Glycol) Hydrogel for Cartilage Tissue Engineering'. *Tissue Engineering. Part A* 16 (2): 565–73. https://doi.org/10.1089/ten.TEA.2009.0173.

Jukes, Jojanneke M., Lorenzo Moroni, Clemens A. van Blitterswijk, and Jan de Boer. 2008. 'Critical Steps toward a Tissue-Engineered Cartilage Implant Using Embryonic Stem Cells'. *Tissue Engineering. Part A* 14 (1): 135–47. https://doi.org/10.1089/ten.a.2006.0397.

Kahn, Joy, Yulia Shwartz, Einat Blitz, Sharon Krief, Amnon Sharir, Dario A. Breitel, Revital Rattenbach, et al. 2009. 'Muscle Contraction Is Necessary to Maintain Joint Progenitor Cell Fate'. *Developmental Cell* 16 (5): 734–43. https://doi.org/10.1016/j.devcel.2009.04.013.

Kalkreuth, Richard Horst, Jan Philipp Krüger, Skadi Lau, Philipp Niemeyer, Michaela Endres, Peter Cornelius Kreuz, and Christian Kaps. 2014. 'Fibronectin Stimulates Migration and

Proliferation, but Not Chondrogenic Differentiation of Human Subchondral Progenitor Cells'. *Regenerative Medicine* 9 (6): 759–73. https://doi.org/10.2217/rme.14.40.

Keene, D. R., E. Engvall, and R. W. Glanville. 1988. 'Ultrastructure of Type VI Collagen in Human Skin and Cartilage Suggests an Anchoring Function for This Filamentous Network'. *The Journal of Cell Biology* 107 (5): 1995–2006.

Kim, Hee Jung, and Jeong-Soo Park. 2017. 'Usage of Human Mesenchymal Stem Cells in Cell-Based Therapy: Advantages and Disadvantages'. *Development & Reproduction* 21 (1): 1–10. https://doi.org/10.12717/DR.2017.21.1.001.

Kim, Hoon, Jun Wu, Shoudong Ye, Chih-I. Tai, Xingliang Zhou, Hexin Yan, Ping Li, Martin Pera, and Qi-Long Ying. 2013. 'Modulation of β-Catenin Function Maintains Mouse Epiblast Stem Cell and Human Embryonic Stem Cell Self-Renewal'. *Nature Communications* 4: 2403. https://doi.org/10.1038/ncomms3403.

Kim, Yushan, and Sanjay Kumar. 2014. 'CD44-Mediated Adhesion to Hyaluronic Acid Contributes to Mechanosensing and Invasive Motility'. *Molecular Cancer Research : MCR* 12 (10): 1416–29. https://doi.org/10.1158/1541-7786.MCR-13-0629.

Koay, Eugene J., Gwen M. B. Hoben, and Kyriacos A. Athanasiou. 2007. 'Tissue Engineering with Chondrogenically Differentiated Human Embryonic Stem Cells'. *Stem Cells (Dayton, Ohio)* 25 (9): 2183–90. https://doi.org/10.1634/stemcells.2007-0105.

Kopesky, P. W., H.-Y. Lee, E. J. Vanderploeg, J. D. Kisiday, D. D. Frisbie, A. H. K. Plaas, C. Ortiz, and A. J. Grodzinsky. 2010. 'Adult Equine Bone Marrow Stromal Cells Produce a Cartilage-like ECM Mechanically Superior to Animal-Matched Adult Chondrocytes'. *Matrix Biology:*

Journal of the International Society for Matrix Biology 29 (5): 427–38. https://doi.org/10.1016/j.matbio.2010.02.003.

Krieg, M., Y. Arboleda-Estudillo, P.-H. Puech, J. Käfer, F. Graner, D. J. Müller, and C.-P. Heisenberg. 2008. 'Tensile Forces Govern Germ-Layer Organization in Zebrafish'. *Nature Cell Biology* 10 (4): 429–36. https://doi.org/10.1038/ncb1705.

Kruse-Lösler, Birgit, Ulrich Meyer, Christian Flören, and Ulrich Joos. 2001. 'Influence of Distraction Rates on the Temporomandibular Joint Position and Cartilage Morphology in a Rabbit Model of Mandibular Lengthening'. *Journal of Oral and Maxillofacial Surgery* 59 (12): 1452–59. https://doi.org/10.1053/joms.2001.28281.

Kuiper, N. J., and A. Sharma. 2015. 'A Detailed Quantitative Outcome Measure of Glycosaminoglycans in Human Articular Cartilage for Cell Therapy and Tissue Engineering Strategies'. *Osteoarthritis and Cartilage* 23 (12): 2233–41. https://doi.org/10.1016/j.joca.2015.07.011.

Kunitomo, Taisuke, Kenji A. Takahashi, Yuji Arai, Kei Sakao, Kuniaki Honjo, Masazumi Saito, Atsuo Inoue, et al. 2009. 'Influence of Extracellular Matrix on the Expression of Inflammatory Cytokines, Proteases, and Apoptosis-Related Genes Induced by Hydrostatic Pressure in Three-Dimensionally Cultured Chondrocytes'. *Journal of Orthopaedic Science: Official Journal of the Japanese Orthopaedic Association* 14 (6): 776–83. https://doi.org/10.1007/s00776-009-1393-0.

Kwon, Heenam, Lin Sun, Dana M. Cairns, Roshni S. Rainbow, Rucsanda Carmen Preda, David L. Kaplan, and Li Zeng. 2013. 'The Influence of Scaffold Material on Chondrocytes in

Inflammatory Conditions'. *Acta Biomaterialia* 9 (5): 6563–75. https://doi.org/10.1016/j.actbio.2013.01.004.

Lafont, Jérôme E. 2010. 'Lack of Oxygen in Articular Cartilage: Consequences for Chondrocyte Biology'. *International Journal of Experimental Pathology* 91 (2): 99–106. https://doi.org/10.1111/j.1365-2613.2010.00707.x.

Larsson, T., Y. Sommarin, M. Paulsson, P. Antonsson, E. Hedbom, M. Wendel, and D. Heinegård. 1991. 'Cartilage Matrix Proteins. A Basic 36-KDa Protein with a Restricted Distribution to Cartilage and Bone'. *The Journal of Biological Chemistry* 266 (30): 20428–33.

Le, Quynh-Thu, and Don Courter. 2008. 'Clinical Biomarkers for Hypoxia Targeting'. *Cancer Metastasis Reviews* 27 (3): 351–62. https://doi.org/10.1007/s10555-008-9144-9.

Lee, Whasil, Holly A. Leddy, Yong Chen, Suk Hee Lee, Nicole A. Zelenski, Amy L. McNulty, Jason Wu, et al. 2014. 'Synergy between Piezo1 and Piezo2 Channels Confers High-Strain Mechanosensitivity to Articular Cartilage'. *Proceedings of the National Academy of Sciences* 111 (47): E5114–22. https://doi.org/10.1073/pnas.1414298111.

Lefebvre, V., W. Huang, V. R. Harley, P. N. Goodfellow, and B. de Crombrugghe. 1997. 'SOX9 Is a Potent Activator of the Chondrocyte-Specific Enhancer of the pro Alpha1(II) Collagen Gene'. *Molecular and Cellular Biology* 17 (4): 2336–46.

Lefebvre, Véronique, and Patrick Smits. 2005. 'Transcriptional Control of Chondrocyte Fate and Differentiation'. *Birth Defects Research. Part C, Embryo Today: Reviews* 75 (3): 200–212. https://doi.org/10.1002/bdrc.20048.

Lesley, J., Q. He, K. Miyake, A. Hamann, R. Hyman, and P. W. Kincade. 1992. 'Requirements for Hyaluronic Acid Binding by CD44: A Role for the Cytoplasmic Domain and Activation by Antibody'. *The Journal of Experimental Medicine* 175 (1): 257–66. https://doi.org/10.1084/jem.175.1.257.

Leslie, Shirae K., Ramsey C. Kinney, Zvi Schwartz, and Barbara D. Boyan. 2017. 'Microencapsulation of Stem Cells for Therapy'. *Methods in Molecular Biology (Clifton, N.J.)* 1479: 251–59. https://doi.org/10.1007/978-1-4939-6364-5_20.

Levenberg, Shulamit, Ngan F. Huang, Erin Lavik, Arlin B. Rogers, Joseph Itskovitz-Eldor, and Robert Langer. 2003. 'Differentiation of Human Embryonic Stem Cells on Three-Dimensional Polymer Scaffolds'. *Proceedings of the National Academy of Sciences* 100 (22): 12741–46. https://doi.org/10.1073/pnas.1735463100.

Li, Wenlin, Woong Sun, Yu Zhang, Wanguo Wei, Rajesh Ambasudhan, Peng Xia, Maria Talantova, et al. 2011. 'Rapid Induction and Long-Term Self-Renewal of Primitive Neural Precursors from Human Embryonic Stem Cells by Small Molecule Inhibitors'. *Proceedings of the National Academy of Sciences of the United States of America* 108 (20): 8299–8304. https://doi.org/10.1073/pnas.1014041108.

Li, Yuting, Hao Meng, Yuan Liu, and Bruce P. Lee. 2015. 'Fibrin Gel as an Injectable Biodegradable Scaffold and Cell Carrier for Tissue Engineering'. Research article. The Scientific World Journal. 2015. https://doi.org/10.1155/2015/685690.

Lian, Xiaojun, Jianhua Zhang, Samira M. Azarin, Kexian Zhu, Laurie B. Hazeltine, Xiaoping Bao, Cheston Hsiao, Timothy J. Kamp, and Sean P. Palecek. 2013. 'Directed Cardiomyocyte Differentiation from Human Pluripotent Stem Cells by Modulating Wnt/β-Catenin Signaling

under Fully Defined Conditions'. *Nature Protocols* 8 (1): 162–75. https://doi.org/10.1038/nprot.2012.150.

Lim, Sung Mook, Sung Hwan Jang, Se Heang Oh, Soon Hong Yuk, Gun Il Im, and Jin Ho Lee. 2010. 'Dual-Growth-Factor-Releasing PCL Scaffolds for Chondrogenesis of Adipose-Tissue-Derived Mesenchymal Stem Cells'. *Advanced Engineering Materials* 12 (1–2): B62–69. https://doi.org/10.1002/adem.200980153.

Liu, Qiang, Xiaoqing Hu, Xin Zhang, Xiaoning Duan, Peng Yang, Fengyuan Zhao, and Yingfang Ao. 2016. 'Effects of Mechanical Stress on Chondrocyte Phenotype and Chondrocyte Extracellular Matrix Expression'. *Scientific Reports* 6 (November): 37268. https://doi.org/10.1038/srep37268.

Loeser, Richard F. 2010. 'Age-Related Changes in the Musculoskeletal System and the Development of Osteoarthritis'. *Clinics in Geriatric Medicine* 26 (3): 371–86. https://doi.org/10.1016/j.cger.2010.03.002.

Lorenzo, P., A. Aspberg, P. Onnerfjord, M. T. Bayliss, P. J. Neame, and D. Heinegard. 2001. 'Identification and Characterization of Asporin. a Novel Member of the Leucine-Rich Repeat Protein Family Closely Related to Decorin and Biglycan'. *The Journal of Biological Chemistry* 276 (15): 12201–11. https://doi.org/10.1074/jbc.M010932200.

Lorenzo, P., M. T. Bayliss, and D. Heinegård. 1998. 'A Novel Cartilage Protein (CILP) Present in the Mid-Zone of Human Articular Cartilage Increases with Age'. *The Journal of Biological Chemistry* 273 (36): 23463–68.

Lorenzo, Pilar, Michael T. Bayliss, and Dick Heinegård. 2004. 'Altered Patterns and Synthesis of Extracellular Matrix Macromolecules in Early Osteoarthritis'. *Matrix Biology: Journal of the International Society for Matrix Biology* 23 (6): 381–91. https://doi.org/10.1016/j.matbio.2004.07.007.

Lowndes, Molly, Sergi Junyent, and Shukry J. Habib. 2017. 'Constructing Cellular Niche Properties by Localized Presentation of Wnt Proteins on Synthetic Surfaces'. *Nature Protocols* 12 (7): 1498–1512. https://doi.org/10.1038/nprot.2017.061.

Lowndes, Molly, Michael Rotherham, Joshua C. Price, Alicia J. El Haj, and Shukry J. Habib. 2016. 'Immobilized WNT Proteins Act as a Stem Cell Niche for Tissue Engineering'. *Stem Cell Reports* 7 (1): 126–37. https://doi.org/10.1016/j.stemcr.2016.06.004.

Ludwig, Tenneille E., Veit Bergendahl, Mark E. Levenstein, Junying Yu, Mitchell D. Probasco, and James A. Thomson. 2006. 'Feeder-Independent Culture of Human Embryonic Stem Cells'. *Nature Methods* 3 (8): 637–46. https://doi.org/10.1038/nmeth902.

Luo, Ziwei, Li Jiang, Yan Xu, Haibin Li, Wei Xu, Shuangchi Wu, Yuanliang Wang, Zhenyu Tang, Yonggang Lv, and Li Yang. 2015. 'Mechano Growth Factor (MGF) and Transforming Growth Factor (TGF)-B3 Functionalized Silk Scaffolds Enhance Articular Hyaline Cartilage Regeneration in Rabbit Model'. *Biomaterials* 52 (June): 463–75. https://doi.org/10.1016/j.biomaterials.2015.01.001.

Mackie, E. J., Y. A. Ahmed, L. Tatarczuch, K. -S. Chen, and M. Mirams. 2008. 'Endochondral Ossification: How Cartilage Is Converted into Bone in the Developing Skeleton'. *The International Journal of Biochemistry & Cell Biology* 40 (1): 46–62. https://doi.org/10.1016/j.biocel.2007.06.009.

Mansour, Joseph M. 2004. 'Biomechanics of Cartilage'. In *Kinesiology: The Mechanics and Pathomechanics of Human Movement*, 66–79. Lippincott Williams & Wilkins.

Marlovits, S., M. Hombauer, M. Truppe, V. Vècsei, and W. Schlegel. 2004. 'Changes in the Ratio of Type-I and Type-II Collagen Expression during Monolayer Culture of Human Chondrocytes'. *The Journal of Bone and Joint Surgery. British Volume* 86 (2): 286–95. https://doi.org/10.1302/0301-620x.86b2.14918.

Mauck, R. L., M. A. Soltz, C. C. Wang, D. D. Wong, P. H. Chao, W. B. Valhmu, C. T. Hung, and G. A. Ateshian. 2000. 'Functional Tissue Engineering of Articular Cartilage through Dynamic Loading of Chondrocyte-Seeded Agarose Gels'. *Journal of Biomechanical Engineering* 122 (3): 252–60.

McCall, Joshua D., Jacob E. Luoma, and Kristi S. Anseth. 2012. 'Covalently Tethered Transforming Growth Factor Beta in PEG Hydrogels Promotes Chondrogenic Differentiation of Encapsulated Human Mesenchymal Stem Cells'. *Drug Delivery and Translational Research* 2 (5): 305–12. https://doi.org/10.1007/s13346-012-0090-2.

McDevitt, C. A., and H. Muir. 1976. 'Biochemical Changes in the Cartilage of the Knee in Experimental and Natural Osteoarthritis in the Dog'. *The Journal of Bone and Joint Surgery. British Volume* 58 (1): 94–101.

McKay, Tristan R., Maria V. Camarasa, Banu Iskender, Jinpei Ye, Nicola Bates, Duncan Miller, Jayne C. Fitzsimmons, et al. 2011. 'Human Feeder Cell Line for Derivation and Culture of HESc/HiPSc'. *Stem Cell Research* 7 (2): 154–62. https://doi.org/10.1016/j.scr.2011.04.005.

Meech, Robyn, David B. Edelman, Frederick S. Jones, and Helen P. Makarenkova. 2005. 'The Homeobox Transcription Factor Barx2 Regulates Chondrogenesis during Limb Development'. *Development (Cambridge, England)* 132 (9): 2135–46. https://doi.org/10.1242/dev.01811.

Mendler, M., S. G. Eich-Bender, L. Vaughan, K. H. Winterhalter, and P. Bruckner. 1989. 'Cartilage Contains Mixed Fibrils of Collagen Types II, IX, and XI.' *The Journal of Cell Biology* 108 (1): 191–97. https://doi.org/10.1083/jcb.108.1.191.

Mérida-Velasco, Juan A., Indalecio Sánchez-Montesinos, Joaquín Espín-Ferra, José R. Mérida-Velasco, José F. Rodríguez-Vázquez, and Juan Jiménez-Collado. 1997. 'Development of the Human Knee Joint Ligaments'. *The Anatomical Record* 248 (2): 259–68. https://doi.org/10.1002/(SICI)1097-0185(199706)248:2<259::AID-AR13>3.0.CO;2-O.

Metallo, CM, SM Azarin, L Ji, JJ De Pablo, and SP Palecek. 2008. 'Engineering Tissue from Human Embryonic Stem Cells'. *Journal of Cellular and Molecular Medicine* 12 (3): 709–29. https://doi.org/10.1111/j.1582-4934.2008.00228.x.

Meyer, E. G., C. T. Buckley, A. J. Steward, and D. J. Kelly. 2011. 'The Effect of Cyclic Hydrostatic Pressure on the Functional Development of Cartilaginous Tissues Engineered Using Bone Marrow Derived Mesenchymal Stem Cells'. *Journal of the Mechanical Behavior of Biomedical Materials* 4 (7): 1257–65. https://doi.org/10.1016/j.jmbbm.2011.04.012.

Mhanna, Rami, Jana Becher, Matthias Schnabelrauch, Rui L. Reis, and Iva Pashkuleva. 2017. 'Sulfated Alginate as a Mimic of Sulfated Glycosaminoglycans: Binding of Growth Factors and Effect on Stem Cell Behavior'. *Advanced Biosystems* 1 (7): 1700043. https://doi.org/10.1002/adbi.201700043.

Mhanna, Rami, Aditya Kashyap, Gemma Palazzolo, Queralt Vallmajo-Martin, Jana Becher, Stephanie Moeller, Matthias Schnabelrauch, and Marcy Zenobi-Wong. 2014. 'Chondrocyte Culture in Three Dimensional Alginate Sulfate Hydrogels Promotes Proliferation While Maintaining Expression of Chondrogenic Markers'. *Tissue Engineering Part A* 20 (9–10): 1454–64. https://doi.org/10.1089/ten.tea.2013.0544.

Mikic, Borjana, Arin Lynn Isenstein, and Abhinav Chhabra. 2004. 'Mechanical Modulation of Cartilage Structure and Function during Embryogenesis in the Chick'. *Annals of Biomedical Engineering* 32 (1): 18–25.

Mills, Kate M., James L. A. Szczerkowski, and Shukry J. Habib. 2017. 'Wnt Ligand Presentation and Reception: From the Stem Cell Niche to Tissue Engineering'. *Open Biology* 7 (8). https://doi.org/10.1098/rsob.170140.

Mitrovic, D. 1982. 'Development of the Articular Cavity in Paralyzed Chick Embryos and in Chick Embryo Limb Buds Cultured on Chorioallantoic Membranes'. *Acta Anatomica* 113 (4): 313–24.

Miyanishi, Keita, Michael C. D. Trindade, Derek P. Lindsey, Gary S. Beaupré, Dennis R. Carter, Stuart B. Goodman, David J. Schurman, and R. Lane Smith. 2006. 'Effects of Hydrostatic Pressure and Transforming Growth Factor-Beta 3 on Adult Human Mesenchymal Stem Cell Chondrogenesis in Vitro'. *Tissue Engineering* 12 (6): 1419–28. https://doi.org/10.1089/ten.2006.12.1419.

Mori-Akiyama, Yuko, Haruhiko Akiyama, David H. Rowitch, and Benoit de Crombrugghe. 2003. 'Sox9 Is Required for Determination of the Chondrogenic Cell Lineage in the Cranial

Neural Crest'. *Proceedings of the National Academy of Sciences of the United States of America* 100 (16): 9360–65. https://doi.org/10.1073/pnas.1631288100.

Morrison, Deborah K. 2012. 'MAP Kinase Pathways'. *Cold Spring Harbor Perspectives in Biology* 4 (11). https://doi.org/10.1101/cshperspect.a011254.

Morrison, Sean J., and Allan C. Spradling. 2008. 'Stem Cells and Niches: Mechanisms That Promote Stem Cell Maintenance throughout Life'. *Cell* 132 (4): 598–611. https://doi.org/10.1016/j.cell.2008.01.038.

Muramatsu, Shuji, Makoto Wakabayashi, Takeshi Ohno, Katsuhiko Amano, Rika Ooishi, Toshinori Sugahara, Satoshi Shiojiri, et al. 2007. 'Functional Gene Screening System Identified TRPV4 as a Regulator of Chondrogenic Differentiation'. *Journal of Biological Chemistry* 282 (44): 32158–67. https://doi.org/10.1074/jbc.M706158200.

Murray, P. D. F., and Doris Selby. 1930. 'Intrinsic and Extrinsic Factors in the Primary Development of the Skeleton'. *Wilhelm Roux' Archiv Für Entwicklungsmechanik Der Organismen* 122 (3): 629–62. https://doi.org/10.1007/BF00573594.

Musumeci, Giuseppe. 2016. 'The Effect of Mechanical Loading on Articular Cartilage'. *Journal of Functional Morphology and Kinesiology* 1 (2): 154–61. https://doi.org/10.3390/jfmk1020154.

Nakagawa, Toshiyuki, Sang Yang Lee, and A. Hari Reddi. 2009. 'Induction of Chondrogenesis from Human Embryonic Stem Cells without Embryoid Body Formation by Bone Morphogenetic Protein 7 and Transforming Growth Factor Beta1'. *Arthritis and Rheumatism* 60 (12): 3686–92. https://doi.org/10.1002/art.27229.

Nakajima, Masahiro, Hideki Kizawa, Masao Saitoh, Ikuyo Kou, Kohei Miyazono, and Shiro Ikegawa. 2007. 'Mechanisms for Asporin Function and Regulation in Articular Cartilage'. *The Journal of Biological Chemistry* 282 (44): 32185–92. https://doi.org/10.1074/jbc.M700522200.

Nastase, Madalina V., Marian F. Young, and Liliana Schaefer. 2012. 'Biglycan'. *Journal of Histochemistry and Cytochemistry* 60 (12): 963–75. https://doi.org/10.1369/0022155412456380.

Natoli, Roman M., and Kyriacos A. Athanasiou. 2008. 'P188 Reduces Cell Death and IGF-I Reduces GAG Release Following Single-Impact Loading of Articular Cartilage'. *Journal of Biomechanical Engineering* 130 (4): 041012. https://doi.org/10.1115/1.2939368.

Nguyen, Lonnissa H., Abhijith K. Kudva, Neha S. Saxena, and Krishnendu Roy. 2011. 'Engineering Articular Cartilage with Spatially-Varying Matrix Composition and Mechanical Properties from a Single Stem Cell Population Using a Multi-Layered Hydrogel'. *Biomaterials* 32 (29): 6946–52. https://doi.org/10.1016/j.biomaterials.2011.06.014.

Nichols, Jennifer, and Austin Smith. 2011. 'The Origin and Identity of Embryonic Stem Cells'. *Development* 138 (1): 3–8. https://doi.org/10.1242/dev.050831.

Nicolae, Claudia, Ya-Ping Ko, Nicolai Miosge, Anja Niehoff, Daniel Studer, Lukas Enggist, Ernst B. Hunziker, Mats Paulsson, Raimund Wagener, and Attila Aszodi. 2007. 'Abnormal Collagen Fibrils in Cartilage of Matrilin-1/Matrilin-3-Deficient Mice'. *Journal of Biological Chemistry* 282 (30): 22163–75. https://doi.org/10.1074/jbc.M610994200.

Nowlan, Niamh C., Céline Bourdon, Gérard Dumas, Shahragim Tajbakhsh, Patrick J. Prendergast, and Paula Murphy. 2010. 'Developing Bones Are Differentially Affected by Compromised Skeletal Muscle Formation'. *Bone* 46 (5): 1275–85. https://doi.org/10.1016/j.bone.2009.11.026.

Nowlan, Niamh C., Gerard Dumas, Shahragim Tajbakhsh, Patrick J. Prendergast, and Paula Murphy. 2012. 'Biophysical Stimuli Induced by Passive Movements Compensate for Lack of Skeletal Muscle during Embryonic Skeletogenesis'. *Biomechanics and Modeling in Mechanobiology* 11 (1–2): 207–19. https://doi.org/10.1007/s10237-011-0304-4.

Nowlan, Niamh C., Paula Murphy, and Patrick J. Prendergast. 2008. 'A Dynamic Pattern of Mechanical Stimulation Promotes Ossification in Avian Embryonic Long Bones'. *Journal of Biomechanics* 41 (2): 249–58. https://doi.org/10.1016/j.jbiomech.2007.09.031.

Nowlan, Niamh C., James Sharpe, Karen A. Roddy, Patrick J. Prendergast, and Paula Murphy. 2010. 'Mechanobiology of Embryonic Skeletal Development: Insights from Animal Models'. *Birth Defects Research. Part C, Embryo Today : Reviews* 90 (3): 203–13. https://doi.org/10.1002/bdrc.20184.

O'Conor, Christopher J., Holly A. Leddy, Halei C. Benefield, Wolfgang B. Liedtke, and Farshid Guilak. 2014. 'TRPV4-Mediated Mechanotransduction Regulates the Metabolic Response of Chondrocytes to Dynamic Loading'. *Proceedings of the National Academy of Sciences* 111 (4): 1316–21. https://doi.org/10.1073/pnas.1319569111.

Ogawa, Rei, Shuichi Mizuno, George F. Murphy, and Dennis P. Orgill. 2009. 'The Effect of Hydrostatic Pressure on Three-Dimensional Chondroinduction of Human Adipose-Derived

Stem Cells'. *Tissue Engineering. Part A* 15 (10): 2937–45. https://doi.org/10.1089/ten.TEA.2008.0672.

Oldershaw, Rachel, Melissa Baxter, Emma Lowe, Nicola Bates, Lisa Grady, Francesca Soncin, Daniel Brison, Timothy Hardingham, and Susan Kimber. 2010. 'A Chemically-Defined Protocol for Generating Chondrocytes from Human Embryonic Stem Cells', November. https://www.nature.com/protocolexchange/protocols/1898#/procedure.

Oliveira, J. T., L. Martins, R. Picciochi, P. B. Malafaya, R. A. Sousa, N. M. Neves, J. F. Mano, and R. L. Reis. 2010. 'Gellan Gum: A New Biomaterial for Cartilage Tissue Engineering Applications'. *Journal of Biomedical Materials Research. Part A* 93 (3): 852–63. https://doi.org/10.1002/jbm.a.32574.

Olson, Michael F. 2008. 'Applications for ROCK Kinase Inhibition'. *Current Opinion in Cell Biology* 20 (2): 242–48. https://doi.org/10.1016/j.ceb.2008.01.002.

Osborne, A. C., K. J. Lamb, J. C. Lewthwaite, G. P. Dowthwaite, and A. A. Pitsillides. 2002. 'Short-Term Rigid and Flaccid Paralyses Diminish Growth of Embryonic Chick Limbs and Abrogate Joint Cavity Formation but Differentially Preserve Pre-Cavitated Joints'. *Journal of Musculoskeletal & Neuronal Interactions* 2 (5): 448–56.

Oseni, Adelola O., Claire Crowley, Maria Z. Boland, Peter E. Butler, and Alexander M. Seifalian. 2011. 'Cartilage Tissue Engineering: The Application of Nanomaterials and Stem Cell Technology'. *Tissue Engineering for Tissue and Organ Regeneration*, August. https://doi.org/10.5772/22453.

Pacifici, Maurizio, Eiki Koyama, and Masahiro Iwamoto. 2005. 'Mechanisms of Synovial Joint and Articular Cartilage Formation: Recent Advances, but Many Lingering Mysteries'. *Birth Defects Research. Part C, Embryo Today: Reviews* 75 (3): 237–48. https://doi.org/10.1002/bdrc.20050.

Pap, Thomas, and Jessica Bertrand. 2013. 'Syndecans in Cartilage Breakdown and Synovial Inflammation'. *Nature Reviews. Rheumatology* 9 (1): 43–55. https://doi.org/10.1038/nrrheum.2012.178.

Paracuellos, Patricia, Sebastian Kalamajski, Arkadiusz Bonna, Dominique Bihan, Richard W. Farndale, and Erhard Hohenester. 2017. 'Structural and Functional Analysis of Two Small Leucine-Rich Repeat Proteoglycans, Fibromodulin and Chondroadherin'. *Matrix Biology: Journal of the International Society for Matrix Biology* 63: 106–16. https://doi.org/10.1016/j.matbio.2017.02.002.

Park, Hyejin, Bogyu Choi, Junli Hu, and Min Lee. 2013. 'Injectable Chitosan Hyaluronic Acid Hydrogels for Cartilage Tissue Engineering'. *Acta Biomaterialia* 9 (1): 4779–86. https://doi.org/10.1016/j.actbio.2012.08.033.

Park, Yong Doo, Nicola Tirelli, and Jeffrey A. Hubbell. 2002. 'Photopolymerized Hyaluronic Acid-Based Hydrogels and Interpenetrating Networks'. In *The Biomaterials: Silver Jubilee Compendium*, edited by D. F. Williams, 203–10. Oxford: Elsevier Science. https://doi.org/10.1016/B978-008045154-1.50023-X.

Parkkinen, J. J., J. Ikonen, M. J. Lammi, J. Laakkonen, M. Tammi, and H. J. Helminen. 1993. 'Effects of Cyclic Hydrostatic Pressure on Proteoglycan Synthesis in Cultured Chondrocytes

and Articular Cartilage Explants'. *Archives of Biochemistry and Biophysics* 300 (1): 458–65. https://doi.org/10.1006/abbi.1993.1062.

Parsons, Philippa, Sophie J. Gilbert, Anne Vaughan-Thomas, David A. Sorrell, Rebecca Notman, Mark Bishop, Anthony J. Hayes, Deborah J. Mason, and Victor C. Duance. 2011. 'Type IX Collagen Interacts with Fibronectin Providing an Important Molecular Bridge in Articular Cartilage'. *Journal of Biological Chemistry* 286 (40): 34986–97. https://doi.org/10.1074/jbc.M111.238188.

Partridge, S. M., H. F. Davis, and G. S. Adair. 1961. 'The Chemistry of Connective Tissues. 6. The Constitution of the Chondroitin Sulphate-Protein Complex in Cartilage'. *The Biochemical Journal* 79 (April): 15–26.

Peake, M. A., L. M. Cooling, J. L. Magnay, P. B. Thomas, and A. J. El Haj. 2000. 'Selected Contribution: Regulatory Pathways Involved in Mechanical Induction of c-Fos Gene Expression in Bone Cells'. *Journal of Applied Physiology (Bethesda, Md.: 1985)* 89 (6): 2498–2507. https://doi.org/10.1152/jappl.2000.89.6.2498.

Peake, Matthew. 2001. 'Regulatory Pathways Involved in Mechanical Induction of C-Fos Gene Expression in Bone Cells'. Ph.D., University of Keele. https://ethos.bl.uk/OrderDetails.do?uin=uk.bl.ethos.392159.

Pereira, R. C., M. Scaranari, P. Castagnola, M. Grandizio, H. S. Azevedo, R. L. Reis, R. Cancedda, and C. Gentili. 2009. 'Novel Injectable Gel (System) as a Vehicle for Human Articular Chondrocytes in Cartilage Tissue Regeneration'. *Journal of Tissue Engineering and Regenerative Medicine* 3 (2): 97–106. https://doi.org/10.1002/term.145.

Pihlajamaa, Tero, Hilkka Lankinen, Joni Ylöstalo, Leena Valmu, Juha Jäälinoja, Frank Zaucke, Luitgard Spitznagel, et al. 2004. 'Characterization of Recombinant Amino-Terminal NC4 Domain of Human Collagen IX INTERACTION WITH GLYCOSAMINOGLYCANS AND CARTILAGE OLIGOMERIC MATRIX PROTEIN'. *Journal of Biological Chemistry* 279 (23): 24265–73. https://doi.org/10.1074/jbc.M402865200.

Poole, A. R., T. Kojima, T. Yasuda, F. Mwale, M. Kobayashi, and S. Laverty. 2001. 'Composition and Structure of Articular Cartilage: A Template for Tissue Repair'. *Clinical Orthopaedics and Related Research*, no. 391 Suppl (October): S26-33.

Popa, Elena G., Sofia G. Caridade, João F. Mano, Rui L. Reis, and Manuela E. Gomes. 2015. 'Chondrogenic Potential of Injectable κ-Carrageenan Hydrogel with Encapsulated Adipose Stem Cells for Cartilage Tissue-Engineering Applications'. *Journal of Tissue Engineering and Regenerative Medicine* 9 (5): 550–63. https://doi.org/10.1002/term.1683.

Popa, Elena G., Vítor E. Santo, Márcia T. Rodrigues, and Manuela E. Gomes. 2016. 'Magnetically-Responsive Hydrogels for Modulation of Chondrogenic Commitment of Human Adipose-Derived Stem Cells'. *Polymers* 8 (2). https://doi.org/10.3390/polym8020028.

Pörtner, Ralf, Stephanie Nagel-Heyer, Christiane Goepfert, Peter Adamietz, and Norbert M. Meenen. 2005. 'Bioreactor Design for Tissue Engineering'. *Journal of Bioscience and Bioengineering* 100 (3): 235–45. https://doi.org/10.1263/jbb.100.235.

Prudnikova, Katsiaryna, Robert W. Yucha, Pavan Patel, Alicia S. Kriete, Lin Han, Lynn S. Penn, and Michele S. Marcolongo. 2017. 'Biomimetic Proteoglycans Mimic Macromolecular

Architecture and Water Uptake of Natural Proteoglycans'. *Biomacromolecules* 18 (6): 1713–23. https://doi.org/10.1021/acs.biomac.7b00032.

Puetzer, Jennifer, John Williams, Allison Gillies, Susan Bernacki, and Elizabeth G. Loboa. 2013. 'The Effects of Cyclic Hydrostatic Pressure on Chondrogenesis and Viability of Human Adipose- and Bone Marrow-Derived Mesenchymal Stem Cells in Three-Dimensional Agarose Constructs'. *Tissue Engineering. Part A* 19 (1–2): 299–306. https://doi.org/10.1089/ten.TEA.2012.0015.

Qi, Maosong, and Elaine A. Elion. 2005. 'MAP Kinase Pathways'. *Journal of Cell Science* 118 (16): 3569–72. https://doi.org/10.1242/jcs.02470.

Qi, Yan, Zhichao Li, Chi-Wing Kong, Nelson L. Tang, Yu Huang, Ronald A. Li, and Xiaoqiang Yao. 2015. 'Uniaxial Cyclic Stretch Stimulates TRPV4 to Induce Realignment of Human Embryonic Stem Cell-Derived Cardiomyocytes'. *Journal of Molecular and Cellular Cardiology* 87 (October): 65–73. https://doi.org/10.1016/j.yjmcc.2015.08.005.

Rampersad, Sephra N. 2012. 'Multiple Applications of Alamar Blue as an Indicator of Metabolic Function and Cellular Health in Cell Viability Bioassays'. *Sensors* 12 (9): 12347–60. https://doi.org/10.3390/s120912347.

Responte, Donald J., Jennifer K. Lee, Jerry C. Hu, and Kyriacos A. Athanasiou. 2012. 'Biomechanics-Driven Chondrogenesis: From Embryo to Adult'. *FASEB Journal: Official Publication of the Federation of American Societies for Experimental Biology* 26 (9): 3614–24. https://doi.org/10.1096/fj.12-207241.

Reza, Anna T., and Steven B. Nicoll. 2008. 'Dose-Dependent Response of Tissue-Engineered Intervertebral Discs to Dynamic Unconfined Compressive Loading'. *Annals of Biomedical Engineering* 36 (2): 204–13. https://doi.org/10.1007/s10439-007-9407-6.

Rhee, David K., Jose Marcelino, MacArthur Baker, Yaoqin Gong, Patrick Smits, Véronique Lefebvre, Gregory D. Jay, et al. 2005. 'The Secreted Glycoprotein Lubricin Protects Cartilage Surfaces and Inhibits Synovial Cell Overgrowth'. *Journal of Clinical Investigation* 115 (3): 622–31. https://doi.org/10.1172/JCI200522263.

Ricard-Blum, Sylvie. 2011. 'The Collagen Family'. *Cold Spring Harbor Perspectives in Biology* 3 (1). https://doi.org/10.1101/cshperspect.a004978.

Richardson, James B., Karina T. Wright, Johanna Wales, Jan Herman Kuiper, Helen S. McCarthy, Peter Gallacher, Paul E. Harrison, and Sally Roberts. 2017. 'Efficacy and Safety of Autologous Cell Therapies for Knee Cartilage Defects (Autologous Stem Cells, Chondrocytes or the Two): Randomized Controlled Trial Design'. *Regenerative Medicine* 12 (5): 493–501. https://doi.org/10.2217/rme-2017-0032.

Rocha, Pedro M. Azevedo, V. Espírito Santo, Manuela Estima Gomes, Rui Luís Reis, and João F. Mano. 2011. 'Encapsulation of Adipose-Derived Stem Cells and Transforming Growth Factor-B1 in Carrageenan-Based Hydrogels for Cartilage Tissue Engineering'. In . https://doi.org/10.1177/0883911511420700.

Rodén, Lennart, John R. Baker, J. Anthony Cifonelli, and Martin B. Mathews. 1972. '[7] Isolation and Characterization of Connective Tissue Polysaccharides'. In *Methods in Enzymology*, 28:73–140. Elsevier. https://doi.org/10.1016/0076-6879(72)28009-0.

Roshanbinfar, Kaveh, and Soheila Salahshour Kordestani. 2013. 'Encapsulating Beta Islet Cells in Alginate, Alginate-Chitosan and Alginate-Chitosan-PEG Microcapsules and Investigation of Insulin Secretion'. Text. April 2013. https://doi.org/info:doi/10.1166/jbt.2013.1082.

Ruano-Gil, D., J. Nardi-Vilardaga, and A. Teixidor-Johé. 1985. 'Embryonal Hypermobility and Articular Development'. *Acta Anatomica* 123 (2): 90–92.

Ruano-Gil, D., J. Nardi-Vilardaga, and A. Tejedo-Mateu. 1978. 'Influence of Extrinsic Factors on the Development of the Articular System'. *Acta Anatomica* 101 (1): 36–44.

Safshekan, Farzaneh, Mohammad Tafazzoli-Shadpour, Mohammad Ali Shokrgozar, Nooshin Haghighipour, Reza Mahdian, and Alireza Hemmati. 2012. 'Intermittent Hydrostatic Pressure Enhances Growth Factor-Induced Chondroinduction of Human Adipose-Derived Mesenchymal Stem Cells'. *Artificial Organs* 36 (12): 1065–71. https://doi.org/10.1111/j.1525-1594.2012.01507.x.

Sajdera, Stanley W., and Vincent C. Hascall. 1969. 'Proteinpolysaccharide Complex from Bovine Nasal Cartilage A COMPARISON OF LOW AND HIGH SHEAR EXTRACTION PROCEDURES'. *Journal of Biological Chemistry* 244 (1): 77–87.

Sakao, K., K. A. Takahashi, Y. Arai, A. Inoue, H. Tonomura, M. Saito, T. Yamamoto, et al. 2008. 'Induction of Chondrogenic Phenotype in Synovium-Derived Progenitor Cells by Intermittent Hydrostatic Pressure'. *Osteoarthritis and Cartilage* 16 (7): 805–14. https://doi.org/10.1016/j.joca.2007.10.021.

Sarrazin, Stephane, William C. Lamanna, and Jeffrey D. Esko. 2011. 'Heparan Sulfate Proteoglycans'. *Cold Spring Harbor Perspectives in Biology* 3 (7). https://doi.org/10.1101/cshperspect.a004952.

Sayyar, Bahareh, Megan Dodd, Leah Marquez-Curtis, Anna Janowska-Wieczorek, and Gonzalo Hortelano. 2015. 'Fibronectin-Alginate Microcapsules Improve Cell Viability and Protein Secretion of Encapsulated Factor IX-Engineered Human Mesenchymal Stromal Cells'. *Artificial Cells, Nanomedicine, and Biotechnology* 43 (5): 318–27. https://doi.org/10.3109/21691401.2014.885446.

Schuette, Hayden B., Matthew J. Kraeutler, and Eric C. McCarty. 2017. 'Matrix-Assisted Autologous Chondrocyte Transplantation in the Knee: A Systematic Review of Mid- to Long-Term Clinical Outcomes'. *Orthopaedic Journal of Sports Medicine* 5 (6). https://doi.org/10.1177/2325967117709250.

Schwartz, E. A., R. Bizios, M. S. Medow, and M. E. Gerritsen. 1999. 'Exposure of Human Vascular Endothelial Cells to Sustained Hydrostatic Pressure Stimulates Proliferation. Involvement of the AlphaV Integrins'. *Circulation Research* 84 (3): 315–22.

Shafiee, Abbas, Masoud Soleimani, Gholamreza Abedi Chamheidari, Ehsan Seyedjafari, Masumeh Dodel, Amir Atashi, and Yousof Gheisari. 2011. 'Electrospun Nanofiber-Based Regeneration of Cartilage Enhanced by Mesenchymal Stem Cells'. *Journal of Biomedical Materials Research. Part A* 99 (3): 467–78. https://doi.org/10.1002/jbm.a.33206.

Shah, Mehul R., Kevin M. Kaplan, Robert J. Meislin, and Joseph A. Bosco. 2007. 'Articular Cartilage Restoration of the Knee'. *Bulletin of the NYU Hospital for Joint Diseases* 65 (1): 51–60.

Shang, Yan-chang, Shu-hui Wang, Fu Xiong, Cui-ping Zhao, Fu-ning Peng, Shan-wei Feng, Mei-shan Li, Yong Li, and Cheng Zhang. 2007. 'Wnt3a Signaling Promotes Proliferation, Myogenic Differentiation, and Migration of Rat Bone Marrow Mesenchymal Stem Cells'. *Acta Pharmacologica Sinica* 28 (11): 1761–74. https://doi.org/10.1111/j.1745-7254.2007.00671.x.

Sharma, Aarti, Lindsay D. Wood, James B. Richardson, Sally Roberts, and Nicola J. Kuiper. 2007. 'Glycosaminoglycan Profiles of Repair Tissue Formed Following Autologous Chondrocyte Implantation Differ from Control Cartilage'. *Arthritis Research & Therapy* 9 (4): R79. https://doi.org/10.1186/ar2278.

Sharma, Shaili, Aeju Lee, Kuiwon Choi, Kwangmeyung Kim, Inchan Youn, Stephen B. Trippel, and Alyssa Panitch. 2013. 'Biomimetic Aggrecan Reduces Cartilage Extracellular Matrix From Degradation and Lowers Catabolic Activity in Ex Vivo and In Vivo Models'. *Macromolecular Bioscience* 13 (9): 1228–37. https://doi.org/10.1002/mabi.201300112.

Shepard, John B., Heidi A. Krug, Brooklynn A. LaFoon, Stanley Hoffman, and Anthony A. Capehart. 2007. 'Versican Expression during Synovial Joint Morphogenesis'. *International Journal of Biological Sciences* 3 (6): 380–84.

Shepherd, D. E., and B. B. Seedhom. 1999. 'The "instantaneous" Compressive Modulus of Human Articular Cartilage in Joints of the Lower Limb'. *Rheumatology (Oxford, England)* 38 (2): 124–32.

Singh, Purva, and Jean E. Schwarzbauer. 2012. 'Fibronectin and Stem Cell Differentiation – Lessons from Chondrogenesis'. *Journal of Cell Science* 125 (16): 3703–12. https://doi.org/10.1242/jcs.095786.

Smith, Alan M., Richard M. Shelton, Yvonne Perrie, and Jonathan J. Harris. 2007. 'An Initial Evaluation of Gellan Gum as a Material for Tissue Engineering Applications'. *Journal of Biomaterials Applications* 22 (3): 241–54. https://doi.org/10.1177/0885328207076522.

Smits, P., P. Li, J. Mandel, Z. Zhang, J. M. Deng, R. R. Behringer, B. de Crombrugghe, and V. Lefebvre. 2001. 'The Transcription Factors L-Sox5 and Sox6 Are Essential for Cartilage Formation'. *Developmental Cell* 1 (2): 277–90.

Snow, Holly E., Lin M. Riccio, Corey H. Mjaatvedt, Stanley Hoffman, and Anthony A. Capehart. 2005. 'Versican Expression during Skeletal/Joint Morphogenesis and Patterning of Muscle and Nerve in the Embryonic Mouse Limb'. *The Anatomical Record. Part A, Discoveries in Molecular, Cellular, and Evolutionary Biology* 282 (2): 95–105. https://doi.org/10.1002/ar.a.20151.

Snyder, Timothy N., Krishna Madhavan, Miranda Intrator, Ryan C. Dregalla, and Daewon Park. 2014. 'A Fibrin/Hyaluronic Acid Hydrogel for the Delivery of Mesenchymal Stem Cells and Potential for Articular Cartilage Repair'. *Journal of Biological Engineering* 8: 10. https://doi.org/10.1186/1754-1611-8-10.

Sokol, Sergei Y. 2011. 'Maintaining Embryonic Stem Cell Pluripotency with Wnt Signaling'. *Development* 138 (20): 4341–50. https://doi.org/10.1242/dev.066209.

Sophia Fox, Alice J., Asheesh Bedi, and Scott A. Rodeo. 2009. 'The Basic Science of Articular Cartilage'. *Sports Health* 1 (6): 461–68. https://doi.org/10.1177/1941738109350438.

Soteriou, Despina, Banu Iskender, Adam Byron, Jonathan D. Humphries, Simon Borg-Bartolo, Marie-Claire Haddock, Melissa A. Baxter, David Knight, Martin J. Humphries, and

Susan J. Kimber. 2013. ‘Comparative Proteomic Analysis of Supportive and Unsupportive Extracellular Matrix Substrates for Human Embryonic Stem Cell Maintenance’. *The Journal of Biological Chemistry* 288 (26): 18716–31. https://doi.org/10.1074/jbc.M113.463372.

Sproul, E., S. Nandi, and A. Brown. 2018. ‘6 - Fibrin Biomaterials for Tissue Regeneration and Repair’. In *Peptides and Proteins as Biomaterials for Tissue Regeneration and Repair*, edited by Mário A. Barbosa and M. Cristina L. Martins, 151–73. Woodhead Publishing. https://doi.org/10.1016/B978-0-08-100803-4.00006-1.

Stanton, Lee-Anne, T. Michael Underhill, and Frank Beier. 2003. ‘MAP Kinases in Chondrocyte Differentiation’. *Developmental Biology* 263 (2): 165–75. https://doi.org/10.1016/S0012-1606(03)00321-X.

Strawich, E., and M. E. Nimni. 1971. ‘Properties of a Collagen Molecule Containing Three Identical Components Extracted from Bovine Articular Cartilage’. *Biochemistry* 10 (21): 3905–11.

Sumi, T., N. Tsuneyoshi, N. Nakatsuji, and H. Suemori. 2008. ‘Defining Early Lineage Specification of Human Embryonic Stem Cells by the Orchestrated Balance of Canonical Wnt/ -Catenin, Activin/Nodal and BMP Signaling’. *Development* 135 (17): 2969–79. https://doi.org/10.1242/dev.021121.

Takahashi, K., T. Kubo, Y. Arai, I. Kitajima, M. Takigawa, J. Imanishi, and Y. Hirasawa. 1998. ‘Hydrostatic Pressure Induces Expression of Interleukin 6 and Tumour Necrosis Factor Alpha MRNAs in a Chondrocyte-like Cell Line’. *Annals of the Rheumatic Diseases* 57 (4): 231–36.

Takigawa, Yoko, Kenji Hata, Shuji Muramatsu, Katsuhiko Amano, Koichiro Ono, Makoto Wakabayashi, Akio Matsuda, Kenji Takada, Riko Nishimura, and Toshiyuki Yoneda. 2010. 'The Transcription Factor Znf219 Regulates Chondrocyte Differentiation by Assembling a Transcription Factory with Sox9'. *Journal of Cell Science* 123 (Pt 21): 3780–88. https://doi.org/10.1242/jcs.071373.

Teo, Jia-Ling, and Michael Kahn. 2010. 'The Wnt Signaling Pathway in Cellular Proliferation and Differentiation: A Tale of Two Coactivators'. *Advanced Drug Delivery Reviews*, Stem Cell Gene Manipulation and Delivery as Systemic Therapeutics, 62 (12): 1149–55. https://doi.org/10.1016/j.addr.2010.09.012.

Tetlow, L. C., D. J. Adlam, and D. E. Woolley. 2001. 'Matrix Metalloproteinase and Proinflammatory Cytokine Production by Chondrocytes of Human Osteoarthritic Cartilage: Associations with Degenerative Changes'. *Arthritis and Rheumatism* 44 (3): 585–94. https://doi.org/10.1002/1529-0131(200103)44:3<585::AID-ANR107>3.0.CO;2-C.

Thomas, G. P., and A. J. el Haj. 1996. 'Bone Marrow Stromal Cells Are Load Responsive in Vitro'. *Calcified Tissue International* 58 (2): 101–8.

Thorfve, A., T. Dehne, A. Lindahl, M. Brittberg, A. Pruss, J. Ringe, M. Sittinger, and C. Karlsson. 2012. 'Characteristic Markers of the WNT Signaling Pathways Are Differentially Expressed in Osteoarthritic Cartilage'. *Cartilage* 3 (1): 43–57. https://doi.org/10.1177/1947603511414178.

Thorlund, J. B., C. B. Juhl, E. M. Roos, and L. S. Lohmander. 2015. 'Arthroscopic Surgery for Degenerative Knee: Systematic Review and Meta-Analysis of Benefits and Harms'. *BMJ* 350 (June): h2747. https://doi.org/10.1136/bmj.h2747.

Tiğli, R. Seda, Chris Cannizaro, Menemşe Gümüşderelioğlu, and David L. Kaplan. 2011. 'Chondrogenesis in Perfusion Bioreactors Using Porous Silk Scaffolds and HESC-Derived MSCs'. *Journal of Biomedical Materials Research. Part A* 96 (1): 21–28. https://doi.org/10.1002/jbm.a.32949.

Toh, Wei Seong, Eng Hin Lee, Xi-Min Guo, Jerry K. Y. Chan, Chen Hua Yeow, Andre B. Choo, and Tong Cao. 2010. 'Cartilage Repair Using Hyaluronan Hydrogel-Encapsulated Human Embryonic Stem Cell-Derived Chondrogenic Cells'. *Biomaterials* 31 (27): 6968–80. https://doi.org/10.1016/j.biomaterials.2010.05.064.

Tortora, Gerard J, and Sandra Reynolds Grabowski. 2003. *Principles of Anatomy and Physiology*. Tenth. United States of America: John Wiley & Sons, Inc.

Towle, C. A., H. H. Hung, L. J. Bonassar, B. V. Treadwell, and D. C. Mangham. 1997. 'Detection of Interleukin-1 in the Cartilage of Patients with Osteoarthritis: A Possible Autocrine/Paracrine Role in Pathogenesis'. *Osteoarthritis and Cartilage* 5 (5): 293–300.

Tsuda, Masanao, Shigeru Takahashi, Yuji Takahashi, and Hiroshi Asahara. 2003. 'Transcriptional Co-Activators CREB-Binding Protein and P300 Regulate Chondrocyte-Specific Gene Expression via Association with Sox9'. *The Journal of Biological Chemistry* 278 (29): 27224–29. https://doi.org/10.1074/jbc.M303471200.

Vilela, Carlos A., Cristina Correia, Alain da Silva Morais, Tírcia C. Santos, Ana C. Gertrudes, Elsa S. Moreira, Ana M. Frias, et al. 2018. 'In Vitro and in Vivo Performance of Methacrylated Gellan Gum Hydrogel Formulations for Cartilage Repair'. *Journal of Biomedical Materials Research. Part A* 106 (7): 1987–96. https://doi.org/10.1002/jbm.a.36406.

Vinardell, Tatiana, Rebecca A. Rolfe, Conor T. Buckley, Eric G. Meyer, Mark Ahearne, Paula Murphy, and Daniel J. Kelly. 2012. 'Hydrostatic Pressure Acts to Stabilise a Chondrogenic Phenotype in Porcine Joint Tissue Derived Stem Cells'. *European Cells & Materials* 23 (February): 121–32; discussion 133-134.

Vincent, T. L., C. J. McLean, L. E. Full, D. Peston, and J. Saklatvala. 2007. 'FGF-2 Is Bound to Perlecan in the Pericellular Matrix of Articular Cartilage, Where It Acts as a Chondrocyte Mechanotransducer'. *Osteoarthritis and Cartilage* 15 (7): 752–63. https://doi.org/10.1016/j.joca.2007.01.021.

Vunjak-Novakovic, G., I. Martin, B. Obradovic, S. Treppo, A. J. Grodzinsky, R. Langer, and L. E. Freed. 1999. 'Bioreactor Cultivation Conditions Modulate the Composition and Mechanical Properties of Tissue-Engineered Cartilage'. *Journal of Orthopaedic Research: Official Publication of the Orthopaedic Research Society* 17 (1): 130–38. https://doi.org/10.1002/jor.1100170119.

Vunjak-Novakovic, Gordana, Lisa E. Freed, Robert J. Biron, and Robert Langer. 1996. 'Effects of Mixing on the Composition and Morphology of Tissue-Engineered Cartilage'. *AIChE Journal* 42 (3): 850–60. https://doi.org/10.1002/aic.690420323.

Wang, Gang, Xiaodong Cao, Hua Dong, Lei Zeng, Chenxi Yu, and Xiaofeng Chen. 2018. 'A Hyaluronic Acid Based Injectable Hydrogel Formed via Photo-Crosslinking Reaction and Thermal-Induced Diels-Alder Reaction for Cartilage Tissue Engineering'. *Polymers* 10 (9). https://doi.org/10.3390/polym10090949.

Wang, Qi Guang, Alicia J. El Haj, and Nicola J. Kuiper. 2008. 'Glycosaminoglycans in the Pericellular Matrix of Chondrons and Chondrocytes'. *Journal of Anatomy* 213 (3): 266–73. https://doi.org/10.1111/j.1469-7580.2008.00942.x.

Wang, Xibin, Paul A. Manner, Alan Horner, Lillian Shum, Rocky S. Tuan, and Glen H. Nuckolls. 2004. 'Regulation of MMP-13 Expression by RUNX2 and FGF2 in Osteoarthritic Cartilage'. *Osteoarthritis and Cartilage* 12 (12): 963–73. https://doi.org/10.1016/j.joca.2004.08.008.

Weber, Alexander E., Philip H. Locker, Erik N. Mayer, Gregory L. Cvetanovich, Annemarie K. Tilton, Brandon J. Erickson, Adam B. Yanke, and Brian J. Cole. 2018. 'Clinical Outcomes After Microfracture of the Knee: Midterm Follow-Up'. *Orthopaedic Journal of Sports Medicine* 6 (2). https://doi.org/10.1177/2325967117753572.

Wiberg, Charlotte, Andreas R. Klatt, Raimund Wagener, Mats Paulsson, John F. Bateman, Dick Heinegård, and Matthias Mörgelin. 2003. 'Complexes of Matrilin-1 and Biglycan or Decorin Connect Collagen VI Microfibrils to Both Collagen II and Aggrecan'. *The Journal of Biological Chemistry* 278 (39): 37698–704. https://doi.org/10.1074/jbc.M304638200.

Willert, Karl, Jeffrey D. Brown, Esther Danenberg, Andrew W. Duncan, Irving L. Weissman, Tannishtha Reya, John R. Yates, and Roel Nusse. 2003. 'Wnt Proteins Are Lipid-Modified and Can Act as Stem Cell Growth Factors'. *Nature* 423 (6938): 448–52. https://doi.org/10.1038/nature01611.

Wu, Xiaolin, Jichun Wang, Hong Jiang, Qi Hu, Jing Chen, Jing Zhang, Rui Zhu, Wenwei Liu, and Bin Li. 2014. 'Wnt3a Activates B1-integrin and Regulates Migration and Adhesion of Vascular Smooth Muscle Cells'. *Molecular Medicine Reports* 9 (4): 1159–64. https://doi.org/10.3892/mmr.2014.1937.

Xu, S. C., M. A. Harris, J. L. Rubenstein, G. R. Mundy, and S. E. Harris. 2001. 'Bone Morphogenetic Protein-2 (BMP-2) Signaling to the Col2alpha1 Gene in Chondroblasts Requires the Homeobox Gene Dlx-2'. *DNA and Cell Biology* 20 (6): 359–65. https://doi.org/10.1089/10445490152122479.

Yegappan, Ramanathan, Vignesh Selvaprithiviraj, Sivashanmugam Amirthalingam, and R. Jayakumar. 2018. 'Carrageenan Based Hydrogels for Drug Delivery, Tissue Engineering and Wound Healing'. *Carbohydrate Polymers* 198 (October): 385–400. https://doi.org/10.1016/j.carbpol.2018.06.086.

Yu, Feng, Xiaodong Cao, Yuli Li, Lei Zeng, Bo Yuan, and Xiaofeng Chen. 2013. 'An Injectable Hyaluronic Acid/PEG Hydrogel for Cartilage Tissue Engineering Formed by Integrating Enzymatic Crosslinking and Diels–Alder "Click Chemistry"'. *Polymer Chemistry* 5 (3): 1082–90. https://doi.org/10.1039/C3PY00869J.

Zhan, T., N. Rindtorff, and M. Boutros. 2017. 'Wnt Signaling in Cancer'. *Oncogene* 36 (11): 1461–73. https://doi.org/10.1038/onc.2016.304.

Zhang, Min, Fa-Ming Chen, An-Hui Wang, Yong-Jin Chen, Xin Lv, Shun Wu, and Rui-Ni Zhao. 2012. 'Estrogen and Its Receptor Enhance Mechanobiological Effects in Compressed Bone Mesenchymal Stem Cells'. *Cells, Tissues, Organs* 195 (5): 400–413. https://doi.org/10.1159/000328003.

Zhang, Shufang, Yang Zi Jiang, Wei Zhang, Longkun Chen, Tong Tong, Wanlu Liu, Qin Mu, et al. 2013. 'Neonatal Desensitization Supports Long-Term Survival and Functional Integration of Human Embryonic Stem Cell-Derived Mesenchymal Stem Cells in Rat Joint Cartilage

without Immunosuppression'. *Stem Cells and Development* 22 (1): 90–101. https://doi.org/10.1089/scd.2012.0116.

Zhang, Y., S. Chen, and M. Pei. 2016. 'Biomechanical Signals Guiding Stem Cell Cartilage Engineering: From Molecular Adaption to Tissue Functionality'. *European Cells & Materials* 31 (January): 59–78.

Zhao, Yin-Hua, Xin Lv, Yan-Li Liu, Ying Zhao, Qiang Li, Yong-Jin Chen, and Min Zhang. 2015. 'Hydrostatic Pressure Promotes the Proliferation and Osteogenic/Chondrogenic Differentiation of Mesenchymal Stem Cells: The Roles of RhoA and Rac1'. *Stem Cell Research* 14 (3): 283–96. https://doi.org/10.1016/j.scr.2015.02.006.

Zhu, Wei, Nathan J. Castro, Xiaoqian Cheng, Michael Keidar, and Lijie Grace Zhang. 2015. 'Cold Atmospheric Plasma Modified Electrospun Scaffolds with Embedded Microspheres for Improved Cartilage Regeneration'. *PLoS ONE* 10 (7). https://doi.org/10.1371/journal.pone.0134729.

Zipper, Hubert, Herwig Brunner, Jürgen Bernhagen, and Frank Vitzthum. 2004. 'Investigations on DNA Intercalation and Surface Binding by SYBR Green I, Its Structure Determination and Methodological Implications'. *Nucleic Acids Research* 32 (12): e103. https://doi.org/10.1093/nar/gnh101.

Appendices

Supplementary figures

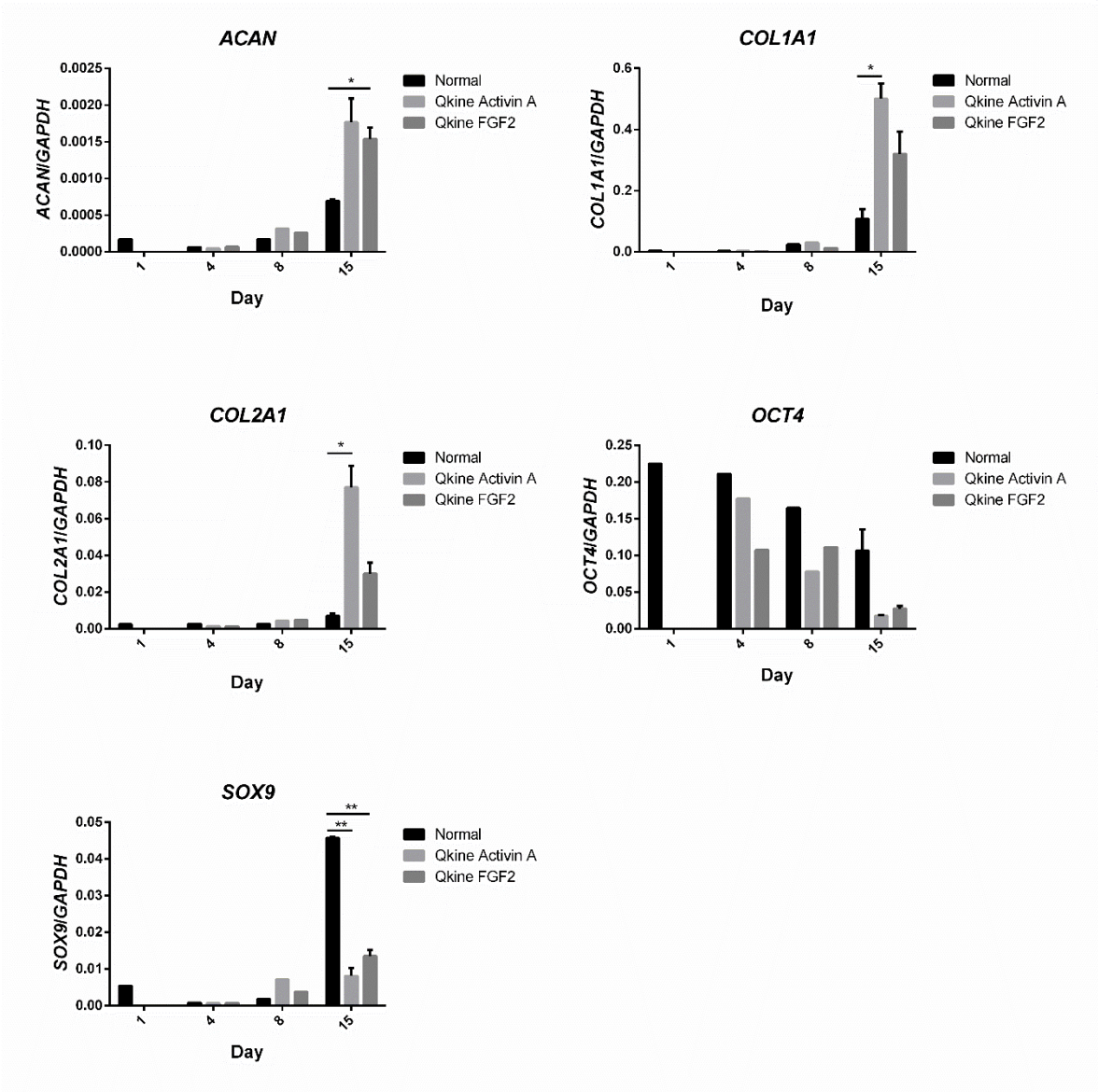

Supplementary figure 1. Downstream chondrogenic gene expressed is significantly increased with addition of GFs from Qkine. Mean expression ($2^{-\Delta Ct}$) of *ACAN*, *COL1A1*, *COL2A1*, *OCT4* and *SOX9* in MAN13 hESC subjected to directed differentiation for 15 days. Data are expressed as the mean ± the standard error, N=1 (days 1-8) and N=3 (day 15). Normal = Activin A (Peprotech) and FGF2 (Gibco™) as detailed in chapter 2.3.

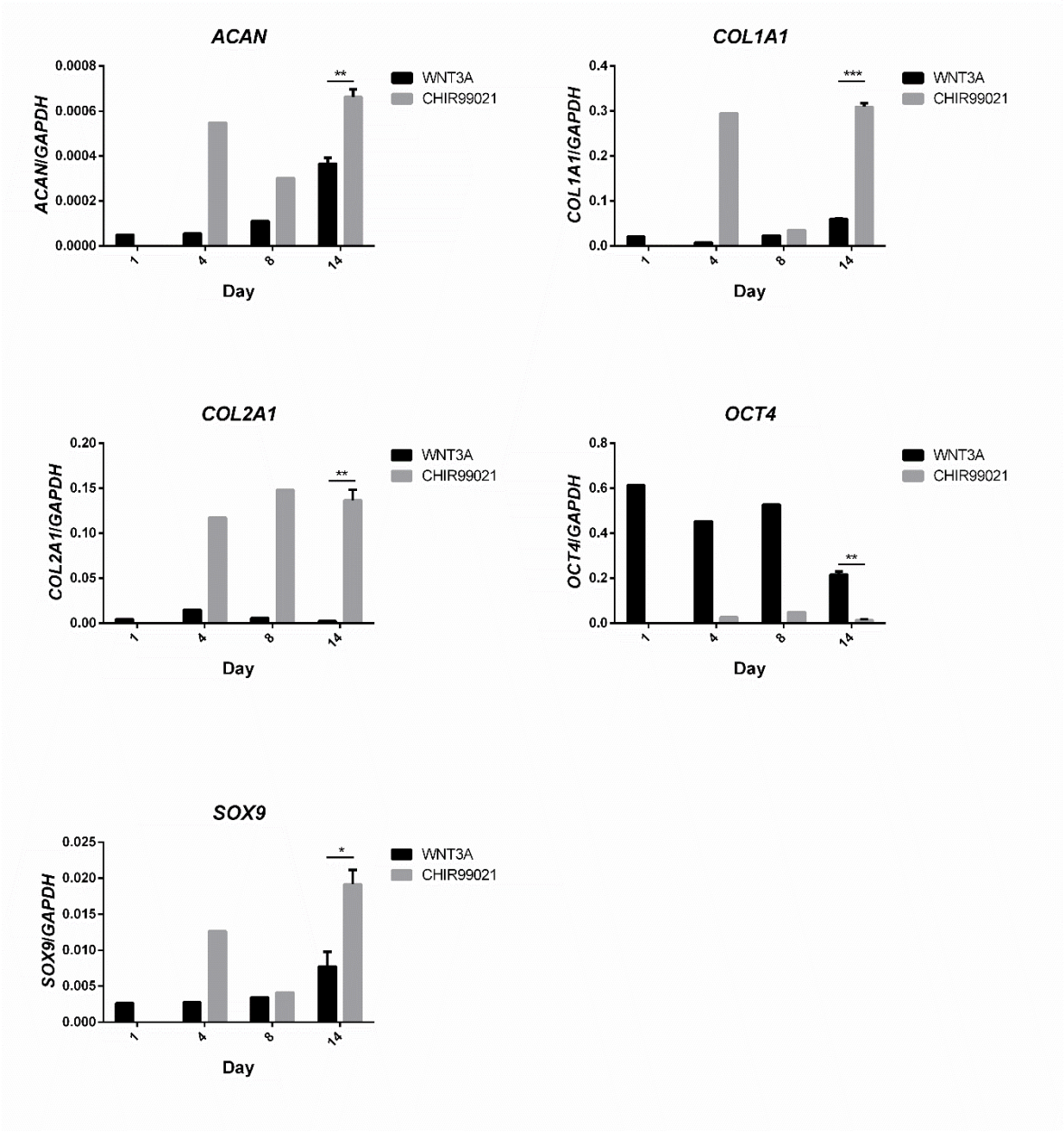

Supplementary figure 2. Chondrogenic gene expression is significantly increased and pluripotency gene expression significantly decreased by substituting WNT3A for CHIR99021. Mean expression ($2^{-\Delta Ct}$) of *ACAN*, *COL1A1*, *COL2A1*, *OCT4* and *SOX9* in MAN7 hESC subjected to directed differentiation for 14 days. Data are expressed as the mean ± the standard error, N=1 (days 1-8) and N=3 (day 15). Either WNT3A or CHIR99021 used during DDP as detailed in chapter 2.3.

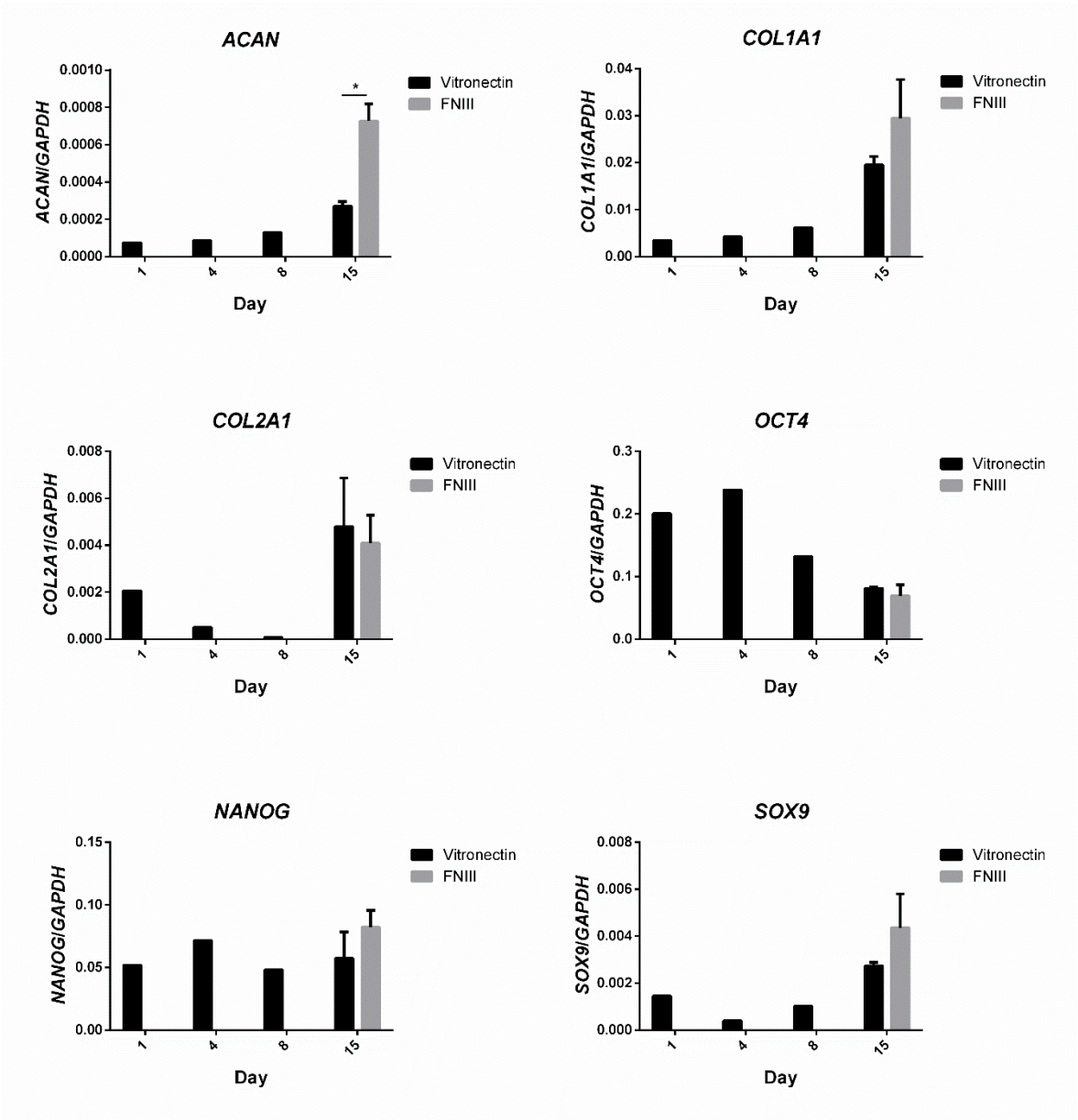

Supplementary figure 3. Chondrogenic and pluripotency gene expressions are not significantly changed by substituting vitronectin for FNIII. Mean expression ($2^{-\Delta Ct}$) of *ACAN*, *COL1A1*, *COL2A1*, *OCT4, NANOG* and *SOX9* in MAN7 hESC subjected to directed differentiation for 15 days. Data are expressed as the mean ± the standard error, N=1 (days 1-8) and N=3 (day 15). Cells were transferred to TCP coated in fibronectin peptide (FNIII) on day 8 of the DDP, as detailed in chapter 2.3.

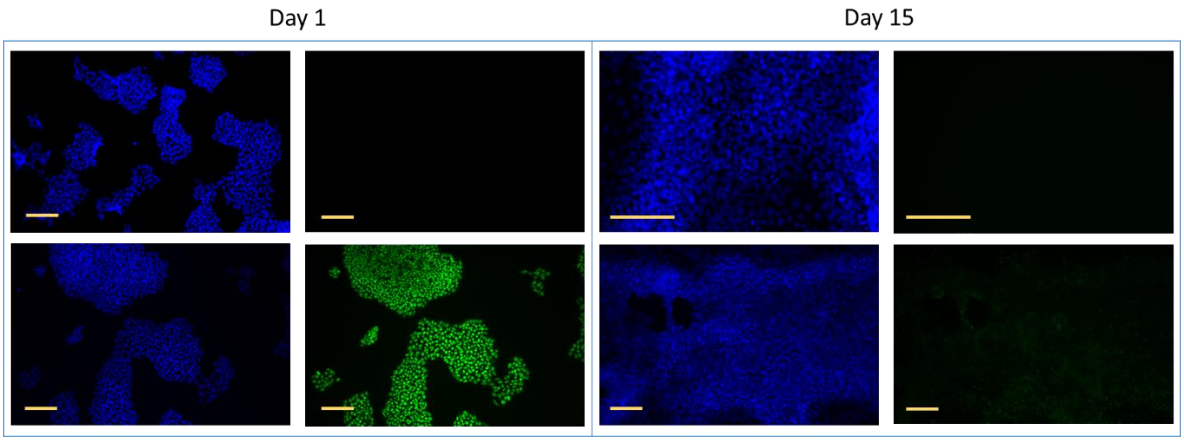

Supplementary figure 4. OCT4 expression diminishes in hESC after application of DDP. MAN7 hESC subjected to directed differentiation for 15 days. Top row = negative control (secondary antibody only), bottom row = positive control (primary and secondary antibodies). Scale bars = 100 µm. DAPI (blue), OCT4 (green).

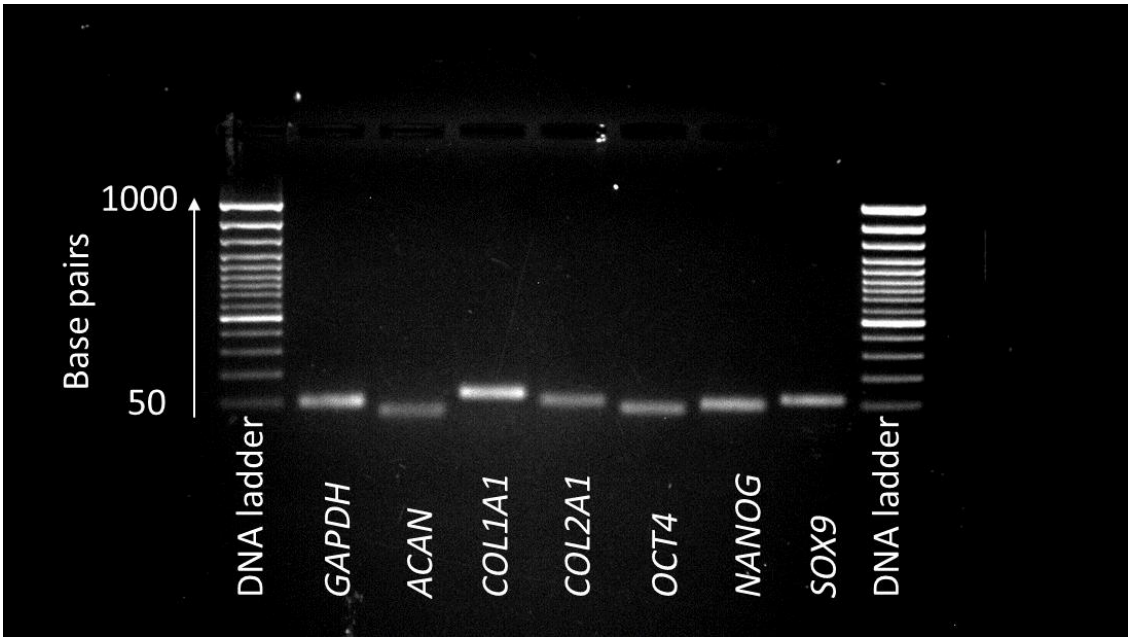

Supplementary figure 5. Gel electrophoresis of qRT-PCR products shows that one product is amplified for each gene. MAN7 hESC subjected to DDP for 16 days. qRT-PCR performed as described in chapter 2.14 and agarose gel electrophoresis performed on products as described in chapter 2.15. GeneRuler 50 bp DNA Ladder (Fisher Scientific UK Ltd) used as reference.

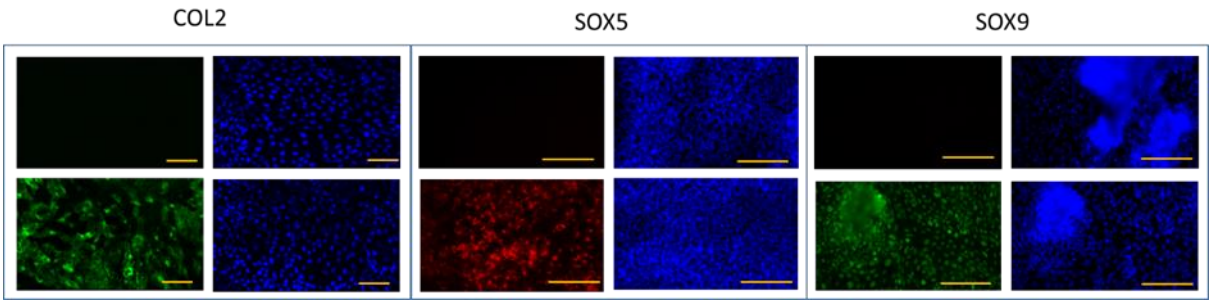

Supplementary figure 6. COL2, SOX5 and SOX9 staining of D14 monolayer hESC-derived chondroprogenitors. Top row = negative control (secondary antibody only), bottom row = positive control (primary and secondary antibodies). Scale bars = 100 µm. DAPI (blue), SOX5 (red), COL2 and SOX9 (green).